Center for Education and Research on Macromolecules (CERM)
Professor C. JEROME

Microfluidic formulation: offering new biomedical perspectives to poly(phospho)ester microparticles

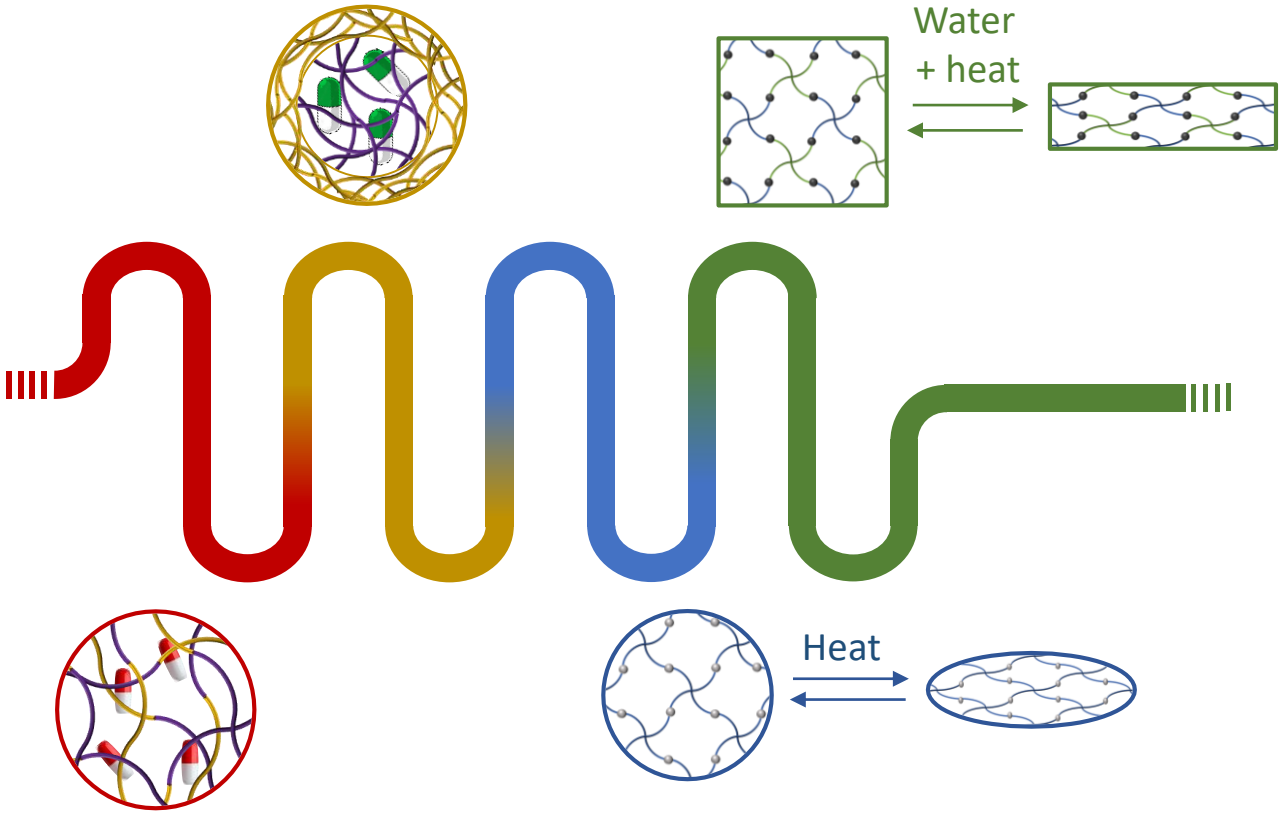

Interreg
Euregio Meuse-Rhin
Fonds Européen de Développement Régional
UNION EUROPÉENNE
INFLOW

Dissertation presented by

Jérémie Caprasse

To obtain the grade of
Doctor in Sciences
Academic Year 2023-2024

Microfluidic formulation: offering new biomedical perspectives to poly(phospho)ester microparticles

By Jérémie CAPRASSE

Drug-loaded microspheres based on biocompatible and biodegradable polymers, mainly aliphatic polyesters, have demonstrated an increasing interest for producing devices with controlled or sustained release profiles of an active ingredient. They rely on the availability of scalable and robust production techniques. Microfluidic technology meets all these requirements and is characterized by high drug encapsulation efficiency and low particles size dispersity. As a result, this formulation process will become increasingly important in the near future for producing commercially available drug delivery systems even though optimizing the formulation process can be time-consuming.

Various microspheres parameters, such as size, polydispersity, composition, structure and shape, have a significant influence on drug release kinetics. The microfluidic technique enables precise control of these parameters which is essential for sustained and predictable drug-release. To modulate the release profile of microfluidically-formulated polylactide (PLA) microspheres, the incorporation of a more hydrophilic polyphosphoester (PPE) component was investigated. On the one hand, a PLA-PPE block copolymer was used as an additive to the polyester microsphere matrix. On the other hand, core-shell microspheres were formulated by adapting the microfluidic chip, enabling a PLA core to be coated with a layer of photo-crosslinked PPE. The impact of this PPE component and its localization on the encapsulation and release profile of model molecules was studied.

The developed microfluidic technologies were further used to produce poly(ε-caprolactone) (PCL) microspheres with shape memory properties. Two types of shape-memory microspheres were designed: (i) a PCL core coated with a crosslinked shell of PPE, and (ii) photo-crosslinked functionalized-PCL microspheres. For both systems, the stimulus for triggering shape memory is temperature (T_m (PCL) ≈ 45°C), which is not always suitable for biomedical applications. To overcome this limitation, a poly(ethylene oxide) (PEO) component was incorporated into PCL to form a hybrid network. In this way, shape memory can be triggered at room temperature by simple immersion in an aqueous medium.

Formulation microfluidique : le nouvel horizon biomédical des microparticules de poly(phospho)esters.

Par Jérémie CAPRASSE

Les microsphères chargées de médicaments utilisées dans le milieu biomédical sont basées sur des polymères biocompatibles et biodégradables, principalement des polyesters aliphatiques, suscitent un intérêt croissant pour la production de dispositifs à libération contrôlée ou prolongée d'un principe actif. Elles s'appuient sur le développement de techniques de production évolutives et robustes. La technologie microfluidique répond à toutes ces exigences et se caractérise par une efficacité d'encapsulation du médicament élevée et une faible dispersion de la taille des particules. Par conséquence, dans un avenir proche, ce processus de formulation prendra de plus en plus d'ampleur pour la production de systèmes médicamenteux disponibles commercialement. Et ce, même si l'optimisation du processus de formulation peut parfois être fastidieuse.

Différents paramètres des microsphères, tels que la taille, la polydispersité, la composition, la structure et la forme, ont une influence significative sur la cinétique de libération des médicaments. La technique microfluidique permet un contrôle précis de ces paramètres, ce qui est essentiel pour une libération de médicament soutenue et prévisible. Afin de moduler le profil de libération des microsphères de polylactide (PLA) formulées par microfluidique, l'incorporation d'un composant plus hydrophile, le polyphosphoester (PPE), a été étudiée. D'une part, un copolymère séquencé PLA-*b*-PPE a été incorporé dans la matrice des microsphères polyester. D'autre part, des microsphères core-shell ont été formulées en adaptant le dispositif microfluidique, permettant au cœur en PLA d'être revêtu d'une couche de PPE photo-réticulé. L'impact de l'addition de ce composant PPE, autour du cœur PLA, sur l'encapsulation et le profil de libération de molécules modèles a été étudié.

La technologie microfluidique développée a ensuite été utilisée pour produire des microsphères de poly(ε-caprolactone) (PCL) présentant des propriétés de mémoire de forme. Deux types de microsphères à mémoire de forme ont été conçus : (i) un noyau en PCL revêtu d'une enveloppe réticulée de PPE, et (ii) des microsphères composées de PCL photo-réticulées. Pour ces deux systèmes, la température (T_m (PCL) ≈ 45°C) est le stimulus utilisé pour déclencher la mémoire de forme, ce qui n'est pas toujours adapté aux applications biomédicales. Pour surmonter cette limitation, un composant poly(éthylène oxide) (PEO) a été incorporé dans la PCL pour former un réseau hybride. De cette manière, la mémoire de forme peut être activée à température ambiante par simple immersion dans un milieu aqueux.

Remerciements

Durant ces 6 (longues) années de thèse, j'ai eu la chance de rencontrer énormément de personnes qui ont eu un impact positif sur mon développement et sur mes recherches. Je ne saurais toutes les citer personnellement dans ces remerciements mais elles se reconnaitront.

J'aimerais tout d'abord remercier le Professeur Christine Jérôme de m'avoir fait confiance en me permettant de réaliser cette thèse de doctorat dans son laboratoire. Merci Christine de m'avoir permis de profiter de ta clairvoyance, de ta science mais aussi de ta bonne humeur et de ton énergie positive. Merci aussi pour le temps et l'implication que tu as mis dans ces corrections afin de rendre ce travail meilleur.

Pour l'attention qu'ils vont porter à mon travail en acceptant de faire partie de mon jury, je tiens à remercier particulièrement le Professeur Benjamin Nottelet, la Docteur Kathy Van Butsele et la Docteur Anna Lechanteur. Anna merci également pour la fourniture des principes actifs, les différentes discussions et les idées.

Je tiens également à remercier chaleureusement le Professeur Jean-Christophe Monbaliu d'avoir accepté de présider mon jury de thèse.

Merci également au Docteur Jean-Michel Thomassin et au Professeur Nicolas Vandewalle pour leur suivi annuel en tant que membre de mon comité de thèse.

Un énorme merci également au Docteur Raphaël Riva qui, grâce à sa grande expertise et sa rigueur scientifique, m'a permis de sortir de nombreuses situations chimiques compliquées que l'on rencontre dans un travail de recherche. Merci aussi pour les discussions, les idées, la motivation, le suivi, les corrections et surtout les Chokotoff.

Thanks a lot to the PhD Nynke as well as the PhD Daniel for the cytotoxocity tests performed in the frame of Interreg IN FLOW project.

Merci au département de Chimie et plus largement à l'Université de Liège pour le financement d'Assistant, grâce auquel je me suis découvert une passion pour l'enseignement et vers lequel je vais sûrement me diriger.

J'ai eu la chance d'encadrer plusieurs mémorantes durant cette thèse sans qui ce travail ne serait sûrement pas aussi complet donc merci à Hajar, Laura et Clémence.

Durant mes 6 années de thèse, j'ai pu m'apercevoir que la particularité du CERM est d'être une grande famille où tout le monde participe du mieux qu'il peut à garder cet esprit. J'aimerais donc remercier tous les membres que j'ai eu la chance de rencontrer durant ces 6 ans.

Parmi eux, j'aimerais particulièrement remercier Christophe pour sa bonne humeur, ses discussions et ses Aïkis de midi. Un énorme merci à Fabi et Bambino pour les cerises, les Spritz

et surtout merci d'avoir accepté d'être mes parents adoptifs durant 2 semaines, c'était un réel plaisir !

Le petit-déjeuner est le repas le plus important de la journée et en étant bien entouré, c'est encore mieux ! Un énorme merci à Charlotte, Greg, Martine et Maxou, merci pour vos discussions (parfois lunaires), vos parties de belote mémorables et vos potions magiques du matin.

Parfois, on a la chance de tomber sur des personnes qui deviennent de véritables ami(e)s. J'ai beaucoup de chance, j'en ai trouvé plusieurs. Vaco et Soph, mes deux mamys-moto (c'est la dernière fois, promis !), vous avez été mon moteur quotidien pour ne pas laisser tomber, merci pour les cafés, les discussions, les coups de gueule, les apéros et tout le reste. Ça va être bizarre de ne plus vous voir tous les jours. Et puis évidemment je gardais les meilleurs pour la fin, merci à mes deux blonds préférés, Phil et Pitt, la bienséance ne me permet pas de donner plus de détails ici mais j'ai vraiment passé d'excellents moments à vos côtés que ça soit au labo ou en sortie, je me suis trouvé deux vrais amis, merci d'avoir toujours été là pour moi !

Quand on a la chance d'être assistant, on est amené à rencontrer beaucoup de belles personnes présentes au département de chimie. Un énorme merci à Steph, Armélinda, Enza, Stéphane, Greg, Carlo, JC, Delphine, Cédric, Romaric, Adrien, Nathan, Edith, Gilles, Damien, Maxime, Thomas, Valentin.

J'ai évidemment une pensée émue pour notre magnifique Alice que je n'oublierai jamais.

Pour finir, j'aimerais remercier les personnes qui m'ont permis d'être l'homme que je suis aujourd'hui grâce à leur soutien et leur confiance inconditionnels. Donc merci à tous mes amis de longue date, Dorian, Hélène, Martial, Nathalie et tous les autres. Un gigantesque merci à mes parents, mes grands-parents, mon frère, ma sœur, ma nièce et mon beau-frère qui transforment chaque moment en famille en moments de fête permettant de se ressourcer. Merci également à ma belle-famille au top pour votre soutien et les bons moments passés ensemble. Et finalement, merci aussi à ma merveilleuse future épouse, Cécile. Tu m'as toujours soutenu et supporté dans tous les différents projets que j'entreprends. J'ai beaucoup de chance de t'avoir à mes côtés.

Bisous à tous.

Table of contents

Table of abbreviations

Acronyms

EMA	European Medicines Agency
FDA	Food and drug administration
API	Active pharmaceutical ingredient
DDSs	Drug delivery systems
EE	Encapsulation efficiency
DL	Drug-loading
$scCO_2$	Supercritical CO_2
RNA	Ribonucleic acid
IgM	Immunoglobulin M
DNA	Deoxyribonucleic acid
Bfb	Bovine fibroblast
HUVEC	Human umbilical vein endothelial cells
MWCO	Molecular-weight cutoff
FT	Fourier-transform
SMPs	Shape-memory polymers
MPs	Magnetic particles
RT	Room temperature
PDA	Photodiode array
MRI	Magnetic resonance imaging
CANs	Covalent adaptable networks
SD	Sustainable development
PDI	Polydispersity
θ	Standard deviation
EF	Environmental factor

Chemical compounds

N_2	Dinitrogen
SDS	Sodium dodecyl sulfate
LA	Lactic acid
GA	Glycolic acid
COP	2-Chloro-3-oxo-1,3,2-dioxaphospholane
TEA	Triethylamine
DBU	1,8 diazobicyclo[5.4.0]undec-7-ene
BEP	Butenyl phosphate
OA	Oleic acid
DMAP	4-dimethylamino-pyridine
DCC	Dicyclohexylcarbodiimide

Solvents

MeOH	Methanol
AcOEt	Ethyl acetate
DMF	Dimethylformamide
DCM	Dichloromethane
THF	Tetrahydrofuran
DMC	Dimethyl carbonate

Polymers

PLGA	Poly(lactic-*co*-glycolic acid)
PLA	Polylactide
PDLLA	Poly-D,L-lactic acid
PLLA	Poly-L-lactic acid
PDLA	Poly-D-lactic acid
PGA	Polyglycolide
PCL	Poly(ε-caprolactone)
PCL-4COU	Poly(ε-caprolactone) bearing 4 coumarin moieties
PCL-4MAL	Poly(ε-caprolactone) bearing 4 maleimide moieties

PEG or PEO	Polyethylene glycol
PEO-4FUR	Polyethylene oxide bearing 4 furan moieties
PPEs	Polyphosphoesters
PBEP	Poly(butenyl phosphate)
PBEP-*b*-PLLA	Poly(butenyl phosphate)-block-poly(L-lactide)
PFA	Perfluoroalkoxy alkanes
PVOH	Polyvinyl alcohol
PVP	Polyvinyl pyrrolidone
PNIPAM	Poly-*N*-isopropylacrylamide

Materials

PDLLA//PBEP	Microparticles with a PDLLA core and a PBEP shell
PCL//PBEP	Microparticles with a PCL core and a PBEP shell
PDLLA//PDLLA	Microparticles with a PDLLA core and a PDLLA shell
IPNs	Interpenetrated networks
TPUs	Thermoplastic polyurethanes

Analysis

DMA	Dynamic mechanical analysis
ESE	Emulsion-solvent evaporation
SD	Spray-drying
ES	Electro-spraying
SCF	Supercritical fluid
MF	Microfluidic technique
NMR	Nuclear magnetic resonance
SEC	Size exclusion chromatography
HPLC	High-Performance Liquid Chromatography
SEM	Scanning electron microscopy
DSC	Dynamic scanning calorimetry
TGA	Thermogravimetric analysis

Fluidic parameters

Re_d	Reynolds number of the dispersed phase
ρ_d	Discontinuous fluid density
l	Characteristic length
U_d	Discontinuous fluid
μ_d	Discontinuous phase viscosity
Ca_c	Capillary number of the continuous phase
μ_c	Continuous phase viscosity
U_c	Continuous fluid average velocity
σ	Surface tension
We	Weber number
Q_d	Flow rate of the discontinuous phase
Q_c	Flow rate of the continuous phase
d	Diameter
w	Width
h	Height

Macromolecular parameters

T_m	Melting temperature
X_c	Crystallinity rate
T_c	Crystallization temperature
ΔH_f^0	Enthalpy of melting for a 100% crystalline polymer
M_w	Molecular weight
T_g	Glass transition temperature

Chapter I : Comprehensive study of parameters influencing the microparticles formulation by microfluidic technique.

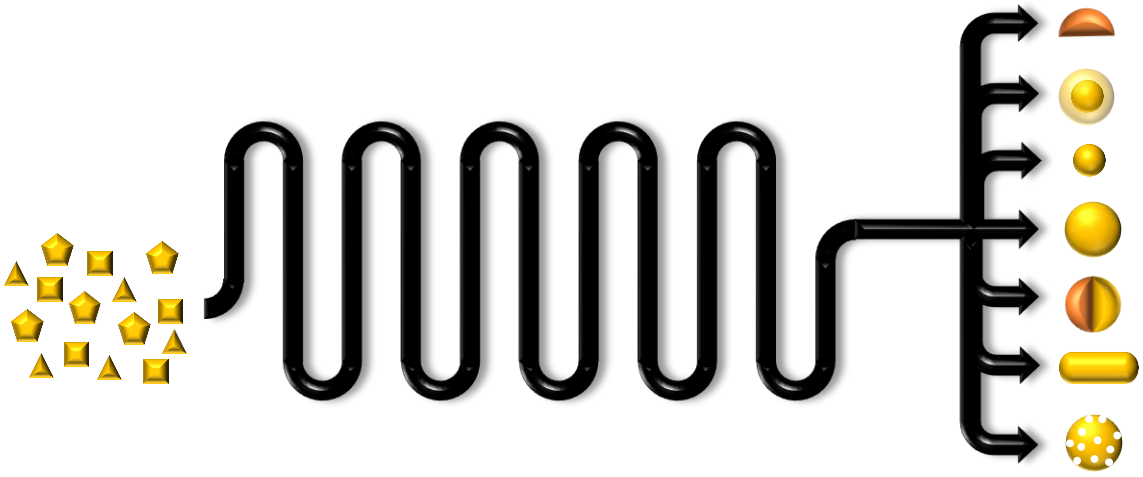

Chapter I : General introduction

I.1 The importance of microparticles in our daily-life and methods to formulate them

Polymer microparticles can have different shapes (even if in most cases, microparticles are spherical) ranging in size from 1 to 1000µm. These microparticles such as microbeads are found more and more frequently in our daily life since they were increasingly used in cosmetics in sunscreen or as exfoliators for example[1–4]. Most of them being made of petro-based non-biodegradable plastics, they create environmental problems because at the end of their life, they constitute one of the many forms of so-called "microplastics" waste[5]. Consequently, there is a strong incentive to develop such microbeads from only biodegradable and/or natural based materials.

Recent developments for the production of biodegradable polymer microparticles were made not only in the field of cosmetics but also in environmental field in which chitosan based microparticles are used to purify water from organic polluting agents[6] or in food and agronomical industries where different kinds of bio-sourced polymers such as chitosan, alginate or methylcellulose are used as microparticles[3,7–9]. Another field where biodegradable microparticles gain more and more interest is the biomedical field[10]. Indeed, microspheres can be incorporated in bone cement[11] or scaffolds[12] and are mostly used for sustained release of an active pharmaceutical ingredient (API)[10,12–17]. Such drug delivery systems (DDSs), which are generally composed of a biocompatible polymer loaded by the API, overcome the disadvantages of the traditional dosage and present many advantages such as the opportunity of encapsulating various APIs, a reduced toxicity, an accurate sustained drug-release, the use of different administration routes and the protection of the encapsulated API.

Different requirements must be achieved to produce suitable and effective DDSs such as: i) the preserved integrity of the encapsulated drug, ii) an optimal drug loading and a high encapsulation efficiency (EE), iii) a suitable release profile for the aimed application and iiii) a simple, scalable and reproducible production process. The first two requirements are

simultaneously inherent to the technique used to produce microparticles and to the characteristic of the particles (size, polydispersity, composition and configuration). The third one depends on the particle's characteristics and the kind of polymer, and the last one is only dependent of the formulation technique[17,18]. It is then obvious that the technique selected to formulate microparticles for drug delivery must produce them in a controlled and reproducible way, with a high EE and preferentially should made accessible a wide range of different kinds of particles.

Thorough the years, plenty ways and techniques were developed in order to prepare these loaded microparticles, as it is shown on Figure 1, leading to a wide variety of morphologies, structures and sizes. The most frequently used techniques allowing to formulate API loaded microparticles (in bold) from a preformed polymer will be detailed in the following and compared in Table 1 on different criteria in order to highlight advantages and limitations of each technique.

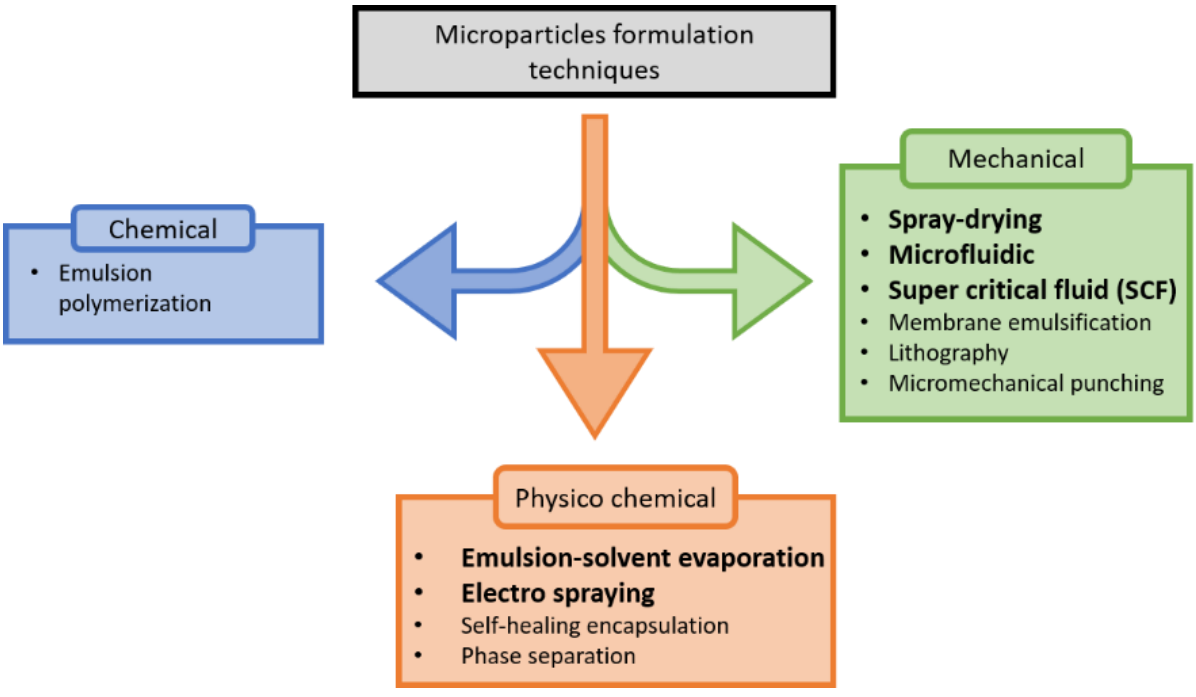

Figure 1 : Overview of the most used techniques to form polymer microparticles.

The emulsion-solvent evaporation (including single and multiple emulsions) (ESE) is the most frequently used approach to formulate microparticles. The principle of this technique (Figure 2) is simple and consists in the emulsification, by mechanical agitation, of a polymer

dissolved in an organic solvent which is completely or partially immiscible with the aqueous phase containing a surfactant. When the organic droplets are formed, the organic solvent is evaporated and the formation of polymer microspheres occurs. These ones are collected by centrifugation or filtration. The single oil-in-water (o/w) emulsion technique is generally applied when hydrophobic or poorly water-soluble ingredients have to be encapsulated. To encapsulate hydrophilic ingredients which tend to diffuse in the aqueous phase during the emulsification process,, a double or a multiple emulsion (most frequently a water-in-oil-in-water, w/o/w, emulsion) is rather applied. The single and multiple emulsion-solvent evaporation methods are simple, low-cost, fast and reproducible techniques allowing the encapsulation of both hydrophobic and hydrophilic components. Moreover, the particles size can be tuned easily by altering the viscosity of the organic and/or the aqueous phase, the mechanical agitation speed and the concentration in emulsifier. However, it is more difficult to entrap hydrophilic ingredients than hydrophobic ones, a large amount of solvents is required, the difficulty of scaling up and the formation of large and non-uniform particles, in the case of the double emulsion, are the principal limitations of this process[17,19–21].

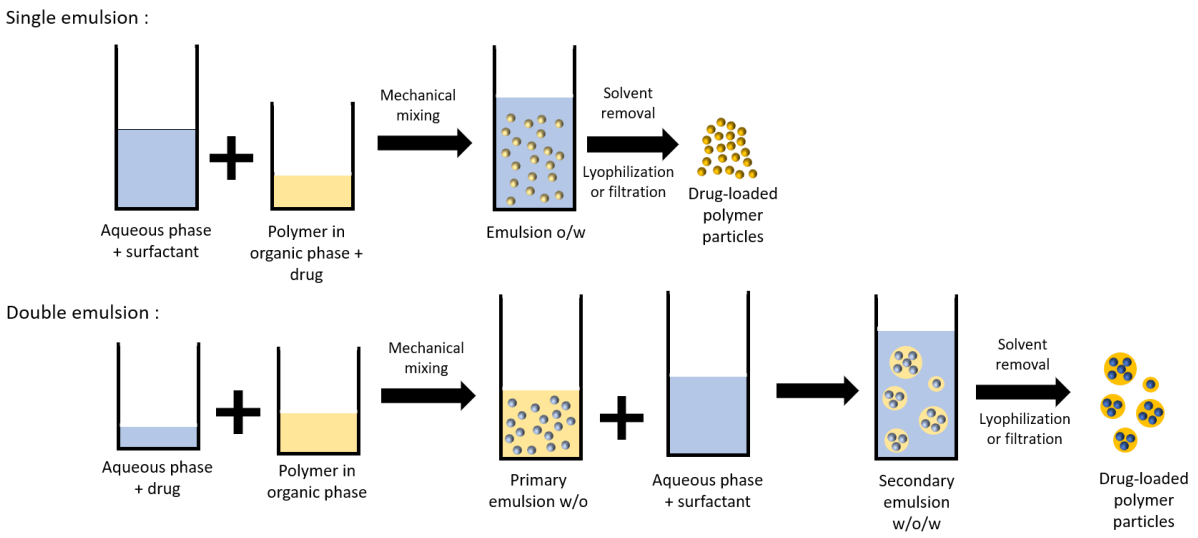

Figure 2: Schematic principle of the single and double emulsion-solvent evaporation

Spray-drying (SD), represented in Figure 3, was used for the first time in 1901 to produce milk powder from liquid milk. This technique is based on the atomization and drying of a feed (which can be either a liquid, a polymer dissolved in aqueous or organic solvent or a dispersion of particles) by spraying it into a hot drying medium. The process can be divided in

three steps: the first one happens in an atomizer in which the feed is atomized into small droplets, the second one consists in the drying of the droplets by a drying gas which can be air or nitrogen for example. The last step is the separation of the dry particles from the drying medium. The simplicity of the method, the versatility, the reproducibility in terms of size and morphology, the fully automatization of all operations, the low production costs and the easy scale up are the major advantages of this technique. However, the reactor cost, the poor thermal efficiency, the significant loss of product because of the adhering particles to the inner walls and the denaturation of natural molecule such as proteins caused by shearing and heating are the main drawbacks of this method[17,22–26].

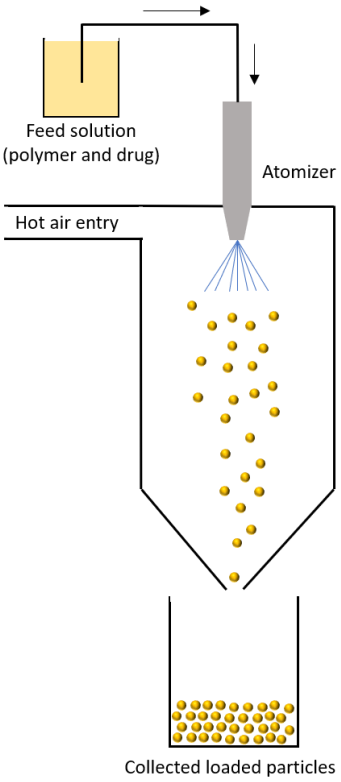

Figure 3 : simple representation of the spray-drying method

The electro-spraying (ES) method is a promising technique to produce microparticles of polymer materials (Figure 4). This technique can overcome some limitations encountered with conventional microparticle formation such as single and double emulsion and spray-drying. In this technique, monodisperse polymer microparticles are produced from a polymer solution, in a conductive enough solvent, by injecting this solution through a capillary or a nozzle where a high electrical potential, on the order of kilovolts, is applied between it and a

collecting plate. During the progression of the polymer droplets, the solvent evaporates and polymer microparticles are collected on the collecting plate. This method has several advantages such as a high control of the particle size, a high drug encapsulation efficiency, the consumption of solvent is lower than other techniques and it is easy to change the particle size and shape by switching the polymer flow rate, the solution viscosity and/or the strength of the electrical field. Even if it is a really promising technique, the main drawback is the low number of produced particles per batch limited by the difficulty to upscale the equipment for industrial production[17,26–29].

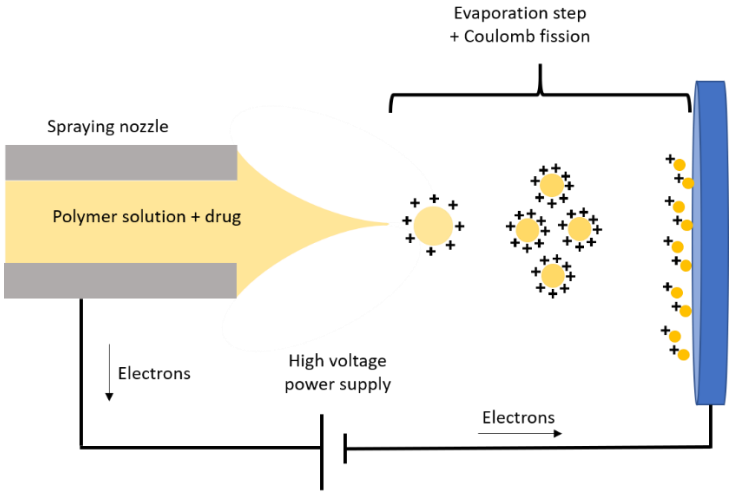

Figure 4 : Scheme of the electro spraying technique

Technologies based on the use of a supercritical fluid (SCF) and especially the supercritical CO_2 ($scCO_2$), because of its low critical temperature (31.1°C) and critical pressure (73.8 bar) and its ability to be a green candidate for the replacement of conventional organic solvents, are recently studied in order to prepare microparticles[17,23,30]. In these processes, the microparticle formation is caused by the rapid expansion of the SCF of the polymer-solvent-SFC solution passing through a nozzle in a vessel where they are collected. The particle properties can be affected by different parameters such as the pressure and the temperature (above the critical point) of the SCF, the nozzle diameter and the solution concentration. Small particles with a narrow size distribution can be obtained, the fact that flammable, toxic solvents are not used or in a very limited amount and the rapid removal of the SCF without the need of an extensive drying step are the main advantages of this method. The non-uniform

mixing, the limited solvation power and the complexity to scale-up are the main limitations[17,23,30,31].

The microfluidic technique (MF) enables the manipulation of microflows in microchannels to produce uniform emulsion droplets. These microchannels are made up of various materials such as polymers (polydimethyl siloxane, poly(methyl methacrylate), polycarbonate and polyimide), metal (aluminum), phenol formaldehyde resin-based and glass capillaries. The principle is the same as the formation of an o/w or a w/o/w emulsion except that the internal phase is pushed in the continuous one by a microchannel system thanks to syringe pumps at constant-flow or constant-pressure with an excellent flow rate control. In the device, the continuous phase, which is generally an aqueous phase containing a surfactant, shears off the organic phase, i.e. the polymer solution, to form small droplets one by one which allows an accurate control over the size and the size distribution (Figure 5). Two different devices can be distinguished in order to form droplets: the droplet-based device also called the segmented device and the continuous microfluidic device. The first one consists in the formation of droplets, by shearing forces, in the microchannel. The droplet-based system can be distinguished by the droplet breakup mechanism: cross-flow, co-flow and flow focusing. This kind of device is preferred to formulate microparticles. In contrast, the second kind of device operates with two or more fluids flow side-by-side in microchannels without segmentation or breakup. Continuous-flow microreactors, which are mainly used for nanoparticles formulation, appear to be easier to handle and more representative of bulk conditions with improved homogeneity leading to better control of nanoparticle characteristics [32,33].

The microfluidic technique is widely used for the preparation of microparticle in the biomedical field because of the possibility to produce microparticles with a narrow size distribution, a precise control on the droplet size and morphology which are directly involved to determine the drug release profiles. In addition to these advantages, the low consumption of solvent, the versatility of the method, the usually better encapsulation efficiency compared to traditional methods are the principal other advantages of this technique. Indeed, the encapsulation efficiency is crucial when drug delivery systems are produced in order to limit the waste of active ingredients which can be very expensive. The encapsulation efficiency can

be related to a dimensionless number: the Peclet number. This number reflects the diffusion or convection of molecules in the fluid. Because of small volumes and the laminar flow pattern, the microfluidic droplets minimize the molecules transition from the dispersed phase to the continuous phase which allows high drug encapsulation efficiency[34]. The prolonged formulation time is the main drawback even if the scale-up of the process is possible[10,16,18,34–38].

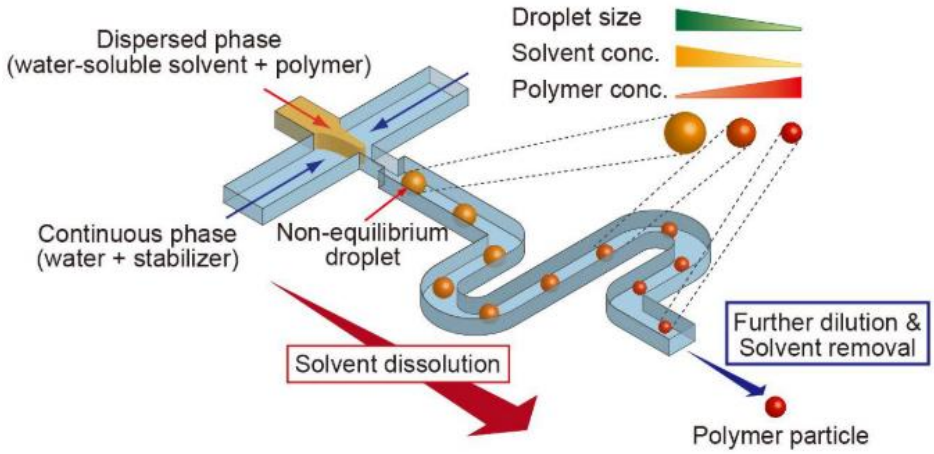

Figure 5 : Simple representation of the microsphere's formulation by microfluidic technique. Reproduced from Suzuki, Y., Yamada, M., Sasamori, K., Taniguchi, T. & Seki, M. One-step synthesis of spherical/non-spherical polymeric particles using non-equilibrium microfluidic droplets. 15th International Conference on Miniaturized Systems for Chemistry and Life Sciences 2011, MicroTAS 2011 ***3****, 1653–1655 (2011).*

The different characteristics of the particles production by the described processes are gathered in the Table 1 which compares them to each other by using the marks "-, + and ++". The "versatility" considers the possibility to change the microparticles structure (porous, core-shell, Janus etc.). The "easy to use" item considers the optimization and the implementation and the "drug stability" reflects the ability to formulate sensitive drugs without alteration during the process.

Table 1 : Comparative table of different important parameters in order to consider a larger pharmaceutical production scale

	Encapsulation efficiency	Versatile	Scalable	Easy to use	Controllable	Drug stability	Reproducible
ESE	-	+	+	-	-	+	+
SD	+	+	+	++	+	-	+
ES	++	++	-	++	++	++	++
SCF	+	-	-	++	++	++	++
MF	++	++	++	+	++	++	++

This table highlights that the microfluidic technique is the most suitable one for the efficient formulation of drug loaded microparticles for DDS. Moreover, as mentioned at the beginning of this section, the particles characteristics, namely the size, the polydispersity, the composition and the configuration, are crucial to reach the targeted drug-release specifications. The control of these microparticles characteristics by microfluidic formulation will be addressed in the following section.

I.2 How the microfluidic formulation parameters can affect the microparticles characteristics and how to control these parameters?

Polymer microparticles are versatile carriers for drug delivery because the drug release profile can easily be tuned by adjusting their physical properties (particle size, structure, shape, …) and/or their chemical properties (polymer nature, composition, molecular weight, …). Nowadays, poly(lactic-*co*-glycolic acid) (PLGA) is the most prevalent type of polymers used to encapsulate an active molecule for drug delivery applications because this synthetic degradable polymer releases the drug over time scales ranging from 1 week to 6 months that are optimal for most of clinical needs[39].

The drug can be released through three different ways from PLGA or other degradable polymer drug delivery systems (DDSs): the first way is the transport of the drug through the polymer matrix; the second is the transport of the drug through water-filled pores (usually the

way for hydrophilic drugs) and finally, the release caused by the dissolution of the encapsulating polymer in the surrounded media. For example, small hydrophobic drugs will pass through the polymer matrix while peptide or proteins, which are large hydrophilic molecules, pass through the water-filled pores of the particle. These three ways lead to three different drug release mechanisms from microparticles systems, which are represented on Figure 6: i) the diffusion which concerns the release of the drug which are at or near the surface of the particle; ii) the release through eroded particle surface caused by the polymer matrix degradation and iii) the release of the drug through the swollen polymer matrix. Nevertheless, in most of cases, more than one release mechanism take place to describe drug release from microparticle[17].

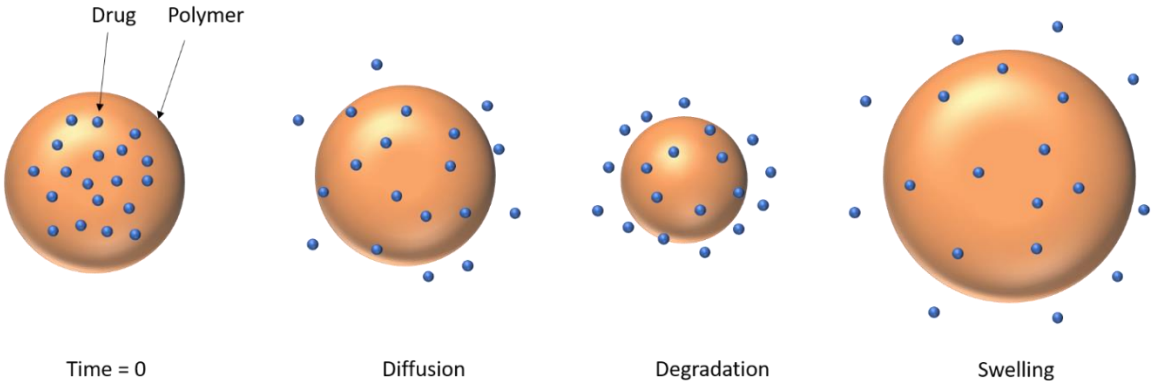

Figure 6 : Representation of the different release mechanisms

Experimentally, the drug release profiles can be summarized in four categories, as it is shown on Figure 7: the monophasic, the burst biphasic, the delayed biphasic and the triphasic. The monophasic profile is a zero-order drug release, meaning that the drug is constantly released from the polymer matrix, which is generally desired because the drug concentration in the body during time is completely predictable. The burst biphasic profile is composed of two parts, a burst release, which is a brutal and rapid drug release in a very short time period (from several hours to 1-2 days) corresponding to release of the drug adsorbed or encapsulated near the surface of the particle. This first phase is followed by a second one, a "progressive" phase, during which the drug is released very slowly. The delayed biphasic phase is composed of a lag phase during which a very slight amount of drug is released, followed by an accelerated release phase occurring because of the polymer degradation and

consequently, the apparition of pores and cracks on the particle surface, leading to the complete release of the active ingredient. This kind of profile is usually observed when particles are very large and no drug is on the microparticle surface or if they are coated with additional protective layer. If there is some drug adsorbed on the particle surface, it leads to the last profile which is the triphasic profile. It is composed of an initial burst effect, often much less significant than the one observed in the burst biphasic profile, followed by a lag-time and accelerated release phase [17,38–40].

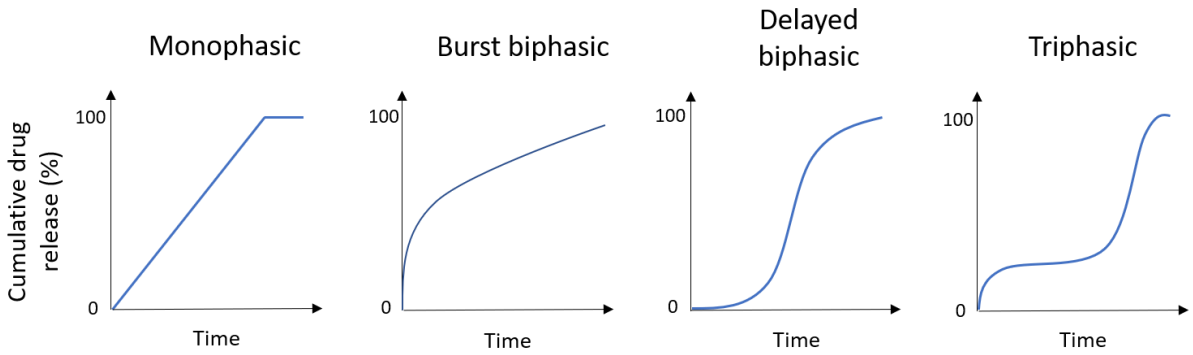

Figure 7 : Different profiles of drug release from loaded polymer microparticles

The control of the release kinetic is key in drug formulation in order to achieve an optimum pharmacokinetic effect. In the following section, we will discuss the influence of different physical parameters (the size, the structure and the shape) on the drug release and how it is possible to tune them, during the formulation of polymer microparticles, by microfluidic in order to obtain the desired release profile.

I.2.1 The size and the polydispersity

According to the definition, the size of a microparticle can be in principle comprised between 1µm and 1000µm, meaning a variation of the surface to volume ratio between 6 and $6*10^{-3}$. This can dramatically affect the drug bioavailability by modifying the drug release profile. Indeed, a higher surface to volume ratio, i.e. for small microparticles, the drug release is faster [40–42]. Moreover, for injectable microparticles formulation which are administrated through sub-cutaneous, intra-muscular or intra-articular routes, the particle size controllability and the polydispersity are crucial parameters because, if the size is not well

controlled, it may require larger needles to inject microparticles to prevent obstruction by larger microparticles and consequently, if larger needles must be used, the patient compliance decreases tremendously[38]. Okedi™ and Signifor™ are injectables drugs composed of microparticles of PLGA containing risperidone, used for the treatment of schizophrenia in adults for Okedi™ and pasireotide used to treat adult patients with Cushing's disease when the surgery is impossible for the Signifor™.

The polydispersity will also play a role on the drug release profile. Indeed, in a high polydispersity sample there will be an important burst effect because the smaller spheres will release the API much faster than larger one[40,41,44,45]. Moreover, particles of the same size can suppress the Ostwald ripening effect by reducing the differences of Laplace pressure between particles[46]. Interestingly, a high polydispersity can be created by purpose to obtain a zero-order release, which corresponds to a constant rate release of the drug with time, which is the panacea for most of the sustained release devices[45,47,48]. In some cases, the burst effect can also be desired when a large quantity of drug is required in a very short period of time[49–51].

In the microfluidic droplet-generation process, the size and the polydispersity of the collected polymer microspheres are directly related to the droplet formation of the organic phase in the continuous aqueous phase both flowing through the microfluidic device (Figure 5). So, it is important to define some constants of fluid mechanics to well understand the process. The first one is the Reynolds number of the dispersed phase (Re_d) which compares the inertial force to viscous force.

$$Re_d = (\rho_d \times l \times U_d)/\mu_d$$

where ρ_d is the discontinuous fluid density, l is the characteristic length, U_d the discontinuous fluid average velocity and μ_d is the discontinuous phase viscosity. Depending on the Reynolds number, different flow patterns are possible (Figure 8). A laminar flow is produced in the microfluidic channel if the Reynolds number is lower than 1800. In this kind of flow, the different streamlines are parallel to the fluid direction. On the other hand, if the Reynolds number is higher than 2300, the flow is turbulent providing a chaotic pattern without distinct

streamlines[34]. In the case of microparticle formulation, laminar flow is preferred in order to accurately manipulate the fluids to create controllable and monodispersed droplets[34,52,53].

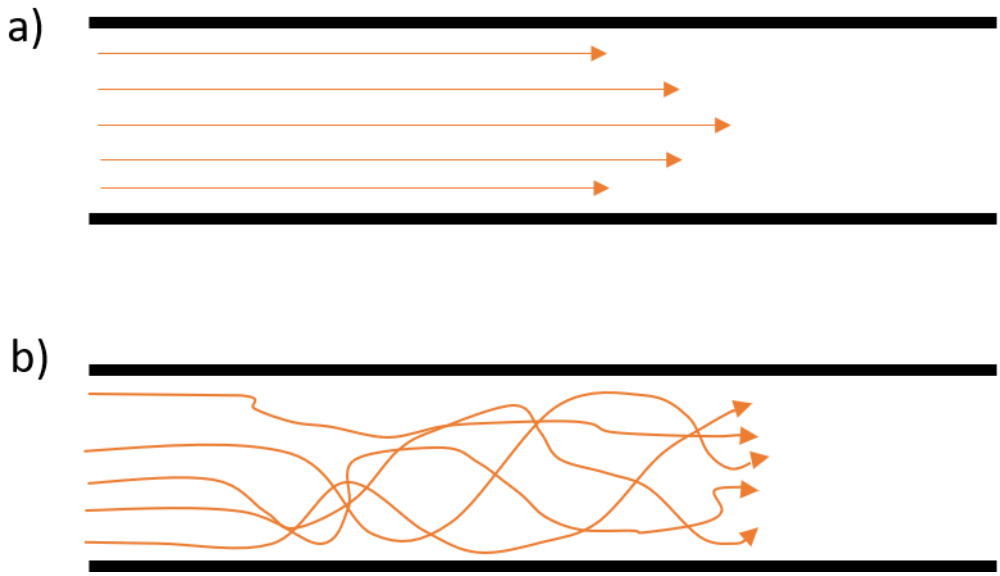

Figure 8 : Streamlines differences between the laminar flow (a) and the turbulent flow (b) in a channel

The second one is the capillary number of the continuous phase (Ca_c) which identifies the ratio of the viscous force to internal tension force.

$$Ca_c = (\mu_c \times U_c/\sigma)$$

where μ_c is the continuous phase viscosity, U_c the continuous fluid average velocity and σ the surface tension. Before continuing, it is important to point that the behavior of a thin stream of liquid is influenced by the Rayleigh-Plateau instability which explains why a liquid breaks up into droplet in order to minimize its surface tension[54,55]. In the experiment, different flow regimes can appear depending on the different two-phases flow rates. The main ones are the squeezing, the dripping and the jetting regime[34,52,54,56]. Ca_c is particularly important in droplet-based microfluidics because it enables the investigation of various break-up patterns depending on the range of capillary number. The droplet formation is not influenced by the shear stress in the case of capillary number values lower than 10^{-2}, the droplet formation is only dependent on the accumulated pressure when the dispersed fluid enters in the main channel. This is defined as the squeezing regime, which is typical for microfluidic devices because of the confinement of the fluids (Figure 9a). This squeezing regime has no interest for

the formulation of microparticles because it takes around ten times more time to produce one particle as compared to other regimes such as dripping or jetting regimes[52]. These dripping and the jetting regimes are two forms of instability observed when the capillary number is higher than 10^{-2} (Figure 9b and c)[34,53]. To visualize the difference between the dripping and the jetting regimes, a parallelism can be made with a dripping faucet, the transition from one regime to another happens by increasing the flow rate of the discontinuous phase and the dimensionless parameters: the capillary force and the Weber number (which will be defined in the next paragraph). In these regimes, the droplet formation is caused by both the shear and the surface tension forces acting on the dispersed fluid after it enters the channel[54].

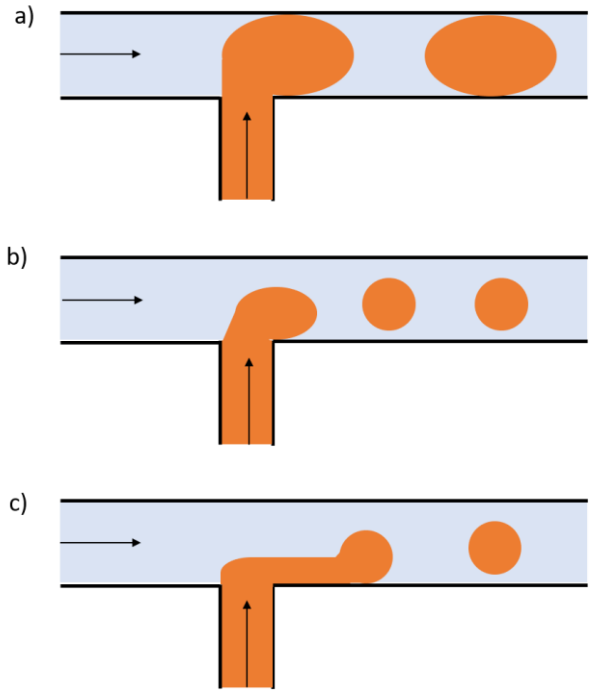

Figure 9 : Schematic representation of the different regimes in a T-junction a) squeezing, b) dripping, c) jetting.

The last dimensionless number is the Weber number which describes the deformation of the droplets and determines the relationship between surface tension and inertial forces. The equation of this number is:

$$We = (\rho_d \times U_d^2 \times l)/\sigma$$

where all variables where previously defined. As mentioned before, this number is very important when the transition between the dripping regime to the jetting regime is studied.

If We < 0.01, the inertial force is small compared to interfacial tension and the dripping regime prevails. In contrast, when We > 0.1, the inertial force dominates the interfacial tension, leading to jetting regime[34,46,52]. Monodisperse droplets are obtained in a dripping instability because the perturbations in the system, leading to the droplet formation, are insensitive to any external interference contrary to the jetting regime that produces polydisperse drops[34]. Nevertheless, Utada et al. succeed to produce monodisperse droplets in a jetting regimen under specific conditions[54].

Considering that the formulation of monodisperse microparticles is reached when a laminar flow is applied and if the system is in a dripping regime, it is still possible to adapt the formulation parameters in order to tune the size of the particles while respecting these conditions. A nice study was conducted by Wehking *et al.* about the limit conditions in a T-junction device to switch from one regime to another[53].

The first parameter that can be modified is the flow ratio between the continuous and the discontinuous solution. The flow rate of the discontinuous phase will be noted Q_d and the one of the continuous phase Q_c. The faster is the Q_d compared to Q_c, the larger are the particles and vice versa as it was observed in different studies[44,46,57–59]. Indeed, if Q_c increases while keeping Q_d constant, the shear forces applied on the discontinuous phase increase, resulting in the formation of smaller droplets[59].

The second parameter is the solutions viscosity. If the viscosity of the discontinuous phase increases e.g. by increasing the polymer concentration, this will lead to the production of highly monodisperse but larger particles[52,57]. As the polymer concentration is increased, a supersaturation in the droplet is easily reached and a faster solidification restricts the shrinkage of the droplets, resulting in larger microspheres[59]. Moreover, increasing the polymer concentration increases also the encapsulation efficiency for the same reason [42]. If the viscosity of the continuous phase in which the emulsifier is solubilized is increased by increasing the concentration of the emulsifier, the size of the particles decreases. This can be explained by the fact that a higher concentration of emulsifier reduced the interfacial tension between the organic and the aqueous phases conducting to the production of smaller particles. Interestingly, the type of surfactants used is important because the dynamic

interfacial tension of surfactants is different. For example, particles formulated with polyvinyl alcohol (PVOH) solution as emulsifier showed larger diameters than the ones formed with Sodium dodecyl sulfate (SDS) solution at the same concentrations[57,60].

The dimension of the channel is another crucial parameter playing on the particles size. Indeed, if the channel dimension is reduced, it will conduct to the formation of smaller particles and conversely[35,46] because if the diameter of the microchannel decreases while keeping the flow constant, the shearing forces applied on the polymer droplets are more important which leads to the formation of smaller particles.

Another parameter depending on the microfluidic device is the channels geometry. The most common geometries are the flow-focusing, the co-flow and the cross-junction. They are represented in Figure 10. In the flow-focusing geometry, the dispersed phase and the continuous phase flow through two sides of the channel and meet before the inner capillary orifice and the droplets are formed at the orifice. Flow-focusing devices are generally easy to manufacture and capable of generating particles with uniform size but the device parameters must be optimized more carefully in order to yield regular droplet. In the co-flow geometry, the two fluids are co-axially aligned and move in the same direction. The dispersed phase flows through the inner capillary into a continuous flow from the outer capillary. In this configuration, droplets are often produced in a jetting regime, which is a drawback to have monodispersed particles. Moreover, this kind of device is much more expensive, compared to the flow-focusing one. The last and the most used geometry is the cross-section geometry, it is also the simplest microfluidic geometry. In cross-flow devices, the two phases come into contact in a junction with various angles such as T-, Y-, double T-, V- or K- junctions[10]. The T-junction is the most common junction and this device is composed of a perpendicular capillary which includes the dispersed phase that intersects the main channel filled by the continuous phase. The droplets are formed at the channel intersection by a combination of the shear forces and the squeezing effect exerted by the continuous phase. In this geometry, the droplet size is not only dependent on the channel width but can also be controlled by changing the flow rates of both solutions or by solutions concentration tuning. The device produces better monodispersed droplets as compared to the co-flow geometry device. As already mentioned, this geometry can be transformed in a Y-junction for example and the process is still the same,

only the angle of the branches is different. Generally, the droplet size increases when the bifurcation angle deviates from 90° because there is the appearance of a horizontal component of the continuous phase on dispersed flow. Additionally, by adding more branches, it is possible to produce multi-emulsion core-shell particles. However, this system is more complicated to scale-up in order to produce a larger quantity of particles during the same time because it can lead to multimodal or chaotic processes in which the droplet size is not uniform[34,52,61,62].

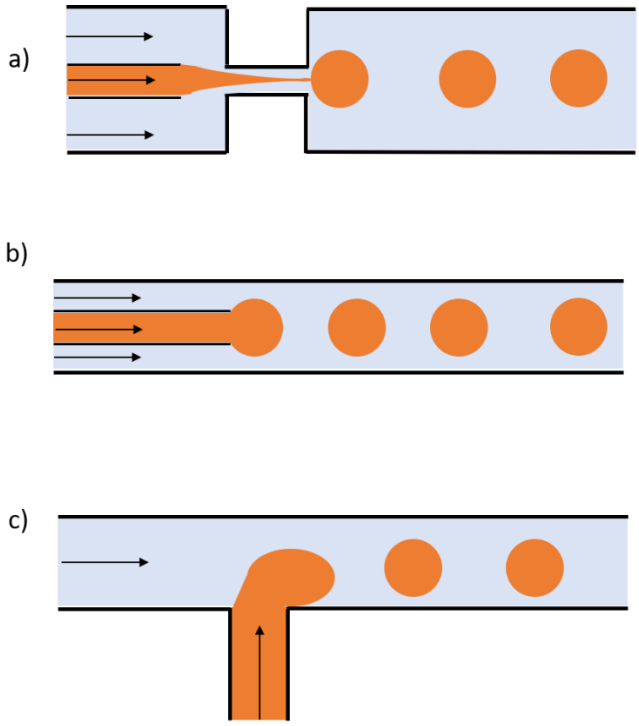

Figure 10 : Schematic droplet formation in different device geometry a) flow-focusing, b) co-flow, c) T-junction.

I.2.2 The microparticle structure

The external and the internal structure of the microparticle can have a tremendous effect on the drug release kinetics. For example, the drug release of porous microparticles will be much steeper than the release from a core-shell particle because the shell is usually there to reduce the burst effect and control the sustained release. Other microstructures can be obtained in spherical microparticles with different release profiles which must be considered for potential biomedical applications. In the following paragraphs, some techniques will be detailed in order to form these different kinds of microparticle structures[42].

I.2.2.1 Porous microparticles

The pore forming appears to be one of the most important phenomena in order to modify the drug release kinetics. Different studies were conducted to compare the release kinetics of porous microparticles with non-porous ones and they observed that the drug release is much faster for porous microparticles than the one for non-porous analogue. Indeed, porous microparticles have larger surface areas and shorter diffusion distance. These particles showed also an intense burst effect of the drug. Nevertheless, these porous particles have also some advantages such as a much larger drug loading capacities, faster overall release of the drug without initial lag period and reduced autocatalytic effect of PLGA degradation. Indeed, the water-soluble degradation products diffuse faster out of the particle which avoids the local acidification responsible of the autocatalyzed degradation of PLGA so as the possible drug degradation[10,14,15,17,39,63–65].

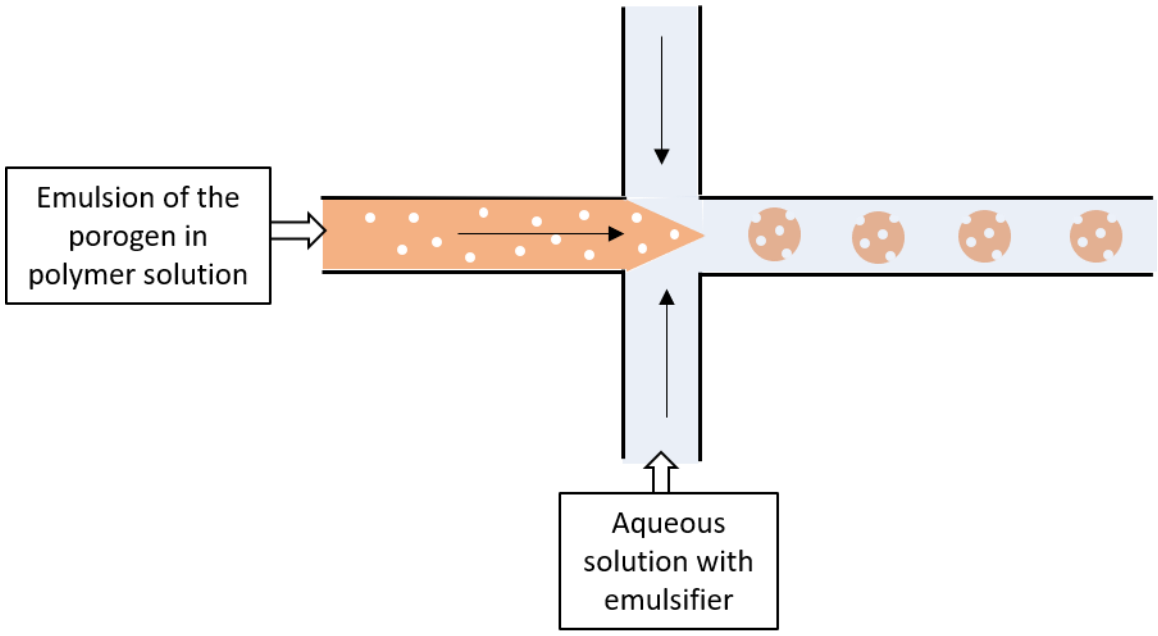

Figure 11 : Schematic formulation of porous microdroplets containing a porogen agent

To produce porous particles, porogen agents can be added as shown in Figure 11. For this purpose, a primary emulsion between an organic solution containing the polymer and an aqueous phase which contains the pore-forming agent is generally produced and injected in microfluidic device as the discontinuous phase. Two of the most commonly used pore-forming agents are ammonium bicarbonate and hydrogen peroxide which will decompose in different

gases leading to the pore's generation. However, several other substances can be used as pore-forming agent such as osmolytes (NaCl), phosphate buffer solution, protein (gelatin), polymers (pluronics) and fatty acid like mustard oil[10,14,15,35,63,66,67]. Typically, the encapsulation of hydrophobic as well as hydrophilic drugs in porous microparticles is generally carried out by double emulsion process, when extractable porogen agent is used, which can lead to a reduced encapsulation efficiency. Nevertheless, Ni *et al*. succeeded to trap a hydrophobic drug for pulmonary drug delivery in a porous PLGA particle in a single emulsion process by using the PVP (polyvinyl pyrrolidone) as porogen agent[68].

The concentration in polymer, and consequently the viscosity of the organic phase, has also an influence on the porosity of a microparticle. If the polymer concentration increases, the degree of porosity decreases. The increased porosity is explained by the fact that a higher viscosity may reduce the ability of the hydrophilic pore-forming gas bubbles to penetrate through the primary emulsion microdroplet to the external membrane of the formulated droplet[10,63].

The inherent characteristics of the polymer also play on the formulation of porous particles based on hydrophilic porogen agent as the ammonium bicarbonate. First, it was demonstrated that pores at the surface of polylactide (PLA) microparticles are bigger compared to PLGA analogues. This was attributed to the difference of the molar masses between the two polymers but also to the difference of hydrophilicity between both polymers. PLA is more hydrophobic than PLGA and consequently, for the same amount of water phase in the emulsion, it absorbs less hydrophilic porogen and then larger pores are formed (Figure 12). The same experiment was made by comparing the porosity of microparticles formed by PLGA 75:25 (75% of polyglycolic acid and 25% of poly(D,L-lactide) and PLGA 50:50 for which bigger pores were obtained, i.e. the most hydrophobic copolymer. Accordingly, poly(ε-caprolactone) (PCL), which is highly hydrophobic is not able to produce porous microparticles with ammonium bicarbonate[63].

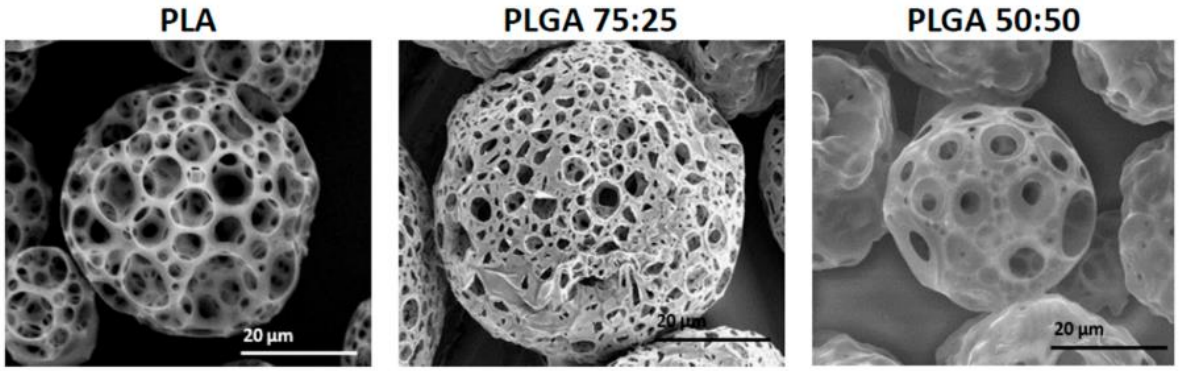

Figure 12 : SEM images of microparticles obtained by using ammonium bicarbonate as porogen with various polymers. Reproduced from: Amoyav, B. & Benny, O. Microfluidic based fabrication and characterization of highly porous polymeric microspheres. Polymers (Basel) 11, (2019).

The polarity of the organic solvent has also an influence on the porosity of the microparticle. When chloroform and dichloromethane are used, porous microparticles are formed which is not the case when ethyl acetate, a more polar solvent, is used. To incorporate the porogen aqueous solution in the organic phase, the two solutions must be immiscible. The chlorinated solvents used here are less polar and then less miscible with the inner aqueous phase. This results in a slow and gradual removal process and then aqueous droplets can develop to form a porous structure[17,63].

The last parameter is the variation of the continuous phase flow. If it increases, the degree of porosity increases as well. This may be explained by the increase of the gas bubble evaporation when the flow is increased[63].

I.2.2.2 Core-shell microparticles

Conversely to porous microparticles, the addition of a shell around a core, containing a drug, can delay and extend the release of the active ingredient[5]. Moreover, it is possible to modulate the release of the drug in function of specific conditions such as temperature and/or pH if the shell is made of a stimuli sensitive material[15,34]. For example, poly-*N*-isopropylacrylamide (PNIPAM) can be used as a shell encapsulating a drug against skin tumor. The PNIPAM has the property to be insoluble in water and blood at a temperature above 32°C and soluble below 32°C. So, if the skin surface is cooled, where the tumor is localized, it allows the release of the drug at the right place[34]. The core-shell structure can protect the drug

against moisture, heat, ultraviolet radiation, oxidation, etc.[69] and then reduce the drug side effects, by avoiding the drug release in the whole body and then increasing the effectiveness by delivering the drug at the right place at the right time[18,55,70]. The shell allows also a stable release which means that the release of the active compound is kept constant through time. Finally, the shell can also avoid or decrease the burst effect encountered in some cases which is useful for the long-term treatment of several diseases such as asthma, angina or psychiatric disorders[34,39,42,71].

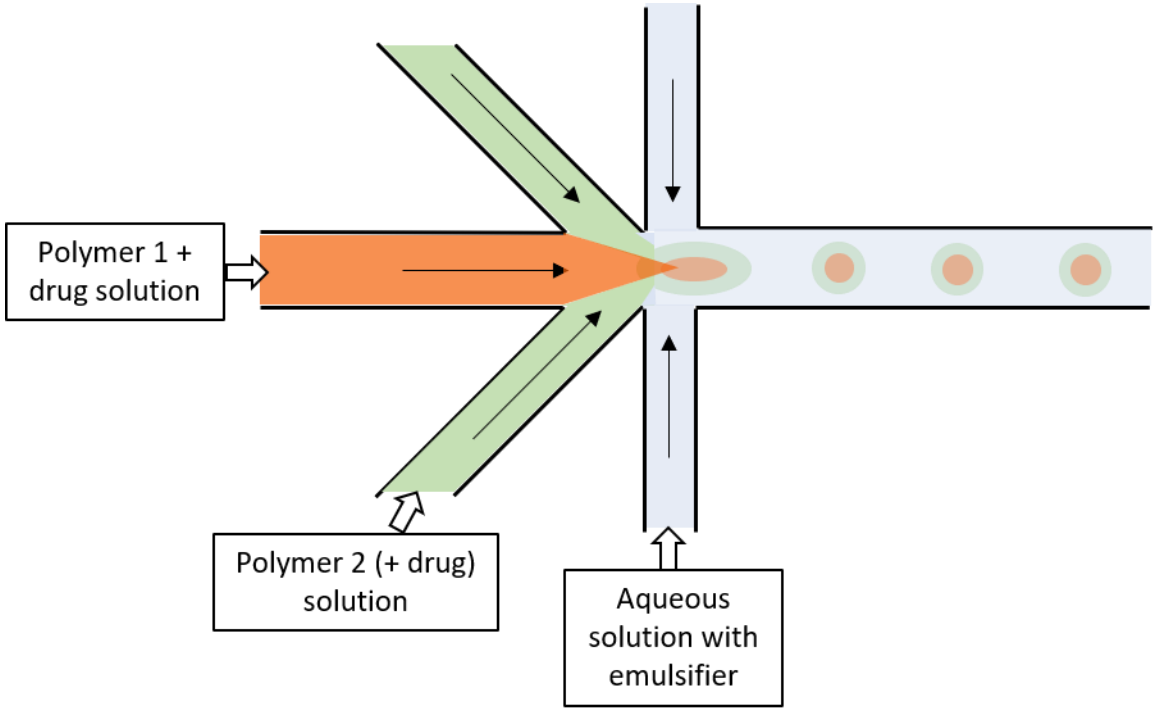

Figure 13 : Schematic of solid-solid core-shell microspheres formulation

The core part can be liquid, gas or solid whereas the shell is usually solid. The scheme of the most common formulation way to formulate core-shell microparticles is represented on the Figure 13[18,34]. Hollow internal microparticles can be used as an encapsulation vehicle to secure biologically active compounds such as proteins, enzymes and DNA in controlled drug release[34]. If the core is composed of a liquid or a gas, it is usually called a microcapsule and this kind of capsules is interesting to encapsulate and protect, with a better encapsulation efficiency, a hydrophilic compound in a hydrophobic shell. It is also possible to trap two incompatible substances, one in the aqueous core and the other in the lipophilic shell. For example, core-shell particles containing two anticancer drugs, one hydrophilic (doxorubicin

hydrochloride) in the aqueous core and the other hydrophobic (paclitaxel) trapped in the shell, can be formulated easily[72]. Nevertheless, a burst release can appear when the shell is degraded and the liquid core is exposed to the outer medium. A solid core structure coated with a shell layer erases this problem because the release of the inner drug appears only after the degradation of the inner polymer, in this case it is referred to microspheres[34].

The shell and the core thicknesses can be modified by changing the solutions concentrations, if the shell polymer concentration increases, the thickness of the shell increases. Concerning the core thickness, it follows the same tendency[61,70–72]. It is also possible to formulate poly-core particles where several particles which can have different sizes, shapes or contents are enclosed within the same shell[5,15,35,61,71] (Figure 14).

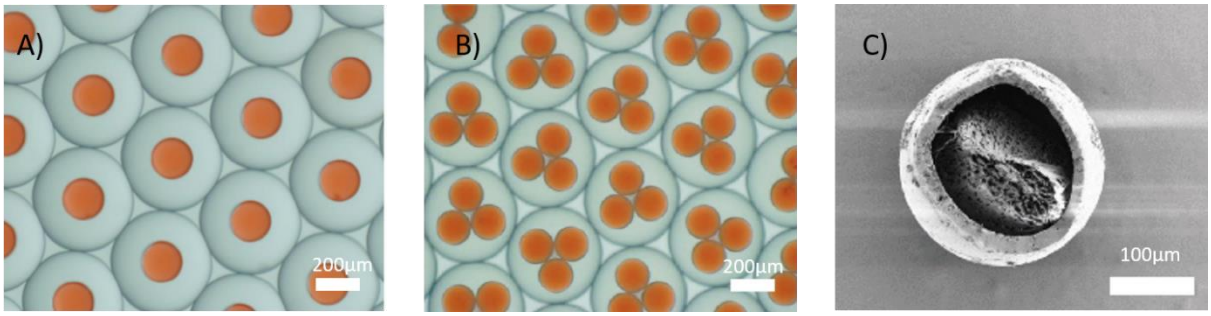

Figure 14: Optical microscope images of different core-shell microparticles composed of gelatin methacrylate (core) and PLGA (shell) with a varying number of cores (A and B). Electron microscope image of a cut core-shell microparticle (C). Reproduced from: Li, Y. et al. Composite core-shell microparticles from microfluidics for synergistic drug delivery. Sci China Mater 60, 543–553 (2017).

I.2.2.3 Janus microparticles

Janus microparticles have two distinct compartments of different physicochemical properties such as electric, magnetic, optical and polar properties. Because of asymmetric composition and structure, Janus particles can integrate different characteristics and perform collaborative functions which makes them really interesting for drug-delivery applications. For example, Janus particles allow the encapsulation of two synergic drugs in each compartment and have a sustained release mode in one phase and a triggered release in the other phase by formulating Janus microparticles composed of biodegradable and pH-responsive or thermo-responsive compartments[15,18,73–76]. Moreover, selective modification of one lobe of Janus

particles was employed to impart additional functionality by adding some magnetic nanoparticles or a porogen agent in one part for example[76–78].

Janus microparticles can be produced by droplet microfluidics as shown in Figure 15. Generally, two dispersed phases flow inside the Y-shaped microchannel and, thanks to a fine flow rate regulation, they merge into the main channel after the first intersection. Then, a second junction is needed to form a droplet of the two combined dispersed phases by the shearing forces applied by the continuous phase[15,61,74].

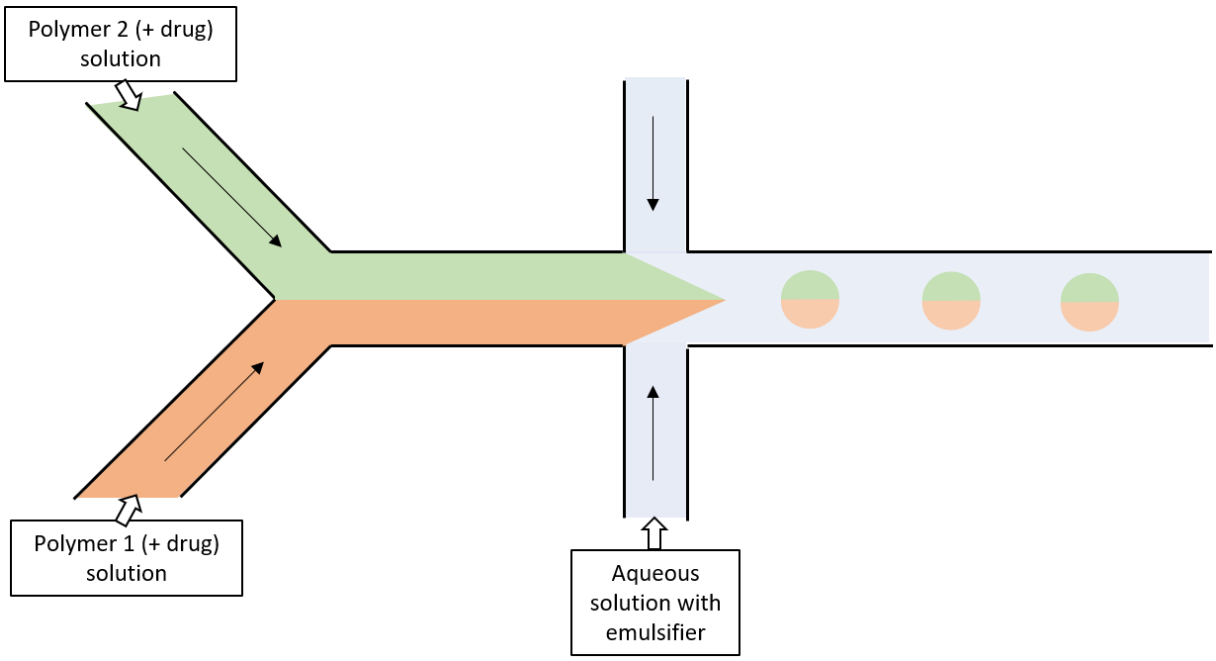

Figure 15 : Schematic formulation of Janus microparticles

The morphology and the structure of Janus particle can be tuned by playing on the type and amount of organic surfactant, the solvent type and the total concentration of both components. For example, if 0.5% (in volume) of Span 80 is used as surfactant in the organic phase, smooth Janus particles are formed but if there is no surfactant, patchy Janus particles are formed. The ratio between the two compartments can be controlled by changing the concentrations of both matrices in the organic phase. Interestingly, the phase ratio in the particle is exactly the same as the predetermined concentration ratio[75].

I.2.3 The shape

The drug release is influenced by the shape of the microparticles. Usually, most of the particles are spherical because of the energy surface minimization while retaining a uniform Laplace pressure. Nevertheless, microfluidic technology offers the unique ability to form non-spherical particles and several methods were developed to produce them[61,79–81].

The simplest one consists in the physical confinement of the droplets. Particles shape is determined by the relation between the diameter (d) of unperturbed droplet and the dimensions of the microchannels the width (w) and the height (h). If the droplets flow through a channel with dimensions that are much larger than their size , i.e. if w and h > d, they will keep a spherical shape and then spherical microparticles are produced. But, when w, > d and h < d, spherical droplet become a discoid shape. In contrast, if w < d and h < d, the droplets become a rod-like shape. If these deformed droplets are photopolymerized, it yields disk-shaped and rod-shaped polymer particles (Figure 16). This method is simple and effective but only convex and flat surface can be obtained[16,35,79,80,82].

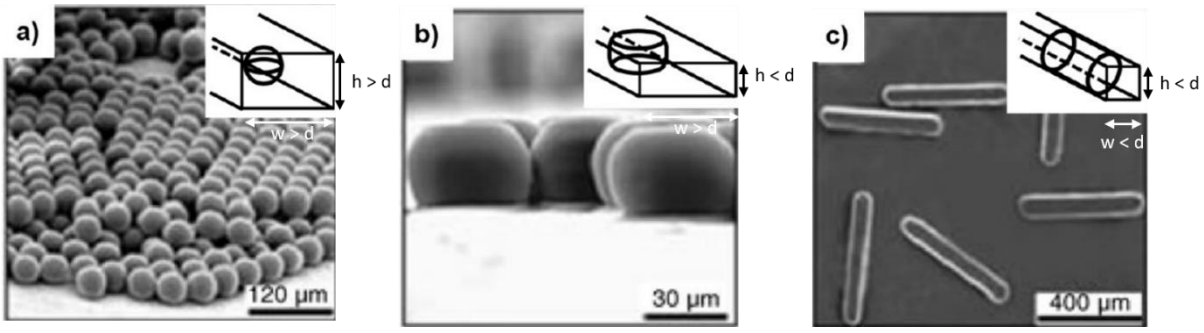

Figure 16 : Scanning electron microscopy pictures of microparticles of different shape obtained with physical confinement of the droplet. Reproduced from : Kim, J. H. et al. Droplet microfluidics for producing functional microparticles. Langmuir 30, 1473–1488 (2014).

Let us mention here that sharp-edged microparticles can be obtained by selectively solubilizing a part of a preformed Janus microparticle (Figure 17a)[35,61,79].

Toroidal particles also called doughnut-shaped particles (Figure 17b) were successfully formulated using emulsion droplet microfluidics under specific conditions. If droplets with a relatively high solubility in the continuous phase (water in dimethyl carbonate for example[83])

flows through the center of a microfluidic channel, the diffusion of the discontinuous phase solvent is not isotropic in the microfluidic device. Indeed, the diffusion toward the side-wall is preferred over the diffusion along the flow direction because the continuous phase is refreshed by the shear flow. This results in a concentration gradient to form an elastic membrane which will be deformed by the continuing anisotropic diffusion, causes buckling instability in the lateral direction and produce a doughnut-shaped microparticle after consolidation[79,83].

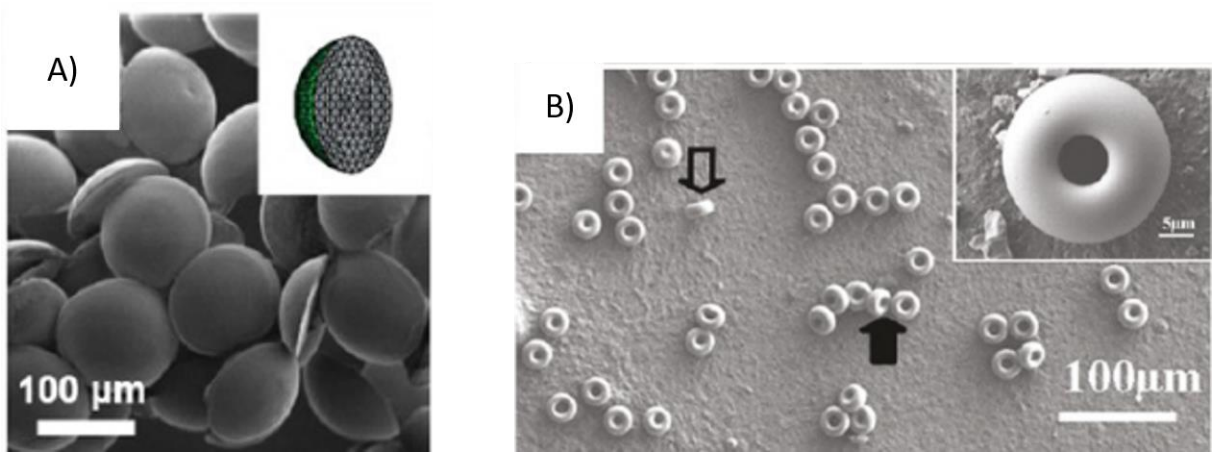

Figure 17 : Scanning electron microscopy pictures of microparticles of different geometries: A) oblate ellipsoids and B) Toroidal particles. Reproduced from : Kim, J. H. et al. Droplet microfluidics for producing functional microparticles. Langmuir 30, 1473–1488 (2014).

An interesting technique allowing directly the production of particles of any shape is the continuous-flow photolithography. This technique relies on the use of masks to provide shape-definition. Arrays of mask-defined polymer particles are obtained by crosslinking a prepolymer, namely PEG-diacrylate shining pulsed UV light through the mask (Figure 18). The as-shaped particles are then flown out of the microfluidic device. Patterned masks define thus the shape of formed particles. Other kinds of photolithography exist such as the stop-flow lithography, the stop-flow interference lithography and the lock and release lithography [61,80–82,84].

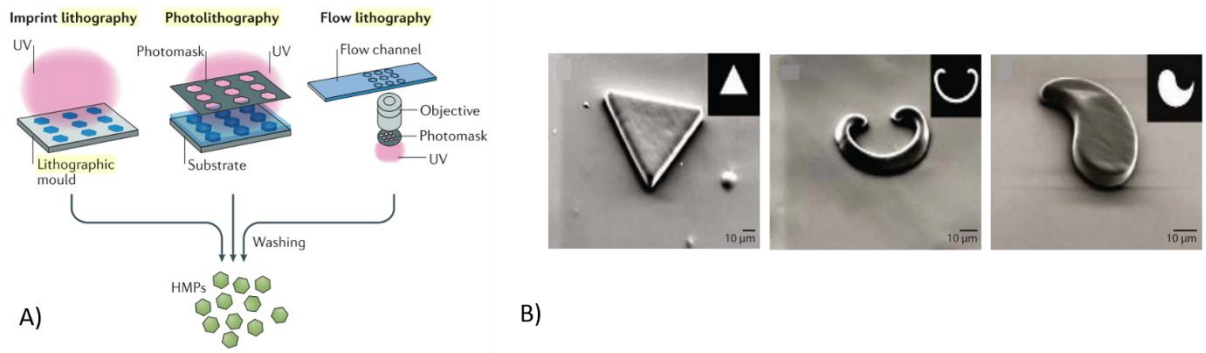

Figure 18 : Lithography technique to produce microparticles : A) different lithography techniques, B) microparticles shapes obtain by lithography. A) Reproduced from Daly, A. C., Riley, L., Segura, T. & Burdick, J. A. Hydrogel microparticles for biomedical applications. Nat Rev Mater ***5****, 20–43 (2020) and B) reproduced from Park, J. Il, Saffari, A., Kumar, S., Günther, A. & Kumacheva, E. Microfluidic Synthesis of Polymer and Inorganic Particulate Materials.* Annu Rev Mater Res ***40****, 415–443 (2010).*

These different geometries will affect some parameters which will influence the drug delivery profile and the drug efficacity[81,84,85].

The degradation of the polymer matrix, which is implied in the release of the therapeutic drug, depends on the particle shape because non-spherical particles that have parts of different thicknesses could conduct unique degradation profiles, as the shape can change during the degradation process[84]. It was demonstrated that the drug release profile from loaded particles of different geometries with almost the same surface area can differ tremendously. The required time to release 90% of the drug for spheres and cylinders was about 12h while about 2h for pyramids. This is related to the surface to volume ratio because spheres have the lowest surface volume ratio and pyramids the highest one[81].

Macrophage phagocytosis is usually undesirable because it prevents the delivery of drugs to the targeted tissues and particles must evade them. The particle geometry is crucial to limit this phenomenon. Indeed, the phagocytosis is an actin-dependent process that internalizes foreign particles with a diameter above 500 nm. The local shape of the particle at the point where the macrophage is attached dictates if a macrophage begins internalization or not. For example, a macrophage attached at the pointed end of an ellipse internalized it in a few minutes while if it is attached to the flat region of the same ellipse, there is no

internalization for over 12h. Concerning spherical particles, due to their symmetry, the internalization occurs at any point of the surface[81,84–86].

The transport of the particles through the body will be also tremendously affected by the shape of the particle. The movement of spheres is easier to predict to their inherent symmetry but non-spherical particles may align or not in the blood flow[84]. For non-spherical particles, the velocity gradients, in a flow environment, cause a nonuniform distribution of forces along the symmetry axis resulting in particle rotation and tumbling. Spherical particles tend to follow the streamlines with hydrodynamic forces correlated to their radius. Then, lateral drift is only affected by external forces such as the gravity and electromagnetic fields. In contrast, anisotropic particles such as discs, spheroids, ellipsoids and rods, because of their rotational motion in flow, can undergo significant lateral drift even in absence of external forces and consequently can achieved improved margination, which describes the fact that particles will move to the vessel wall, before to target the endothelium[80,81,84].

The particle shape will also influence the efficacity of the medicine. According to the particle shape, it will be possible to cross purifying organs such as liver and spleen or not. For example, spheres larger than 200 nm in diameter cannot cross the spleen but flexible disk-shape of 10 µm, like red blood cells, are able to easily cross it[84].

Finally, the targeting ability will also be influenced by the particle geometry because the overall surface and the local curvature affect ligands and opsonins adsorption and so the degree to which particles fit the contours of target cell membranes. Moreover, the shear forces induced by the blood flow applied on the attached particle could detached it from the desired location since depending on the shape, the shear forces will change[84].

As discussed, the shape is a crucial parameter on which it is possible to play in order to tune the drug delivery kinetics and the drug efficacity triggering an increasing interest for researches. For example, new morphologically biomimetic particles such as virus-like spiky particles, red blood cell-shape particles or pollen-shape particles were developed in order to enhance the bio-affinity[87,88]. Another example concerns the formulation of shape-memory particles which can change their shapes when a stimulus is applied, impacting their properties as discussed above[89–93].

Besides properties of the microparticle itself, the composition of the microparticle will play a key role in the drug release kinetics. This will be discussed in the next part.

I.3 The role of the polymers in the drug delivery kinetic profile

Ideally, biomaterials are materials that temporarily or permanently become a part of the body to restore, augment, heal or replace the natural functions of the living tissues or organs. Consequently, they should not induce any systemic, immunologic, cytotoxic, mutagenic, carcinogenic or teratogenic reactions when there are introduced in the body. In the medical or in the pharmaceutical fields, biodegradable polymers are an interesting class of materials that can degrade into non-toxic products and then find different applications such as scaffolds for tissues engineering, degradable implants in orthopedic surgery or as matrices for drug delivery. Among the various synthetic biodegradable polymers, aliphatic polyesters have been the most extensively investigated and developed for medical applications. Homopolymers based on lactide or glycolide, respectively the polylactide (PLA) and the polyglycolide (PGA) as well as their random copolymers poly(lactic-*co*-glycolic acid) (PLGA) were developed for drug delivery systems because of their biocompatibility and their degradation in non-toxic species. The PLGA has especially emerged as an important biocompatible and non-toxic polymer with numerous applications in drug delivery in particular because it is approved by the US FDA (food and drug administration) for several therapeutic applications[94–96].

For the successful development of any drug delivery systems, it is crucial to understand the degradation behavior of the (bio)degradable polymer used as drug delivery material. Different kinds of polymer degradation processes exist such as photo-, thermal, mechanical and chemical degradation. In the case of *in vitro* degradation, photo- and thermal degradation are irrelevant to consider. The mechanical degradation can also be neglected in the case of drug delivery applications because this kind of degradation affects the polymers implied in sutures, mechanical implants etc., i.e. those which are subjected to significant mechanical stress. In contrast, the chemical degradation is the most important to occur in the drug delivery systems because polyesters contain hydrolysable bonds which can be cleaved by

hydrolysis and enzyme-catalyzed hydrolysis. Nevertheless, the role of the enzymatic degradation is not significant to hydrolyze the bonds in lactide/glycolide-based polymers[94].

The hydrolytic degradation of PLGA occurs in aqueous environment and consists in the random hydrolysis of ester bounds present along the polymer backbone. Each hydrolyzed ester linkage forms one hydroxyl and one carboxylic acid moiety. The scission of the polymer chains will lead to the reduction of the molecular weight of polymer which increases its hydrophilicity and then conducts to the formation of water-soluble fragments. These fragments are ultimately hydrolyzed in lactic and glycolic acids which are finally transformed in energy, carbon dioxide and water by the normal metabolic pathways in the body. PLGA can also undergo auto-catalytic degradation because the carboxylic group remains attached to the polymer backbone and consequently decreases the local pH in the polymer bulk which catalyzes the hydrolytic degradation. The formation of acid such as lactic acid or glycolic acid increases the acidity of the medium which can lead to irritation of the surrounding tissues and this can also affect the stability of the encapsulated drugs as proteins or peptide. The drug stability can be improved by controlling the pH by adding suitable excipients such as poorly soluble bases. The particle surface is less subject to the auto-catalytic degradation because the degraded product can diffuse more easily out of the polymer[96]. This kind of particle consequently undergoes a bulk degradation (Figure 19).

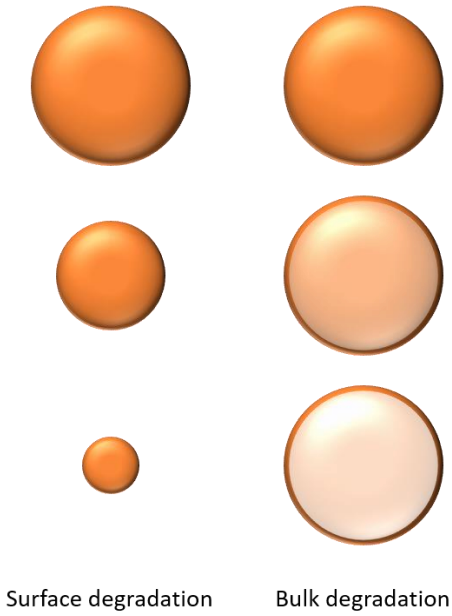

Figure 19 : Sketch of degradation pathways that particles can undergo in the body

To produce a PLGA-based DDSs with higher efficiency and efficacy within a desired therapeutic window, it is essential to understand the influence of the factors on the degradation rate as well as the drug release kinetics and properly accommodate these factors with the formulation of the drug-polymer composites.

In the following paragraphs, different parameters such as the copolymer composition, the crystallinity, the molar mass of the polymer, the chain-ends functionalization, the glass transition temperature, and the influence of the drug will be discussed in order to determine how they impact the polymer degradation and therefore the drug release profile.

I.3.1 The copolymer composition

Table 2 shows physical properties of different PLGA with various ratios between lactide and glycolide moieties as well as the properties of the two homopolymers, the PLA and PGA. It can be seen that the comonomers ratio (LA:GA) has a major impact on the properties of the copolymer. Indeed, the *in vivo* resorption of PLA is between 12 and 24 months whereas the complete resorption of the PGA is between 6 and 12 months and the one for the PLGA is between 1 and 6 months depending on the copolymer composition[95]. This variation on the degradation period is partially caused by the difference of hydrophilicity between the

polymers. Indeed, the PLA is more hydrophobic than the PGA which explains its lower hydrolytic degradation rate. The amorphous PLGA copolymers have higher degradation rates than their corresponding semi-crystalline homopolymers and this degradation slows down when the proportion in lactide increases. Therefore, the use of PLGA in biomedical applications depends on the selection of appropriate ratio of LA and GA that would determine the degradation rate and then the drug delivery profile. For example, the release rate of the imatinib mesylate from microspheres is 1.5 times higher for PLGA 50/50 compared to PLGA 85/15 (85% LA and 15% GA)[95].

Table 2 : Physical properties of some polyesters

Polymer	**Glass transition temperature (°C)**	**Melting temperature (°C)**	**Degradation time (months)**
PGA	35-40	225-230	6-12
PLLA	60-65	173-178	>24
PDLLA	50-60	Amorphous	12-16
PLGA (50:50)	45-50	Amorphous	1-2
PLGA (65:35)	45-50	Amorphous	3-4
PLGA (75:25)	50-55	Amorphous	4-5
PLGA (85:15)	50-55	Amorphous	5-6

I.3.2 The polymer crystallinity

The crystallinity of the polyesters affects the degradation rate and the drug release. Indeed, lower crystallinity accelerates the hydrolysis and then the degradation of the polyester because the water can diffuse more easily in the amorphous regions than in the crystalline regions. The PLA can exist in three different forms, the poly-L-lactic acid (PLLA), the poly-D-lactic acid (PDLA) and the poly-D,L-lactic acid (PDLLA), depending on the kind of lactic acid used: the L-lactic acid and the D-lactic acid or a combination of both. The PDLA exhibits a higher crystallinity than the PLLA whereas the PDLLA is completely amorphous. Despite the

semi-crystallinity of the PGA (Table 2) the PLGA composed of PLLA and PGA is amorphous if the proportion of GA varies between 25% and 70%. PLGAs composed of PDLLA and PGA are also amorphous if there is less than 70% of PGA in the copolymer. The use of amorphous polymers is preferred since it allows a more homogeneous drug dispersion in the polymer matrix[10,42,94–98]. Indeed, the active ingredient will be mainly encapsulated in the amorphous region of the microparticle, the crystalline region will act as a barrier for the drug diffusion. Therefore, the EE of the drug encapsulated will dramatically decrease when highly crystalline polymers are used [97,98].

I.3.3 The polymer molecular weight

The molecular weight (M_w) influence also considerably the degradation behavior and the drug release profile. It is generally observed that the drug release increases when the molar mass of the polymer decreases. For example, the drug release from PLGA (50/50) decreases by almost 4 times when the M_w increase from 14,500 g/mol to 213,000 g/mol[95]. Indeed, higher molecular weight means longer polymer chains, thus the breakdown of the polymer chains in small water-soluble molecules requires more time compared to smaller polymer chains[96]. The lag-time generally observed for PLGA degradable microparticles is then tremendously decreased for low molecular weight PLGA compared with high molar mass PLGA. In addition, the water diffusion in lower M_w chains particles is easier compared to the higher M_w polymer particles which favors the hydrolytic degradation of the polymer[10,99]. Nevertheless, the use of higher molecular weight polymers reduces the initial burst effect, increases the bioavailability, the drug-loading and the encapsulation efficiency. This can be explained by the fact that the viscosity of the polymer solution increases with the molar mass which reduces the diffusion of the drug before the hardening of the particle[98].

I.3.4 Glass transition temperature

The glass transition temperature (T_g) is defined as a temperature at which the polymer starts transition from a glassy solid state to a viscous rubbery state. In a microscopic way, it means that the chains have enough energy to move and disentangled. The T_g mainly depends on the macromolecular structure and the stereochemistry of the polymer. The presence of flexible chains will decrease the T_g and oppositely. The molecular weight and the copolymer composition, see Table 2, will affect the transition temperature. Indeed, the both decrease in lactide content and in molecular weight of the PLGA lead to a decrease of the T_g which increases the polymer chains mobility and allows the drug molecules to escape more easily from the polymer chain entanglement, resulting in an increased release rate[95,96,98,100,101]. It is important to notice that the encapsulation of a drug in the copolymer matrix can decrease the T_g of the copolymer playing as a plasticizer[100].

I.3.5 Chain-ends functionalization

Depending on the chain ends on the PLGA, the degradation rate and the encapsulation efficiency will change. Indeed, the PLGA with an ester as chain-ends is more resistant to the hydrolytic degradation than the PLGA end-capped with a carboxylic acid since acid catalyzes the hydrolytic degradation and increase the hydrophilicity. Moreover, it was demonstrated that a PLGA with an ethyl end-capping group will showed a faster degradation rate than the one with the hexyl group because of the lower reduction of the hydrophilicity[10,96,98,102].

I.3.6 Drug-polymer interactions

The last parameter is not really an intrinsic property of the polymer but it can influence the degradation profile of the polymer matrix. Indeed, if the encapsulated drug is an acid or a weak base, the effect of drug-polymer interaction on polymer degradation must be considered. If acidic drug is entrapped, it will catalyze hydrolysis as well as the autocatalytic degradation of the polymer matrix. Concerning the encapsulation of basic drugs, it will lead to two conflicted effects. Indeed, the hydrolytic degradation is also accelerated in basic conditions and then the release will increase but there is also the fact that the basic function on the active ingredient can minimize the autocatalytic effect by neutralizing the carboxylic

acid functions generated by the hydrolytic degradation which leads to a slower degradation rate and a reduced release rate[95].

The PLGA is the most used degradable polymer for biomedical applications but it is not the only one and more and more researchers develop drug delivery microparticle based on other biodegradable polymer. The most used of them are described in the following part.

I.4 Biocompatible and biodegradable polymers used for drug delivery systems.

The first polymers used to formulate particles were non-degradable polymers because they exhibit a rapid and efficient clearance. Unfortunately, they show also chronic toxicity and inflammatory responses caused by the accumulation in the body[12]. In the past twenty years, the development of biodegradable polymer particles becomes more and more significant because of their notable biocompatibility and biosafety. Biodegradable polymers have the property to self-degrade *in vivo* via either enzymatically or non-enzymatically ways, such as hydrolysis, and yield biocompatible or harmless by-products which are typically oligomers or monomers which can be eliminated from the body through classical ways. These biodegradable materials must not induce constant inflammatory response, should not produce toxic degradation products and should have medicinal properties for the targeted medical application. Another characteristic of these polymers is that they show a reduced toxicity and side-effects, and the drug-release kinetic can be easily modulated, as discussed in the third part of this work [103,104].

Biodegradable polymers can be divided in two different categories, the bio-sourced polymers provided by animals, vegetal and microorganisms, and the synthetic polymers which are created in the laboratory.

Bio-sourced polymers, such as chitosan, alginate, agarose and albumin are used to formulate drug-delivery microparticles[15]. Nevertheless, they can cause immunogenicity and require frequently chemical modification before being used. On the other hand, the chemical synthesis of polymers allows to obtain very well controlled polymers in term of molar mass,

hydrophilicity, crystallinity and functionality. Consequently, only synthetic polymers will be discussed in the next section.

I.4.1 Synthetic polymers used for the fabrication of drug-loaded microparticles

I.4.1.1 Polyesters

Polyesters (Figure 20a) represent the most widely studied and used family of synthetic biodegradable polymers. The most known polymers in this family are the PGA, the PLA, the PLGA and PCL. The first three were already detailed in the section 3. PCL is also biocompatible, bio-absorbable, and (bio)degradable but it is more hydrophobic than PLA, PLGA or PGA, which has an influence on the degradation time. Indeed, the PCL, that degrades in the same way as other polyesters (i.e. hydrolytic degradation and autocatalytic degradation), takes around two-three years to be fully degraded *in vivo*. This polymer is also semi-crystalline, with a melting temperature around 50°C-60°C, which slows down its degradation time. Nevertheless, the degradation rate can be improved by making copolymers with lactide or glycolide. The PCL was approved by the FDA for suture wire, as a drug-delivery device and as adhesion barrier[103–108].

I.4.1.2 Polyanhydrides

Polyanhydrides (Figure 20b) are non-toxic promising materials for drug delivery devices. This family of polymers is hydrophobic but the hydrolysis of the anhydride bond is especially fast and faster than the water penetration rate, which conducts to the production of surface-eroding devices. Polyanhydrides have been designed to develop nano- or micro spheres for injectable, oral or aerosol delivery. They have been investigated for controlled release of a bunch of drugs to treat eye disorders, as local anesthetics or as anticoagulants for example. Drugs are protected inside the polymer because the water cannot penetrate inside the particle until the surface is eroded[15,104,108–110]. Moreover, as previously discussed, the

polymer structure and composition, crystallinity, hydrophobicity, pH of the release medium, microspheres size, configuration, etc. can influence the rate of drug-delivery[110].

Polyanhydrides are very promising for drug delivery applications due to their controlled biodegradability, zero-order release kinetics for drugs and low toxicity of the degradation products. For example, poly(sebacic acid) microparticles prepared by emulsion-evaporation technique released their active ingredient, the Olaparib, an anti-cancerous molecule, in 7 days[109]. Core-shell microparticles with a hydrophilic PGA core containing blue brilliant as hydrophilic molecule and a copolymer of sebacic acid and 1,3-bis(p-carboxyphenoxy) propane as shell containing curcumin as hydrophobic molecule present a sustained release over 30 days[111]. Another example concerns the formulation of a sebacic acid and 1,3-bis(p-carboxyphenoxy) propane copolymer containing carmustine, used for the therapy of brain cancer. This last example is the only one FDA approved formulation. This can be explained by the difficult handling, storage and fabrication of polyanhydride due to their high degradation rate[15,104,108,110].

I.4.1.3 Poly(amino-acids)

Poly(amino-acids) are the component of different tissues and they are *in vivo* hydrolyzed to produce non-toxic oligopeptides or amino acids. The poly(aspartic acid) and its derivatives emerge among all poly(amino-acids) due to their easy synthesis and adaptable functionalization comparing to the polymerization of other poly(amino-acids). These anionic biopolymers are extensively used in a variety of biomedical applications such as drug carriers or injectable hydrogels. Ring-opening reactions of polysuccinimide leads to an amphiphilic poly(aspartic acid) derivative with both pH and redox sensitive properties. The polymer being hydrophilic, drugs or active ingredients is encapsulated in the core of microcapsules via hydrophobic interactions. The structural integrity of the microcapsules is preserved in a neutral environment but when they are subject to acid or reducing substances, the decomposition of the material starts and the drug release is achieved[15,112,113]. A nucleophilic reaction on polysuccinimide can lead to polyelectrolytes and then open the way to a lot of interesting *in vivo* applications[113,114]. Poly(aspartic acid) (Figure 20c) is also widely used, like other poly(amino-acids), in water treatment, paint additives and paper processing[115].

I.4.1.4 Polyphosphoesters

Polyphosphoesters (PPEs) are one type of synthetic polymers with a phosphate ester bond in the backbone. These polymers contain two substitution sites, R and R', and following the nature of R', the PPE properties will change (Figure 20d). If the R' = H it is a poly(phosphite), if R'= alkyl or aryl moiety, it is called a polyphosphonate and if R' = alkoxy or aryloxy, it is a polyphosphate. In the 1970s, the study of this kind of polymers began with the work of Penczek's team and with time, different research groups bring to light various desirable characteristics such as their biocompatibility, their physicochemical properties and their versatility and flexibility[15,108,116,117].

Biocompatible polyphosphoesters can be synthetized via different ways, such as polyaddition, polycondensation or enzymatic polymerization, based on nontoxic alcohol and diols resulting in harmless and biocompatible hydrolytic products[15]. Moreover, polyphosphoesters have structural similarity with biomacromolecules such as DNA, RNA and nucleic acids. The physicochemical properties are interesting comparing with polyesters because the T_g is reduced thanks to the flexibility of the phosphate ester bond. Finally, properties of these polymers can be tuned by changing the backbone structure or side chain. The pentavalency of the phosphorus atom offers a large diversity of structures compared to the "classical" polyesters allowing to tune both the degradation and physicochemical properties[15,108,116,118–120]. For example, the PPE with a methyl side group is soluble in water but if the length of the alkyl side chain increases, the hydrophilicity decreases. The PPE with an ethyl side group has a low critical solubility temperature in water (LCST = 45°C) and the PPE with a propyl pendant group is insoluble in water[116]. It is also possible to tune the crystallinity of the PPE by increasing the backbone chain length or by modifying the pendant group[121,122].

Polyphosphoesters are already used as drug delivery systems for various applications and thanks to their high versatility, their biocompatibility and their biomimicry, they have a great potential in the medical field and especially for drug delivery applications[117,123–125]. Recently, water soluble polyphosphoesters were even evidenced as good candidates to replace the poly(ethylene glycol) (PEG) which can accumulate in the body and produce immunogenic responses as hypersensitivity and the production of anti-PEG IgM antibodies[117].

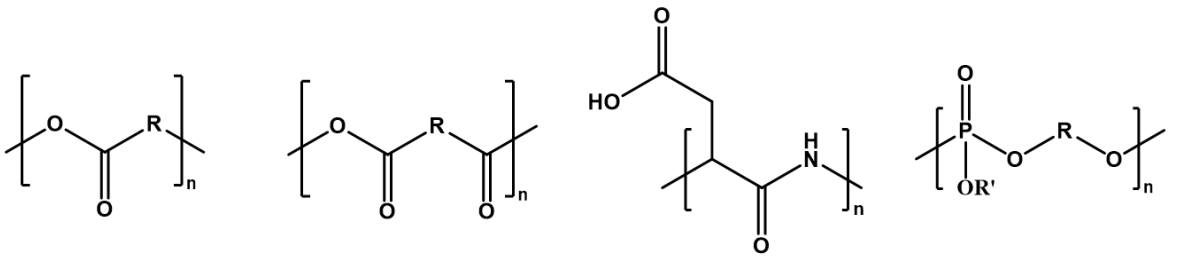

Figure 20 : Chemical structures of synthetic polymers used for drug-delivery

As highlighted in this chapter, microfluidic technique is a very powerful technique allowing to formulate a wide range of microparticles with different characteristics and functionalities. That is why this technique will become more and more significant in the near future to produce commercially available DDSs even if it can be time-consuming to optimize the formulation process.

I.5 References

1 E. Vatankhah, S. Hamedi and O. Ramezani, *Polym Test*, 2020, **81**, 106180.

2 C. Gu, C. Hu, C. Ma, Q. Fang, T. Xing and Q. Xia, *European Journal of Lipid Science and Technology*, 2016, **118**, 1093–1103.

3 A. Łętocha, M. Miastkowska and E. Sikora, *Polymers (Basel)*, , DOI:10.3390/polym14183834.

4 J. Kozlowska, W. Prus and N. Stachowiak, *Int J Biol Macromol*, 2019, **129**, 952–956.

5 H. El Itawi, S. Fadlallah, F. Allais and P. Perré, *Green Chemistry*, 2022, **24**, 4237–4269.

6 I. C. da Silva Grem, B. N. B. Lima, W. F. Carneiro, Y. G. de Carvalho Queirós and C. R. E. Mansur, *Polimeros*, 2013, **23**, 705–711.

7 C. G. Barreras-Urbina, B. Ramírez-Wong, G. A. López-Ahumada, S. E. Burruel-Ibarra, O. Martínez-Cruz, J. A. Tapia-Hernández and F. Rodríguez Félix, *Int J Food Prop*, 2016, **19**, 1912–1923.

8 S. Martin-Saldaña, M. T. Chevalier, M. J. Iglesias, S. L. Colman, C. A. Casalongué, V. A. Álvarez and A. A. Chevalier, *Carbohydr Polym*, 2018, **200**, 321–331.

9 D. A. Popović, D. D. Milinčić, M. B. Pešić, A. M. Kalušević, Ž. L. Tešić and V. A. Nedović, *Encapsulation technologies for polyphenol-loaded microparticles in food industry*, 2019.

10 E. Lagreca, V. Onesto, C. Di Natale, S. La Manna, P. A. Netti and R. Vecchione, *Prog Biomater*, 2020, **9**, 153–174.

11 M. Ventura, Y. Sun, S. Cremers, P. Borm, Z. T. Birgani, P. Habibovic, A. Heerschap, P. M. van der Kraan, J. A. Jansen and X. F. Walboomers, *Biomaterials*, 2014, **35**, 2227–2233.

12 A. C. Daly, L. Riley, T. Segura and J. A. Burdick, *Nat Rev Mater*, 2020, **5**, 20–43.

13 C. Y. Wong, H. Al-Salami and C. R. Dass, *Int J Pharm*, 2018, **537**, 223–244.

14 F. Molavi, M. Barzegar-Jalali and H. Hamishehkar, *Journal of Controlled Release*, 2020, **320**, 265–282.

15 Z. Chen, Y. Lan, S.-D. Ling, Y.-H. Dong, Y.-D. Wang and J.-H. Xu, *Adv Mater Technol*, , DOI:10.1002/admt.202100733.

16 A. N. Serra C., Khan I., Cortese B., Ono T., *Encyclopedia of Polymer Science and Technology*, 2013, 1–37.

17 A. Vlachopoulos, G. Karlioti, E. Balla, V. Daniilidis, T. Kalamas, M. Stefanidou, N. D. Bikiaris, E. Christodoulou, I. Koumentakou, E. Karavas and D. N. Bikiaris, *Pharmaceutics*, , DOI:10.3390/PHARMACEUTICS14020359.

18 W. Li, H. Lee, D. A. Weitz, L. Zhang, X. Ge, B. Xu, W. Zhang, L. Qu, C.-H. Choi, J. Xu and A. Zhang, *Chem. Soc. Rev*, 2018, **47**, 5646–5683.

19 V. Percec, *Hierarchical Macromolecular Structures: 60 Years after the Staudinger Nobel Prize II (Advances in Polymer Science)*, 2014.

20 M. Iqbal, N. Zafar, H. Fessi and A. Elaissari, *Int J Pharm*, 2015, **496**, 173–190.

21 M. G. Nava-Arzaluz, E. Pinon-Segundo, A. Ganem-Rondero and D. Lechuga-Ballesteros, *Recent Pat Drug Deliv Formul*, 2012, **6**, 209–223.

22 A. Gonçalves, B. N. Estevinho and F. Rocha, *Powder Technol*, 2017, **305**, 411–417.

23 F. Wan and M. Yang, *Int J Pharm*, 2016, **498**, 82–95.

24 M. Amdadul Haque, Y. Timilsena, B. Adhikari, M. Amdadul Haque and Y. Prasad Timilsena, *Drying Technologies for Foods: Fundamentals & Applications : Spray Drying*, 2015.

25 W. Liu, X. D. Chen and C. Selomulya, *Particuology*, 2015, **22**, 1–12.

26 A. Í. S. Morais, E. G. Vieira, S. Afewerki, R. B. Sousa, L. M. C. Honorio, A. N. C. O. Cambrussi, J. A. Santos, R. D. S. Bezerra, J. A. O. Furtini, E. C. Silva-Filho, T. J. Webster and A. O. Lobo, *J Funct Biomater*, , DOI:10.3390/jfb11010004.

27 D. M. Correia, R. Gonçalves, C. Ribeiro, V. Sencadas, G. Botelho, J. L. G. Ribelles and S. Lanceros-Méndez, *RSC Adv*, 2014, **4**, 33013–33021.

28 M. Jeyhani, S. Y. Mak, S. Sammut, H. C. Shum, D. K. Hwang and S. S. H. Tsai, *ChemPhysChem*, 2018, **19**, 2113–2118.

29 M. E. Tasci, B. Dede, E. Tabak, A. Gur, R. B. Sulutas, S. Cesur, E. Ilhan, C. C. Lin, P. Paik, D. Ficai, A. Ficai and O. Gunduz, *Applied Sciences (Switzerland)*, 2021, **11**, 1–13.

30 S. H. Soh and L. Y. Lee, *Pharmaceutics*, , DOI:10.3390/pharmaceutics11010021.

31 R. M. Obaidat, B. M. Tashtoush, M. F. Bayan, R. T. Al Bustami and M. Alnaief, *AAPS PharmSciTech*, 2015, **16**, 1235–1244.

32 S. Rezvantalab and M. Keshavarz Moraveji, *RSC Adv*, 2019, **9**, 2055–2072.

33 A. Abou-Hassan, R. Bazzi and V. Cabuil, *Angewandte Chemie - International Edition*, 2009, **48**, 7180–7183.

34 S. Yazdian Kashani, A. Afzalian, F. Shirinichi and M. Keshavarz Moraveji, *RSC Adv*, 2020, **11**, 229–249.

35 M. Zhang, W. Wang, R. Xie, X. Ju, Z. Liu, L. Jiang, Q. Chen and L. Chu, *Particuology*, 2016, **24**, 18–31.

36 R. K. Shah, H. C. Shum, A. C. Rowat, D. Lee, J. J. Agresti, A. S. Utada, L. Y. Chu, J. W. Kim, A. Fernandez-Nieves, C. J. Martinez and D. A. Weitz, *Materials Today*, 2008, **11**, 18–27.

37 K. E. Washington, R. N. Kularatne, V. Karmegam, M. C. Biewer and M. C. Stefan, *WIREs Nanomed Nanobiotechnol*, 2017, **9**, 1446.

38 R. Bhujel, R. Maharjan, N. A. Kim and S. H. Jeong, *J Drug Deliv Sci Technol*, 2021, **64**, 102608.

39 J. Yoo and Y. Y. Won, *ACS Biomater Sci Eng*, 2020, **6**, 6053–6062.

40 C. Busatto, J. Pesoa, I. Helbling, J. Luna and D. Estenoz, *Int J Pharm*, 2018, **536**, 360–369.

41 W. Chen, A. Palazzo, W. E. Hennink and R. J. Kok, *Mol Pharm*, 2017, **14**, 459–467.

42 S. Freiberg and X. Zhu, *Int J Pharm*, 2004, **282**, 1–18.

43 B. L. Laube, *Journal of Aerosol Medicine: Deposition, Clearance, and Effects in the Lung*, 1996, **9**, 77–91.

44 Q. Xu, M. Hashimoto, T. T. Dang, T. Hoare, D. S. Kohane, G. M. Whitesides, R. Langer, D. G. Anderson and H. David, *Small*, 2009, **5**, 1575–1581.

45 C. Berkland, M. King, A. Cox, K. Kim and D. W. Pack, *Journal of Controlled Release*, 2002, **82**, 137–147.

46 G. T. Vladisavljević, H. Shahmohamadi, D. B. Das, E. E. Ekanem, Z. Tauanov and L. Sharma, *J Colloid Interface Sci*, 2014, **418**, 163–170.

47 X. Li, Q. Li and C. Zhao, *ACS Omega*, 2021, **6**, 13774–13778.

48 K. Park, *Journal of Controlled Release*, 2014, **190**, 3–8.

49 K. T. M. Tran, T. D. Gavitt, N. J. Farrell, E. J. Curry, A. B. Mara, A. Patel, L. Brown, S. Kilpatrick, R. Piotrowska, N. Mishra, S. M. Szczepanek and T. D. Nguyen, *Nat Biomed Eng*, 2021, **5**, 998–1007.

50 K. E. Broaders, S. J. Pastine, S. Grandhe and J. M. J. Fréchet, *Chemical Communications*, 2011, **47**, 665–667.

51 K. J. Rambhia and P. X. Ma, *Journal of Controlled Release*, 2015, **219**, 119–128.

52 W. Yu, X. Liu, B. Li and Y. Chen, *International Journal of Multiphase Flow*, , DOI:10.1016/j.ijmultiphaseflow.2022.103973.

53 J. D. Wehking, M. Gabany, L. Chew and R. Kumar, *Microfluid Nanofluidics*, 2014, **16**, 441–453.

54 F. Fontana, M. P. A. Ferreira, A. Correia, J. Hirvonen and H. A. Santos, *J Drug Deliv Sci Technol*, 2016, **34**, 76–87.

55 Z. Liu, F. Fontana, A. Python, J. T. Hirvonen and H. A. Santos, *Small*, , DOI:10.1002/smll.201904673.

56 M. de menech, P. Garstecki, F. Jousse and H. A. Stone, *J Fluid Mech*, 2008, **595**, 141–161.

57 B. Amoyav and O. Benny, *Applied Nanoscience (Switzerland)*, 2018, **8**, 905–914.

58 S. W. Choi, I. W. Cheong, J. H. Kim and Y. Xia, *Small*, 2009, **5**, 454–459.

59 T. Watanabe, T. Ono and Y. Kimura, *Soft Matter*, 2011, **7**, 9894–9897.

60 K. Park, A. Otte, F. Sharifi, J. Garner, S. Skidmore, H. Park, Y. K. Jhon, B. Qin and Y. Wang, *Journal of Controlled Release*, 2021, **329**, 1150–1161.

61 D. Dendukuri and P. S. Doyle, *Advanced Materials*, 2009, **21**, 4071–4086.

62 P. S. Clegg, J. W. Tavacoli and P. J. Wilde, *Soft Matter*, 2016, **12**, 998–1008.

63 B. Amoyav and O. Benny, *Polymers (Basel)*, , DOI:10.3390/POLYM11030419.

64 D. Klose, F. Siepmann, K. Elkharraz, S. Krenzlin and J. Siepmann, *Int J Pharm*, 2006, **314**, 198–206.

65 M. Brzeziński, M. Socka and B. Kost, *Polym Int*, 2019, **68**, 997–1014.

66 M. Nasr, G. A. S. Awad, S. Mansour, A. al Shamy and N. D. Mortada, *Pharm Dev Technol*, 2013, **18**, 1078–1088.

67 C. M. Kim, A. Ullah, C. H. Chang and G. M. Kim, *International Journal of Precision Engineering and Manufacturing*, 2017, **18**, 599–604.

68 R. Ni, U. Muenster, J. Zhao, L. Zhang, E. M. Becker-Pelster, M. Rosenbruch and S. Mao, *Journal of Controlled Release*, 2017, **249**, 11–22.

69 Y. Oh and S. H. Kim, *Journal of Polymer Science*, 2022, **60**, 1700–1709.

70 T. Watanabe, Y. Kimura and T. Ono, *Langmuir*, 2013, **29**, 14082–14088.

71 Y. Li, D. Yan, F. Fu, Y. Liu, B. Zhang, J. Wang, L. Shang, Z. Gu and Y. Zhao, *Sci China Mater*, 2017, **60**, 543–553.

72 M. Windbergs, Y. Zhao, J. Heyman and D. A. Weitz, *J Am Chem Soc*, 2013, **135**, 7933–7937.

73 Z. Feng, B. Zhou, X. Su, T. Wang, S. Guo, H. Yang and X. Sun, *Mater Des*, 2023, **225**, 111516.

74 M. Saqib, P. A. Tran, B. Ercan and E. Yegan Erdem, *Int J Nanomedicine*, 2022, **17**, 4355–4366.

75 X. T. Sun, R. Guo, D. N. Wang, Y. Y. Wei, C. G. Yang and Z. R. Xu, *J Colloid Interface Sci*, 2019, **553**, 631–638.

76 T. Nisisako, *Curr Opin Colloid Interface Sci*, 2016, **25**, 1–12.

77 R. al Nuumani, S. K. Smoukov, G. Bolognesi and G. T. Vladisavljevic, *Langmuir*, 2020, **36**, 12702–12711.

78 K. P. Yuet, D. K. Hwang, R. Haghgooie and P. S. Doyle, *Langmuir*, 2010, **26**, 4281–4287.

79 J. H. Kim, T. Y. Jeon, T. M. Choi, T. S. Shim, S. H. Kim and S. M. Yang, *Langmuir*, 2014, **30**, 1473–1488.

80 A. Sen Gupta, *Wiley Interdiscip Rev Nanomed Nanobiotechnol*, 2016, **8**, 255–270.

81 S. Nejati, E. Mohseni Vadeghani, S. Khorshidi and A. Karkhaneh, *Eur Polym J*, 2020, **122**, 109353.

82 J. Il Park, A. Saffari, S. Kumar, A. Günther and E. Kumacheva, *Annu Rev Mater Res*, 2010, **40**, 415–443.

83 A. Fang, C. Gaillard and J. P. Douliez, *Chemistry of Materials*, 2011, **23**, 4660–4662.

84 J. A. Champion, Y. K. Katare and S. Mitragotri, *Journal of Controlled Release*, 2007, **121**, 3–9.

85 J. Di, X. Gao, Y. Du, H. Zhang, J. Gao and A. Zheng, *Asian J Pharm Sci*, 2021, **16**, 444–458.

86 Y. Yang, D. Nie, Y. Liu, M. Yu and Y. Gan, *Drug Discov Today*, 2019, **24**, 575–583.

87 J. Wang, Q. Li, J. Xue, W. Chen, R. Zhang and D. Xing, *Chemical Engineering Journal*, 2021, **410**, 127849.

88 Y. Wang, L. Shang, G. Chen, C. Shao, Y. Liu, P. Lu, F. Rong and Y. Zhao, *Appl Mater Today*, 2018, **13**, 303–309.

89 C. Wischke and A. Lendlein, *Langmuir*, 2014, 2820–2827.

90 C. Wischke, M. Schossig and A. Lendlein, *Small*, 2014, **10**, 83–87.

91 Y. Bai, J. Zhang, J. Ju, J. Liu and X. Chen, *React Funct Polym*, 2020, **157**, 104770.

92 J. Huang, L. Lai, H. Chen, S. Chen and J. Gao, *Mater Lett*, 2018, **225**, 24–27.

93 L. M. Cox, J. P. Killgore, Z. Li, R. Long, A. W. Sanders, J. Xiao and Y. Ding, *Langmuir*, 2016, **32**, 46.

94 C. Engineer, J. Parikh and A. Raval, *Trends Biomater Artif Organs*, 2011, **25**, 79–85.

95 Y. Xu, C. S. Kim, D. M. Saylor and D. Koo, *J Biomed Mater Res B Appl Biomater*, 2017, **105**, 1692–1716.

96 D. N. Kapoor, A. Bhatia, R. Kaur, R. Sharma, G. Kaur and S. Dhawan, *Ther Deliv*, 2015, **6**, 41–58.

97 I. Takeuchi, K. Tomoda, A. Hamano and K. Makino, *Colloids Surf A Physicochem Eng Asp*, 2017, **520**, 771–778.

98 S. Sonam, H. Chaudhary, V. Arora, K. Kholi and V. Kumar, *Polymer Reviews*, 2013, **53**, 546–567.

99 W. Guo, P. Quan, L. Fang, D. Cun and M. Yang, *Asian J Pharm Sci*, 2015, **10**, 405–414.

100 G. Liu and K. McEnnis, *Polymers (Basel)*, , DOI:10.3390/polym14050993.

101 K. Park, A. Otte, F. Sharifi, J. Garner, S. Skidmore, H. Park, Y. K. Jhon, B. Qin and Y. Wang, *Mol Pharm*, 2021, **18**, 18–32.

102 J. Wang, L. Helder, J. Shao, J. A. Jansen, M. Yang and F. Yang, *Int J Pharm*, 2019, **564**, 1–9.

103 A. Gagliardi, E. Giuliano, E. Venkateswararao, M. Fresta, S. Bulotta, V. Awasthi and D. Cosco, *Front Pharmacol*, 2021, **12**, 1–24.

104 S. K. Prajapati, A. Jain, A. Jain and S. Jain, *Eur Polym J*, 2019, **120**, 109191.

105 V. Ogay, E. A. Mun, G. Kudaibergen, M. Baidarbekov, K. Kassymbek, Z. Zharkinbekov and A. Saparov, *Polymers (Basel)*, 2020, **12**, 1–25.

106 N. Asadi, A. R. del Bakhshayesh, S. Davaran and A. Akbarzadeh, *Mater Chem Phys*, 2020, **242**, 122528.

107 B. Wang, S. Wang, Q. Zhang, Y. Deng, X. Li, L. Peng, X. Zuo, M. Piao, X. Kuang, S. Sheng and Y. Yu, *Acta Biomater*, 2019, **96**, 55–67.

108 G. S. Kwon and D. Y. Furgeson, *Biodegradable polymers for drug delivery systems*, Woodhead Publishing Limited, 2007.

109 S. G. Kala and S. Chinni, *Indian Journal of Pharmaceutical Education and Research*, 2022, **56**, 429–437.

110 P. G. Reddy and A. J. Domb, *Biomacromolecules*, 2022, **23**, 4959–4984.

111 I. M. Chu, T. H. Liu and Y. R. Chen, *Journal of Polymer Research*, 2019, **26**, 1–6.

112 C. Gong, M. Shan, B. Li and G. Wu, *Colloids Surf B Biointerfaces*, 2016, **146**, 396–405.

113 H. Adelnia, H. D. N. Tran, P. J. Little, I. Blakey and H. T. Ta, *ACS Biomater Sci Eng*, 2021, **7**, 2083–2105.

114 P. S. Yavvari, A. K. Awasthi, A. Sharma, A. Bajaj and A. Srivastava, *J Mater Chem B*, 2019, **7**, 2102–2122.

115 S. H. S. Boddu, P. Bhagav, P. K. Karla, S. Jacob, M. D. Adatiya, T. M. Dhameliya, K. M. Ranch and A. K. Tiwari, .

116 C. J. Ergul Yilmaz Z., *Macromol Biosci*, 2016, 1745–1761.

117 C. Pelosi, M. R. Tinè and F. R. Wurm, *Eur Polym J*, 2020, **141**, 110079.

118 T. Steinbach and F. R. Wurm, *Angewandte Chemie - International Edition*, 2015, **54**, 6098–6108.

119 Z. Zhao, J. Wang, H. Q. Mao and K. W. Leong, *Adv Drug Deliv Rev*, 2003, **55**, 483–499.

120 S. Vanslambrouck, R. Riva, B. Ucakar, V. Préat, M. Gagliardi, D. G. M. Molin, P. Lecomte and C. Jérôme, *Molecules*, , DOI:10.3390/molecules26061750.

121 H. T. Tee, K. Koynov, T. Reichel and F. R. Wurm, *ACS Omega*, 2019, **4**, 9324–9332.

122 H. Busch, S. Majumder, G. Reiter and S. Mecking, *Macromolecules*, 2017, **50**, 2706–2713.

123 H. Elzeny, F. Zhang, E. N. Ali, H. A. Fathi, S. Zhang, R. Li, M. A. El-Mokhtar, M. A. Hamad, K. L. Wooley and M. Elsabahy, *Drug Des Devel Ther*, 2017, **11**, 483–496.

124 G. Ma, J. Liu, J. He, M. Zhang and P. Ni, *ACS Biomater Sci Eng*, 2018, **4**, 2443–2452.

125 P. Ju, J. Hu, F. Li, Y. Cao, L. Li, D. Shi, Y. Hao, M. Zhang, J. He and P. Ni, *J Mater Chem B*, 2018, **6**, 7263–7273.

Aim of the thesis

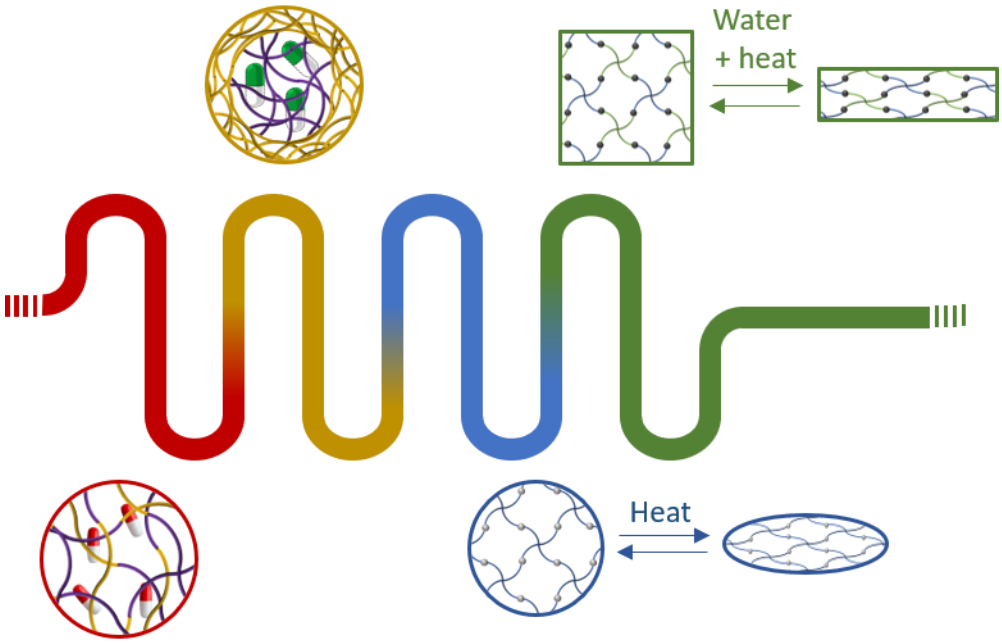

Aim of the thesis

As presented in **Chapter I**, the release kinetics of a drug encapsulated in a polymer-microsphere depend on both the microsphere characteristics (shape, size, morphology, porosity…) and the chemical composition (polymer structure, molecular weight, hydrophilicity, glass transition temperature, crystallinity,…), which offers many levers to finely adapt the release profile for a targeted therapeutic application.

This work aims to formulate innovative (bio)degradable, biocompatible and well-defined drug loaded microspheres presenting advanced functionalities or abilities able to rule the drug-release kinetics. To reach this goal, the microfluidic droplet generation technique is selected as formulation process according to its high potential in terms of versatility, reproducibility, controllability and high encapsulation efficiency.

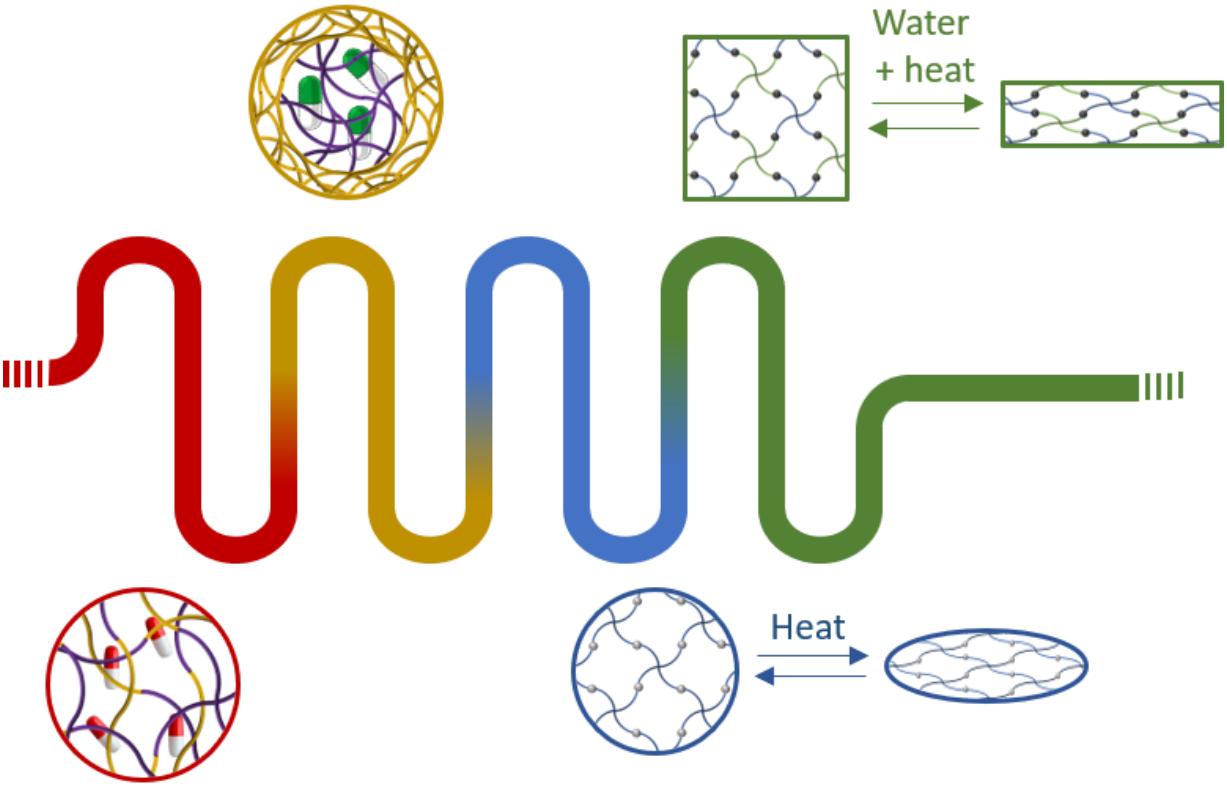

Figure 1 : Overview of the different challenges of the thesis

For this purpose, improvement is imparted on commonly used drug delivery carriers made of aliphatic polyesters, such as poly-D,L-lactic acid (PDLLA) or poly(ε-caprolactone) (PCL), microspheres already largely investigated in the biomedical field as drug carrier.

In **Chapter II**, the increasing of the hydrophilicity, impacting the degradation rate, of classical aliphatic polyester microspheres is investigated by incorporating polyphosphoesters (PPEs) in particle matrix. Indeed, PPEs are biocompatible and biodegradable polymer presenting tunable properties, as hydrophilicity, thanks to the lateral pendant chain, and are synthesized through ring-opening polymerization similarly to conventional aliphatic polyesters, enabling the synthesis of well-defined block copolymer PPE-*b*-PLLA . The microfluidics formulation of microspheres made of copolymer is investigated and the impact of PPE on the drug release kinetics and on the cytocompatibility are discussed and compared with traditional aliphatic polyester microspheres.

The presence of a shell around the microspheres allows a constant release through time with a decrease of the undesired burst effect. The development of a microfluidic process allowing the formulation of core-shell microparticles, composed of a polyphosphoester shell and an aliphatic polyester core is the topic of **Chapter III**. Due to the very low polyphosphoester glass transition temperature (around -60°C), avoiding their direct application as polymer shell, a strategy to allow an in-line crosslinking by UV radiation is set up by the use of unsaturated poly(butenyl phosphate). The effect of the nature of the shell on the release kinetics of a model molecule and on the cytotoxicity of the carrier is discussed.

The UV radiation can also be used to form a fully crosslinked polymer network to implement functionality. In **Chapter IV**, this property will be exploited to formulate shape-memory microspheres. The shape-memory property is the ability of a material to switch from one stable macroscopic shape to another one under the action of a stimulus, mainly heat. In the case of shape-memory microparticles, they find a potential application as embolization agents (Figure 2).

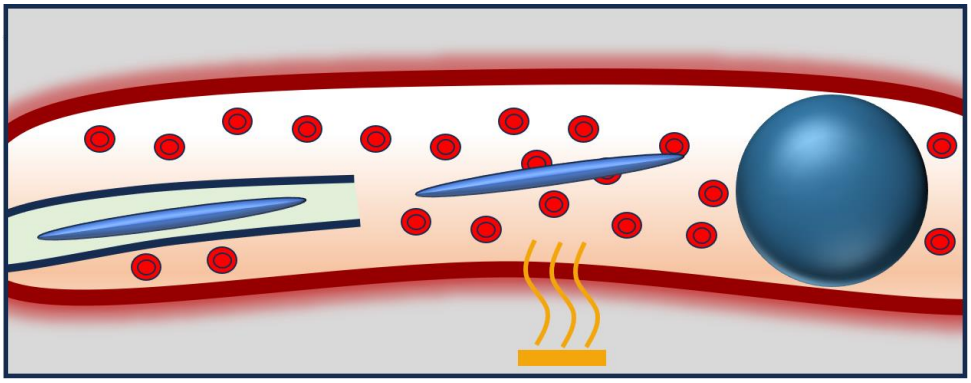

Figure 2 : Schematic principle of shape-memory microparticles for embolization: injection in the programmed elongated shape through a microcatheter, recovery of the spherical shape by local heating, blocking further blood supply.

A complete microfluidics process is successfully implemented to formulate UV-crosslinked microspheres made of 4-arm star-shaped PCL functionalized with coumarins at each chain-end. The ability of programming temporary shapes on these microparticles with different deformation techniques is discussed and shape-memory properties are determined.

Moreover, shape-memory tests are realized on the core-shell microparticles formulated in the **Chapter III**, which could have a real interest for injected microparticles.

The thermal stimulus, required to induce the shape recovery, may pose problems for biomedical applications so that an alternative approach is explored by the introduction of magnetite nanoparticles finely dispersed into the matrix of the microspheres in order to confer magnetic response and induce the shape-memory effect by application of a magnetic field leading to Joule effect. Furthermore, another suitable stimulus for biomedical applications able to induce shape-memory effect is water or moisture. When water penetrates a material, it disturbs the polymer chains, triggering the shape-memory effect. This concept was tested on a macroscopic hybrid network composed of PCL and poly(ethylene oxide), detailed in **Chapter V**.

Finally, the **Chapter VI** is dedicated to a comprehensive discussion that aims to place this work and its associated results within the broader context of sustainable development.

Chapter II : Accelerated drug-release from polylactide microspheres by using polyphosphoester.

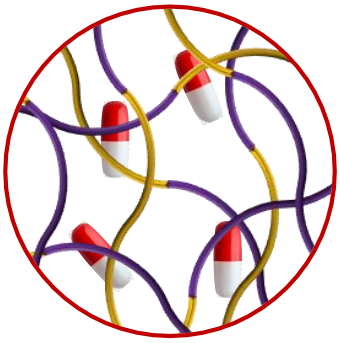

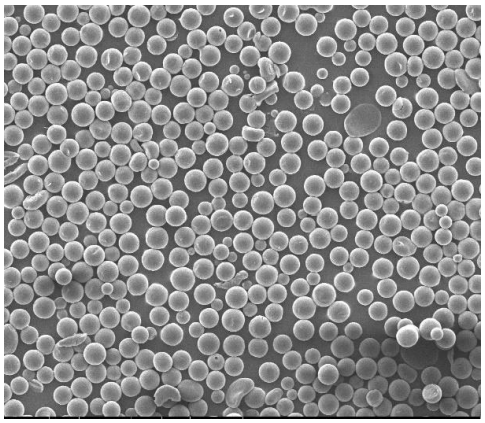

Chapter II : Accelerated drug-release from polylactide microspheres by using polyphosphoester.

Controlled drug-delivery systems based on microspheres of degradable polymers allows to decrease adverse effects caused by an important fluctuation of the drug concentration, a higher drug efficiency and a better patient compliance. Different techniques exist to formulate such drug loaded microspheres and amongst all of them the microfluidics droplet generation emerges as the most powerful because of its high versatility, its excellent reproducibility and especially its high controllability which allows to decrease the main drawback of microspheres sustained release namely the burst effect. PDLLA (co)polymers are the most commonly used degradable polyesters for this application allowing to modulate sustained release from few weeks to several months, especially by controlling their degradation rate by copolymerization with the less hydrophobic glycolide. Recently, polyphosphoesters emerge as new kind of degradable materials showing strong promise for drug-delivery applications. Moreover, the structure of these biocompatible polymers can be easily adapted thanks to the pentavalency of the phosphorous atom allowing a remarkable tunability of their physicochemical properties, typically hydrophilicity, or the introduction of chemical functionalities. In the present work, we investigate the impact of adding a poly(butenyl phosphate) component to polylactide microspheres formulated by microfluidic technique on the encapsulation efficiency and release profile of an active pharmaceutical ingredient, namely budesonide compare to conventional PDLLA and PLGA microspheres as reference. The absence of cytotoxicity of these innovative microspheres is also assessed.

II.1 Introduction

Sustained and controlled drug delivery systems allow to decrease the potential adverse effects, a higher drug efficiency and a better patient compliance[1]. These systems must be able to achieve their purpose during a certain period of time before being eliminated from the body either by degradation and renal filtration. Amongst all kinds of DDSs, degradable polymer-based microspheres remain the most used and studied. Several parameters influence the release of the active ingredient from the polymer matrix such as the degradation rate of the polymer, the morphology of the particles, the solubility of the encapsulated drug and the drug distribution in the particle[2].

One recurring problem with most of controlled drug delivery microspheres is the burst effect occurring when a significant amount of the encapsulated drug is prematurely released within a short period of time after systemic injection[3]. The most efficient way to minimize this burst effect is to produce highly monodisperse particles. Indeed, the smaller particles of a polydisperse sample release faster their active ingredient, compared to their bigger counterparts, causing the burst effect[3,4]. Today, amongst all existing techniques to produce highly monodisperse microspheres with an excellent reproducibility and a minimum of waste, the microfluidic droplet technology appears as the most relevant[4–8].

Different criteria must be considered when degradable materials are involved for biomedical applications and were already discussed in the introduction. Biocompatible and (bio)degragrable aliphatic polyesters, with a wide range of physical properties in terms of crystallinity, mechanical stress and degradation time, are already successfully applied in a wide range of biomedical applications, such as drug delivery carriers or in tissue engineering[1,9–14].

The drug release from these microspheres can occur through different pathways, notably by diffusion or upon degradation or erosion of the polymer matrix. Drug release profiles are therefore highly dependent on polymer characteristics, particularly hydrophilicity, crystallinity and free volume, as already discussed in the introduction[15,16,17,18]

In this context, polyphosphoesters appear to be prime candidates for potentially accelerating drug release from aliphatic polyester-based microspheres and have already been successfully applied for the elaboration of drug loaded nanocarriers or hydrogels for drug-delivery applications[19–24]. PPEs are characterized by a low T_g (≈-60°C) with adjustable hydrophilicity thanks to the length of the pendant alkyl chain[25] granting a tunability of the degradation rate[7,19]. Furthermore, these PPEs are efficiently synthesized by ring-opening polymerization, like conventional aliphatic polyesters, allowing the synthesis of well-defined block copolymer by sequential copolymerization with D,L-lactide[26,27].

This work aims at reporting on the addition of poly(butenyl phosphate)-block-poly(L-lactide (PBEP-*b*-PLLA) block copolymer PLLA microspheres formulation and to studied its impact on the encapsulation of a model active pharmaceutical ingredient (API), namely budesonide. These PPE/PLLA blend microspheres are formulated by microfluidic technique and compared to PDLLA and PLGA microspheres formulated under similar conditions for the sake of comparison. A size range between 50µm and 100µm is aimed because such microspheres exhibit a release profile that is more sigmoidal compared to smaller particles, which is more suitable for sustained release[28]. The impact of the PPE-based additive on API encapsulation efficiency and release profile is reported, as well as the cytotoxicity evaluation of these new microspheres.

II.2 Experimental section

II.2.1 Materials

2-Chloro-3-oxo-1,3,2-dioxaphospholane (COP, TCI), methanol (MeOH, VWR), calcium hydride (CaH_2, Aldrich), Ethyl acetate (AcOEt, Fisher), dimethylformamide (DMF, Fisher), poly(vinyl alcohol) (PVOH, Mowiol 8-88, M_w = 67 Kg/mol, Merck), poly(lactide-*co*-glycolide) (75:25, M_w 76-115 Kg/mol, PLGA, Merck) and poly-L-(lactide) (M_n 20 Kg/mol, PLLA, Merck) were used as received. L-Lactide (L-LA, Aldrich) was recrystallized 3 times in anhydrous toluene before use and stored under inert atmosphere. 3-buten-1-ol (Aldrich), benzyl alcohol (Aldrich), triethylamine (TEA, Aldrich) and 1,8 diazobicyclo[5.4.0]undec-7-ene (DBU, Aldrich) were dried

over calcium hydride at room temperature, following by distillation under reduced pressure just before use. Tetrahydrofuran (THF, VWR), toluene (VWR), dichloromethane (CH_2Cl_2, VWR) were dried under molecular sieves. 1-[3,5-bis (trifluoromethyl)phenyl]-3-cyclohexyl-thiourea (TU) was synthesized according to a described method [29]. Poly-D,L-lactide (PDLLA, Purasorb® PDL04, η_{inh}= 0.4dl/g) was kindly provided by Corbion.

II.2.2 Synthesis of PBEP macroinitiator

925 mg (2.5 mmol) of TU was transferred in a round bottom flask and dried by three azeotropic distillations with anhydrous toluene. 3 g (17 mmol) of BEP (synthesis reported elsewhere[25]) was added in the flask containing the TU and the system was put under vacuum during 15 min. After addition of 10mL of anhydrous CH_2Cl_2, 0.1mL of freshly distilled benzylic alcohol (0.9 mmol) was added under N_2 atmosphere. The mixture was cooled down to 0°C and 0.4mL (2.6 mmol) of DBU was finally introduced under a N_2 atmosphere with a syringe equipped with a stainless-steel capillary. The reaction medium was stirred at 0°C for 30 min. After concentration of the solution under vacuum, the copolymer was precipitated in cold diethyl ether. After decantation, the recovered copolymer was dissolved in methanol and dialyzed against methanol (MWCO = 1 kDa) overnight in order to remove impurities. After evaporation of methanol under vacuum, the copolymer was collected and characterized by NMR and SEC analyses.

^{1}H NMR (CDCl3) δ= 7.5 (m, 5H, aromatic protons), 5.8 ppm (m, 15 H, $–CH_2–C\mathbf{H}=CH_2$) ,5.1 ppm (m, 30 H, $C\mathbf{H}_2=CH-CH_2$), 4.25 ppm (m, 90 H, $O–C\mathbf{H}_2–C\mathbf{H}_2–O$ and $O-C\mathbf{H}_2-CH_2-CH=CH_2$ of BEP), 2.41 ppm (m, 30 H, $O–CH_2–C\mathbf{H}_2–CH=CH_2$)

^{31}P NMR (CDCl3) δ= -1.36 ppm.

Mn(^{1}H NMR) = 2700 g/mol, Đ = 1.5 (SEC).

II.2.3 Synthesis of PBEP-*b*-PLLA

2.15 g (0.8 mmol) of PBEP macroinitiator and 450 mg (1.2 mmol) of TU were transferred in a round bottom flask and dried by three azeotropic distillations with anhydrous toluene. 4.1 g (28.4 mmol) of freshly recrystallized L,L-LA was added in the flask and the system was put under vacuum during 15 min. After addition of 15mL of anhydrous CH_2Cl_2, the solution was placed in a bath at 25°C and 0.6mL (0.4 mmol) of freshly distilled DBU was finally introduced under a N_2 atmosphere with a syringe equipped with a stainless-steel capillary. The reaction medium was stirred at 25°C for 20 min. After concentration of the solution under vacuum, the copolymer was precipitated in cold diethyl ether and recovered by filtration and dried under vacuum.

^{1}H NMR ($CDCl_3$) δ= 7.5 (m, 5H, aromatic protons), 5.8 ppm (m, 15 H, –CH_2–C**H**=CH_2) ,5.1 ppm (m, 30 H, C**H$_2$**=CH-CH_2 + m, 82 H, C**H**-O), 4.25 ppm (m, 90 H, O–C**H$_2$**–C**H$_2$**–O and O-C**H$_2$**-CH_2-CH=CH_2 of BEP), 2.41 ppm (m, 30 H, O–CH_2–C**H$_2$**–CH=CH_2), 1.55 ppm (d, 246 **H**, CH_3)

^{31}P NMR ($CDCl_3$) δ= -1.37 ppm.

M_n(^{1}H NMR) = 8600 g/mol, Đ = 1.9 (SEC).

II.2.4 General microspheres formulation process by microfluidics

II.2.4.1 First microfluidics device

Two 50mL syringes (Terumo) were filled with aqueous PVOH solution and placed in Chemyx Fusion 4000-X syringe pump. The 10mL syringe (Braun) was filled with polymer organic phase and placed in a Chemyx 6000-X syringe pump. Three 1/16'' PFA tubing (IDEX (1632L)) were connected to each syringe thanks to a 1/16'' connector (IDEX XP-161) and a luer adapter (IDEX P658). These three tubes were connected together in a cross-junction (IDEX P722). The two aqueous tubes were connected perpendicularly to the organic phase tube. The 4th connection was the outlet pipe in PFA (Swagelock, PFA-T2-030-100). This fourth tubing was connected to the cross-junction connection (Idex, XP-131) .

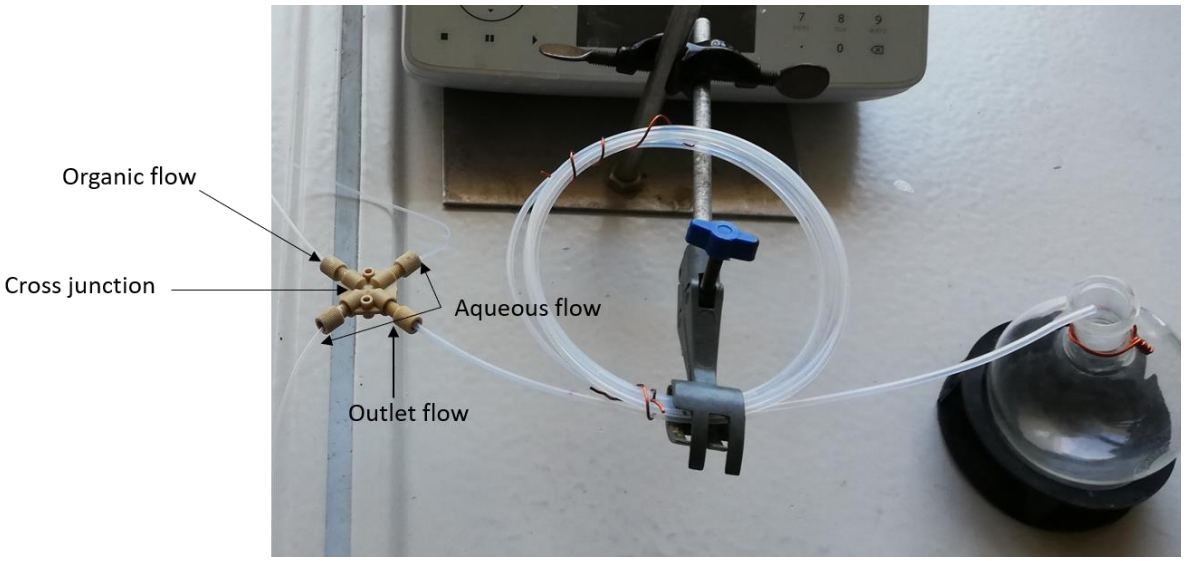

Figure 1 : Microfluidic cross-junction used to formulate microspheres

II.2.4.2 Second microfluidics device

A Y-junction device, provided by Sirris (Figure 2), was used instead the cross-junction for most of the experiments. All the tubing, pumps, connectors, syringes and adapters remain exactly the same.

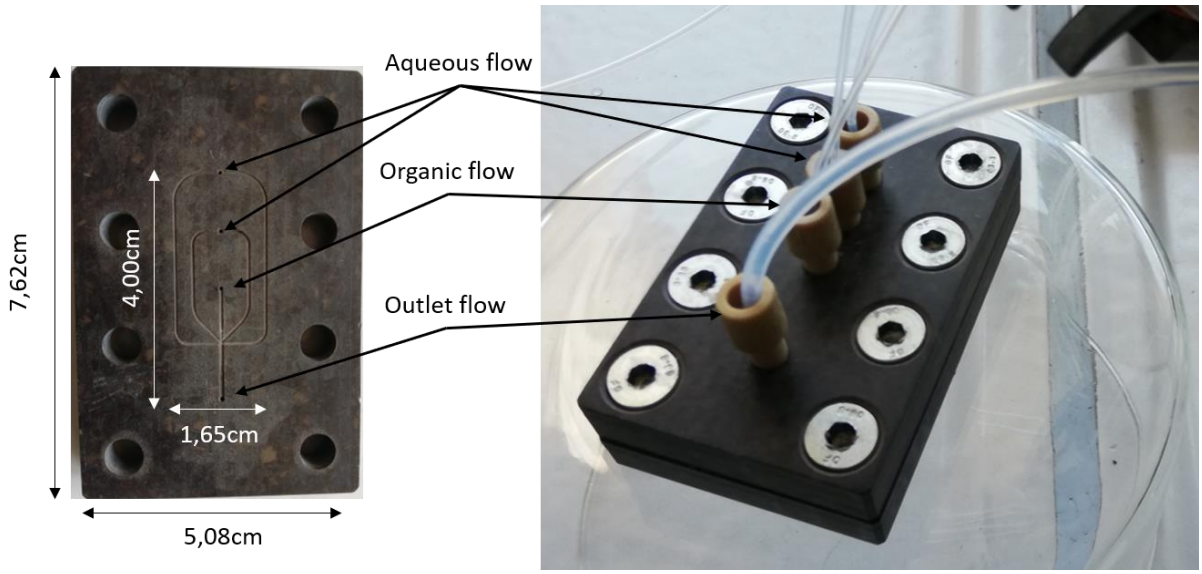

Figure 2 : Microfluidic core-shell device used to formulate microspheres

II.2.5 Formulation of PDLLA, PLLA and PLGA particles

Empty microspheres

Typically, 500 mg of PDLLA or PLGA was dissolved in 9.5 g of AcOEt and 500 mg of PLLA was dissolved in 9.5 g of CH_2Cl_2. The polymer solution, freshly heated at 70°C for 30sec) was then transferred in a 10mL syringe. A 2w% PVOH aqueous solution was transferred into two 50mL syringes. Once syringe drivers were set up, the system can run following the selected parameters (listed in table 2). Microspheres were collected in a 250mL round-bottom flask under gentle stirring containing a small amount of PVOH solution. Microspheres were then washed three times with MilliQ water in order to remove all the PVOH stabilizer, dried by freeze-drying before to be analyzed by scanning electron microscope.

Budesonide loaded particles

The formulation protocol is exactly the same excepted the addition of 100 mg of budesonide in the polymer solution.

II.2.6 Formulation of 80:20 (PLLA: PBEP-*b*-PLLA), 45:55 (PLLA: PBEP-*b*-PLLA) and PBEP-*b*-PLLA particles

Empty microspheres

For each formulation, a 500 mg of polymer mix was dissolved in 9.5 g of CH_2Cl_2 and transferred in a 10mL syringe. Two 50mL syringes were filled with a 5w% or a 2w% PVOH aqueous solution. Once syringe drivers were set up, the system can run following the selected parameters. Microspheres were collected in a 250mL round-bottom flask under gentle stirring containing a small amount of PVOH solution. Microspheres were then washed three times with MilliQ water in order to remove all the PVOH stabilizer, then they were freeze with liquid nitrogen and placed on a lyophilizator at -48°C under a pressure of 0.5 mbar before to be analyzed by scanning electron microscope.

Budesonide loaded particles

The formulation protocol is exactly the same excepted the addition of 100 mg of budesonide in the polymer solution.

II.2.7 Drug-loading (DL) and encapsulation efficiency (EE) determination

A precise amount of microspheres (typically 5.0mg) were dissolved in 5mL of DMF and then submitted to ultrasound for 30sec. Then, the solution was diluted 10 times with the mobile phase (MeOH:H_2O 35:65), filtrate on Acrodisc 0.2µm filters, and the concentration of budesonide was determined by High-Performance Liquid Chromatography (HPLC) method. The HPLC equipment consisted of a Waters equipment composed of an Autosampler 2707, a Controller 600 and a PDA 996. Briefly, budesonide concentration was analyzed using a Polaris C18-A end-capped analytical column with particles of 5 µm (L 250 mm, d.i. 4.6 mm) and a mobile phase in an isocratic mode composed of a mixture of water and methanol (35/65 % v/v) at a flow rate of 1 mL/min. 50 µL of the samples were injected at 30°C and the run time was set to 15 min (detection wavelength was 245 nm) and the retention time was 11min. This method was developed previously by the Brigitte Evrard's group[30,31]

Thanks to a calibration curve (calibration solutions consisted of 6 concentrations: 100, 20, 10, 5, 0.5 and 0.25 µg/mL) with a R^2=0.999, it was possible to quantify the amount of budesonide in the microspheres. Then, the DL and the EE can be calculated with these formulae :

$$DL\ (\%) = \left(\frac{m_{\ loaded\ budesonide}}{m_{microparticles}}\right) \text{x } 100\ ; \qquad EE\ (\%) = \left(\frac{Experimental\ DL}{Targeted\ DL}\right) \text{x } 100$$

II.2.8 Drug-release kinetic analysis

Drug-release measurements were realized in triplicates for each sample (PDLLA, PLGA, 80:20, 45:55 and copolymer). A precise amount of each batch of microspheres (between 15mg and 30mg) was placed in a 30mL centrifugation vial. 10 mL of PBS buffer 0.1M (pH=7.4)

containing 0.5w% of Tween 80 as surfactant were added in the vial before being transferred in an incubator at 37°C. After 2h of release, all the solution was removed and collected in a glass vial in order to be filtrated on Acrodisc 0.2µm and analyzed by HPLC. 10mL of a fresh buffer was then added in the centrifugation vial and the kinetic study continues. The release medium analysis was performed after 2h, 4h, 6h, 24h, 48h, 72h, 1 week, 2 weeks, 3 weeks, 4 weeks and 6 weeks. After the kinetic point at 6h, 15mL of PBS buffer solution was added instead of 10mL in order to be sure to stay in the SINC conditions.

II.2.9 Cytotoxicity assays

Bovine fibroblast (Bfb) cells and Human umbilical vein endothelial cells (HUVEC) were seeded in 96 well plates at a concentration of 5000 cells per well. The plates were incubated for 72 hours after which different concentrations of each formulated microparticles (PLA, PLA + Budesonide, PLGA, PLGA + Budesonide, PBEP-b-PLLA and PBEP-b-PLLA + budesonide) suspensions were added. Suspensions were made at a concentration of 20.000 beads/mL by adding to each formulated microparticles batch medium without any FBS or growth factors. These suspensions were incubated for 24 hours at 37˚C, 5% CO2. Prior to addition to the cells, suspensions were centrifuged and supernatant was separated from the pellet. The pellet was resuspended in culture medium. The plates were incubated with different concentrations of resuspended beads (direct assay) or bead supernatant (indirect assay) for 24 hours at 37˚C and 5% CO2. Cytotoxicity was determined with a live/dead staining. In short, cells were stained with Hoechst 33342 (3.25 µM) and Ethd-1 (650 nM) and imaged with a BD pathway 855 high content analyzer. The images were analyzed with MetaXpress (Molecular Devices) software. Viable cell number per well was calculated by subtracting the dead cells (Ethd-1 positive nuclei) from all the cells (Hoechst positive nuclei) present in the wells. The average amount of viable cells in the culture control wells (wells that underwent the same treatment as the conditions) was set to 100% and the percentage of viable cells per condition was determined.

II.2.10 Characterization techniques

^{1}H and ^{31}P nuclear magnetic resonance (NMR) spectra were recorded on a Bruker Avance 400 apparatus at 25 °C at 400MHz in the Fourier-transform (FT) mode and using $CDCl_3$ as solvent.

The surface and the morphology of the formulated microspheres were characterized by scanning electron microscopy (SEM) images recorded with a FEI Quanta 600 apparatus. SEM pictures were used to determine the mean microspheres diameter and the polydispersity of each sample. Typically, 50 microspheres of batch were analyzed by ImageJ software in order to calculate the mean diameter (d), the standard deviation (θ) and the polydispersity (PDI) index according the following equation.

$$PDI = \left(\frac{\theta}{d}\right)^2$$

Glass transition temperature (T_g) and melting temperature (T_m) were determined by dynamic scanning calorimetry (DSC) on a TA Instruments DSC250. Approximately, a sample of 5.0mg was heating up to 200°C with a rate of 10°C/min, cooled down to 0°C with a rate of 10°C/min before being heated with a rate of 10°C/min . The T_g and T_m were recorded on the second heating step.

II.3 Results and discussion

II.3.1 Flow formulation of microspheres of aliphatic polyesters

Microfluidic technique (MF) enables the manipulation of microflows in microchannels to produce uniform emulsion droplets. The principle is the same as the formation of an O/W emulsion except that the internal phase is pushed in the continuous phase by a microchannel system thanks to syringe pumps at constant-flow with an excellent flow rate control (Figure 3). The aqueous phase contains an emulsifier, the PVOH, at a concentration varying between 2w% and 5w% which is a common concentration found in the literature[6,32]. The organic phase

contains the polymer at a concentration of 5w% in ethyl acetate, which is a good solvent of the PDLLA and is a class 3 solvent which is compatible if biomedical applications are aimed. These solutions were pushed in different capillaries and arrive in a cross-junction in which microdroplets of organic solution were formed by shearing and capillary forces. The aimed microspheres size must be in the 50µm to 100µm range to have a more suitable sustained release.

Based on reported works, the selected size of the cross-junction device and accessible flow rates of the pumps were suitable to target this particles size range[32–34]. Once the droplet was formed in the tubing, the ethyl acetate can leave the droplet thanks to its partial miscibility with water and at the end of the formulation process, completely solid microspheres were recovered.

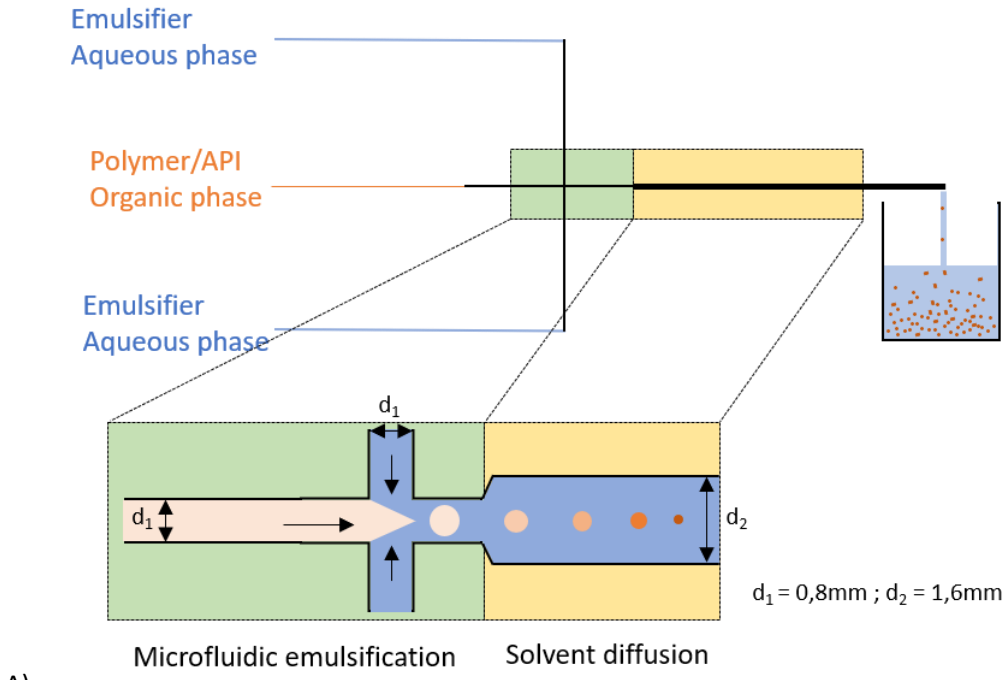

A)

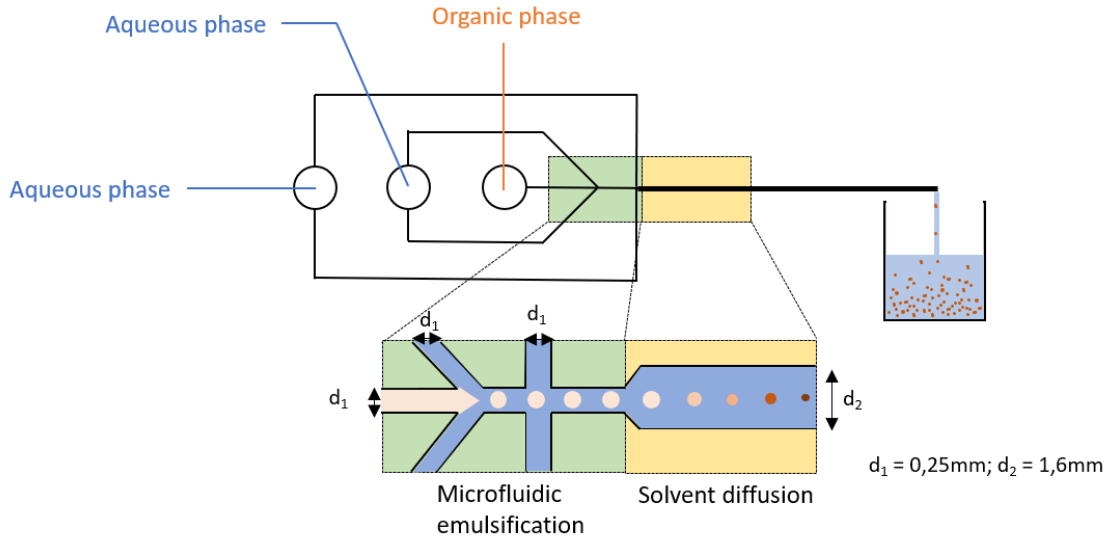

B)

Figure 3 : Scheme of the microfluidic devices used for formulations: A) Cross-junction and B) Y-junction devices

Microspheres formulation was first tested with commercially available PDLLA in order to determine the impact of the surfactant flow rate on the droplet size. The concentration in PDLLA in the AcOEt solution equals 5wt% with a flow rate fixed at 0.025mL/min and the concentration of the PVOH in the aqueous phase was 2wt% with a flow rate varying between

0.25mL/min and 1mL/min for both PVOH aqueous solution inlet. The results as well as the formulation conditions are listed in Table 2.

Table 1 : Formulation parameters used for PDLLA microspheres formulation with the cross-junction microfluidic device and diameter and PDI of the collected microspheres determined by SEM analysis.

Entry	PVOH concentration (wt%)	PVOH flow rate (mL/min)	Polymer concentration (wt%)	Polymer flow rate (mL/min)	Mean size (µm)	PDI
1	2	0.5	5	0.025	155.1	$9.3*10^{-4}$
2	2	1	5	0.025	130.6	$8.7*10^{-4}$
3	2	2	5	0.025	98.6	$5.1*10^{-3}$
4	2	0.5	5	**0.05**	165.6	$1.2*10^{-2}$
5	2	1	5	**0.05**	135.5	$4,6*10^{-3}$
6	2	2	5	**0.05**	103.5	$2.3*10^{-3}$
7	**5**	0.5	5	0.025	84.7	$3,6*10^{-2}$
8	**5**	1	5	0.025	63.4	$1,7*10^{-2}$
9	**5**	2	5	0.025	47.1	$1,4*10^{-2}$
10	2	0.5	**2**	0.025	109.9	$3,3*10^{-2}$
11	2	1	**2**	0.025	88.3	$1,3*10^{-2}$
12	2	2	**2**	0.025	70.1	$4*10^{-3}$

A microsphere sample is considered as monodisperse if the PDI is below 0.1[35]. With the cross-junction flow droplet generation system, all collected particles exhibit remarkable monodispersity with a PDI far below 0.1 (Table 2). Interestingly, increasing the surfactant flow rate decreases the microspheres size as illustrated by Figure 4 and Table 2, which was explained by the increase of shearing forces at higher flow rates leading to earlier droplet separation which is in line with other studies[32,36].

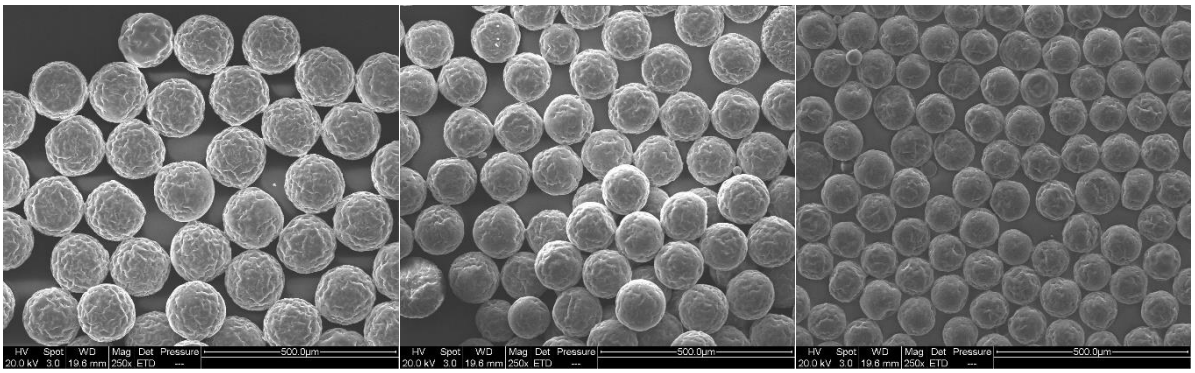

Figure 4 :SEM images of PDLLA particles formulated from a 5wt% solution in AcOEt (flow rate 0.025mL/min.) with 2wt% PVOH aqueous solution in a cross-junction device with a flow rate of a) 0.5mL/min; b) 1mL/min and c) 2mL/min

Increasing polymer flow rate to 0.05mL/min slightly increases the particles size (Table 1, entries 4-6). In that case, the PDI increases which can be explained by the change of droplet formation regime from a dripping to a jetting regime when the flow rates of both the continuous and the discontinuous phases become closer[37].

Smaller particles were obtained at higher concentration of emulsifier (Table 1, entries 7-9) due to the reduction of the interfacial tension between the organic and the aqueous phases leading to the stabilization of smaller droplets [38,39]. In this case, PDI increases but remains well below 0.1. Finally, decreasing the PDLLA concentration in the organic phase from 5wt% to 2wt% leads to smaller particles ranging from 70 to 110µm (Table 1, entries 10-12). Indeed, with higher polymer concentration, the saturation state of the polymer in the solvent is more easily reached and favor a faster precipitation restrict the droplets shrinkage, resulting in larger microspheres[32].

Considering all the collected results, the optimum conditions to formulate microspheres presenting the lowest PDI were 5wt% polymer solution with a flow rate of 0.025mL/min coupled with a 2wt% continuous phase. With these conditions, the size of the monodispersed particles is between 100 and 155µm depending on the flow rate of the emulsifier aqueous phase (Table 1, entries 1-3). These sizes were slightly higher than the targeted ones. Therefore, a Y-junction microchip was then considered.

When these optimized conditions were applied to the Y-junction microfluidic device (Figure 2), i.e. having a smaller angle between the aqueous and organic phases channels (45° instead of 90°) the particles were smaller (Entries 1-3 of tables 2 and 3). This is explained by the additional horizontal component of the aqueous flow in this microchip geometry which makes easier the droplets separation leading thus to smaller droplets generation and smaller particles formulation[40]. The flow rate of the aqueous phase was exactly the same for each syringe.

The PDI remains very low with this device and the particles size is controlled between 55 to 70µm by adjusting the aqueous phase flow rate which fits perfectly with the targeted values. Therefore, this Y-junction device will be selected for all the following experiments.

Table 2 : Formulation parameters used for microspheres formulation with the Y-junction microfluidic device the PVOH concentration equals 2w% and the organic flow rate equals 0.025mL/min for each formulation process.

Entry	PVOH flow rate (mL/min)	Aliphatic polyester	Polymer/API concentration (wt%)	Size (µm)	PDI
1	0.5	PDLLA	5/0	71.1	$3.5*10^{-3}$
2	1	PDLLA	5/0	69.1	$2.5*10^{-3}$
3	2	PDLLA	5/0	55.7	$3*10^{-3}$
4	0.5	PDLLA	5/1	113.7	$2.5*10^{-3}$
5	1	PDLLA	5/1	78.0	$3.5*10^{-3}$
6	2	PDLLA	5/1	69.8	$6.2*10^{-3}$
7	1	PLGA	5/0	46.5	$8*10^{-3}$
8	1	PLGA	5/1	71.7	$2.5*10^{-3}$
9	1	PLLA	5/1	71.5	$5.1*10^{-3}$
10	1	PLLA	5/1	72.8	$9.8*10^{-4}$

II.3.2 Formulation of PDLLA microspheres with budesonide

The optimized formulation conditions were then applied for the encapsulation of an API in PDLLA microspheres. Budesonide was chosen as the API because it is a drug commonly used as an anti-inflammatory that has already been encapsulated in PLGA and PLA[41–43]. Advantageously, this API is soluble in AcOEt and is easily quantified by HPLC analysis. The polyester concentration was kept constant at 5wt% and 1wt% of budesonide relative to the polymer was added. This corresponds to a maximum drug loading of 16.7wt%.

In presence of budesonide, the same trend was observed: higher is the flow rate, smaller are the particles. Nevertheless, the particles size was increased by the addition of the API due to the increasing of solid compound dissolved in each microdroplet. Controlling the aqueous solution flow rate from 0.5 to 2 mL/min allows to reach monodispersed particles with a size in the range between 70 and 115µm (entries 4-6, Table 2). The microspheres of entry 5 being in the targeted size range (between 50 and 100µm), they were selected to further determine the drug loading (DL) and encapsulation efficiency (EE) by HPLC dosing.

For this purpose, 5.0 mg of Budesonide loaded PDLLA microspheres (Entry5, Table 3) microspheres were dissolved in DMF and diluted 10 times with the HPLC mobile phase (MeOH/H_2O; 35/65 in volume). After the analysis and quantification according, the calibration curve generated by successive dilution of a Budesonide solution in the HPL mobile phase, a DL of 11.8% ± 0.3% and an EE of 71% ± 1.8% were determined for the PDLLA microspheres formulation (entry 5, Table 3) which is in line with reported data for different encapsulation techniques[41,44].

II.3.3 Formulation of PLGA particles with and without budesonide

In order to determine the impact of the nature of the microsphere matrix on the DL and EE of Budesonide, PLGA microspheres were formulated in the same conditions as previously applied to PDLLA microspheres formulation (Table 3, entries 7-8). Indeed, PLGA is

known to degrade faster than PDLLA due to higher hydrophilicity which may have also an impact on Budesonide encapsulation.

As previously observed and discussed, the Budesonide loaded PLGA microspheres were highly monodispersed and perfectly spherical with a size similar to Budesonide loaded PDLLA microspheres obtained with the same formulation conditions,. The DL was equal to 10.6% ± 0.03%, corresponding to an EE of 64% ± 0.2%, which was slightly smaller than for PDLLA. Nevertheless, this is in the range of previously reported data on the encapsulation of budesonide in PLGA[43,45,46].

II.3.4 PBEP-*b*-PLLA copolymer microspheres

In order to increase the hydrophilicity of the formulated PLGA and PDLLA microspheres, and thus their degradation rate, the addition of biocompatible and hydrophilic polyphosphoester polymers (PPE) was investigated (scheme 1). For this purpose, PBEP bearing a butenyl side chain was selected amongst the wide diversity of phosphoesters reported in the literature for its moderate hydrophilicity brought by a four-carbon unsaturated side-chain. Moreover, the unsaturation makes possible additional π-interactions with the API which could enhance the drug-loading and the encapsulation efficiency. Since the PBEP homopolymer is amorphous and has a T_g of around -60°C, its direct addition into microspheres is impossible as it will flow out with time leading to particle aggregation. PBEP was therefore combined with a PLLA block to bring crystallinity to the copolymer, converting the viscous liquid PBEP into a plastic diblock at room temperature and so enabling the potential formation of stable microspheres.

The copolymer synthesis was inspired from literature data. The PBEP block was firstly synthesized by ROP of the BEP monomer in CH_2Cl_2 in the presence of TU/DBU catalytic system using benzylic alcohol as initiator. Then, it was used as macroinitiator to polymerize L,L-Lactide in similar conditions. After 20min, the copolymer was recovered by precipitation and dried before being used for microspheres formulation. The expected structure was confirmed by ^{1}H-NMR (Figure S1) giving the composition of 31wt% of PBEP and 69wt% of PLLA. The block

structure was confirmed by the shift of the SEC peak towards higher molar mass after addition of the LLA monomer (Figure S2).

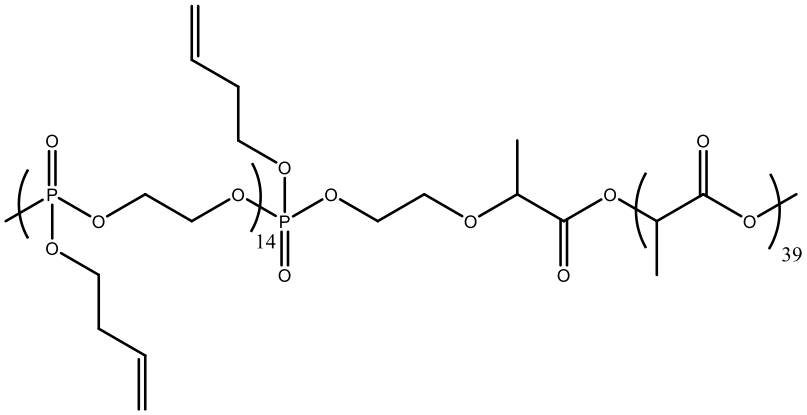

Scheme 1 : Structure of the polyphosphoester-polyester diblock copolymer

DSC analysis performed on the synthesized PBEP-*b*-PLLA copolymer with a 39:61 composition shows only one T_g of 16.5°C and a T_m of 177°C with a crystallinity rate of 1% (Figure S3). The single T_g which is intermediate to that of the two homopolymers indicates that the PBEP segment is miscible with PLLA. The introduction of the PBEP segment thus lowers the T_g of the pure PLLA and decreases the crystallinity rate. However, at this composition, the copolymer is a solid at room temperature even if the crystallinity rate is low and the T_g at 16.5°C, which make it suitable for microspheres formulation.

The Y-junction microfluidic device was thus used to formulate the block copolymer. This copolymer being not soluble in AcOEt, CH_2Cl_2 was used as organic phase. Different formulation conditions were tested varying the solutions flow rates and concentrations. The results are reported in Table 4.

Table 3 : Formulation conditions used for the microfluidic of PBEP-b-PLLA copolymer microspheres by using Y-junction chip.

Entry	PVOH concentration (wt%)	PVOH flow rate (mL/min)	Copolymer[(1)]/API[(2)] concentration (wt%)	Copolymer solution flow rate (mL/min)	Size (µm)	PDI
1	2	2	5/0	0.025	44.2	$7.2*10^{-3}$
2	2	1	5/0	0.025	58.9	$1.6*10^{-2}$
3	2	2	5/0	0.0125	49.2	$8.4*10^{-3}$
4	2	1	5/0	0.0125	39.6	$2.3*10^{-2}$
5	5	2	5/0	0.025	32.3	$1.1*10^{-1}$
6	2	2	5/1	0.025	/	/
7	5	2	5/1	0.025	46.6	$3.4*10^{-2}$

(1) Copolymer concentration in DCM

(2) API content relative to the copolymer

For most conditions, well-defined and highly monodisperse microspheres of PBEP-b-PLLA were successfully obtained presenting comparable size to polyester microspheres previously described, except for the formulation conditions with an emulsifier equal to 5wt% (Figure 5a and b). However, the addition of Budesonide in the copolymer organic phase led to the formation of highly polydisperse, porous and destroyed microspheres (entry 6, Table 4 and Figure 5c), suggesting that they were not enough stabilized by the PVOH 2wt% continuous aqueous phase. Increasing the PVOH concentration to 5wt% improved the microspheres stability; particles with a size of 46.6µm and a PDI of $3.4*10^{-2}$ were collected (Figure 5d) and turned to be non-porous which is an important parameter to control the sustained release.

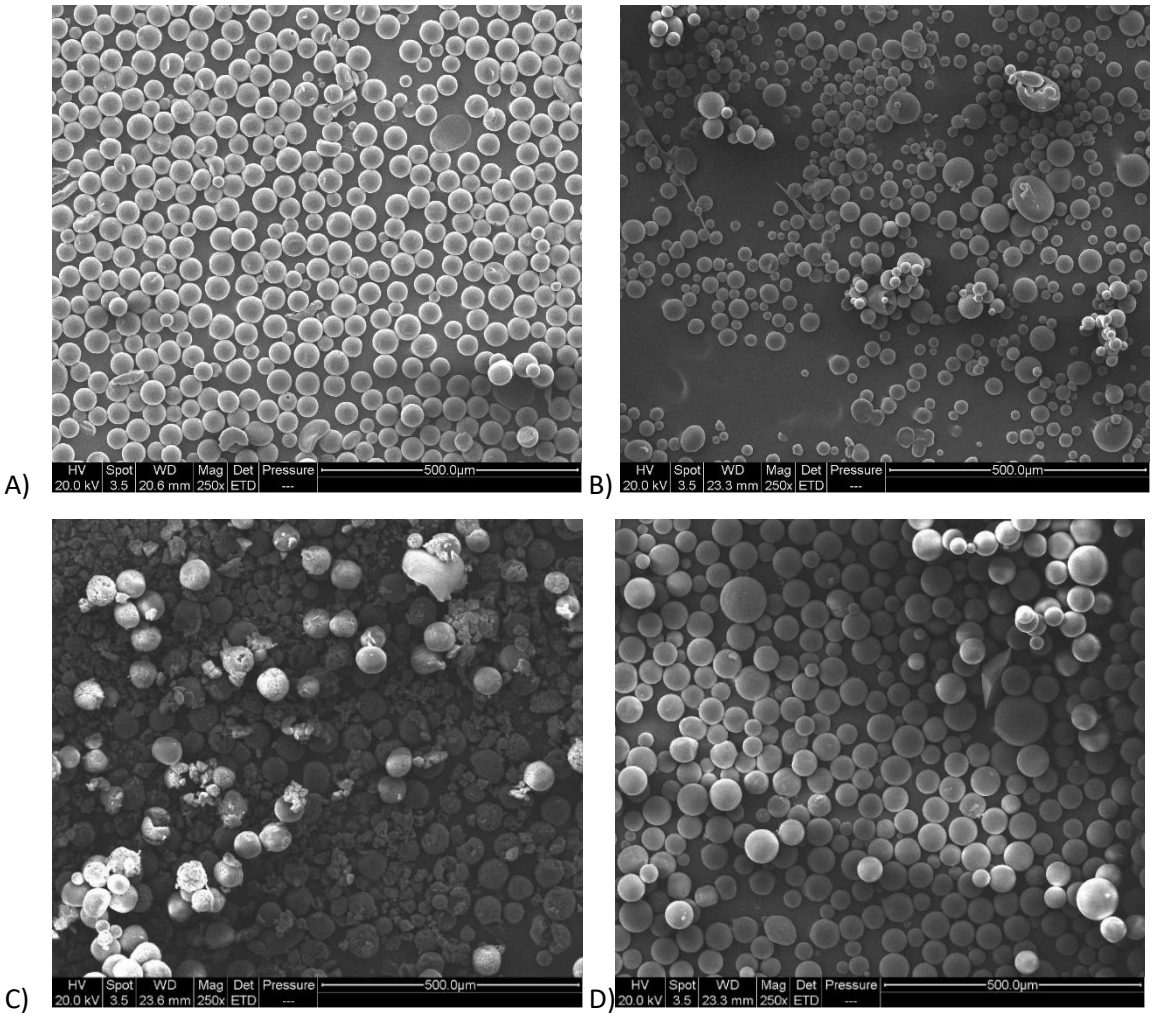

Figure 5 : SEM images of copolymer microspheres without budesonide: a) PVOH 2wt%; b) PVOH 5wt%. and with budesonide: c): PVOH 2wt%; d): PVOH 5wt%.

II.3.5 Microspheres formulation based on blends of PLLA and PBEP-*b*-PLLA

As mentioned above, there is a full miscibility between PLLA and the PBEP-*b*-PLLA copolymer. Therefore, the glass transition temperature of the microspheres could be tuned by varying the composition of blends between commercially available PLLA and the PBEP-*b*-PLLA. So, the impact of the T_g on the drug loading and release profile could be investigated.

Table 4: Thermal properties of the pure PBEP-b-PLLA copolymers and two blends with PLLA as determined from DSC traces. The crystallinity ratio is determined for per gram of polymer and not only for the PLLA part with a $\Delta H_{melting}$ =123 J/g.

PBEP-*b*-PLLA/PLLA	T_g (°C)	T_m (°C)	Crystallinity ratio (%)
100:0	17	177	1.5
55:45	30	160	25
20:80	43	164	37

The two PLLA/PBEP-*b*-PLLA blends with composition of 45:55 (45w% of PLLA and 55w% in copolymer) and 80:20 were prepared by mixing both materials in DCM followed by solvent evaporation. These compositions were selected so that the resulting T_g surround the body temperature. Indeed, applying the Fox equation, these blends should exhibit a T_g of 32°C and 49°C respectively. DSC analysis of these blends shows a T_g of 30°C and 43°C, respectively (Figure SI3 and Table 5), which is in good agreement with the predicted values. DSC also reveals an increase of the blend crystallinity degree while increasing the PLLA content.

Microspheres of both blends containing budesonide were formulated in the same conditions as the pure copolymer, as summarized in table 6:

Table 5 : Formulation parameters for the production of microspheres of the two different blend compositions the PVOH concentration =2w% with a flow rate = 2mL/min.

Entry	**PLLA/PBEP-*b*-PLLA blend**	**Blend/API concentration (wt%)**	**Polymer/API flow rate (mL/min)**	**Size (µm)**	**PDI**
1	45:55	5/1	0.025	50.6	$3.9*10^{-3}$
2	80:20	5/1	0.025	59.8	$6.7*10^{-3}$

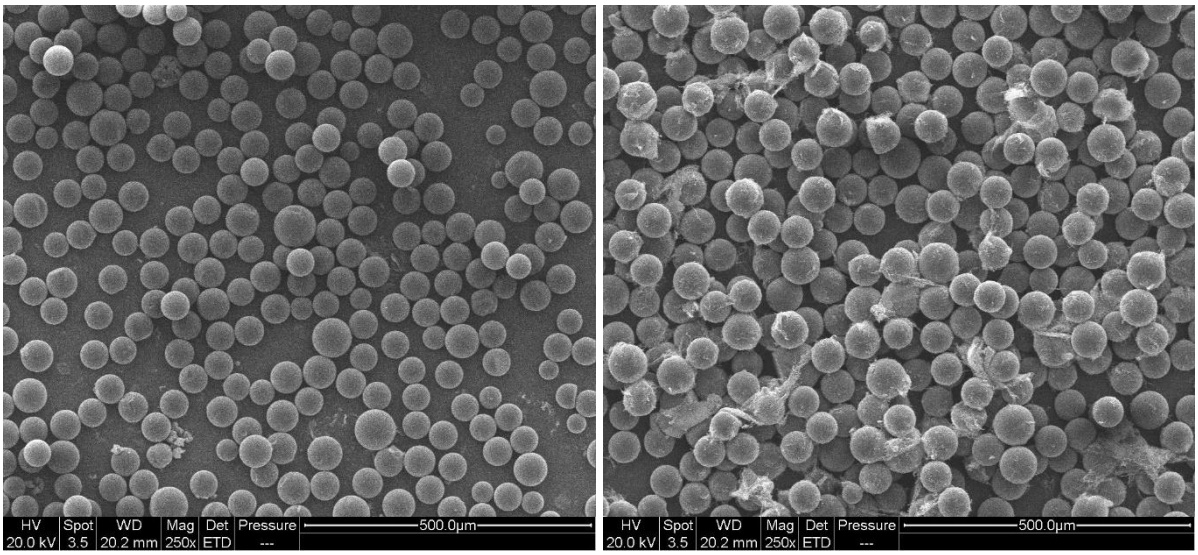

*Figure 6 : SEM images of PLLA:/PBEP-*b*-PLLA blend microspheres with budesonide. (Left 45:55 and right 80:20)*

DSC analysis were also performed on the Budesonide loaded blend microspheres. The incorporation of the Budesonide leads to significant shifts of the T_g, of 10°C for 80:20 microspheres (T_g 53.2°C) and about 18°C for the 45:55 blend (T_g 48.2°C). This anti-plasticizing effect induced by the budesonide could traduce a strong interaction of this API with the polymer chains of the blend. The impact being stronger for the 45:55 blend, the PBEP block appears particularly involved in these interactions. Accordingly, the crystallization of the blends involving PLLA chains, appears less affected by the presence of Budesonide. A melting temperature was still measured between 165°C and 170°C and the crystallinity rate reaches 45% for the 80:20 and 30% for the 45:55 formulated microspheres. The drug-loading and the release kinetic were then determined for all the three types of microspheres containing the PBEP. The results are gathered in Table 7.

Table 6 : Drug-loading and encapsulation efficiency for the different microspheres. The first column refers to the table and entry giving the formulation conditions applied to prepare the particles.

Table / entry	Type of microspheres	Solvent	Size (µm)	PDI	Drug-loading (%)	Encapsulation efficiency (%)
3 / 5	PDLLA	AcOEt	78.0	$3.5*10^{-3}$	11.8 ± 0.3	71 ± 1.8
3 / 8	PLGA	AcOEt	71.7	$2.5*10^{-3}$	10.6 ± 0.03	64 ± 0.2
3 / 9	PDLLA	CH_2Cl_2	71.5	$5.1*10^{-3}$	9.2 ± 0.3	55 ± 1.8
3 / 10	PLLA	CH_2Cl_2	72.8	$9.8*10^{-4}$	9.3 ± 0.4	56 ± 2.3
4 / 5	PBEP-b-PLLA	CH_2Cl_2	46.6	$3.4*10^{-2}$	$9.7 ± 4*10^{-3}$	58 ± 0.02
5 / 1	Blend 45:55	CH_2Cl_2	50.6	$3.9*10^{-3}$	9.3 ± 0.1	56 ± 0.6
5 / 2	Blend 80:20	CH_2Cl_2	59.8	$6.7*10^{-3}$	8.5 ± 0.2	51 ± 1.3

In order to complete the comparison, PLLA and PDLLA microspheres were also formulated in dichloromethane (DCM) following the same procedure. One can observe from Table 7 that the encapsulation efficiency was lower when the formulation was performed in CH_2Cl_2 rather than in AcOEt. This shows that the decrease of EE can be at least partly accounted for the solvent used for the formulation which requires different purification procedures. AcOEt is partially miscible to water and it is extracted in the aqueous phase very gently during the formulation step. Therefore, a simple filtration allows to collect the microspheres free from the organic solvent. In contrast, DCM is completely immiscible with water so that the microspheres remain swollen by DCM after filtration. Therefore, an additional evaporation step is required to remove it. This has been performed either under the fume hood at room temperature overnight or by rotavapor under reduced pressure at RT for 5 min. During this process, the budesonide can be partly extracted with the CH_2Cl_2. The encapsulation efficiency determined for microspheres purified by each extraction methods evidenced that both methods were quite equivalent (EE=54% by rotavapor and EE=55% under fume hood).

Remarkably, the incorporation of polyphosphoester in the polyester matrix does not influence the DL compared to 100% polyester microspheres. In fact, microspheres composed of 100% copolymer perform even better. The drug-loading and the encapsulation efficiency of microspheres containing polyphosphoester in their matrix were similar. A slight decrease was observed when the proportion of PLLA increases. This decrease can be attributed to the higher crystallinity of the matrix. Essentially, the active ingredient is primarily encapsulated in the non-crystalline region of the microsphere, while the crystalline region acts as a barrier for the drug[15,16].

II.3.6 Kinetics release profiles

Release profiles of the three types of microspheres containing various amounts of PBEP-*b*-PLLA were compared to the one of PDLLA and PLGA in the Figure 7. Clearly, the addition of the polyphosphoester to the polyester increases tremendously the drug-release rate. Even with a very small proportion of PBEP, as in the blend 80:20, where PBEP represents no more than 6.2wt% of the microspheres, the drug-release was much faster. The enhanced hydrophilicity of the PBEP backbone, when compared to polyester, along with its lower glass transition temperature (T_g) which increases free volume, accelerates the drug release mechanism through diffusion. Being more hydrophilic, the water can easier penetrate in the microspheres and extract the budesonide. Moreover, the T_g of the copolymer (16.5°C) is below the temperature of the release medium (37°C) and then the polymeric chains are very flexible which can favor again the diffusion of the API.

a)

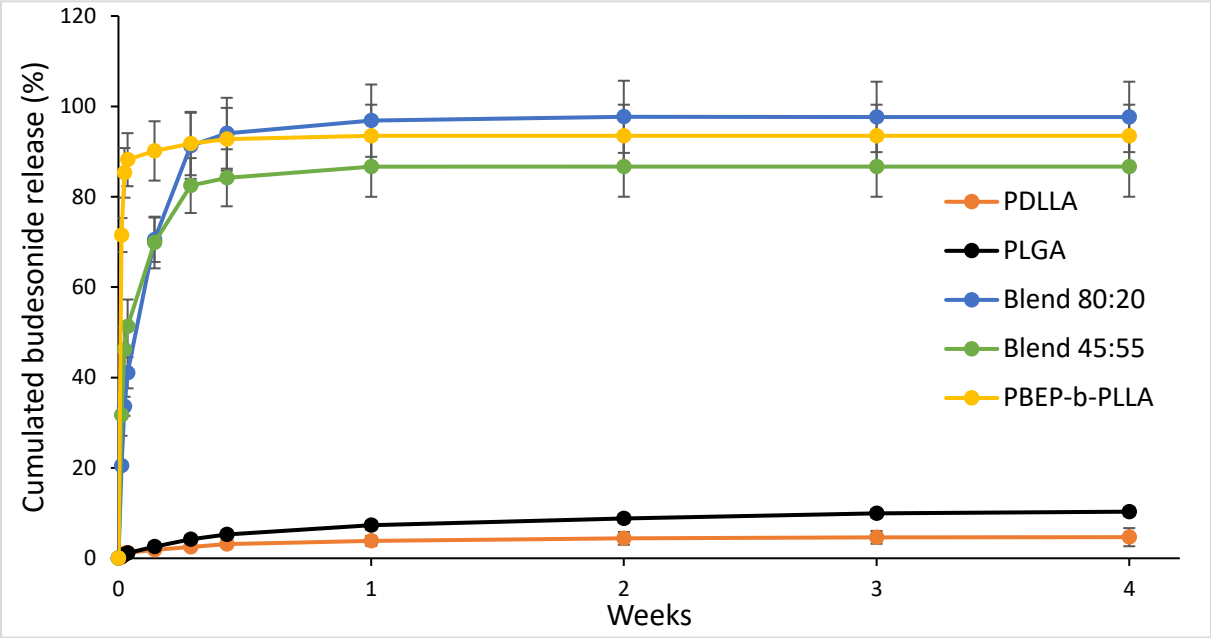

b)

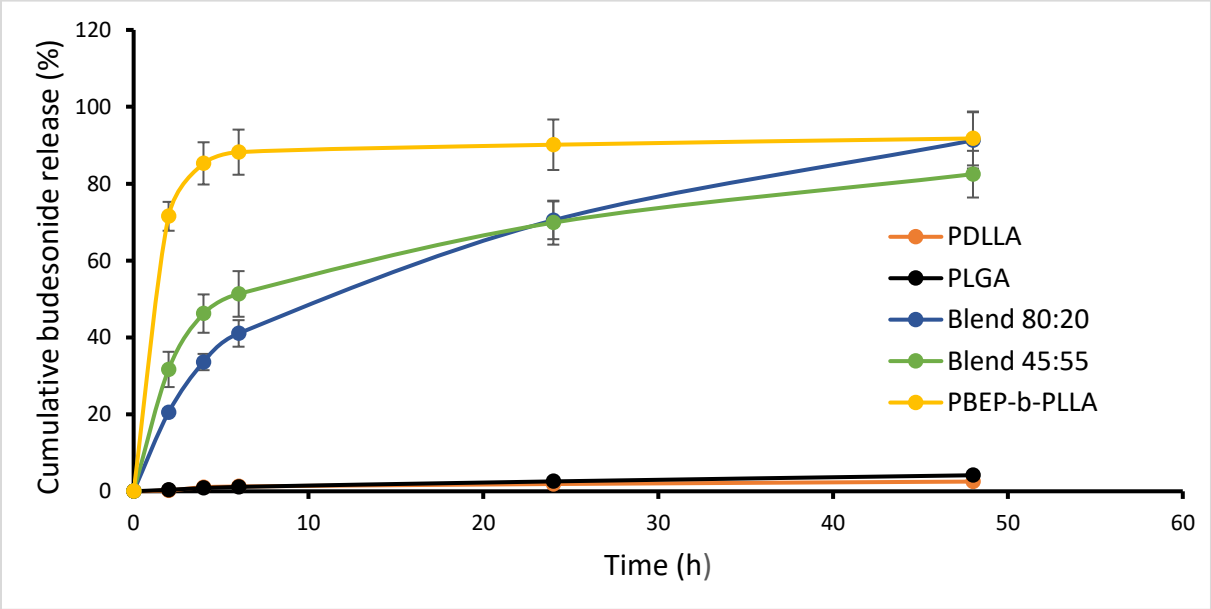

Figure 7 : Budesonide release profiles a) over 6 weeks b) during the first 48h from the different microspheres prepared by microfluidic.

Figure 7b illustrates the drug release patterns during the initial 48 hours. When examining the microspheres containing PBEP, the release profiles of budesonide exhibit some

variations. In the case of microspheres composed of 100% copolymer, the budesonide was rapidly released within less than 6 hours, whereas complete release takes place over the course of 48 hours for the other two compositions. Consequently, depending on the specific composition, the drug release kinetics can be adjusted to occur within a range of 6 to 48 hours.

II.3.7 Cytotoxicity assays

Cytotoxicity assays were performed to confirm the absence of toxicity. Different cytotoxicity tests were performed by direct or indirect contact between cells and by using two different primary cell types.

The first assay by indirect contact is reported on the figure 8 for bovine fibroblast and HUVEC cells.

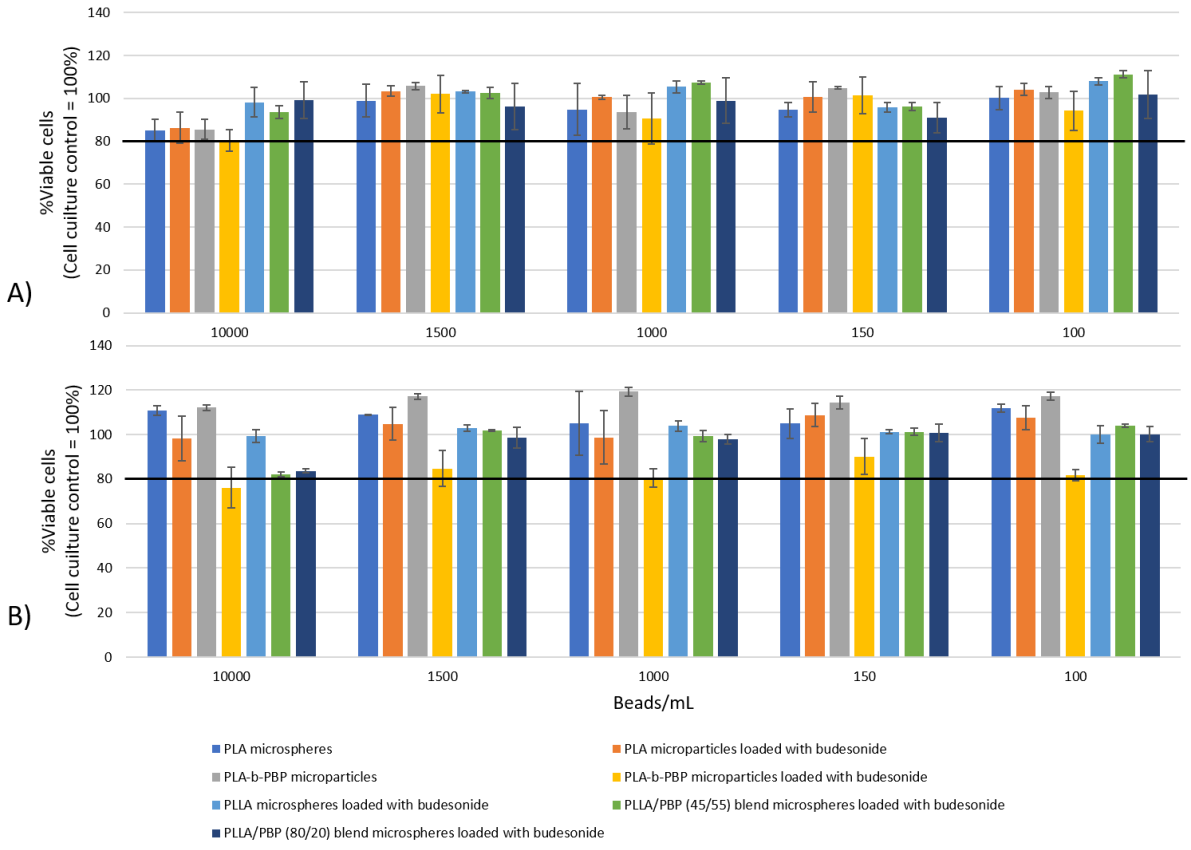

Figure 8 : Cytotoxicity tests by indirect contact between a) bovine fibroblasts or b) HUVEC and formulated microspheres

The Figure 8 shows that bovine fibroblasts as well as HUVEC cells were viable for all formulated microparticles. The cytotoxicity is slightly higher for the microspheres containing the copolymer at a 10.000 mg/mL concentration on HUVEC. This decrease in viability is caused by the budesonide that was faster released from these microspheres (Figure 7) and has more cytotoxic impact on HUVEC cells than on Bfb (Figure 9).

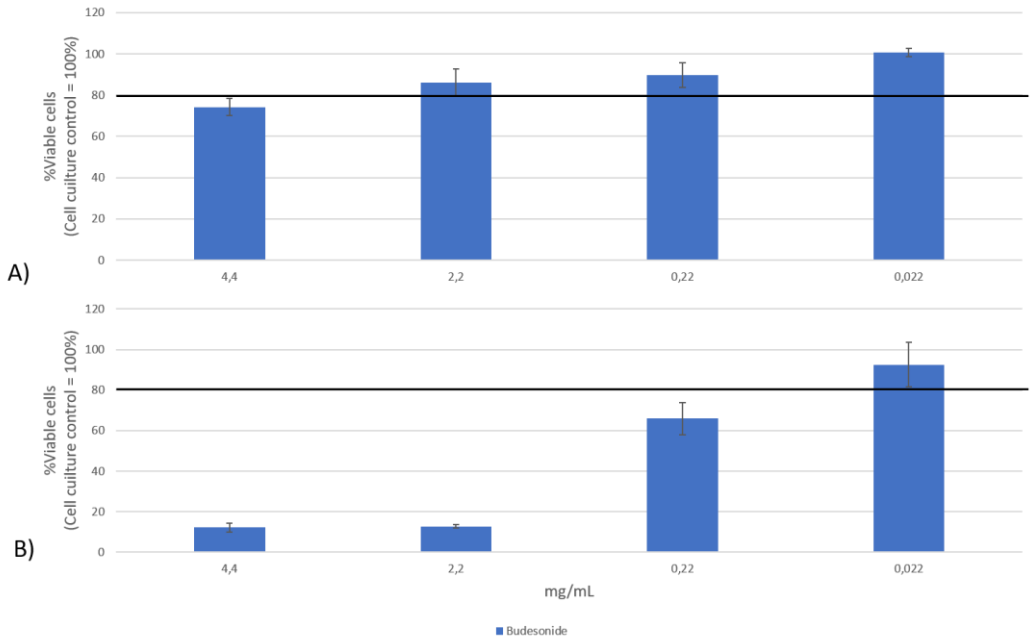

Figure 9 : Budesonide cytotoxicity tests on a) bovine fibroblasts and b) HUVEC

Cytotoxicity tests by direct contact between fibroblasts or HUVEC are shown in Figure 10.

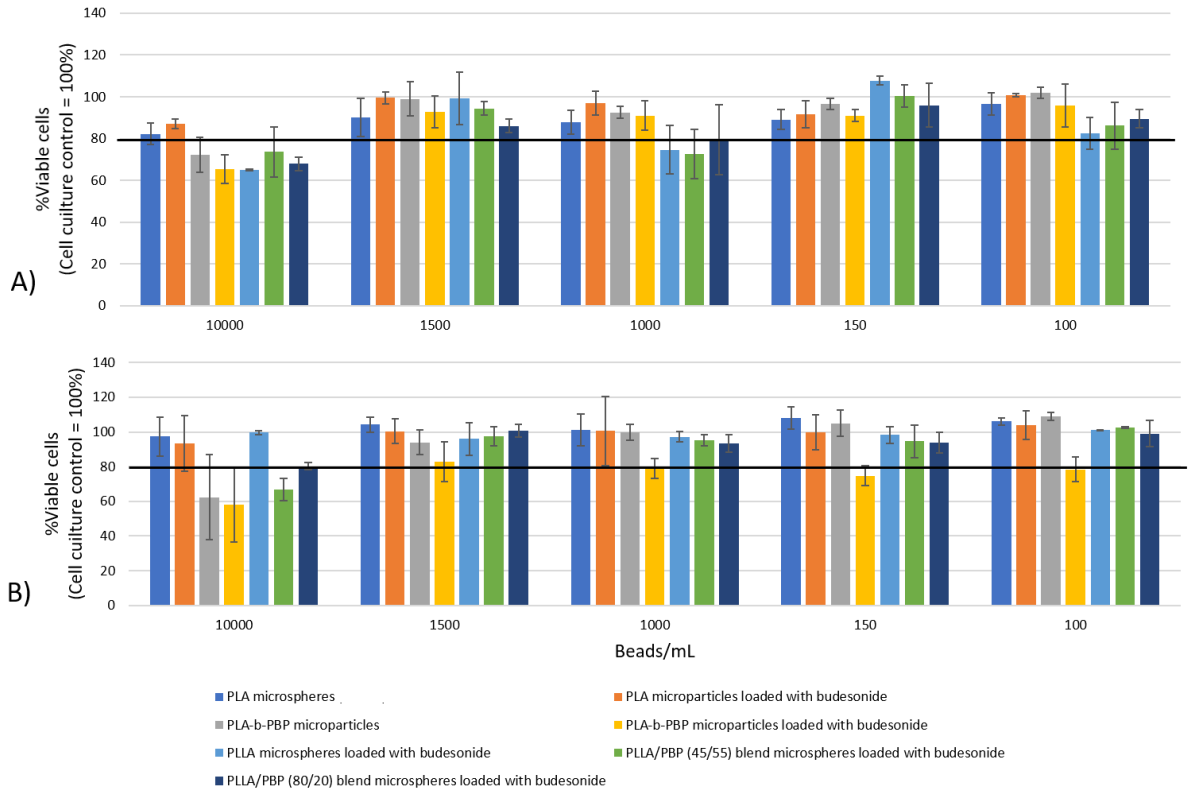

Figure 10 : Cytotoxicity tests by direct contact between a) fibroblasts or b) HUVEC and formulated microspheres.

The results indicate that the microparticles containing the PBEP-b-PLLA copolymer, both with and without budesonide, exhibit a higher cytotoxic effect at a concentration of 10,000 mg/mL. This could be explained if it remains some DBU traces after the precipitation of the copolymer in diethyl ether. To address this issue, a second precipitation step could be implemented to ensure the complete removal of all DBU traces. Furthermore, additional cytotoxicity tests should be conducted using newly formulated microparticles to validate this hypothesis and assess their safety.

II.4 Conclusions

Polylactide microspheres containing different amount of polyphosphoester and a model active pharmaceutical ingredient were successfully formulated by microfluidic droplet generation technique. These particles, as well as microspheres formed with classical

polyesters, were monodispersed and reproducible. The drug-loading and the encapsulation efficiency were quite similar to the ones of polyesters microspheres formulated in the same conditions. In contrast, the drug-release profiles were deeply impacted by the microspheres' composition, the PBEP being responsible of a tremendous fastening of the release. This kind of release profile is interesting if the patient has a crisis, such as a Crohn's disease crisis. Nevertheless, after 48h, the patient must take another dose if he has another crisis. But if these copolymer microspheres are blended with PLGA or PDLLA microspheres a biphasic profile release could be obtained. Indeed, there would be a fast release followed by a sustained release during weeks, preventing other crisis.

The cytotoxicity is higher on more sensitive HUVEC. The indirect contact test between microspheres and HUVEC suggest that the budesonide cause some toxicity and the direct contact tests suggest that the copolymer induce cytotoxicity which can be due to remaining DBU traces.

In order to enhance the encapsulation efficiency, one approach to consider is the addition of KH_2PO_4 to the continuous phase. This addition has the potential to increase both the drug-loading and the EE [47], thus enabling the achievement of a consistent drug-loading percentage across all formulated microspheres.

II.5 References

1 U. Edlund and A. C. Albertsson, *Advances in Polymer Science*, 2002, **157**, 67–112.

2 Q. Xu, M. Hashimoto, T. T. Dang, T. Hoare, D. S. Kohane, G. M. Whitesides, R. Langer, D. G. Anderson and H. David, *Small*, 2009, **5**, 1575–1581.

3 J. Yoo and Y. Y. Won, *ACS Biomater Sci Eng*, 2020, **6**, 6053–6062.

4 Y. Oh and S. H. Kim, *Journal of Polymer Science*, 2022, **60**, 1700–1709.

5 S. W. Choi, I. W. Cheong, J. H. Kim and Y. Xia, *Small*, 2009, **5**, 454–459.

6 B. Amoyav and O. Benny, *Polymers (Basel)*, , DOI:10.3390/POLYM11030419.

7 Z. Chen, Y. Lan, S.-D. Ling, Y.-H. Dong, Y.-D. Wang and J.-H. Xu, *Adv Mater Technol*, , DOI:10.1002/admt.202100733.

8 S. T. Sanjay, W. Zhou, M. Dou, H. Tavakoli, L. Ma, F. Xu and X. J. Li, *Adv Drug Deliv Rev*, 2018, **128**, 3–28.

9 B. Massoumi, R. Sarvari and S. Agbolaghi, *International Journal of Polymeric Materials and Polymeric Biomaterials*, 2018, **67**, 808–821.

10 H. Ye, K. Zhang, D. Kai, Z. Li and J. Loh, *Chem. Soc. Rev*, 2018, **47**, 4545.

11 K. E. Washington, R. N. Kularatne, V. Karmegam, M. C. Biewer and M. C. Stefan, *WIREs Nanomed Nanobiotechnol*, 2017, **9**, 1446.

12 L. S. Nair and C. T. Laurencin, *Progress in Polymer Science (Oxford)*, 2007, **32**, 762–798.

13 K. Park, *Journal of Controlled Release*, 2014, **190**, 3–8.

14 S. Freiberg and X. Zhu, *Int J Pharm*, 2004, **282**, 1–18.

15 S. Sonam, H. Chaudhary, V. Arora, K. Kholi and V. Kumar, *Polymer Reviews*, 2013, **53**, 546–567.

16 I. Takeuchi, K. Tomoda, A. Hamano and K. Makino, *Colloids Surf A Physicochem Eng Asp*, 2017, **520**, 771–778.

17 G. Liu and K. McEnnis, *Polymers (Basel)*, , DOI:10.3390/polym14050993.

18 K. Park, A. Otte, F. Sharifi, J. Garner, S. Skidmore, H. Park, Y. K. Jhon, B. Qin and Y. Wang, *Mol Pharm*, 2021, **18**, 18–32.

19 C. J. Ergul Yilmaz Z., *Macromol Biosci*, 2016, 1745–1761.

20 C. Pelosi, M. R. Tinè and F. R. Wurm, *Eur Polym J*, 2020, **141**, 110079.

21 H. Elzeny, F. Zhang, E. N. Ali, H. A. Fathi, S. Zhang, R. Li, M. A. El-Mokhtar, M. A. Hamad, K. L. Wooley and M. Elsabahy, *Drug Des Devel Ther*, 2017, **11**, 483–496.

22 P. Ju, J. Hu, F. Li, Y. Cao, L. Li, D. Shi, Y. Hao, M. Zhang, J. He and P. Ni, *J Mater Chem B*, 2018, **6**, 7263–7273.

23 T. Steinbach and F. R. Wurm, *Angewandte Chemie - International Edition*, 2015, **54**, 6098–6108.

24 Y. C. Wang, Y. Y. Yuan, J. Z. Du, X. Z. Yang and J. Wang, *Macromol Biosci*, 2009, **9**, 1154–1164.

25 Z. E. Yilmaz, S. Vanslambrouck, S. Cajot, J. Thiry, A. Debuigne, P. Lecomte, C. Jérôme and R. Riva, *RSC Adv*, 2016, **6**, 42081–42088.

26 Q. Wu, C. Wang, D. Zhang, X. Song, D. Liu, L. Wang and G. Zhang, *React Funct Polym*, 2012, **72**, 372–377.

27 R. Sun, X. J. Du, C. Y. Sun, S. Shen, Y. Liu, X. Z. Yang, Y. Bao, Y. H. Zhu and J. Wang, *Biomater Sci*, 2015, **3**, 1105–1113.

28 A. Vlachopoulos, G. Karlioti, E. Balla, V. Daniilidis, T. Kalamas, M. Stefanidou, N. D. Bikiaris, E. Christodoulou, I. Koumentakou, E. Karavas and D. N. Bikiaris, *Pharmaceutics*, , DOI:10.3390/PHARMACEUTICS14020359.

29 R. Riva, U. Shah, J. M. Thomassin, Z. Yilmaz, A. Lecat, A. Colige and C. Jérôme, *Biomacromolecules*, 2020, **21**, 349–355.

30 N. Penoy, K. L. Delma, H. A. Tonakpon, B. Grignard, B. Evrard and G. Piel, *Int J Pharm*, , DOI:10.1016/j.ijpharm.2022.122212.

31 G. Dufour, W. Bigazzi, N. Wong, F. Boschini, P. De Tullio, G. Piel, D. Cataldo and B. Evrard, *Int J Pharm*, 2015, **495**, 869–878.

32 T. Watanabe, T. Ono and Y. Kimura, *Soft Matter*, 2011, **7**, 9894–9897.

33 N. N. Deng, Z. J. Meng, R. Xie, X. J. Ju, C. L. Mou, W. Wang and L. Y. Chu, *Lab Chip*, 2011, **11**, 3963–3969.

34 J. Y. Chang, C. H. Yang and K. S. Huang, *Nanotechnology*, , DOI:10.1088/0957-4484/18/30/305305.

35 K. N. Clayton, J. W. Salameh, S. T. Wereley and T. L. Kinzer-Ursem, *Biomicrofluidics*, 2016, **10**, 20048.

36 G. T. Vladisavljević, H. Shahmohamadi, D. B. Das, E. E. Ekanem, Z. Tauanov and L. Sharma, *J Colloid Interface Sci*, 2014, **418**, 163–170.

37 S. Yazdian Kashani, A. Afzalian, F. Shirinichi and M. Keshavarz Moraveji, *RSC Adv*, 2020, **11**, 229–249.

38 B. Amoyav and O. Benny, *Applied Nanoscience (Switzerland)*, 2018, **8**, 905–914.

39 K. Park, A. Otte, F. Sharifi, J. Garner, S. Skidmore, H. Park, Y. K. Jhon, B. Qin and Y. Wang, *Journal of Controlled Release*, 2021, **329**, 1150–1161.

40 W. Yu, X. Liu, B. Li and Y. Chen, *International Journal of Multiphase Flow*, , DOI:10.1016/j.ijmultiphaseflow.2022.103973.

41 T. M. Martin, N. Bandi, R. Shulz, C. B. Roberts and U. B. Kompella, *AAPS PharmSciTech*, 2002, **3**, 1–11.

42 M. D. Buhecha, A. B. Lansley, S. Somavarapu and A. S. Pannala, *J Drug Deliv Sci Technol*, 2019, **53**, 101128.

43 Y. J. Oh, J. Lee, J. Y. Seo, T. Rhim, S. H. Kim, H. J. Yoon and K. Y. Lee, *Journal of Controlled Release*, 2011, **150**, 56–62.

44 M. D. Buhecha, A. B. Lansley, S. Somavarapu and A. S. Pannala, *J Drug Deliv Sci Technol*, 2019, **53**, 101128.

45 H. Ali, B. Weigmann, E. M. Collnot, S. A. Khan, M. Windbergs and C. M. Lehr, *Pharm Res*, 2016, **33**, 1085–1092.

46 F. Leonard, S. Srinivasan, X. Liu, E. M. Collnot, M. Ferrari, C. M. Lehr and B. Godin, *European Journal of Pharmaceutics and Biopharmaceutics*, 2020, **151**, 61–72.

47 M. Mestiri, F. Puisieux and J. P. Benoit, *Int J Pharm*, 1993, **89**, 229–234.

Chapter III : Poly(phosphoester) core-shell microspheres as tunable degradable drug-release vehicles.

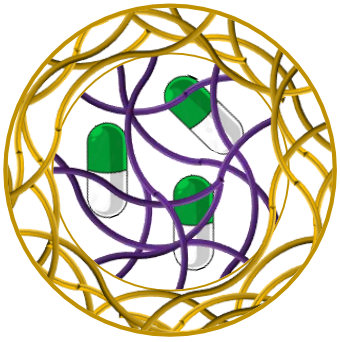

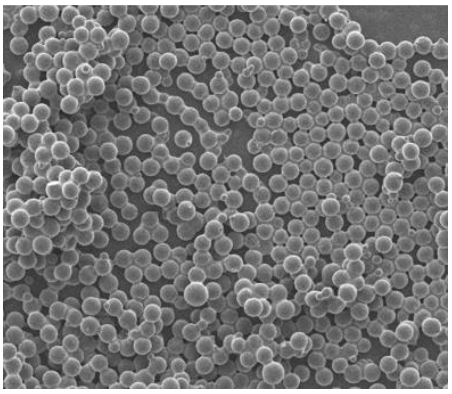

Chapter III : Poly(phosphoester) core-shell microspheres as tunable degradable drug-release vehicles.

The use of core-shell microspheres for drug-delivery is one promising strategy to improve therapeutic outcomes and minimize side effects. Indeed, the shell protect the drug against moisture, UV irradiation, heat or oxidation. The addition of a shell can also improves the drug-loading efficiency and can limit the burst effect of the drug. Different techniques are already used to produce core-shell microspheres but amongst them, droplet microfluidic generation technique is the most powerful one to have reproducible and monodisperse microspheres. Aliphatic polyesters such as poly(D,L-lactide) or poly(ε-caprolactone) are widely used to produce drug-loaded degradable microspheres, allowing to modulate sustained release from few weeks to several months, especially by controlling their degradation rate by copolymerization with the less hydrophobic glycolide. Nowadays, polyphosphoesters are a new kind of degradable materials showing strong promise for drug-delivery applications. Being biocompatible, their structure can be easily adapted thanks to the pentavalency of the phosphorous atom allowing precise tunability of their hydrophilicity or chemical functionality. In this work, the formulation, by microfluidic technique, of different core-shell microspheres loaded with acetylsalicylic acid is optimized. These microspheres have a PDLLA or a PCL core and a poly-(butenylphosphate) shell. Finally, the drug-loading, the encapsulation efficiency and the drug-release profile are determined and the results are compared with PDLLA microspheres with and without a PDLLA shell.

III.1 Introduction

The field of drug delivery has witnessed remarkable advancements over the years, aiming to improve therapeutic outcomes and minimize side-effects associated with conventional drug administration. One promising strategy that has emerged is the use of core-shell microspheres for drug delivery[1,2]. These microspheres offer a versatile and efficient platform for controlled release, targeted delivery, and protection of drugs, thereby revolutionizing the field of pharmaceuticals. The core shelling protects the drug against moisture, heat, ultraviolet radiation or oxidation and enable a higher encapsulation efficiency[1–4]. Besides, the shell allows also the release of the active compound which is kept constant through time and also avoid or decrease the burst effect encountered in some cases which is useful for the long-term treatment of several diseases such as asthma, angina or psychiatric disorders[5–8]. The core part can be liquid, gas or solid whereas the shell is usually solid. Hollow internal microspheres are used as an encapsulation vehicle to secure biologically active compounds such as proteins, enzymes and DNA in controlled drug release[7]. If the core is composed of a liquid or a gas, it is usually called a microcapsule allowing to encapsulate and protect, with a better encapsulation efficiency, a hydrophilic compound in a hydrophobic shell or to trap two incompatible substances, one in the aqueous core and the other in the lipophilic shell. For example, core-shell particles containing two anticancer drugs, hydrophilic doxorubicin hydrochloride in the aqueous core and hydrophobic paclitaxel trapped in the shell, are formulated easily[9]. Nevertheless, a burst release can appear when the shell is degraded and the liquid core is exposed to the outer medium. A solid core structure coated with a shell layer erases this problem because the release of the inner drug appears only after the degradation of the inner polymer[7].

A wide range of techniques, including polymerization, spray drying, solvent evaporation and self-assembly, have been used for the fabrication of core-shell structures. Within these physical and chemical methods, there is a growing demand for the controlled generation of monodisperse core-shell microspheres with a narrow size distribution. The properties of core-shell microspheres, such as their size, morphology and structure, exert a

significant influence on their applications. However, achieving the desired size distribution of core-shell microspheres using conventional methods has long been a major challenge. These traditional approaches often result in core-shell particles with high polydispersity, while also offering limited control over morphology and exhibiting poor reproducibility. Recently, significant advancements have been made in the development of core-shell drug carrier particles due to their unique characteristics. In addressing the aforementioned issues, microfluidics has emerged as a promising solution. Microfluidics has been extensively developed and holds great potential for overcoming the challenges associated with traditional methods, enabling enhanced control over particle size distribution, morphology, and reproducibility. Moreover, the UV-irradiation during the flow formulation process, in order to crosslink polymer for example, is also easily accessible[10–12]. This advancement has paved the way for the production of core-shell microspheres with specific attributes, making microfluidics a valuable tool in the field of core-shell drug delivery systems[4,5,7,9,13,14].

PLGA polymers are well-known synthetic biomaterials approved by the U.S. Food and Drug Administration (FDA) and the European Medicines Agency (EMA) for their biodegradability, biocompatibility and ease of property manipulation. These polymers, along with other biocompatible and biodegradable materials such as PLA and PCL, have been used as matrix materials for encapsulating and controlling the release of lipophilic drugs. The drugs are incorporated into microspheres formed through emulsification and consolidation of the polymer-drug solution. These microspheres exhibit sustained release of lipophilic drugs as the polymers gradually degrade through hydrolysis in the presence of water[4,15].

Polyphosphoesters represent another category of polymers that are biocompatible and degradable. These polymers, already used as micellar nanocarriers or hydrogels for drug-delivery applications[16–22], are characterized by a low T_g (≈-60°C) and can be easily adjusted in term of hydrophilicity thanks to the length of the alkyl side-chain[23,24] with a consequence that the degradation rate is also tunable[13,16]. Moreover, they present the advantages to be easily crosslinked by introducing vinyl moieties in the side chain[24].

In this chapter, the formulation by microfluidics of core-shell microspheres composed of a polyester core (PLA or PCL) and a crosslinked polyphosphoester shell is investigated (Figure 1A). The PPE, being viscous at RT, the poly(butenyl phosphate) (PBEP, Figure 1B) bearing a butenyl side-chain is selected for the shell to be crosslinked under UV irradiation.

Firstly, the core of these microspheres is loaded with a drug, the acetylsalicylic acid (Aspirin) which is an anti-inflammatory drug used to reduce pain or fever. The impact of the PPE shell on the encapsulation efficiency and the drug-release profiles is studied. The cytotoxicity of these core-shell microspheres is also evaluated.

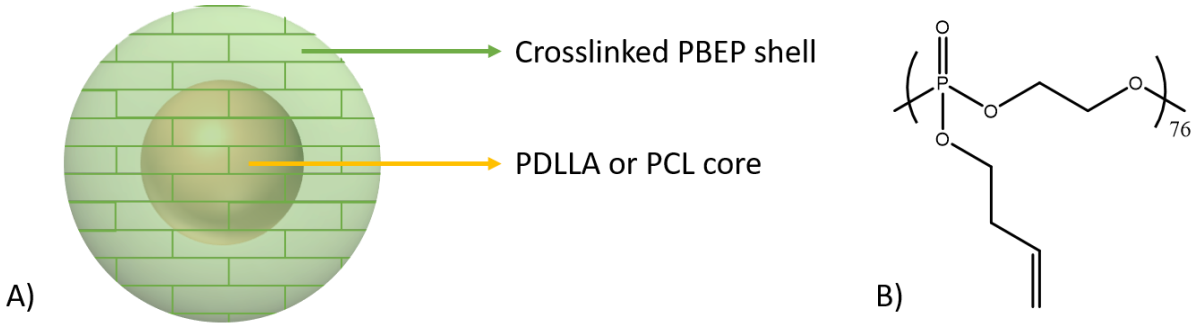

Figure 1 : A) Sketch of the targeted core-shell microspheres and B) structure of the selected PPE.

III.2 Experimental section

III.2.1 Materials

2-Chloro-3-oxo-1,3,2-dioxaphospholane (COP, TCI), calcium hydride (CaH_2, Aldrich), Irgacure (>98%, TCI), methyl red (Aldrich), concentrated phosphoric acid (Janssen chimica, P.A., 85w%), acetonitrile (>99.9%, Fisher), methanol (MeOH, VWR), ethyl acetate (AcOEt, Fisher), dimethylformamide (DMF, Fisher), poly(vinyl alcohol) (PVOH, Mowiol 8-88, M_w = 67,000g/mol, Merck) and poly(ε-caprolactone) (CAPA 6400, PCL-2OH, M_n = 37.000 g/mol, Perstorp), are used as received. 3-buten-1-ol (Aldrich), benzyl alcohol (Aldrich), triethylamine (TEA, Aldrich) and 1,8 diazobicyclo[5.4.0]undec-7-ene (DBU, Aldrich) are dried over calcium hydride at room temperature, following by distillation under reduced pressure just before use. Tetrahydrofuran (THF, VWR), toluene (VWR), dichloromethane (DCM, CH_2Cl_2, VWR) are dried

under molecular sieves. TU (thiourea) is synthesized according to a described method[24]. Poly-(D,L-lactide) (PDLLA, Purasorb PDL04) was kindly provided by Corbion.

III.2.2 Synthesis of PBEP

420 mg (1.1 mmol) of TU and 50mg (0.52mmol of OH) of tetraethylene glycol are transferred in a round bottom flask and dried by three azeotropic distillations with anhydrous toluene. 5 g (28 mmol) of BEP, the synthesis is reported elsewhere[23], is added in the flask containing the TU and the system is put under vacuum during 15 min. After addition of 20mL of anhydrous CH_2Cl_2. The mixture is cooled down to 0°C and 0.4mL (2.6 mmol) of DBU is finally introduced under a N_2 atmosphere with a syringe equipped with a stainless-steel capillary. The reaction medium is stirred at 0°C for 30 min. After concentration of the solution under vacuum, the polymer is precipitated in cold diethyl ether and recovered by decantation before being characterized by NMR and SEC analyses.

^{1}H NMR (CDCl3) δ= 5.8 ppm (m, 76 H, –CH_2–C**H**=CH_2) ,5.1 ppm (m, 152 H, C**H**$_2$=CH-CH_2), 4.25 ppm (m, 456 H, O–C**H**$_2$–C**H**$_2$–O and O-C**H**$_2$-CH_2-CH=CH_2 of BEP; 4H, P-O-C**H**$_2$- TEG), 3.71 ppm (t, 4H, P-O-CH_2-C**H**$_2$-O TEG), 3.64 ppm (t, 8H, O-C**H**$_2$-C**H**$_2$-O TEG), 2.41 ppm (m, 152 H, O–CH_2–C**H**$_2$–CH=CH_2)

^{31}P NMR (CDCl3) δ= -1.36 ppm.

Mn(^{1}H NMR) = 14000 g/mol, Đ = 1.3 (SEC).

III.2.3 Microfluidics formulation of the core-shell microspheres

The formulation of core-shell particles requires the preparation of two organic solutions and one aqueous solution:

Organic solution 1 (core): 5w% PDLLA solution containing acetylsalicylic acid is prepared by dissolving 250mg of PDLLA and 50mg of acetylsalicylic acid in 4.75g of AcOEt. Similarly, the 5w% PCL solution containing acetylsalicylic acid is prepared by dissolving 250mg of PCL and 50mg of acetylsalicylic acid in 4.75g of AcOEt.

Organic solution 2 (shell): 5w% PBEP solution is prepared by dissolving 250mg of PBEP (1.4mmol) and 16mg of Irgacure (0.7mmol) , the photosensitizer, in 4.75g of AcOEt.

Aqueous solution: 10w% of a PVOH stock solution is prepared by dissolving 100g of PVOH in 900g of MilliQ water. 2w% and 5w% PVOH solutions are prepared by dilution of this stock solution.

One 50mL syringe (Terumo), is filled with the aqueous solution and placed in Chemyx Fusion 6000-X syringe pump. Two 5mL syringes (Hamilton) are filled with the organic phases 1 and 2 and they are placed in a Chemyx 4000-X syringe pump. Three 1/16'' PFA tubing (IDEX 1632L) are connected to each syringe thanks to a 1/16'' connector (IDEX XP-161) and a luer adapter (IDEX P658). These three tubes are connected to a core-shell device provided by Sirris as described on Figure 2. The last connection is the outlet pipe composed of PFA (Swagelock, PFA-T2-030-100). This fourth tubing is connected to the device with a XP-131 connection (IDEX) and has a length of 200cm that allows the irradiation by UV light (Figure 2 and Figure 3). This homemade UV device is composed of four pylons with 4 LEDs (operating at 365nm). Each LED has a power of 1.76W and they are fabricated by AMS OSRAM. The tubing length being equal to 2.0m and the internal diameter being equal to 1.6mm, the internal volume is equal to 4.0mL. The irradiation time depends on the selected flow conditions. Subsequently, the microspheres are collected in a 250mL round-bottom flask under gentle stirring, which contained a small amount of 5w% PVOH solution. To remove any excess of PVOH, the microspheres underwent three washes with MilliQ water. After the washing steps, they are transferred to a 30mL vial and dried in a vacuum oven at 30°C, enabling subsequent analysis using a scanning electron and optical microscope.

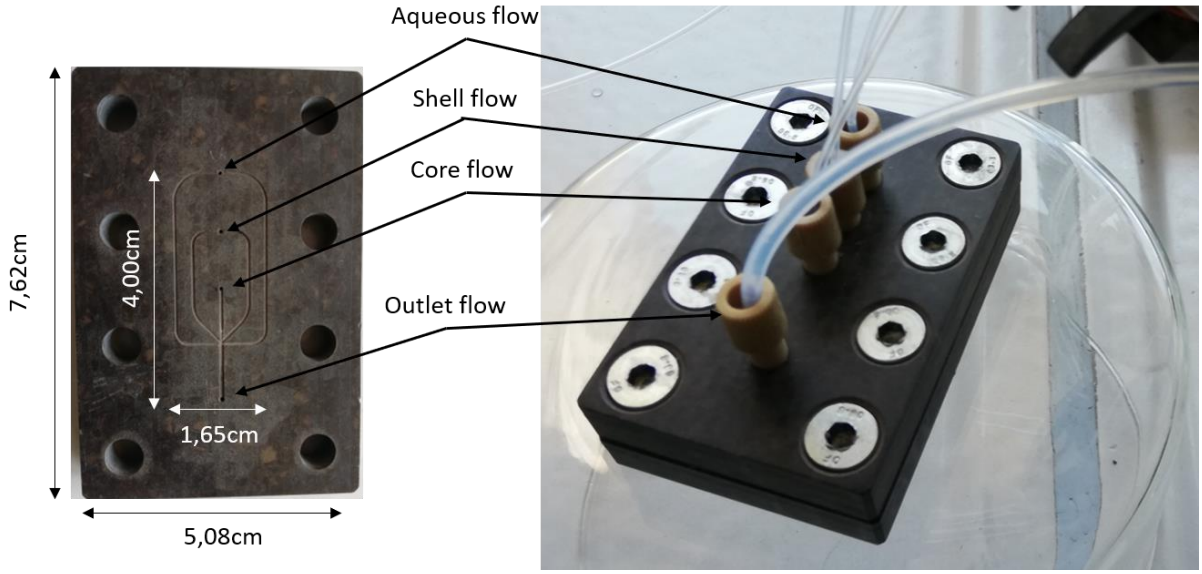

Figure 2 : Microfluidic core-shell device used to formulate the targeted microspheres

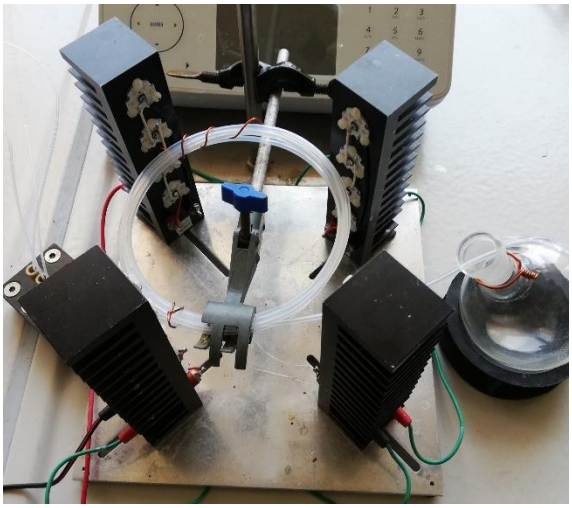

Figure 3 On line irradiation set-up to crosslink the PBEP shell of the microspheres

III.2.4 Drug-loading (DL) and encapsulation efficiency (EE) determination

A precise amount of microspheres (typically 5.0mg) are dissolved in 5mL of CH_2Cl_2 and then submitted to ultrasound for 30sec. Then, the solution is analyzed by UV spectrophotometer. Thanks to a calibration curve, with a R^2=0.998, the amount of

acetylsalicylic acid in the microspheres is quantified and the DL and the EE are calculated according to the following formulae :

$$DL\ (\%) = \left(\frac{m_{loaded\ aspirin}}{m_{microparticles}}\right) \text{x } 100\ ;\quad EE\ (\%) = \left(\frac{Experimental\ DL}{Targeted\ DL}\right) \text{x } 100$$

III.2.5 Drug-release kinetic analysis

Drug-release measurements are realized in triplicates for each sample (PDLLA//PBEP, PCL//PBEP and PDLLA//PDLLA). A precise amount of each microspheres (between 5mg and 10mg) is placed in a 10mL vial. 5mL of PBS buffer 0.1M (pH=7.4) containing 0.5w% of Tween 80 as surfactant are added in the vial before being transferred in an incubator at 37°C. After 2h of release, all the solution is removed and collected in a glass vial in order to be filtrated on Acrodisc 0.2µm and analyzed by High-Performance Liquid Chromatography HPLC. 5mL of a fresh buffer solution is then added in the vial and the kinetic release continues. The release medium analysis is performed after 2h, 4h, 24h, 48h, 72h, 1 week, 2 weeks, 3 weeks, 4 weeks, 5 weeks and 6 weeks.

The HPLC equipment consisted of a Waters equipment composed of an Autosampler 2707, a Controller 600 and a PDA 996. Briefly, acetylsalicylic acid concentration is analyzed using a Polaris C18-A analytical column with particles of 5 µm (L 250 mm, d.i. 4.6 mm) and a mobile phase in an isocratic mode composed of a mixture of concentrated H_3PO_4, acetonitrile and water (2/400/600, v/v/v) at a flow rate of 1 mL/min. 20 µL of the samples is injected at 30°C and the run time is set to 10 min (detection wavelength is 275 nm) and the retention time is 3min.

III.2.6 Cytotoxicity assays

Bovine fibroblast (Bfb) cells and Human umbilical vein endothelial cells (HUVEC) were seeded in 96 well plates at a concentration of 5000 cells per well. The plates were incubated for 72 hours after which different concentrations of each formulated microparticles containing acetylsalicylic acid (PDLLA//PBEP, PCL//PBEP, PDLLA//PDLLA) suspensions were added.

Suspensions were made at a concentration of 20.000 beads/mL by adding to each formulated microparticles batch medium without any FBS or growth factors. These suspensions were incubated for 24 hours at 37˚C, 5% CO_2. Prior to addition to the cells, suspensions were centrifuged and supernatant was separated from the pellet. The pellet was resuspended in culture medium. The plates were incubated with different concentrations of resuspended beads (direct assay) or bead supernatant (indirect assay) for 24 hours at 37˚C and 5% CO_2. Cytotoxicity was determined with a live/dead staining. In short, cells were stained with Hoechst 33342 (3.25 µM) and Ethd-1 (650 nM) and imaged with a BD pathway 855 high content analyzer. The images were analyzed with MetaXpress (Molecular Devices) software. Viable cell number per well was calculated by subtracting the dead cells (Ethd-1 positive nuclei) from all the cells (Hoechst positive nuclei) present in the wells. The average amount of viable cells in the culture control wells (wells that underwent the same treatment as the conditions) was set to 100% and the percentage of viable cells per condition was determined.

III.2.7 Characterization techniques

^{1}H and ^{31}P nuclear magnetic resonance (NMR) spectra are recorded on a Bruker Avance 400 apparatus at 25 °C at 400MHz in the Fourier-transform (FT) mode and using $CDCl_3$ as solvent.

Size exclusion chromatography (SEC) analysis are recorded in THF at 45°C with a flow of 1 mL min^{-1} on a Viscotek 305 TDA liquid chromatograph equipped with 2 PSS SDV linear M columns calibrated with polystyrene standards.

The surface and morphology of the formulated and washed microspheres are observed by scanning electron microscopy (SEM) images are collected with FEI Quanta 600 apparatus. SEM pictures are used to determine the mean diameter and the polydispersity of each sample. Indeed, 50 microspheres of each kind of sample are analyzed by ImageJ software in order to calculate the mean diameter (d), the standard deviation (θ) and the polydispersity. The PDI (polydispersity index) is calculated thanks to this formula:

$$PDI = \left(\frac{\theta}{d}\right)^2$$

Differential scanning calorimetry (DSC) is performed on a Discovery series TA DSC250 calibrated with indium. Between 5-10mg of the core-shell microspheres is transferred in the DSC oven at 20°C and a cooling ramp of 10°C.min^{-1} is applied until -80°C. After 5 min of temperature stabilization, a heating ramp of 10°C.min^{-1} is applied until 200°C. This cooling–heating cycle is repeated two times, the melting temperature (T_m) and the enthalpy (ΔH_m) being recorded during the second heating ramp.

An Amscope MD35 optical microscope with a magnification of 200x is used to take pictures and videos of microparticles swelling experiments.

III.3 Results and discussion

III.3.1 Flow formulation of core-shell microspheres composed of a PDLLA or PCL core and a crosslinked PBEP shell (PLA//PBEP or PCL//PBEP)

Microfluidic technique (MF) enables the manipulation of microflows in microchannels to produce uniform emulsion droplets. The principle is the same than the formation of an o/w emulsion except that the internal phase is pushed in the continuous one by a microchannel system thanks to syringe pumps at constant-flow with an excellent flow rate control. In the core-shell device, microdroplets of the organic solvent containing the core polymer are formed inside a Y-shape junction by shearing and capillary forces and are carried away by the second polymeric phase constituting the shell. Both organic phases contain the polymer at a concentration of 5w% in ethyl acetate, which is a good solvent of the PDLLA, PCL and PBEP and is a class 3 solvent which is better if biomedical applications are aimed. Then the aqueous phase cuts regularly the polymer flow to form core-shell microspheres (Figure 4). The aqueous phase contains an emulsifier, the PVOH, at a concentration varying between 2w% and 5w% which is a common concentration found in the literature[25,26]. The shell is crosslinked under UV

in order to have solid core-shell microspheres. Once the droplet is formed in the tubing, the ethyl acetate leaves the droplet thanks to its partial miscibility with water and at the end of the formulation process, completely solid microspheres are recovered.

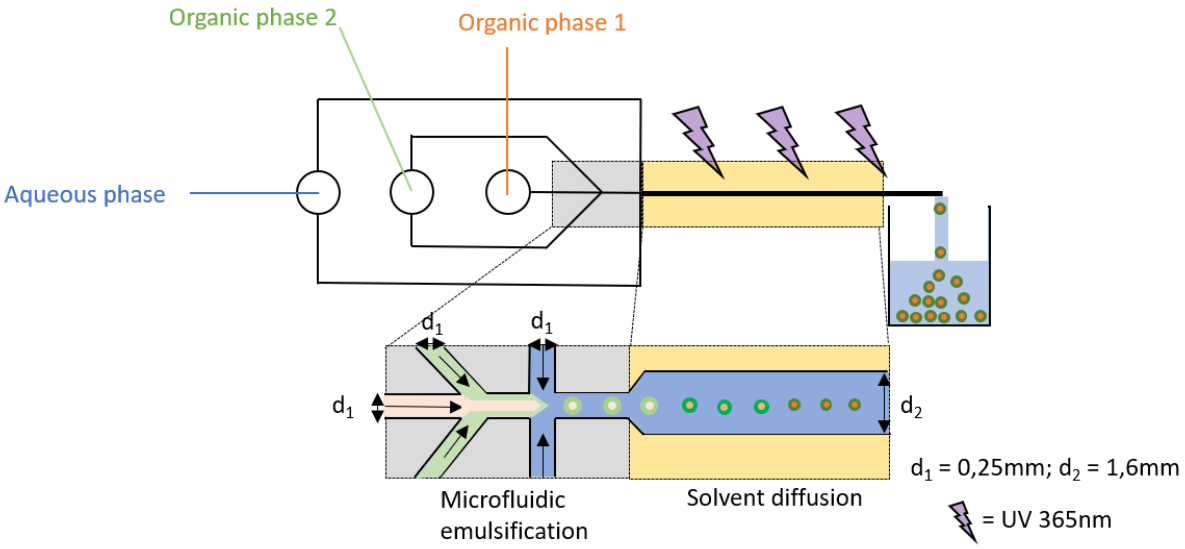

Figure 4 : Scheme of the microfluidic device used for core-shell formulation

Microspheres formulation is first optimized by using a solution of PDLLA without acetylsalicylic acid as core and a solution of synthesized PBEP as shell, which is crosslinked during the formulation process. The emulsifier concentration, the aqueous flow as well as the organic flows are varied. All results are gathered in the Table 1. The flow rate of both organic solutions 1 and 2 containing either PLA or PBEP is always kept identical to each other. Some microscope pictures are gathered in the Figure 5.

Table 1 : Formulation parameters to formulate PLA//PBEP core-shell microspheres and the corresponding diameter and PDI of the collected microspheres as determined by optical microscope analysis.

Entry	PVOH concentration (wt%)	PVOH flow rate (mL/min)	PLA and PBEP concentrations (wt%)	flow rate (mL/min)	Mean diameter (µm)	PDI
1	2	0.5	5	0.025	/	/
2	2	0.5	5	0.0125	/	/
3	2	**1.0**	5	0.025	/	/
4	2	**1.0**	5	0.0125	/	/
5	**5**	0.5	5	0.025	/	/
6	**5**	0.5	5	0.0125	/	/
7	5	**0.75**	5	0.025	/	/
8	5	**0.75**	5	0.0125	109.6	$3.9\ 10^{-2}$
9	5	**1.0**	5	0.025	112.4	$7.4\ 10^{-3}$
10	5	**1.0**	5	0.0125	102.9	$6.1\ 10^{-3}$

These findings suggest that at lower concentrations of emulsifier, microsphere formation does not occur (Table 1, entries 1-4). Additionally, if the ratio between the aqueous flow and organic flow rates is too small (Table 1, entries 5-6-7), the microspheres are not stable. This can be explained by the lower shearing forces and delayed droplet formation, leading to larger microspheres with excessive AcOEt content. Due to the inability of AcOEt to escape from the microspheres before collection, they explode. However, by increasing the aqueous flow rate, the collected microspheres become stable and monodisperse, as microspheres are considered monodisperse when their PDI is below 0.1.

Decreasing both organic flows rate while keeping the aqueous flow rate constant (Table 1, entries 7-8 or 9-10) reduces the size of the microspheres due to the shearing forces. Similarly, increasing the aqueous flow rate also results in smaller microspheres for the same reason. Moreover, selecting a larger aqueous flow rate improves the PDI. Therefore, the conditions corresponding to the entry 10 (Table 1) are chosen for subsequent experiments.

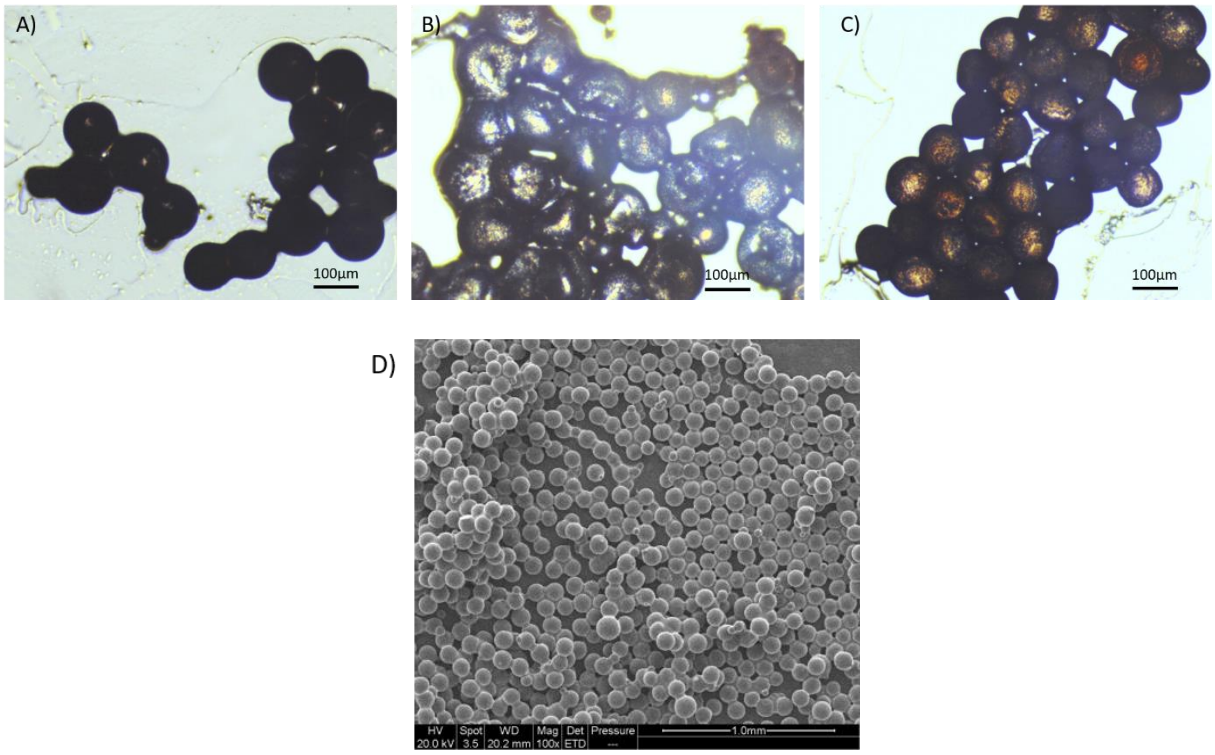

Figure 5 : optical microscope pictures of PDLLA//PBEP core-shell microspheres: A) Entry 8; B) Entry 9; C) Entry 10 and D) SEM picture of the core-shell microspheres formulated in the selected parameters (entry 10)

With the selected conditions, the irradiation time is equal to 4min. In order to determine if the shell of the microspheres is crosslinked or not, some CH_2Cl_2 is added on a microsphere sample and the behavior is observed by optical microscopy (Figure 6).

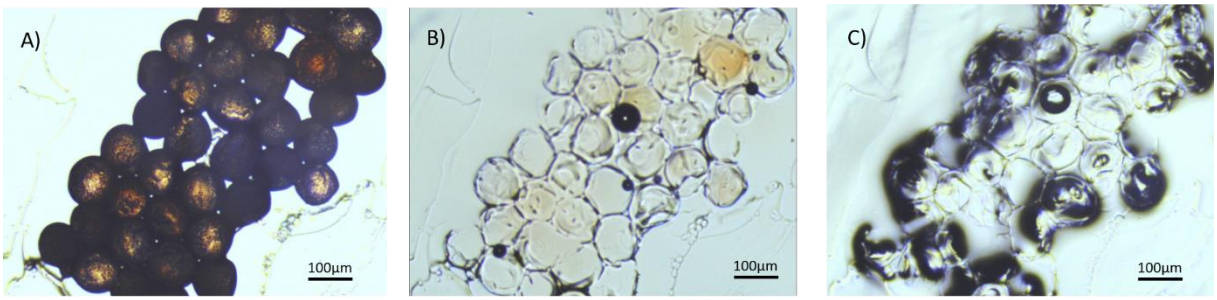

Figure 6 : Swelling experiment for the selected PDLLA//PBEP core-shell microspheres in dichloromethane

For the sake of the core visualization, during the optimization process, 1mg of methyl red is added in the PDLLA core solution before formulation. The DCM is chosen because it is a

good solvent of PLA and PBEP. On Figure 6A, orange microspheres with a size of 109 µm are well-formed and stable when placed in water. When the DCM is added, the crosslinked PBEP swells until reaching a diameter of 135µm, which means that the volume doubles while the orange dye diffuses out with the PDLLA because they are soluble in the solvent . At the end only PBEP capsule remains and shrinks because the PDLLA is gone. These results confirm the effective crosslinking of the shell of the microspheres.

III.3.2 Flow formulation of core-shell microspheres containing acetylsalicylic acid

Once the optimal conditions for creating uniform core crosslinked shell microspheres have been established, the core of the microspheres can be used to encapsulate the selected active pharmaceutical ingredient (API). Acetylsalicylic acid, a commonly used drug for pain and fever reduction that is unaffected by the UV light necessary for the crosslinking the polyphosphoester shell, is chosen as the API. Various types of microspheres are produced for the study. Initially, core-shell microspheres are formulated with a poly(D,L-lactide) (PDLLA) core and a crosslinked shell. Subsequently, the PDLLA core is replaced with poly(ε-caprolactone) (PCL) to assess the impact of crystallinity on the encapsulation efficiency (EE) and drug release of acetylsalicylic acid. A control sample consisting of PDLLA as both the core and shell is also prepared. To examine the effect of adding a shell on the encapsulation efficiency, PDLLA microspheres containing acetylsalicylic acid are created without a shell. The results of these experiments are summarized in the table below.

Table 2 : Characteristics of core-shell microspheres formulated with the following parameters: PVOH concentration : 5w%; PVOH flow : 1.0mL/min; polymer concentrations : 5w%.

Entry	Core Polymer	Shell polymer	Polymer flow rate (mL/min)	Mean diameter (µm)	PDI	Drug-loading (%)	Targeted drug-loading (%)	EE (%)
1	PDLLA	PBEP	0.0125	119.6	$2.2\ 10^{-3}$	6.51	9.1	71.5
2	PCL	PBEP	0.0125	104.7	$2.1\ 10^{-3}$	4.92	9.1	54.1
3	PDLLA	PDLLA	0.0125	62.4	$1,2\ 10^{-2}$	4.54	9.1	49.9
4	PDLLA	/	0.0125	43.4	$2.7\ 10^{-3}$	0.61	16.7	3.7

Comparing entry 4 (Table 2) with the other entries reveals a significant impact of the shell on the encapsulation efficiency, as it effectively reduces the extraction of acetylsalicylic acid during the formulation process. The inclusion of a PDLLA shell leads to an increased EE due to the dilution of acetylsalicylic acid within the polymer matrix, which limits its extraction into the aqueous phase. By incorporating a crosslinked PBEP shell around the polyester core, the extraction of acetylsalicylic acid into the aqueous phase is partially obstructed, resulting in a substantial increase in EE, particularly for microspheres with a PDLLA core. The difference in EE between entry 1 and entry 2 may be attributed to the crystallinity of PCL. Indeed, the active ingredient is mainly encapsulated in the amorphous region of the microsphere, the crystalline region acts as a barrier for the drug. Therefore, the EE of the drug encapsulated decreases dramatically when highly crystalline polymers are used [27,28].

III.3.3 Kinetics release profiles

Considering that the EE is very low for the PDLLA microspheres without shell, the drug-release is performed on the three different core-shell microspheres. It is quite clear than the polyphosphoester shell have a tremendous effect on the drug release acting like a barrier against the drug-release.

The release profiles are similar for each kind of microspheres (Figure 7). They correspond to a triphasic profile, which is frequently observed for larger microspheres[29]. A triphasic profile is composed of three steps : an initial burst effect, corresponding to the

release of some drug adsorbed near the surface, a lag-time during which there is a very small amount of drug which is released and finally an accelerated release phase occurring because of the polymer degradation[29]. The acetylsalicylic acid release is almost complete after 5 weeks for all formulated compositions and the release is slightly faster for the PCL core than for the PDLLA core, which is explained by the lower T_g of the PCL compare to PDLLA allowing faster API diffusion in a higher free volume.

The Figure 7B illustrates the drug release patterns during the initial 48 hours. When examining the different microspheres, the release profiles of acetylsalicylic acid exhibit some variations. The microspheres containing the PBEP have a higher burst effect, mainly because it is more hydrophilic than aliphatic polyesters and consequently, the water can penetrate a bit deeper to extract the acetylsalicylic acid which is near the surface. The slight burst effect difference between the PDLLA//PBEP and the PCL//PBEP can also be explained by this difference of hydrophilicity because the PDLLA is more hydrophilic than the PCL.

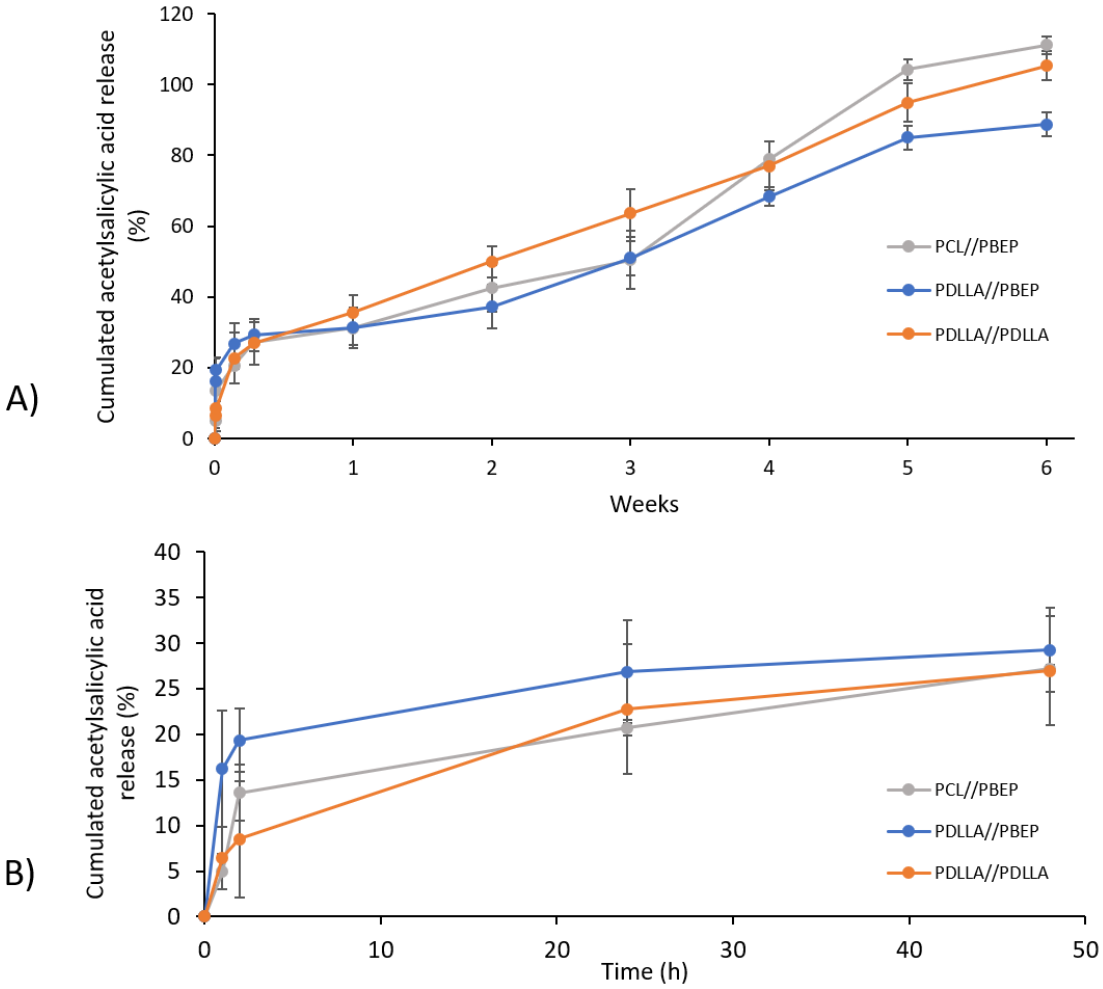

Figure 7 : Acetylsalicylic acid release profiles a) over 4 weeks b) during the first 48h from the various core-shell microspheres prepared by microfluidic.

III.3.4 Cytotoxicity assays

Cytotoxicity assays are performed on microspheres in order to confirm the absence of toxicity. Different cytotoxicity tests are performed by direct or indirect contact between cells and by using two different cell lines.

The first assay by indirect contact is reported on the Figure 8 for bovine fibroblast and HUVEC cells.

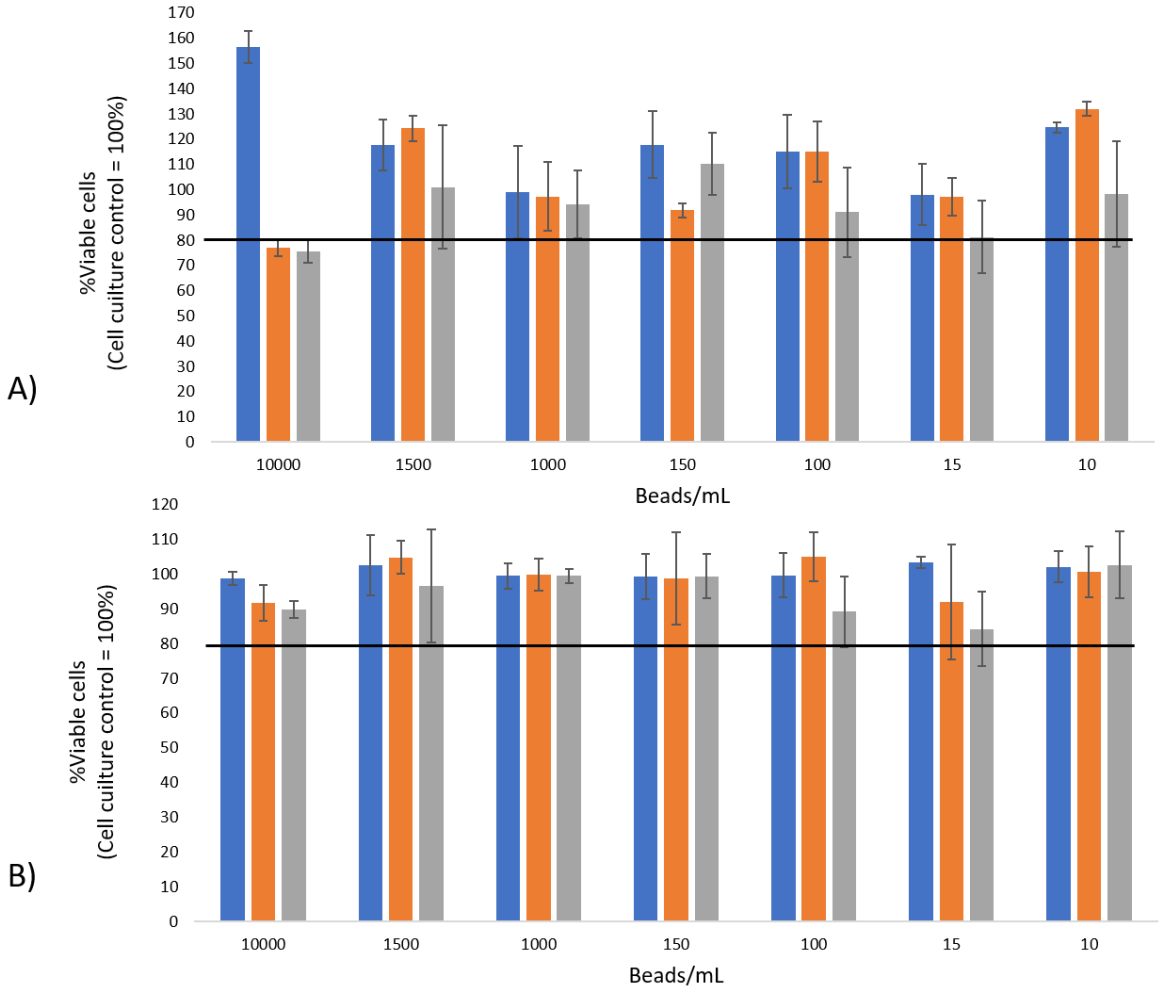

Figure 8 : Cytotoxicity tests by indirect contact between a) bovine fibroblasts or b) HUVEC and PDLLA//PBEP (blue) or PDLLA//PDLLA (orange) or PCL//PBEP (grey) microspheres loaded with acetylsalicylic acid.

The Figure 8a shows that bovine fibroblasts are viable for all formulated microspheres, except at very high concentration for the PDLLA//PDLLA and PCL//PBEP microspheres. Interestingly, the viability of the PDLLA//PBEP microspheres is almost always better than the reference at 100%. Moreover, the viability is always better for the PDLLA//PBEP microspheres compared to the PCL//PBEP microspheres. These results show that there is no toxicity caused by the release of the acetylsalicylic acid in the medium. The HUVEC cells are less sensitive to the different microspheres' compositions (Figure 8b) and there is no cytotoxicity whatever the concentration.

Cytotoxicity tests by direct contact between fibroblasts (Figure 9a) or HUVEC (Figure 9b) are performed by incubating microspheres for 24h in the culture medium, collecting them and placing them during 24h in contact with fibroblasts or HUVEC.

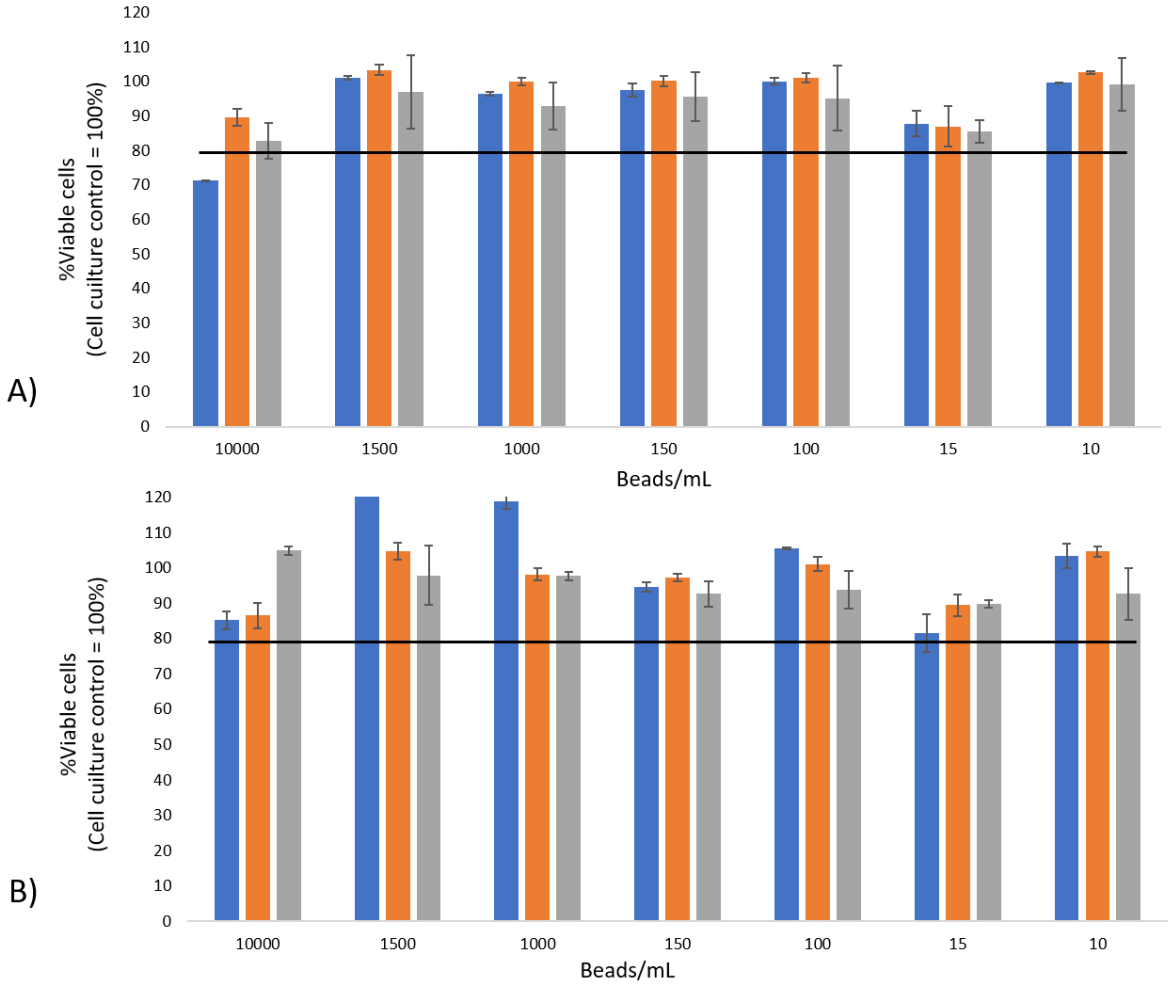

Figure 9 : Cytotoxicity tests by direct contact between a) bovine fibroblasts or b) HUVEC and PDLLA//PBEP (blue) or PCL//PBEP (grey) or PDLLA//PDLLA (orange) microspheres loaded with acetylsalicylic acid.

These results show that there is no toxicity caused by the microspheres except for the PDLLA//PBEP in contact with fibroblasts at high concentration. For the other results, the toxicity is not influence by the kind of microspheres.

III.4 Conclusion

Core-shell microspheres composed of an aliphatic polyester core and a crosslinked polyphosphoester shell and containing a model active pharmaceutical ingredient are successfully synthesized by microfluidic droplet generation technique. These formulated microspheres are monodisperse and the formulation is reproducible. The shell crosslinking by UV irradiation is proven according to swelling experiment in dichloromethane. As expected, the addition of a crosslinked polyphosphoester shell increase the drug-loading of the API by limiting it extraction to the external environment during formulation. Moreover, the nature of the polymer constituting the core of the microspheres have also an influence on the drug loading as PDLLA-based core exhibit a much higher drug loading compared to PCL core, which is explained by the difference of thermal properties between these aliphatic polyesters.

Finally, release profiles of core-shell microspheres correspond to a triphasic profile. All profiles are similar but the burst release differs according to the polymer composition. Indeed, the more hydrophilic microspheres (PDLLA//PBEP) have a more important burst effect compared to others. The drug-release is complete after 6 weeks for all formulation microspheres.

III.5 References

1 T. Watanabe, Y. Kimura and T. Ono, *Langmuir*, 2013, **29**, 14082–14088.

2 W. Li, H. Lee, D. A. Weitz, L. Zhang, X. Ge, B. Xu, W. Zhang, L. Qu, C.-H. Choi, J. Xu and A. Zhang, *Chem. Soc. Rev*, 2018, **47**, 5646–5683.

3 Z. Liu, F. Fontana, A. Python, J. T. Hirvonen and H. A. Santos, *Small*, , DOI:10.1002/smll.201904673.

4 Y. Oh and S. H. Kim, *Journal of Polymer Science*, 2022, **60**, 1700–1709.

5 Y. Li, D. Yan, F. Fu, Y. Liu, B. Zhang, J. Wang, L. Shang, Z. Gu and Y. Zhao, *Sci China Mater*, 2017, **60**, 543–553.

6 S. Freiberg and X. Zhu, *Int J Pharm*, 2004, **282**, 1–18.

7 S. Yazdian Kashani, A. Afzalian, F. Shirinichi and M. Keshavarz Moraveji, *RSC Adv*, 2020, **11**, 229–249.

8 J. Yoo and Y. Y. Won, *ACS Biomater Sci Eng*, 2020, **6**, 6053–6062.

9 M. Windbergs, Y. Zhao, J. Heyman and D. A. Weitz, *J Am Chem Soc*, 2013, **135**, 7933–7937.

10 E. Lagreca, V. Onesto, C. Di Natale, S. La Manna, P. A. Netti and R. Vecchione, *Prog Biomater*, 2020, **9**, 153–174.

11 A. Vlachopoulos, G. Karlioti, E. Balla, V. Daniilidis, T. Kalamas, M. Stefanidou, N. D. Bikiaris, E. Christodoulou, I. Koumentakou, E. Karavas and D. N. Bikiaris, *Pharmaceutics*, , DOI:10.3390/PHARMACEUTICS14020359.

12 E. Baeten, S. Vanslambrouck, C. Jérôme, P. Lecomte and T. Junkers, *Eur Polym J*, 2016, **80**, 208–218.

13 Z. Chen, Y. Lan, S.-D. Ling, Y.-H. Dong, Y.-D. Wang and J.-H. Xu, *Adv Mater Technol*, , DOI:10.1002/admt.202100733.

14 B. Amoyav and O. Benny, *Applied Nanoscience (Switzerland)*, 2018, **8**, 905–914.

15 H. W. Yeh and D. R. Chen, *Int J Pharm*, 2017, **528**, 637–645.

16 C. J. Ergul Yilmaz Z., *Macromol Biosci*, 2016, 1745–1761.

17 C. Pelosi, M. R. Tinè and F. R. Wurm, *Eur Polym J*, 2020, **141**, 110079.

18 H. Elzeny, F. Zhang, E. N. Ali, H. A. Fathi, S. Zhang, R. Li, M. A. El-Mokhtar, M. A. Hamad, K. L. Wooley and M. Elsabahy, *Drug Des Devel Ther*, 2017, **11**, 483–496.

19 P. Ju, J. Hu, F. Li, Y. Cao, L. Li, D. Shi, Y. Hao, M. Zhang, J. He and P. Ni, *J Mater Chem B*, 2018, **6**, 7263–7273.

20 T. Steinbach and F. R. Wurm, *Angewandte Chemie - International Edition*, 2015, **54**, 6098–6108.

21 Y. C. Wang, Y. Y. Yuan, J. Z. Du, X. Z. Yang and J. Wang, *Macromol Biosci*, 2009, **9**, 1154–1164.

22 X. Xu, H. Yu, S. Gao, H. Q. Mao, K. W. Leong and S. Wang, *Biomaterials*, 2002, **23**, 3765–3772.

23 Z. E. Yilmaz, S. Vanslambrouck, S. Cajot, J. Thiry, A. Debuigne, P. Lecomte, C. Jérôme and R. Riva, *RSC Adv*, 2016, **6**, 42081–42088.

24 R. Riva, U. Shah, J. M. Thomassin, Z. Yilmaz, A. Lecat, A. Colige and C. Jérôme, *Biomacromolecules*, 2020, **21**, 349–355.

25 T. Watanabe, T. Ono and Y. Kimura, *Soft Matter*, 2011, **7**, 9894–9897.

26 B. Amoyav and O. Benny, *Polymers (Basel)*, , DOI:10.3390/POLYM11030419.

27 S. Sonam, H. Chaudhary, V. Arora, K. Kholi and V. Kumar, *Polymer Reviews*, 2013, **53**, 546–567.

28 I. Takeuchi, K. Tomoda, A. Hamano and K. Makino, *Colloids Surf A Physicochem Eng Asp*, 2017, **520**, 771–778.

29 C. Busatto, J. Pesoa, I. Helbling, J. Luna and D. Estenoz, *Int J Pharm*, 2018, **536**, 360–369.

Chapter IV: Microfluidic formulation of shape-memory microspheres for embolization applications.

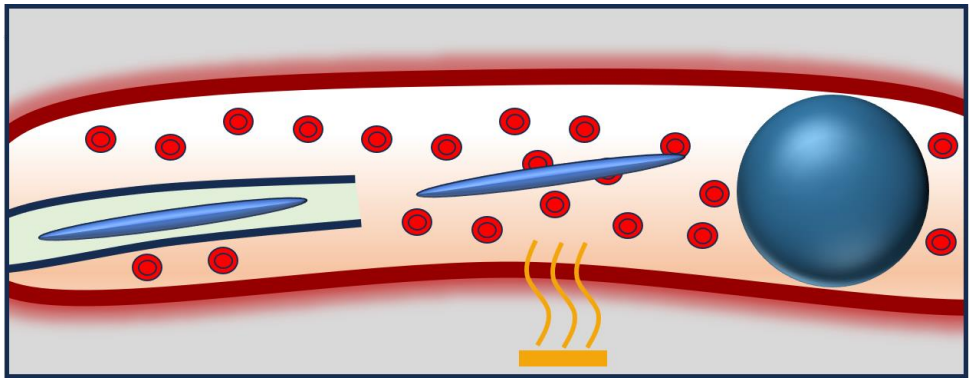

Chapter IV: Microfluidic formulation of shape-memory microspheres for embolization applications.

Minimally invasive procedures guided by real-time imaging have gained popularity over traditional open surgery due to their reduced post-operative complications and expanded treatment options for vascular pathologies. Embolization involves blocking blood flow in targeted vessels using agents delivered through a catheter. Amongst them, microparticles are widely used due to their versatility, calibrated size, and functionality. However, controlling their size and shape is challenging, as irregular shapes and smaller diameters can lead to unpredictable behavior and aggregation. Shape-memory polymer microparticles offer improved injectability and embolization capabilities. The microfluidic droplet technology allows formation of highly uniform and crosslinked microspheres. In this study, we developed well-defined shape-memory microspheres of chemically crosslinked poly(ε-caprolactone). For that purpose, 4-arm star-shape PCL end-capped with coumarin were formulated by microfluidic droplet generation coupled to UV-light irradiation. The formulation parameters were optimized to achieve highly uniform microspheres with a size greater than 100µm and the shape programming and recovery capabilities of these microspheres were demonstrated. Finally, by using the same formulation process, iron oxide nanoparticles could be loaded in the microspheres to afford radio-opacity for *in vivo* imaging during surgery.

IV.1 Introduction

Minimally invasive procedures guided by real-time imaging have gained increasing interest over the past few decades compared to open surgery. One of the main reasons for this is the reduction of post-operative complications compared to traditional surgical methods. Additionally, they have expanded the range of vascular pathologies that can be effectively treated[1,2].

Embolization, which involves delivering an agent through a catheter to obstruct blood flow in a targeted vessel, is a highly common endovascular procedure. Various interventions require embolization procedures, such as blocking the blood supply to eradicate a hepatic tumor or preventing the rupture of an intracranial aneurysm[1–6]. The selection of an embolic agent is based on several factors, including the clinical indication for the procedure, the desired level of occlusion (temporary or permanent), the extent of occlusion, flow dynamics and collateral circulation, the risk of complications like necrosis or unintended embolization, and cost considerations [3,6].

There are different types of embolic agents available for clinical use, including metallic coils, and polymer microparticles, foams and liquids/gels. Among these options, polymer microparticles were the first to be developed and remain the most widely used due to their versatility and functionality. They can be calibrated in size or have irregular shapes, be degradable or not, have a natural or synthetic origin, and can be loaded with various chemical drugs making possible chemo-embolization[1,2,5,6]. Occlusin™ 503 and Embosphere™ microspheres are currently marketed artificial embolization devices. These agents consist of biodegradable poly(lactic acid-*co*-glycolic acid) microspheres with a size comprised within 150–212 µm and 300–500 µm, respectively.

The precise control of microparticle size and shape presents a significant challenge, as it is crucial for achieving efficient injection without clogging the syringe capillary and preventing undesired aggregation within blood vessels, which can lead to unpredictable occlusion of unintended vessels with potentially severe consequences[1,2,7,8]. Microspheres with

smaller diameters (<100 µm) are particularly hazardous due to their unpredictable behavior in the bloodstream. Furthermore, the shape of the particles greatly affects their transport throughout the body[8].

Spherical particles, with their inherent symmetry, generally exhibit more predictable movement. On the other hand, non-spherical particles may align or not with the blood flow[9]. In a flow environment, non-spherical particles experience velocity gradients that result in non-uniform forces along their symmetry axis, causing rotation and tumbling. In contrast, spherical particles tend to follow the streamlines dictated by hydrodynamic forces relative to their radius, with lateral drift primarily influenced by external factors such as gravity and electromagnetic fields. Anisotropic particles, such as discs, spheroids, ellipsoids, and rods, due to their rotational motion in flow, can undergo significant lateral drift even in the absence of external forces. This phenomenon, known as improved margination, describes the tendency of particles to migrate towards the vessel wall [9–11].

Shape-memory materials are remarkable stimuli-responsive materials able to switch from one stable macroscopic shape to another one**.** These materials must contain soft segment that will fix the temporary shape, typically crystallinity, and hard segments that will fix the permanent shape, such as crosslinking. While this property has already been widely exploited in coils of shape-memory alloys for embolization purposes[12], microspheres made of degradable synthetic shape-memory polymers have been disregarded even if this type of materials is receiving an increasing attention for other types of biomedical applications[1,13–17].

Considering this knowledge gap, we aim to explore the design of well-defined microspheres made of a (bio)degradable and biocompatible polymer and exhibiting shape-memory properties for enhancing both injectability and embolization capabilities. These shape-memory microparticles would adapt their shape to flow through narrow catheters, and subsequently, once reaching the embolization site would effortlessly recover their spherical shape without undergoing structural collapse upon a dedicated thermal trigger.

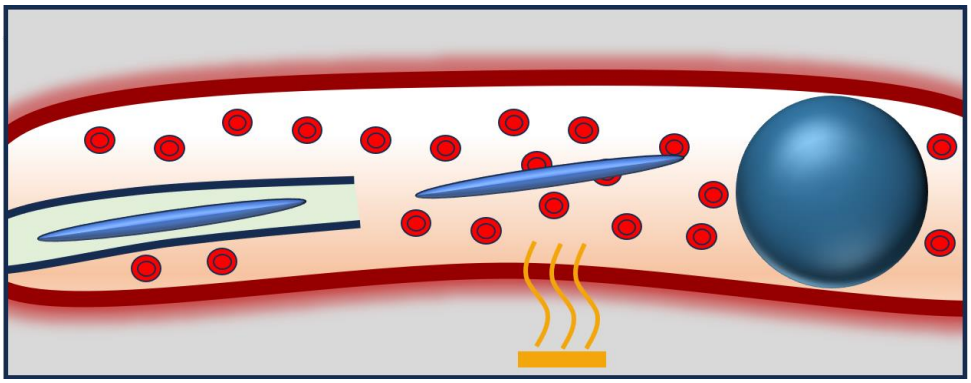

Figure 1 : Schematic principle of shape-memory microparticles for embolization: injection in the programmed elongated shape through a microcatheter, recovery of the spherical shape by local heating, blocking further blood supply.

In order to afford optimal shape memory properties to the targeted microspheres, chemically crosslinked PCL appears as one of the best candidates[18,19]. The easiest way to implement the continuous crosslinking of the PCL is by UV. Accordingly, the photo-crosslinking of 4-arms star-shaped PCL end-capped with coumarin moieties under UV irradiation leading to PCL networks, with remarkable thermo-sensitive shape-memory properties, has been already studied and optimized by our group. Moreover, the network formed is more regular compared to a network formed with acrylate moeities[20].

Among the various techniques available for formulating microparticles, microfluidic droplet technology stands out as the most suitable method for producing highly uniform microspheres with excellent reproducibility. Moreover, the UV-irradiation during the flow formulation process, in order to crosslink polymer for example, is also easily accessible[21–23].

The shell of the PCL//PBEP microparticles, synthetized in the Chapter III, are also UV crosslinked. Thanks to the crystallinity of the PCL and the UV crosslinking of the shell, the potential of these microspheres to exhibit shape memory properties has been investigated, which could be significant added-value when chemoembolization applications would be foreseen.

The microfluidic technique enables also the formulation of loaded microparticles with high encapsulation efficiency[24]. The loading can be a drug when chemoembolization is

foreseen or a magnetic agent such as the magnetite (Fe_3O_4) nanoparticles to get magnetic shape-memory microspheres.

The design of monodispersed microspheres of crosslinked PCL with a targeted diameter about a hundred of micrometers is thus investigated here formulating 4-arm PCL stars bearing coumarin at the chain-ends by the microfluidic droplet generation technology coupled to in line UV-crosslinking. The shape programming and shape recovery of these microspheres as well as PCL//PBEP microspheres is also demonstrated. Finally, the developed technology is investigated to load iron oxide nanoparticles in the microspheres bringing them radio-opacity[25].

IV.2 Experimental section

IV.2.1 Materials

Ethyl acetate (AcOEt, Fisher), dichloromethane (DCM, CH_2Cl_2, Fisher), benzophenone (Aldrich), poly(vinyl alcohol) (PVOH, Mowiol 8-88, M_w = 67,000 g/mol, Merck) and PEO (8,000 g/mol, Merck) were used as received.

PCL-4COU was obtained starting from 7-hydroxy-4-methylcoumarin (Aldrich) and CAPA 4801® (4-arm star-shaped PCL (PCL-4OH), M_n = 8,800 g/mol, Đ = 1.2) kindly offered by Perstorp. The conversion of the 7-hydroxy-4-methylcoumarin in 7-hydroxypropyl-4-methylcoumarin as well as the chain-end functionalization of the PCL-4-OH by coumarin moieties to get the photo-crosslinkable star PCL (PCL-4COU) was performed following the same procedure as described in the literature[20].

IV.2.2 Microfluidic System and Chip

Two 50mL syringes (Terumo) were filled with the aqueous solution and placed in Chemyx Fusion 4000-X syringe pump. The 20mL stainless steel syringe (Chemyx) was filled with the organic phase and it was placed in a Chemyx 6000-X syringe pump. Three 1/16'' PFA tubing (IDEX 1632L) were connected to each syringe thanks to a 1/16'' connector (IDEX XP-

161) and a luer adapter (IDEX P658). These three tubes were connected together in a cross-junction (IDEX P722) (Figure 2). The two aqueous tubes are connected perpendicularly to the organic phase and the last connection is the outlet pipe composed of PFA (Swagelock, PFA-T2-030-100). This fourth tubing is connected to the cross-junction with a XP-131 (IDEX) connection. A 365nm UV lamp, kindly provided by the CiTOS, was connected to the system in order to crosslink coumarin moieties. The UV device (Figure 2) is a homemade device composed of four pylons with 4 LED on them. Each LED has a power of 1.76W and they are fabricated by AMS OSRAM. The tubing length being equal to 2.0m and the internal diameter being equal to 1.6mm, the internal volume is equal to 4.0mL. The irradiation time will depend on the selected flow conditions.

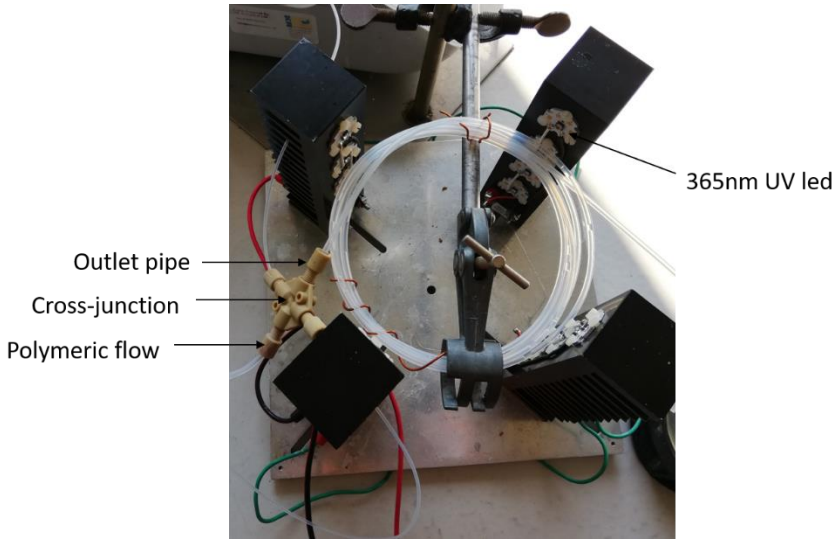

Figure 2 : Microfluidic setup for the formulation of crosslinked PCL microparticles

IV.2.3 Formulation of crosslinked PCL microspheres

For the 2w% PCL-4COU (10,000g/mol) solution, 200mg of PCL-4COU (8 10^{-2} mmol) and 7.3mg of benzophenone (4 10^{-2} mmol) were dissolved in 9.8g of AcOEt. Similarly, the 5w% PCL-4COU (10,000g/mol) solution was prepared by dissolving 500mg of PCL-4COU and 18.2mg of benzophenone (0.1 mmol) in 9.5g of AcOEt. A 20mL syringe was filled with this solution which was previously slowly heated (70°C for 30sec) in order to favor the formulation. 1w%, 2w% and 3w% of PVOH aqueous solution was also prepared and two 50mL syringes were filled

with this solution. Once the syringe drivers were configured, the system was ready to run with the selected parameters. During the formulation process, the microparticles were crosslinked using a UV lamp at 365nm which will irradiate them during the whole formulation process. Subsequently, the microparticles were collected in a 250mL round-bottom flask under gentle stirring, which contained a small amount of PVOH solution. To remove the PVOH, the microparticles were washed three times with MilliQ water. After the washing steps, they were transferred to a 30mL vial and dried through lyophilization, enabling subsequent analysis using a scanning electron microscope.

IV.2.4 Synthesis of Fe_3O_4 nanoparticles

21.6 g of ferric chloride was added to 200 ml of deionized water and stirred for at least 20 min under closed condition with nitrogen bubbling. 8.1 g of ferrous chloride was added to 100 ml of deionized water, stirred also for 20 min under closed conditions with nitrogen bubbling. The two solutions were then mixed and the mixture was stirred under a closed condition for 25 min. Aqueous ammonia and oleic acid (OA) were slowly added into the mixture at a relative rate of 10 drops of aqueous ammonia for 1 drop of OA until 50 ml of aqueous ammonia and 3 ml of oleic acid were added. The mixture was then stirred for another 25 min. A magnet was placed at the bottom of the flask to obtain wet precipitate of magnetic particles (MPs) which was washed twice with deionized water and alcohol, respectively. Then, the wet precipitate was stirred for 5 min at 75 °C. Finally, the wet precipitate was mixed with toluene at a desired ratio and stirred for 30 min to obtain the dispersion of Fe_3O_4@OA. The final concentration of nanoparticles is equal to 20mg/ml.

IV.2.5 Preparation of the PCL-4COU solution containing Fe_3O_4 nanoparticles

1.5mL of nanoparticles solution was added to a solution of 5w% PCL-4COU (10,000g/mol) solution, prepared by dissolving 500mg of PCL-4COU and 18.2mg of benzophenone (0.1 mmol) in 9.5g of AcOEt.

IV.2.6 Temporary shape programming methods

Method for the production of a disc shape:

50mg of crosslinked PCL microparticles is dispersed in 10g of molten PEO at 100°C and mixed for 5min with a magnetic stirrer. This melted suspension was recovered on a Teflon sheet and cooled down to RT. The solidified PEO block containing the microparticles is then crushed in small pieces. 200mg of this powder is placed between two microscope slides and heated at 80°C until the complete melting of the PEO. Then there were pressed into a binder clip with a force of 1.15N[26] and cooled down to RT. The two slides were separated and the resulting deformed PCL microspheres are then observed with an optical microscope.

Method for the production of a rod shape:

50mg of crosslinked PCL or core-shell PCL//PBEP microparticles is placed in a rectangular mold (50mm x 10mm x 1mm) and coated with a 10w% PVOH solution. After the complete evaporation of the water, the plastic film containing the microparticles is recovered. This film is placed in the heat gun flow at 100°C for 30 s and then gently manually stretched to avoid the film rupture and cooled down to RT. Stretched microparticles are recovered by placing the film in water to dissolve the PVOH. Deformed microparticles are then observed with an optical microscope.

IV.2.7 Characterization techniques

The surface and morphology of the formulated and washed microparticles were observed by scanning electron microscopy (SEM) images were collected with FEI Quanta 600 apparatus. SEM pictures are used to determine the mean diameter and the polydispersity of each sample. Indeed, 50 microparticles of each kind of samples are analyzed by ImageJ software in order to calculate the mean diameter (d), the standard deviation (θ) and the polydispersity index(PDI) which is calculated thanks to the following formula:

$$PDI = \left(\frac{\theta}{d}\right)^2$$

Differential scanning calorimetry (DSC) was performed on a Discovery series TA DSC250 calibrated with indium. Between 5-10mg of the crosslinked microparticles is transferred in the DSC oven at 20°C and a cooling ramp of 10°C.min^{-1} is applied until -80°C. After 5 min of temperature stabilization, a heating ramp of 10°C.min^{-1} is applied until 100°C. This cooling–heating cycle is repeated two times, the melting temperature (T_m) and the enthalpy (ΔH_m) being recorded during the second heating ramp.

Thermogravimetric analysis was performed with a TGA2 Mettler Toledo. Typically, 5.0mg of products are weighted in a ceramic pan are heated at 10°C.min^{-1} until 600°C under dry air. The mass loss in function of the time is determined and reported on a thermogram.

An Amscope MD35 optical microscope with a magnification of 200x was used to take pictures and videos of microparticles shape-memory and swelling experiments.

IV.3 Results and discussion

IV.3.1 Flow formulation of crosslinked PCL microparticles

Microfluidic technique (MF) enables the manipulation of microflows in microchannels to generate uniform emulsion droplets. The principle is the same as the formation of an o/w emulsion, i.e. drops of the polymer in an organic solvent are dispersed in an aqueous phase in the presence of a surfactant, except that the internal organic phase is pushed in the continuous aqueous one by a microchannel system thanks to syringe pumps at constant-flow and controlling the flow rate. The aqueous phase must contain an emulsifier to stabilize the polymer particles. Poly(vinyl alcohol) (PVOH) is a common surfactant used to stabilize polyester microspheres with a concentration varying between 1w% and 3w% as reported for such microfluidic formulations[27,28]. On the other hand, the organic phase contains the polymer, typically at a concentration of 5w%. Ethyl acetate is selected as organic solvent as it allows the solubilization of PCL and is a class 3 solvent which is better than chlorinated solvents especially

when biomedical applications are foreseen. These solutions are pushed in different capillaries and reach a cross-junction in which microdroplets of organic solution are formed by shearing and capillary forces (Figure 3). Once the polymer droplet is formed in the tubing, ethyl acetate leaves the droplet thanks to its partial miscibility with water leading to a progressive concentration of the polymer solution with, at the end of the formulation process, the recovery of a completely solid microparticles (zoom in Figure 3). In order to have shape-memory properties, these microspheres must be crosslinked. This crosslinking is achieved by photodimerization of coumarin moieties under UV irradiation. Thanks to the transparency to UV light of the tubing, this irradiation is performed all along, during the solvent diffusion and polymer microspheres formation (Figure 3).

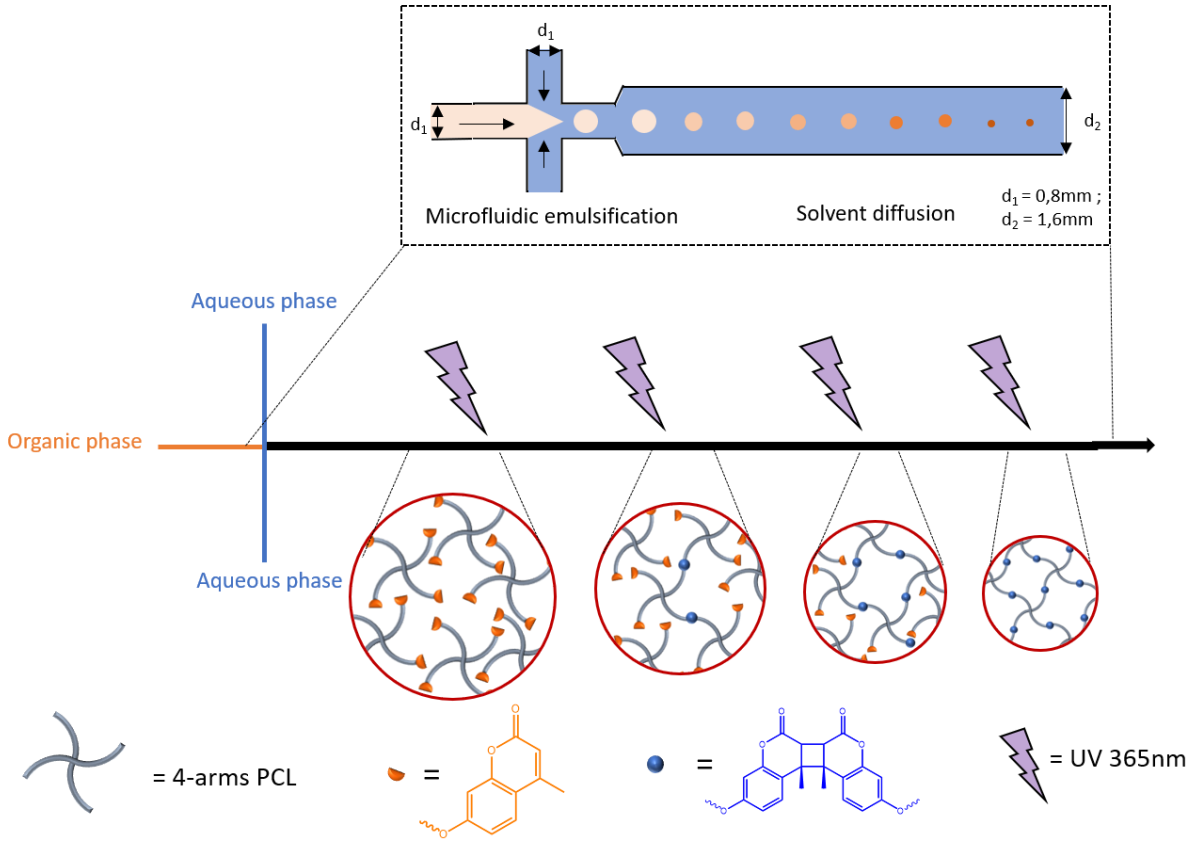

Figure 3 : Scheme of the microfluidic cross-junction device used for the formulation of SM microspheres.

In the cross-junction device, the size of the microdroplets will be related to the size of the final PCL microspheres once the organic solvent is extracted. Different parameters

influence the size and the polydispersity of these droplets. These include the flow rate of both solutions and their ratio, the organic phase viscosity, which is dependent on the polymer concentration, or the concentration of the PVOH stabilizer. These parameters have to be optimized in order to reach the targeted diameter of the microspheres as well as a high particles size homogeneity (i.e. above 100µm to avoid the more unpredictable behavior of the smaller microspheres in blood vessels[8]).

Firstly, the role of the surfactant concentration on the droplet size was investigated. The PCL concentration in the AcOEt solution was thus fixed to 2wt% and the concentration of PVOH in the aqueous phase was varied between 1 and 3wt%[27,28]. The flow of the organic phase is fixed at 0.025mL/min and the total flow of the PVOH solution is kept constant at 2mL/min. The size and size dispersity of the collected microspheres in regards to the formulation conditions are summarized in Table 1 (entries 1-3). Considering that a microsphere sample is monodisperse for a PDI below 0.1[29], we can conclude that all these formulation conditions have produced well-defined monodisperse microspheres. Figure 4a shows a representative SEM image of the microspheres produced in conditions of entry 2 Table 1 where the size homogeneity can be visually appreciated.

Table 1 : Formulation parameters to formulate crosslinked PCL-4COU-based microparticles with the T-junction microfluidic device and the corresponding diameter and PDI of the collected microspheres as determined by SEM analysis.

Entry	PVOH concentration (wt%)	PVOH flow rate (mL/min)	Polymer concentration (wt%)	Polymer flow rate (mL/min)	Size (µm)	PDI
1	1	2	2	0.025	/	/
2	2	2	2	0.025	57.5	$2.3\ 10^{-3}$
3	3	2	2	0.025	48.8	$1.0\ 10^{-2}$
4	1	2	**5**	0.025	86.1	$4.4\ 10^{-3}$
5	2	2	**5**	0.025	67.9	$4.7\ 10^{-3}$
6	3	2	**5**	0.025	53.2	$3.1\ 10^{-3}$
7	1	**1**	5	0.025	147.7	$3.0\ 10^{-2}$
8	2	**1**	5	0.025	110.1	$7.3\ 10^{-3}$
9	3	**1**	5	0.025	64.2	$5.4\ 10^{-3}$
10	1	2	5	**0.05**	149.2	$1.6\ 10^{-2}$
11	2	2	5	**0.05**	91.2	$9.4\ 10^{-3}$
12	3	2	5	**0.05**	69.3	$5.2\ 10^{-3}$

Increasing the emulsifier concentration (entries 1 to 3, Table 1) leads to the formulation of smaller particles due to the reduction of the interfacial tension between the organic and the aqueous phases leading to the stabilization of smaller droplets and thus smaller polymer particles[30,31]. The conditions of entry 1 give highly polydisperse microparticles without a spherical shape. This can be attributed to the higher polymer dilution and lower concentration of the emulsifier used. For entries 2 and 3, the PDI perfectly suits embolization applications but the particles diameters are far below 100µm.

Increasing the concentration of PCL in the organic phase from 2wt% to 5wt% leads to bigger particles ranging from 53µm to 86µm (entries 4-6, Table 1). Indeed, when the polymer concentration is higher, the saturation state of the polymer in the solvent is more easily reached and a faster solidification restrict the droplets shrinkage, resulting in larger microspheres[27]. Although, the PDI is still very low, the microspheres size remains below 100µm.

A solution is found by decreasing the surfactant flow rate (entries 7-8, Table 1) which increases the microparticles size above 100µm, which is explained by the decreased shearing forces at lower flow rate of the aqueous phase leading to later droplet separation which is in line with other studies[27,32].

Expectedly, increasing the PCL solution flow rate to 0.05mL/min increases also the particles size (Table 1, entries 10-12). In that case, the PDI increases which can be explained by the change of droplet formation regime that shifts from a dripping to a jetting regime when the flow rates of both the continuous and the discontinuous phases become closer[24].

In all the tested conditions, the collected particles produced by the cross-junction flow droplet generation system exhibit remarkable monodispersity with a PDI far below 0.1 (Table 1, Figure 4).

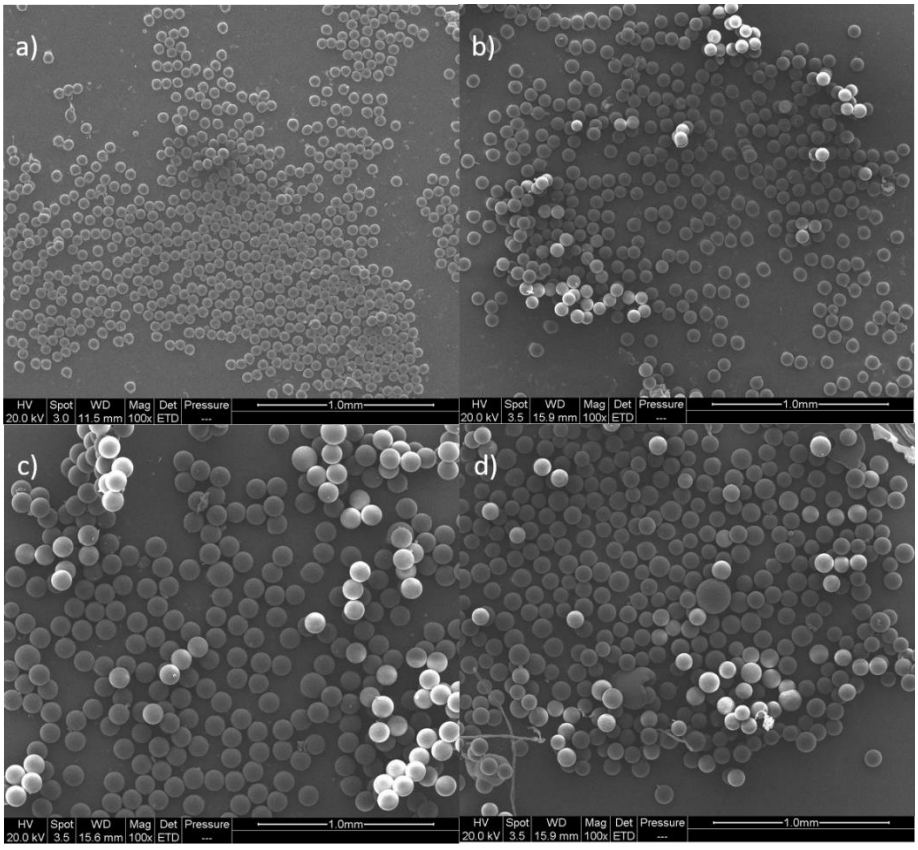

Figure 4 : SEM images of microparticles formulated with conditions reported in Table 1 a) Entry 2; b) Entry 5 ; c) Entry 8; d) Entry 11

Considering the specifications in terms of size and dispersity required to a further application, the formulation conditions of entry 8 Table 1 (Figure 4c) turn out to be the most appropriated with PCL microspheres size of 110.1µm with a PDI of 7.3 10^{-3}.

In order to impart shape-memory properties to PCL-4COU-based microspheres, a UV irradiation was applied during the 4 min of formulation process. This appears suitable to reach an efficient crosslinking by photodimerization of the coumarin in presence of the low amount (0.1mmol) of benzophenone as photosensitizer. Indeed, these crosslinking conditions are quite similar to reported data for the crosslinking of thin film made of PCL-4COU stars [20]. In order to confirm the efficiency of the crosslinking, CH_2Cl_2 was added on the collected microspheres and the behavior was observed by optical microscope (Figure 5).

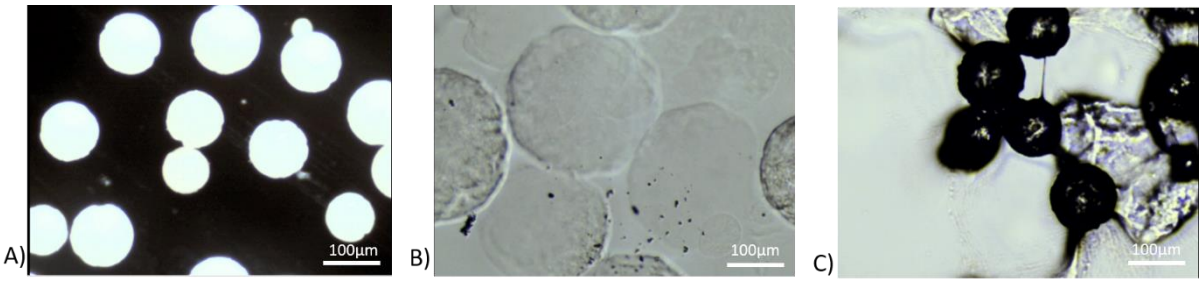

Figure 5 : Swelling experiment of crosslinked microspheres followed with an optical a) before addition of DCM, b) after swelling in DCM and c) after evaporation of DCM.

Prior addition of CH_2Cl_2, the microspheres diameter is about 110µm. In presence of DCM, a good solvent for PCL, the microspheres swell and reach a diameter of 280µm. In addition, after DCM evaporation, the microspheres return to their initial size and shape indicating an efficient and homogeneous crosslinking over the entire volume of the microspheres.

IV.3.2 Thermal properties of crosslinked PCL-4COU-based microspheres

The programming of a temporary shape in a crosslinked PCL relies on the melting and recrystallization of the material. Therefore, it is mandatory that the designed microspheres

kept their ability to crystallize. Therefore, the melting temperature (T_m), the crystallinity rate (X_c), and the crystallization temperature (T_c) of the microspheres were determined by DSC and compared to corresponding crosslinked 4-arm PCL star-shaped thin film[18] (Table 2).

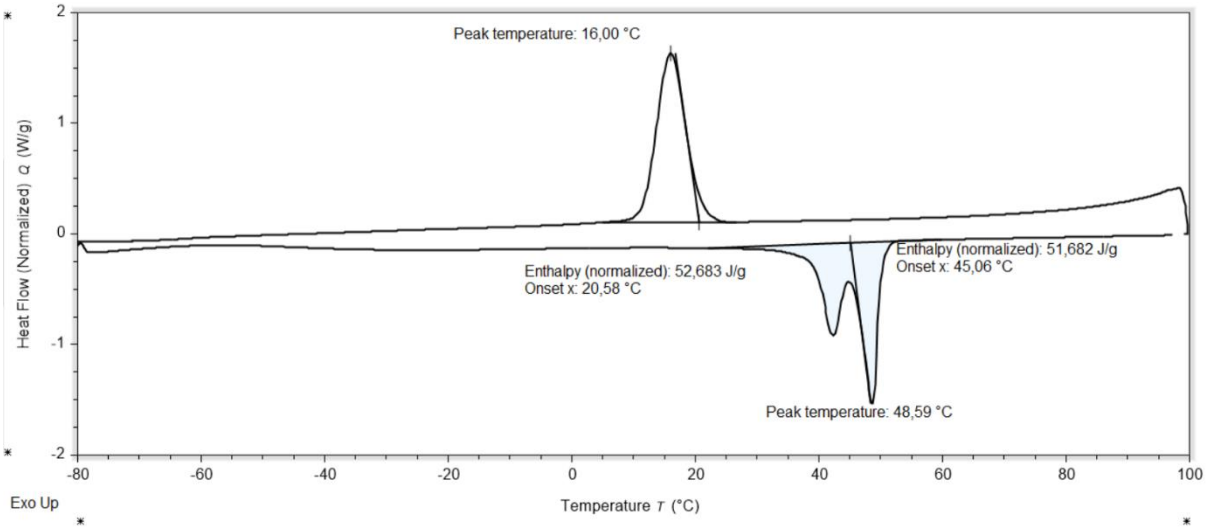

Figure 6 : DSC traces for the PCL-4COU-based microspheres

The thermogram recorded for the microspheres is presented on Figure 6. Clearly, during the heating ramp, a melting process is observed by a split endotherm around 45°C. During the cooling ramp, the crystallization requires to reach lower temperature, below 16°C. This type of DSC trace is commonly observed for crosslinked PCL. The crystallinity rate was calculated by dividing the ΔH_f (T_m), i.e. the enthalpy of melting measured by DSC, by ΔH_f^0 (T^0_m), i.e. the enthalpy of melting for a 100% crystalline PCL which is equal to 139.5 J g^{-1} according to the literature[20]. A crystallinity rate of 37% is determined which is enough to fix the temporary shape by stocking the energy induced by the material deformation. The higher T_m and X_c suggest that the microparticles are less crosslinked than the thin film because an increased crosslinking density decreases the melting temperature[20]. The lower crosslinking ratio is explained by a shorter irradiation time in the case of microspheres (4 min) formulation compared to thin film (5 min). The dilution of the chain-ends in AcOEt could also disfavor the photodimerization reaction considering that the thin film was crosslinked in bulk.

Table 2 : Melting temperature (Tm), crystallization temperature (Tc) and crystallinity degree determined by DSC for UV-crosslinked PCL-4COU as thin film or as microspheres.

Sample	T_m (°C)	T_c (°C)	X_c (%)
4-arm star-shape PCL-4COU	50	28	59
PCL-4COU-based thin film	44	20	29
PCL-4COU-based microspheres	48	16	37

IV.3.3 Shape-memory properties of crosslinked PCL microspheres

In order to achieve shape-memory, programming the temporary shape is essential. This is accomplished by subjecting the microspheres to a temperature above their melting point, causing the crystallites melting. Subsequently, mechanical stress is applied to deform the particles, which is maintained until the microspheres have completely cooled to room temperature (RT). At this point, the mechanical stress can be released, and the temporary shape is fixed due to the crystallites storing the deformation energy. Finally, to initiate the recovery process, the microparticles are heated above the melting temperature without applying any mechanical stress, allowing shape recovery to occur through elasticity.

A first test was performed to demonstrate the shape-memory of UV crosslinked PCL microspheres. The programmed shape was obtained by compressing between two microscope slides, a molten dispersion of the microspheres in PEO. The microspheres are dispersed in PEO to have a better separation of them and observe them individually. After cooling under stress and stress release at low temperature, thin discs were obtained as evidenced by their transparency when they are observed by optical microscope (Figure 7a). On this picture, no gap between the three discs and the PEO matrix is observed, which traduces an excellent fixity, i.e. the ability of the sample to keep its temporary shape when the mechanical stress is removed. The obtained discs exhibit a diameter between 200-250µm and a thickness between 12-15µm while we started from spheres of 110µm, showing the good

ability to store a strong deformation. After heating at 60°C for 20 sec (Figure 7b), the microspheres recovered their initial shape confirming the imparted shape-memory property. Indeed, the top view image shows three black dots, efficiently blocking the light of the microscope, corresponding to the recovered three-dimensional spherical shape with a diameter back to 110-130µm.

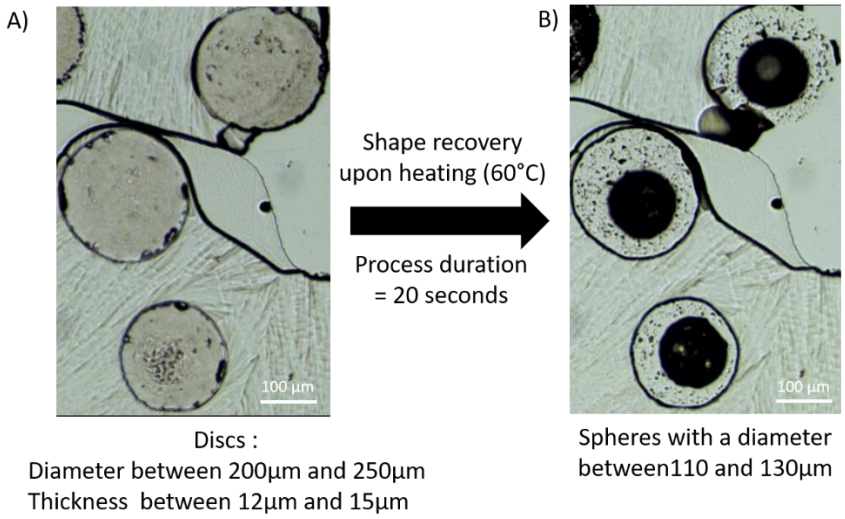

Figure 7 : Optical microscope images of shape-memory experiment based on PCL-4COU-based microspheres dispersed in a PEO film: a) after programming the disc shape (top view) and b) after recovery of the sphere shape upon simple heating at 60°C for 20sec.

Other shapes, such as rod-like shapes that would be better suited for traveling through a catheter have been programmed by a film stretching technique[9,10,16,33,34]. This technique consists in dispersing the PCL shape-memory microspheres in a PVOH film before to heat it at 80°C in order to melt the PCL and stretched it to obtain oblate PCL microparticles with different aspect ratio (l/d) depending on the stretching amplitude. After cooling of the stretched composite film, the PCL chains crystallize and fix the elongated shape. After dissolution of PVOH, rod-like shapes particles are collected. Two different experiments were performed on the same microsphere batch to obtain rod-like microparticles with an aspect ratio of 3 and 5 (Figure 8).

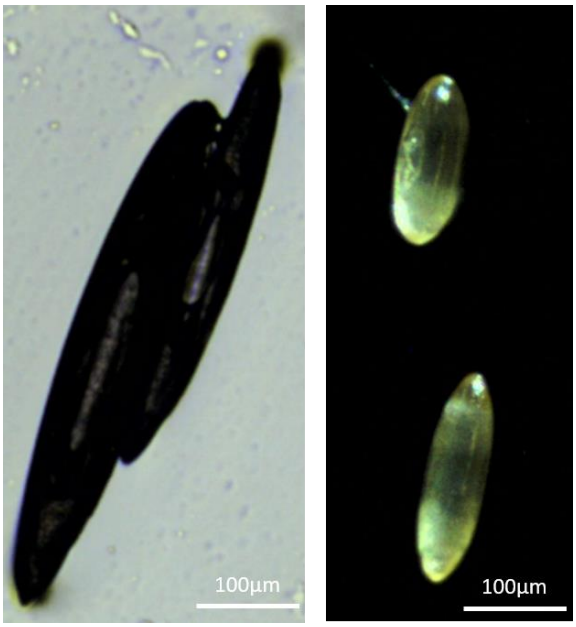

Figure 8 : Optical microscope images of rod-shaped shape-memory microparticles with different aspect ratio. Left : aspect ratio = 5 and Right: aspect ratio = 3.

Similar to the microparticles with disc shape, most of the microparticles achieve a complete recovery after heating. However, a few of them exhibit a lemon shape after deformation, particularly the ones that were subjected to the highest degree of stretching due to an applied stretching force significantly greater in the deformation direction. As a result,

the stretching energy becomes excessive, causing the elasticity threshold to be exceeded (Figure 9).

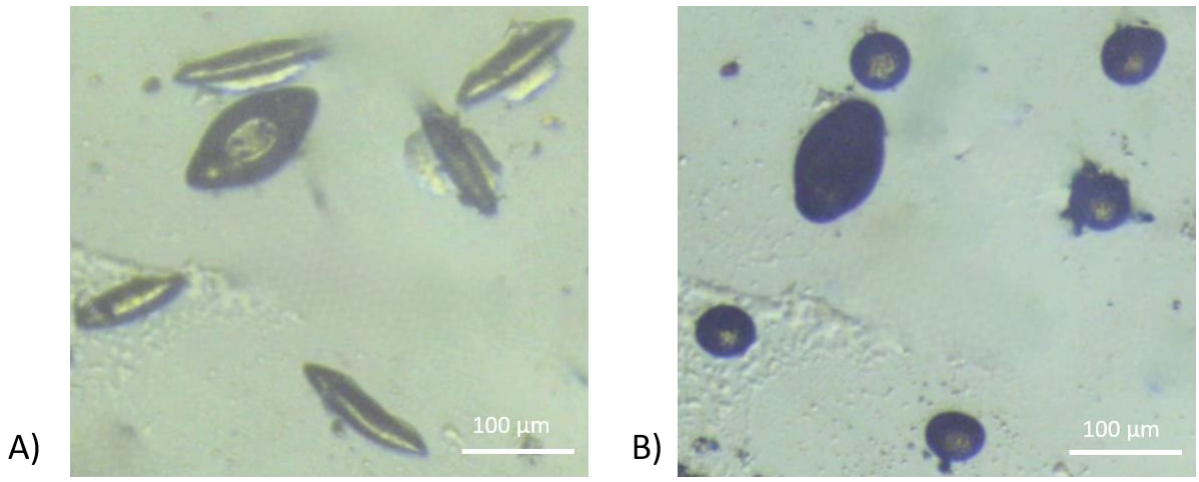

Figure 9 : Shape-memory experiment on stretched microparticles (from entry 5 Table 1). A) programmed shape before heating B) recovered shape after heating at 60°C.

Some cytotoxicity assays were also carried out on these microspheres. Four different cytotoxicity tests were performed. Two tests, one direct and one indirect, on bovine fibroblast and the same on human umbilical vein endothelial cells (HUVEC). All results show a cell viability above 80% (See SI).

IV.3.4 Shape-memory properties of crosslinked PCL//PBEP microspheres

Concerning the core-shell microparticles, DSC analysis (Figure 10) is performed on the different core-shell microspheres and expectedly, the PCL//PBEP microspheres exhibit crystallinity with a melting enthalpy of 35.3 J/g and T_m at 55.6°C, thanks to the semi-crystalline PCL core. This corresponds to a crystallinity rate of 25.8% which is far enough to program a temporary shape stable up to 40°C, i.e. the measured melting temperature. In case of PDLLA//PBEP, the T_g of the PDLLA core is observed at 43°C, which can also be used to fix a temporary shape.

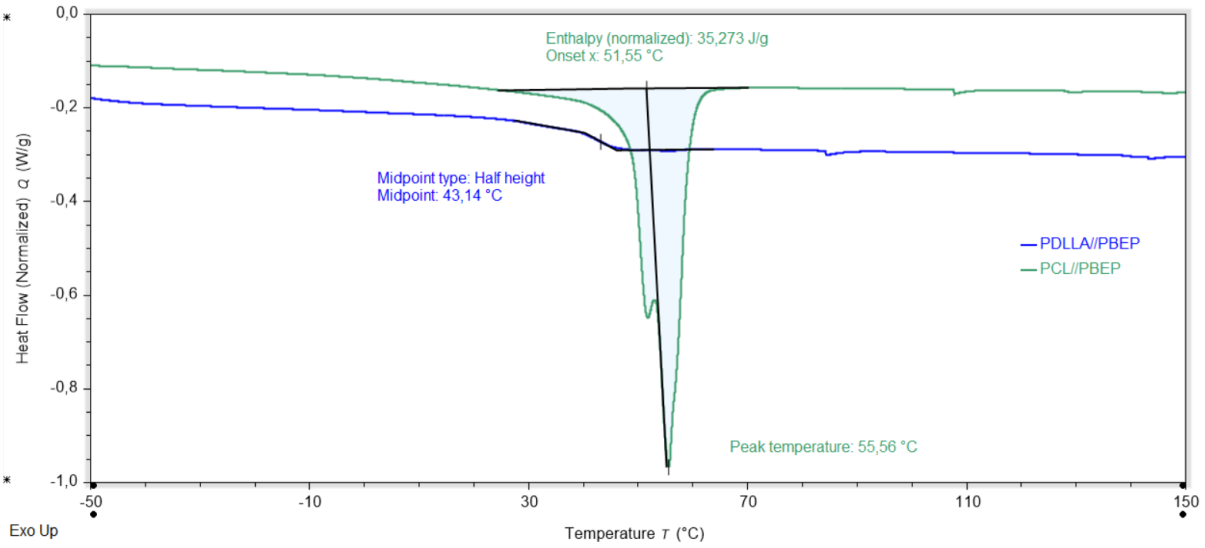

Figure 10 : DSC traces of PDLLA//PBEP (blue) and PCL//PBEP (green) microspheres

Figure 11 illustrates the schematic representation of the shape-memory cycle observed in PCL//PBEP microspheres. Upon heating the microsphere above its melting temperature, the crystallites of the PCL melt, resulting in a softening of the microsphere that allows its deformation under mechanical stress. Throughout the cooling process, the deformation is maintained, and once the microparticle reaches a sufficiently cooled state, the temporary shape is fixed. Finally, when the microparticle is reheated without any applied mechanical stress, it undergoes elastic recovery, returning to its permanent shape.

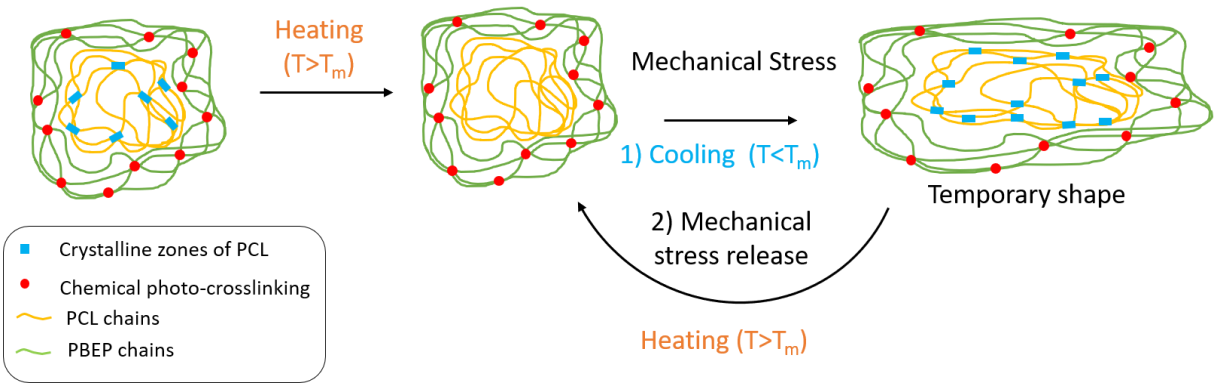

Figure 11 : Schematic shape-memory experiment of core-shell PCL//PBEP microspheres

An ovoid temporary shape is thus tentatively programmed and fixed by applying the film stretching technique to the starting spherical microspheres [9,10,16,33,34] (Figure 12A and B). The recovery is then performed by heating the microparticles at 80°C (Figure 12C). As evidenced by the optical microscope images of Figure 12, the microspheres exhibit shape-memory properties. An ovoid shape is indeed observed after film stretching which is partly recovered after heating. Nevertheless, the spherical shape recovery is not complete because of some leaking of uncrosslinked PCL through the PBEP shell. To avoid leaking, crosslinking of the PCL is considered in the next chapter by using 4-arm PCL stars functionalized by UV reactive coumarins moieties as chain-ends[20].

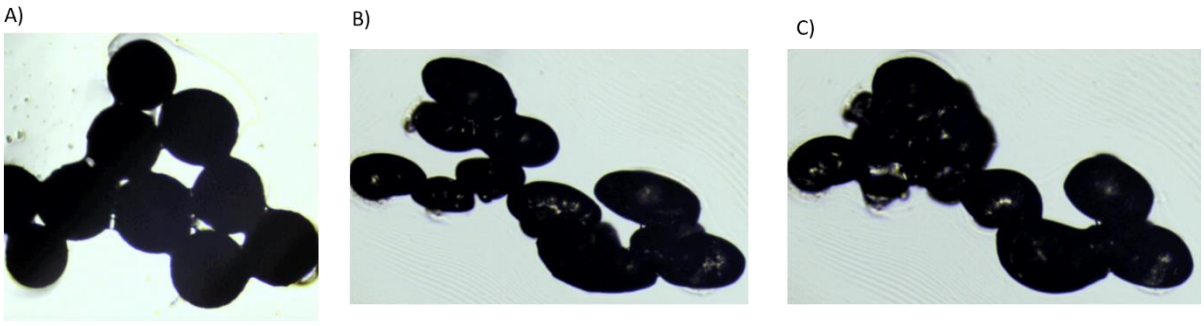

Figure 12 : Optical microscope images of PCL//PBEP microparticles during a shape-memory experiment: A) initial spherical shape ; B) Programmed elongated shape by film stretching method and C) microparticles shape recovery after being heated.

IV.3.5 Encapsulation of magnetite in crosslinked PCL microparticles

The developed microfluidic process allows the easy loading of the microspheres by ingredients soluble or easily dispersed in the organic phase. In order to make the PCL microspheres radio-opaque, they were loaded with magnetite nanoparticles. The PCL-4COU solution containing the nanoparticles were formulated using the same conditions as previously described (entry 8 table 2). The recovered suspension is colorless and the microparticles are dark brown which indicates a high encapsulation efficiency. This was confirmed by a TGA experiment (Figure 13). The nanoparticle loading corresponds to 5.4% and

the calculated according to a quantitative encapsulation is equal to 5.47% which means that the encapsulation efficiency equals 98.7%.

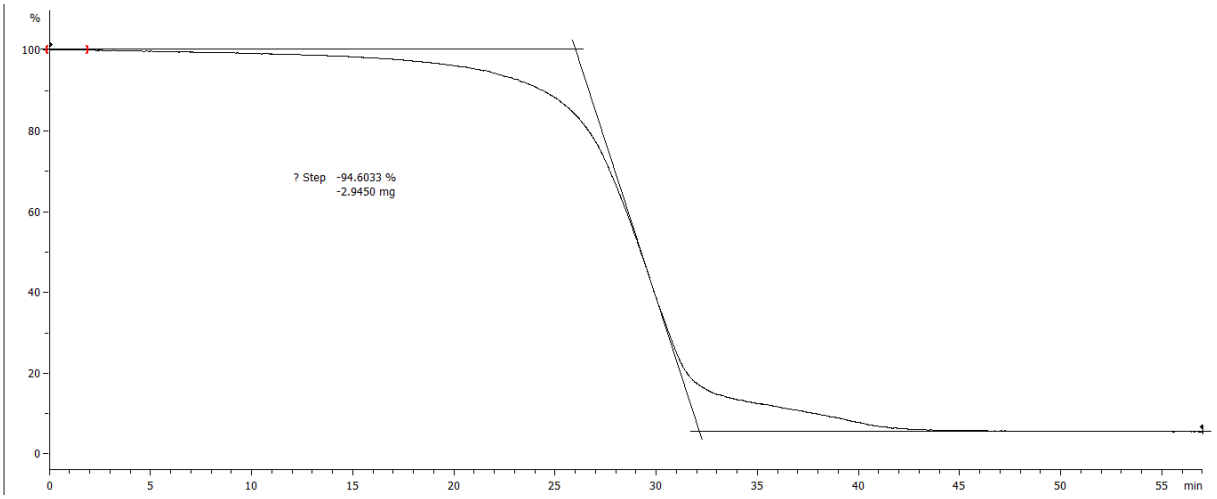

Figure 13 : Thermogravimetric analysis profile of PCL-4COU loaded with magnetite nanoparticles

Microscope images of the magnetic microspheres were taken by SEM (Figure 14). The size and the PDI were determined and gathered in the following Table 3. The magnetic microspheres are smaller than previously formulated microspheres without magnetite. This can be explained by the presence of toluene in the polymer solution coming from the magnetite nanoparticles suspension which dilute the solution and produce smaller microspheres, as it was discussed previously.

Table 3 : Mean size and PDI comparison between microparticles with and without magnetic nanoparticles

PVOH concentration (wt%)	PVOH flow rate (mL/min)	Polymer concentration (wt%)	Polymer flow rate (mL/min)	Magnetite	Mean Size (µm)	PDI
2	1	5	0.025	NO	110.1	$7.3\ 10^{-3}$
2	1	5	0.025	YES	90.7	$6.2\ 10^{-3}$

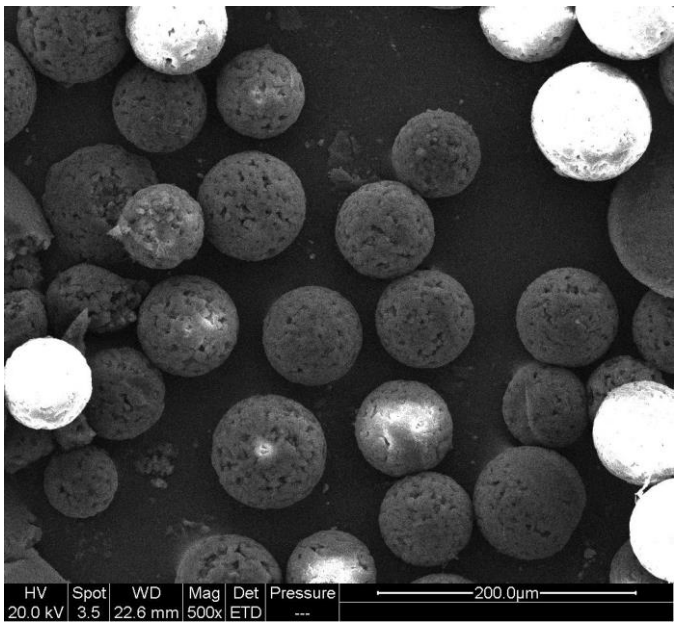

Figure 134 : SEM picture of magnetite loaded microspheres

Finally, it was confirmed that the magnetic microparticles respond to the magnetic field of a magnet (Figure 15).

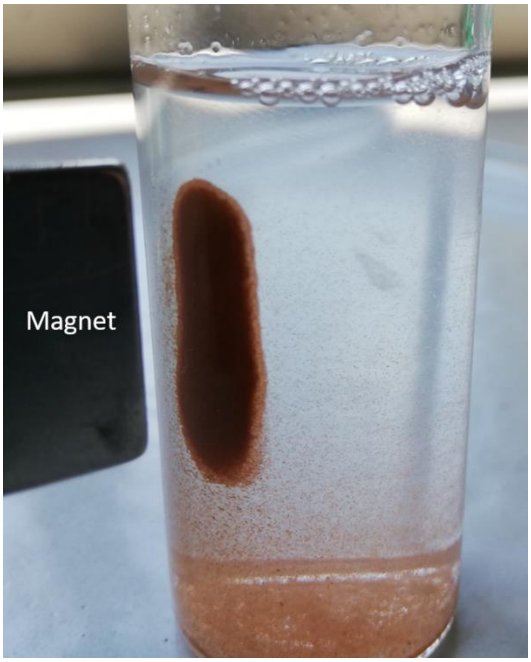

Figure 145 : Magnetic microparticles responsiveness to a magnet

IV.4 Conclusion and perspective

Shape-memory microparticles can play a key role in drug-delivery applications or as embolization agents in the future. In this work, we formulate, with a very simple microfluidic device, highly monodisperse crosslinked microspheres composed of PCL, a biodegradable and biocompatible material. The selected microparticles have similar thermal properties than a thin film composed of crosslinked PCL-4COU with a melting temperature of 48°C. The crystallinity rate used to fix the temporary shape, a crucial step for shape-memory application, is also similar to the one of crosslinked thin film close to 35%. Finally, different shapes were obtained by two different deformation techniques and these deformed microparticles present excellent fixity and recovery. The shape recovery occurs in 20 seconds when the microparticles were heated at 60°C.

Microspheres composed of PCL and PBEP exhibit shape-memory properties. The shape-memory properties could still be improved by a better crosslinking of the PPE shell or by improving the PPE hydrophilicity making the shell less permeable to molten PCL.

The temperature stimulus could be problematic for biomedical purpose. For this reason, the development of magnetite-loaded microspheres was investigated to induce shape-memory properties through the application of a magnetic field.

Moreover, the encapsulation of magnetic nanoparticles in microspheres could allow the direct MRI observation of the microparticles in the body during the surgery and at low costs[35–37]. The development of a full microfluidics process, from the formulation to the deformation of the PCL crosslinked microspheres, is currently under investigation to allow further potential application in the biomedical field.

IV.5 References

1 N. Wang, X. Jiang and J. Wang, *Prog. Biomed. Eng*, , DOI:10.1088/2516-1091/ab6c7d.

2 J. Hu, H. Albadawi, B. W. Chong, A. R. Deipolyi, R. A. Sheth, A. Khademhosseini and R. Oklu, *Advanced Materials*, , DOI:10.1002/adma.201901071.

3 B. Liu, Z. Xu, H. Gao, C. Fan, G. Ma, D. Zhang, M. Xiao, B. Zhang, Y. Yang, C. Cui, T. Wu, X. Feng and W. Liu, *Adv. Funct. Mater.*, 2020, **1910197**, 1–12.

4 P. F. Chiang, C. L. Peng, Y. H. Shih, Y. H. Cho, C. S. Yu, Y. M. Kuo, M. J. Shieh and T. Y. Luo, *ACS Biomater Sci Eng*, 2018, **4**, 3425–3433.

5 J. Doucet, L. Kiri, K. O'Connell, S. Kehoe, R. J. Lewandowski, D. M. Liu, R. J. Abraham and D. Boyd, *J Funct Biomater*, , DOI:10.3390/jfb9010014.

6 Y. Chen, J. Zhang, Y. Zou and Y. Wu, *Front. Chem.*, 2019, **7**, 1–11.

7 M. Sarmadi, A. M. Behrens, K. J. McHugh, H. T. M. Contreras, Z. L. Tochka, X. Lu, R. Langer and A. Jaklenec, *Sci Adv*, 2020, **6**, 1–14.

8 A. Laurent, *Tech Vasc Interv Radiol*, 2007, **10**, 248–256.

9 J. A. Champion, Y. K. Katare and S. Mitragotri, *Journal of Controlled Release*, 2007, **121**, 3–9.

10 S. Nejati, E. Mohseni Vadeghani, S. Khorshidi and A. Karkhaneh, *Eur Polym J*, 2020, **122**, 109353.

11 A. Sen Gupta, *Wiley Interdiscip Rev Nanomed Nanobiotechnol*, 2016, **8**, 255–270.

12 W. Small IV, P. Singhal, T. S. Wilson and D. J. Maitland, *J Mater Chem*, 2010, **20**, 3356–3366.

13 Y. Bai, J. Zhang, J. Ju, J. Liu and X. Chen, *React Funct Polym*, 2020, **157**, 104770.

14 L. M. Cox, J. P. Killgore, Z. Li, R. Long, A. W. Sanders, J. Xiao and Y. Ding, *Langmuir*, 2016, **32**, 46.

15 J. Huang, L. Lai, H. Chen, S. Chen and J. Gao, *Mater Lett*, 2018, **225**, 24–27.

16 C. Wischke and A. Lendlein, *Langmuir*, 2014, 2820–2827.

17 R. Liu, H. Dai, Q. Zhou, Q. Zhang and P. Zhang, *J Biomater Sci Polym Ed*, 2016, **27**, 1248–1261.

18 T. Defize, R. Riva, C. Jérôme and M. Alexandre, *Macromol Chem Phys*, 2012, **213**, 187–197.

19 T. Defize, R. Riva, J. M. Thomassin, M. Alexandre, N. Van Herck, F. Du Prez and C. Jérôme, *Macromol Rapid Commun*, 2017, **38**, 1–7.

20 T. Defize, J. Thomassin, H. Ottevaere, G. Eppe, C. Jérôme and R. Riva, *Macromolecules*, 2019, 444–456.

21 E. Lagreca, V. Onesto, C. Di Natale, S. La Manna, P. A. Netti and R. Vecchione, *Prog Biomater*, 2020, **9**, 153–174.

22 A. Vlachopoulos, G. Karlioti, E. Balla, V. Daniilidis, T. Kalamas, M. Stefanidou, N. D. Bikiaris, E. Christodoulou, I. Koumentakou, E. Karavas and D. N. Bikiaris, *Pharmaceutics*, , DOI:10.3390/PHARMACEUTICS14020359.

23 E. Baeten, S. Vanslambrouck, C. Jérôme, P. Lecomte and T. Junkers, *Eur Polym J*, 2016, **80**, 208–218.

24 S. Yazdian Kashani, A. Afzalian, F. Shirinichi and M. Keshavarz Moraveji, *RSC Adv*, 2020, **11**, 229–249.

25 E. Y. Chung, H. M. Kim, G. H. Lee, B. K. Kwak, J. S. Jung, H. J. Kuh and J. Lee, *Carbohydr Polym*, 2012, **90**, 1725–1731.

26 N. S. Yagnick, R. Singh, M. Tripathi, S. Mohindra, H. Deora, A. Suri and S. K. Gupta, *World Neurosurg*, 2019, **121**, 222–226.

27 T. Watanabe, T. Ono and Y. Kimura, *Soft Matter*, 2011, **7**, 9894–9897.

28 B. Amoyav and O. Benny, *Polymers (Basel)*, , DOI:10.3390/POLYM11030419.

29 K. N. Clayton, J. W. Salameh, S. T. Wereley and T. L. Kinzer-Ursem, *Biomicrofluidics*, 2016, **10**, 20048.

30 B. Amoyav and O. Benny, *Applied Nanoscience (Switzerland)*, 2018, **8**, 905–914.

31 K. Park, A. Otte, F. Sharifi, J. Garner, S. Skidmore, H. Park, Y. K. Jhon, B. Qin and Y. Wang, *Journal of Controlled Release*, 2021, **329**, 1150–1161.

32 G. T. Vladisavljević, H. Shahmohamadi, D. B. Das, E. E. Ekanem, Z. Tauanov and L. Sharma, *J Colloid Interface Sci*, 2014, **418**, 163–170.

33 Y. Yang, D. Nie, Y. Liu, M. Yu and Y. Gan, *Drug Discov Today*, 2019, **24**, 575–583.

34 R. A. Meyer, R. S. Meyer and J. J. Green, *J Biomed Mater Res Part A*, 2015, **103**, 2747–2757.

35 E. Y. Chung, H. M. Kim, G. H. Lee, B. K. Kwak, J. S. Jung, H. J. Kuh and J. Lee, *Carbohydr Polym*, 2012, **90**, 1725–1731.

36 J. Li, J. Wang, J. Li, X. Yang, J. Wan, C. Zheng, Q. Du, G. Zhou and X. Yang, *Acta Biomater*, 2021, **131**, 532–543.

37 K. H. Lee, E. Liapi, J. A. Vossen, M. Buijs, V. P. Ventura, C. Georgiades, K. Hong, I. Kamel, M. S. Torbenson and J. F. H. Geschwind, *Journal of Vascular and Interventional Radiology*, 2008, **19**, 1490–1496.

Chapter V: Hybrid covalent adaptable networks from cross-reactive poly(ε-caprolactone) and poly(ethylene-oxide) stars towards advanced shape-memory materials.

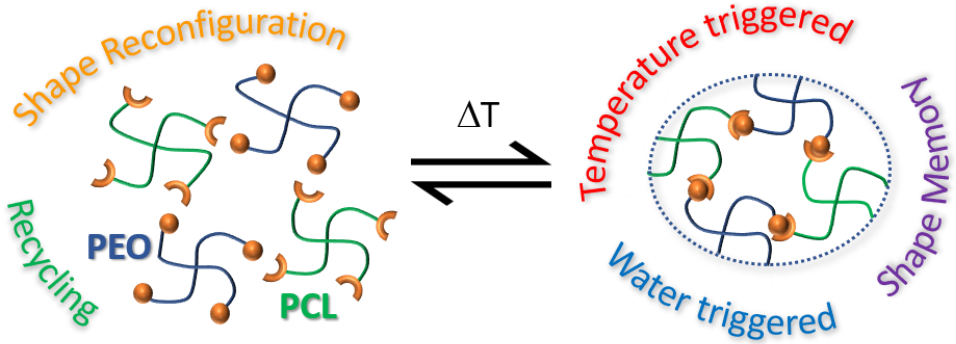

Paper published in 2021 in Materials Advances
J. Caprasse, R. Riva, J. M. Thomassin and C. Jérôme, *Mater Adv*, 2021, **2**, 7077–7087.

Chapter V: Hybrid covalent adaptable networks from cross-reactive poly(ε-caprolactone) and poly(ethylene-oxide) stars towards advanced shape-memory materials

The synthesis and properties of hybrid poly(ε-caprolactone) (PCL)–poly(ethylene oxide) (PEO) covalent adaptable networks have been investigated. This novel material uniquely combines recycling and reconfiguration capabilities with temperature and water-triggered shape-memory properties. Firstly, 4-arm star-shaped PEO and PCL were end-capped with furan and maleimide moieties, respectively. Then, equimolar mixtures of these cross-reactive stars were melt-blended and cured leading to PCL-PEO hybrid networks by Diels-Alder addition between chain-ends. The PCL/PEO content of the networks was varied by using PCL stars of different molar masses allowing to tailor the material hydrophilicity. We evidenced that the as-obtained hybrid networks exhibit not only excellent temperature-triggered shape-memory properties (high fixity and high and rapid recovery) but also valuable water-triggered shape-memory properties characterized by a high fixity and a recovery-rate controlled by the network composition. Remarkably, thanks to the introduction of thermo-reversible Diels-Alder adducts within the covalent network, we demonstrated that this material can be easily recycled while preserving the shape-memory performances. Therefore, the reconfiguration of the so-called permanent shape is straightforward making this material a potential candidate for applications as water responsive medical devices. The hydrolytic stability of these networks was demonstrated over a period of one month of immersion in water at physiological pH.

V.1 Introduction

Shape-memory polymers are a class of stimuli-responsive materials that can be elastically deformed and then fixed into a temporary shape by immobilization of the network chains. They later recover to their original (also called permanent) shape when exposed to an external stimulus that gives back their mobility to the network chains. The formation of three-dimensional covalent networks by chemical crosslinking of the polymer chains enhances the thermal stability and the structural integrity of the materials leading to an improvement of the mechanical properties, typically a significant increase of the elastic behavior in response to strain deformations. Moreover, chemically cross-linked SMPs exhibit most often better performances as compared to physical networks[1]. Nevertheless, these covalent networks suffer from the severe drawback to prevent recycling or reconfiguration in contrast to thermoplastics. The creation of covalent but reversible bonds between polymer chains was thus developed to overcome this limitation. In 2010, C. Kloxin and C. Bowman defined this family of materials that include reversible covalent bonds as covalent adaptable networks (CANs)[2]. Inserting reversible binding groups in shape-memory covalent networks has thus emerged as a successful strategy for imparting them recyclability and also generating additional functionality such as self-healing properties as reviewed by Lewis et al.[3] or Wu et al.[4]. In that context, Defize et al. reported on the preparation of PCL CANs based on the integration of furan-maleimide Diels-Alder adducts in the network[5–7]. These CANs not only exhibit excellent shape-memory properties, i.e. high fixity and temperature-triggered recovery but thanks to the thermo-reversible character of this Diels-Alder reaction, they are also fully recyclable at high temperature where the cleavage of the furan-maleimide adducts occurs. This biocompatible and bioresorbable material is thus promising for the development of medical devices.

Recently, new types of SMPs have been developed towards the production of multi-stimuli-responsive SMPs, such as combined electro- and thermo-responsive[8,9],

magneto- and thermo-responsive[10], photo- and thermo-responsive[11] as well as chemo- and thermo-responsive materials[12].

When biomedical applications are envisioned temperature-triggered SMPs might induce undesirable effects since heat could damage the surrounding tissue and cells when triggering the shape recovery of such smart implant. In that framework, water responsive SMPs, that recover their shape by immersing the sample in water at constant body temperature, are particularly interesting and preferred over heat-triggered onesl[13–16]. To impart such water sensitivity to polyesters based SMPs, they have been combined notably with poly(ethylene oxide) (PEO), a highly hydrophilic and bio-eliminable component. PCL and PEO were combined in multiblock polyurethanes leading to water-triggered SM thermoplastics[17,18]. As far as covalent networks are concerned, the synthesis of polyesters (PLA, PLGA, PCL) and PEO double interpenetrated networks (IPNs) was reported[19,20] evidencing potential of these fully bioresorbable materials as water-induced shape-memory materials. Nevertheless, these IPNs combining two interpenetrated covalent networks without reversible bond cannot be recycled, reprocessed nor reconfigured.

Herein, we investigated for the first time the PCL and PEO combination in a single covalent adaptable network to provide novel recyclable and reconfigurable water-triggered shape-memory materials. The mechanical so as the temperature and water-triggered shape-memory properties were evaluated in function of the PCL/PEO content of the networks and their recyclability was demonstrated. This hybrid PEO-PCL covalent network was obtained by mixing 4-arm star-shaped PEO and PCL bearing furan and maleimide end-groups, respectively. The formation of the Diels-Alder adducts allowed the intimate network formation between both types of cross-reactive stars (Scheme 1). The thermo-reversibility of these adducts allowed reprocessing and recyclability of the material while preserving the water-triggered shape-memory performances.

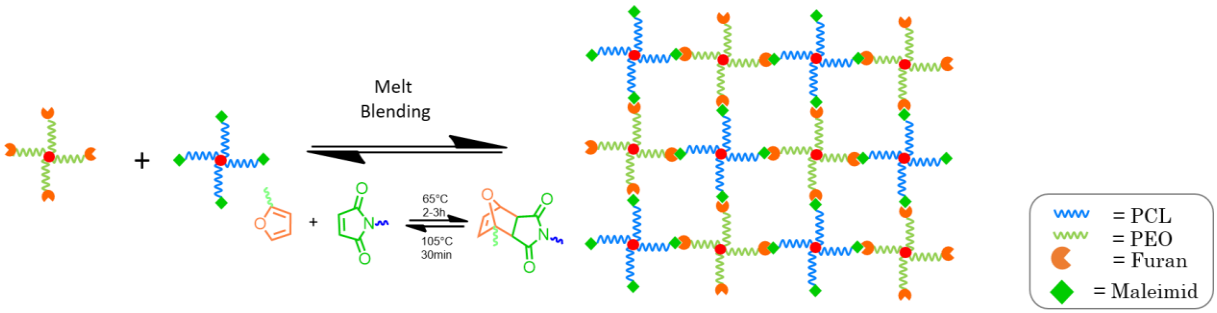

Scheme 1 : Strategy for the synthesis of the PCL-PEO hybrid covalent adaptable network by introduction of thermo-reversible Diels-Alder adducts.

V.2 Experimental section

V.2.1 Materials

Toluene, dichloromethane (CH_2Cl_2), diethyl ether, chloroform and methanol, from Chem-Lab, as well as N,N-dimethylformamide (DMF), succinic anhydride, triethylamine (NEt_3), dicyclohexylcarbodiimide (DCC), 4-dimethylamino-pyridine (DMAP), dibutyltin dilaurate and 2-(isocyanatomethyl)-furan from Aldrich were used as received. 4-arm star-shaped PCL bearing hydroxyl groups at the end of each arm (Mn = 8000 g/mol, PCL-4OH) were kindly provided by Perstop-caprolactones. PCL-4OH of lower molar mass (Mn = 4000 g/mol) was synthesized following a procedure adapted from literature[5,6] (see supporting information). The 4-arms star-shaped PEO bearing hydroxyl groups as chain-ends (Mn = 10000 g/mol, PEO-4OH) was supplied by CreativePEGWorks.

V.2.2 Synthesis of 4-arm star-shaped maleimide end-capped PCL (PCL-4MAL)

The conversion of the hydroxyl end-groups of PCL-4OH in maleimide moieties to get PCL-4MAL is a well optimized and already reported process[6,7]. It was applied to PCL-4OH of two molar masses, 8000 and 4000 g/mol (see supporting information) with a conversion equal to 85% in both cases leading to the PCL-4MAL8k (Đ 1.21) and PCL-4MAL4k (Đ 1.23), respectively.

V.2.3 Synthesis of 4-arm star-shaped furan end-capped PEO (PEO-4FUR)

The chain-ends functionalization of the PEO-4FUR was achieved by the reaction between the hydroxy groups of PEO-4OH stars with furfuryl isocyanate as shown on scheme S1. For that purpose, 10g of PEO-4OH (4.0 mmol in hydroxyl group) were transferred into a previously dried round bottom glass flask and three azeotropic distillations with anhydrous toluene, were performed. Then, 100mL of anhydrous CH2Cl2 was added in the flask. After the complete dissolution of the PEO, 0.471mL (4.4 mmol) of furfuryl isocyanate and 0.01mL (0.4mol%) of dibutyltin dilaurate were transferred into the reactive medium. After 24h of stirring at 40°C, the reaction was stopped and the PEO-4FUR is recovered by precipitation in diethyl ether. PEO-4FUR was finally purified by dialysis (MWCO = 1 kDa) against water during 12h to remove the tin catalyst and recovered after freeze-drying. A white powder (8.5g) is recovered (PEO-4FUR). A quantitative functionalization was determined by 1H NMR analysis (Figure S1). The SEC chromatogram (Figure S2) showed a slight shift to lower elution volume of the peak apex demonstrating that the functionalization occurred properly.

1H NMR (CDCl3, δ): 7.35 (d, 4H, H furan); 6.31 (d, 4H, H furan); 6.22 (d, 4H, H furan); 4.31 (d, 8H, -C(O)-N(H)-CH2-Fur); 4.2 (t, 8H, -CH2-O-C(O)-N(H)-), 3.62 (m, 1060H, H PEO). Conversion of the chain-ends in furan moiety > 99%.

V.2.4 Preparation of the PEO-PCL hybrid networks

Hybrid networks are formed by mixing PEO-4FUR and PCL-4MAL stars in an extruder at 90°C in equimolar amounts of reactive functions, followed by a thermal post-curing in a mould. Two types of networks have been prepared based on the same PEO-4FUR 10400 g/mol mixed with the PCL-4MAL 9700 g/mol (51:49 network, numbers represent the mass proportion in each polymer in the blend) or with PCL-4MAL 4000 g/mol (70:30 network). More precisely, for the first network, 2.3g of PEO-4FUR and 2.2g of PCL-4MAL8k stars were grinded together and injected in a 6 cm3 co-rotating twin screw mini-extruder (Xplore, DSM). They were melt-blended at 90°C during 45 min at 150 rpm. The blend was collected in a 0.5 mm thick mould and processed by compression moulding at 100°C and 75 bars during 1h in order to obtain a flat sheet shape of material. It was followed by a post-curing of 72h at 65°C to obtain a fully crosslinked material.

The same procedure is followed to synthesize the second network, except for stars quantities. In this blend, 3g of PEO-4FUR 10400 g/mol and 1.4g of PCL-4MAL 8800 g/mol were used to achieve the equimolar ratio of reactive functions.

V.2.5 Swelling experiment

Samples (0.5cm x 0.5cm x 0.5mm) were immersed in chloroform for 48h at room temperature in order to reach swelling equilibrium. The resulting gels were collected carefully and weighted in order to determine the amount of solvent absorb by the cross-linked materials. Then, they were dried under vacuum until constant weight in order to determine the insoluble fraction. The swelling ratio and the insoluble fraction were calculated according to the following equations.

$$\text{Swelling ratio} = \frac{\text{weight of the swollen material} - \text{weight of the dried material}}{\text{weight of the dried material}} * 100$$

$$\text{Insoluble fraction} = \frac{\text{weight of the dried material}}{\text{weight of the initial dry material}} * 100$$

Water swelling ratios were also measured by similar swelling experiments using water instead of chloroform.

V.2.6 Characterization techniques

Proton nuclear magnetic resonance (^{1}H NMR) spectra were carried out by a Bruker Avance 400 apparatus at 25 °C at 400MHz in the Fourier-transform (FT) mode and using $CDCl_3$ as solvent.

Size exclusion chromatography (SEC) analysis were recorded in THF at 45°C with a flow of 1ml.min-1 on a Viscotek 305 TDA liquid chromatograph equipped with 2 PSS SDV linear M columns calibrated with polystyrene standards.

Raman spectra were recorded at room temperature using a Horiba-Jobin-Yvon Labram 300 confocal spectrometer provided with an Olympus BX40 microscope. The 647.1 nm line of a Spectra Physics model 168 Krypton ion laser was focused on a rectangular-shaped solid sample with an Olympus 50x (NA 0.5) objective. The laser power at the sample level was of the order of 25 mW. Every spectrum was accumulated 6 times for 60 seconds. The detector is an Andor iDus BR-DD 401 CCD. All spectra were scaled up and, if necessary, baseline corrected with homemade software. All spectra were normalized by the area under the PEO peak at 842 cm-1 and analysed thanks to the program OriginPro2016.

Differential scanning calorimetry (DSC) was performed on a DSC Q100 (TA Instruments) calibrated with indium. For the dry material, a sample is transferred in the DSC oven at 20°C and a cooling ramp of 10°C.min^{-1} is applied until -80°C. After 5min of temperature stabilization, a heating ramp of 10°C.min^{-1} is applied until 100°C. This cooling-heating cycle is repeated for each sample, the melting temperature (Tm) and the enthalpy (ΔHm) being recorded during the second heating ramp. In case of water-swollen materials, the sample is transferred in the DSC oven at 20°C and a cooling ramp of 10°C.min^{-1} is

applied until 5°C. After 5min of temperature stabilization, a heating ramp of 10°C.min^{-1} is applied until 80°C.

Temperature shape-memory properties (fixity and recovery) were determined with a DMA Q800 (TA Instruments) using the tensile film clamp in controlled force mode. The sample (2.5cm x 5mm x 0.5mm) is introduced and then heated at 65°C. After 5min of temperature stabilization, an elongation stress ramp of 0.06MPa.min^{-1} is applied to reach 0.6MPa. The sample is cooled down under stress to 0°C at 3°C/min. and the temperature is maintained for 5min. Then, the stress is released and the fixity is determined at this stage by applying the eq.1. Finally, still in absence of stress, the sample is heated to 65°C and the recovery is determined from the eq.2. This cycle is repeated four times.

The fixity ratio:

$$R_f = \frac{\text{Strain after stress release at 0°C}}{\text{Strain before stress release at 0°C}} * 100 \quad \text{eq 1}$$

The recovery ratio:

$$R_r = \frac{\text{Strain at 65°C wihtout stress for cycle N}}{\text{Strain at 65°C without stress for cycle (N}-1)} * 100 \quad \text{eq 2}$$

Water shape-memory properties were determined by immersing a flat strip (2.5cm x 0.5cm x 0.5mm) in water for 1h. The dimension of the water swollen strip is then measured, especially the distance between the strip ends (initial hydrated shape). A stress is applied to bend the hydrated strip into a ring, the latter being dried at room temperature for 24h under stress. After drying, the stress is released to reach the curved temporary shape. The fixity is calculated by measuring the distance between the two ends of the bended strip before and after stress release. To determine the recovery, the curved sample is immersed in water for 30 min., the distance between the two strip ends is measured and compared to the initial hydrated shape.

Tensile properties were performed with an Instron 5586 machine linked to the BlueHill software on dried and hydrated samples (2.5cm x 0.5cm x 0.5mm) at room temperature at a rate of 10mm/min. The modulus was determined by measuring the slope at the beginning of the curve.

V.2.7 Local network reconfiguration

For the local reconfiguration, a piece of material was heated at 120°C during 30min and then cooled under stress. After that, the material was heated at 65°C in order to verify if the network reconfiguration happened. This operation is repeated two times at different spot of the material piece.

V.2.8 Material recycling

The 70:30 material was cut into small pieces and injected into a mini extruder at 120°C during 2h. After that, a viscous material was collected and pressed at 65°C during 30min. Finally, a post-curing of 48h was performed at 65°C. The 51:49 was cut into small pieces which are placed into a mould, pressed at 130°C, to make the retro Diels-Alder predominant, under a pressure of 75 bars, for 1h and then cured for 72h at 60°C.

V.2.9 Hydrolytic stability test

The sample (2.5cm x 0.5cm x 0.5mm) is immersed in 30mL of phosphate buffer at pH=7.2 and kept at room temperature for two weeks or one month. Then, the material is dried during 24h and analysed by DMA and swelling to evidence any degradation of network.

V.3 Results and discussion

V.3.1 Networks synthesis and characterization

V.3.1.1 Network synthesis

As presented in Scheme 1, we aim to prepare a thermo-reversible covalent PEO-PCL hybrid network by the formation of Diels-Alder adducts between 4-arm star-shaped PEO end-capped with furan with 4-arm star-shaped PCL end-capped with maleimide (see SI for synthesis and characterization of both precursors).

Table 1: Swelling experiments in chloroform and water for several PEO-4FUR/PCL-4MAL blend compositions measured after melt-blending at 90°C for 45 min followed by a post-curing treatment.

Sample composition PEO:PCL	Curing time at 65°C (h)	Insoluble fraction in chloroform(%)	Swelling ratio in chloroform (%)	Insoluble fraction in water (%)	Swelling ratio in water (%)
51 :49	1	60	2500	/	/
51 :49	72	96	1000	100	90
70 :30	72	86	1900	95	206
70:30	Recycling[a]	76	2600	82	260
51:49	PBS[b]	91	1500	100	90

[a]Recycled material as described in section 4, [b] Entry 2 sample after 1-month immersion in PBS buffer as described in section 5.

Typically, PEO-4FUR (Mn = 10000 g/mol) was mixed with the PCL-4MAL8k or PCL-4MAL4k in a proportion respecting a 1:1 stoichiometric amount between furan and

maleimide moieties, i.e. a PEO/PCL weight ratio of 51:49 and 70:30 is reached when the PEO-4FUR is blended with PCL-4MAL8k or PCL-4MAL4k, respectively. Knowing that PEO and PCL are non-miscible polymers[21–23], the two polymer precursors were firstly grinded at room temperature together to intimately mix both powders before introducing them into the extruder. It is also important to mention that the temperature of the extruder is crucial to observe a homogeneous blend and the network formation. Indeed, if the blending temperature is too high (above 90°C), the recovered blend is inhomogeneous and the network is not formed as evidenced by the important swelling and dissolution of the sample during the swelling test in chloroform, a good solvent for both PEO and PCL stars. Indeed, after extrusion at 105°C, only a few Diels-Alder adducts are formed, the retro-Diels-Alder reaction dominating at high temperature[24–26]. Thus, a very limited coupling reactions between PCL and PEO stars occurs, the blend is loosely crosslinked so that it highly swells and dissolves in chloroform and cannot be recovered. The inhomogeneity of the mixture after blending at 105°C was evidenced by Raman spectroscopy microscope. About 15 different areas of the sample extruded at 105°C were analyzed by focalizing the laser on a 2 µm diameter spot and recording the Raman spectrum for each place. Depending on the spot location, an important variation of the Raman intensity ratio between the characteristic peaks of PEO and PCL are observed. Normalizing all the 15 spectra on the peak at 842 cm-1 corresponding to PEO[27], the intensity of the peak at 1108 cm-1 corresponding to PCL was measured and a standard deviation of 0.26 was calculated (Figure S3a). This traduces the inhomogeneity of the sample induced by the macrophase separation between the two immiscible PEO and PCL polymers. At high temperature, very few Diels-Alder adducts are formed and thus only a few couplings between PEO and PCL occurs limiting the mixture compatibilization. In contrast, when a temperature of 90°C is selected for the extrusion, the resulting blend collected after 45min. is more homogeneous. This is evidenced by the reduced variation of the Raman spectra measured on 15 different spot areas (Figure S3b). In this case, the standard deviation is only 0.11. To complete the Diels-Alder adducts formation, this homogeneous blend is then cured at 65°C, under 75bars, for various times then shaped as a sheet with a thickness about

0.5mm. Swelling tests in chloroform evidenced the network formation with an insoluble fraction of 60% obtained after 1h of curing (Table 1). The crosslinking is improved by increasing the curing time. It is nearly complete for 72h at 65°C as evidenced by the very high insoluble fraction (96%) and the decrease of the swelling ratio down to 1000% for the 51:49 composition (Table 1). This is also confirmed by the disappearance of the characteristic peaks of the furan at 1503cm^{-1} (C=C stretching) and maleimide at 1587 cm^{-1} (C=C stretching) and at 1770 cm^{-1} (C=O stretching) moieties on the Raman spectrum recorded on the PEO-PCL mixture after 72h of curing (Figure S4).

When the same process is applied to the 70:30 PEO/PCL mixture, the insoluble fraction remains high (Table 1). The swelling ratio in chloroform increases but it is partially caused by the higher PEO content that swells more than PCL in this solvent. It is remarkable to observe that for both compositions, a high insoluble fraction is observed at the end of the post-curing process, which traduces the efficient coupling between furan and maleimide moieties whereas these are capping the chain-ends of the two immiscible PEO and PCL stars. The peculiar multi-arm architecture of the selected precursors which favors the network formation combined with the well-adjusted extrusion temperature to allow enough Diels-Alder adducts formation and thus enough coupling between PEO and PCL stars is most probably responsible for the success in reaching the covalent networks in so high yields. These yields are indeed fully comparable to those observed for other reported covalent networks, i.e. PCL/PEO IPNs crosslinked by the polymerization of acrylic chain-ends for which the insoluble fraction varies from 87 to 91%[20]. In the present case, the cross-reactivity between both PCL and PEO partners that are not reacting with themselves in contrast to acrylic systems, also favors the rapid compatibilization and thus the intimate blending of both partners accounting for the observed very high insoluble fraction.

V.3.1.2 Water swelling of the networks

In these hybrid covalent networks, the PEO component was selected to bring the hydrophilicity necessary to impart the foreseen water triggered shape-memory effect. The swelling behaviour in water was thus investigated for these hybrid CAN of both compositions. They exhibit a significant water uptake that expectedly increases with the PEO content (Table 1). The swelling ratio reaches 90% for the 51:49 sample. Considering that only the PEO phase is swelling in water, this swelling ratio measured for the 51:49 PEO: PCL stars-based network exhibiting PEO segment length between crosslinks of 2500g/mol logically falls in between previously described 50:50 PCL: PEO systems that report a water swelling of 50% for covalent IPN with PEO length 2000 g/mol[20] and 120% for TPU with PEO length 10000 g/mol[18]. It is worth mentioning that in this selective solvent for PEO, the insoluble fraction is very high for both sample compositions which confirms the efficiency of the multi-arm PEO stars to covalently bind to the PCL ones leading to a stable network. The rate of water swelling of these hybrid CANs was also investigated (Figure 1). The equilibrium is reached after 15min for the most hydrophilic network (70:30) and 30 min for the 51:49 for samples with a thickness of 0.5mm. Knowing that the swelling rate is limited by the water diffusion in the sample and is thus thickness dependent, these data are quite comparable to the reported PCL:PEO TPU of lower thickness and crosslinking density (8 min. for a thickness of 350µm, PEO:PCL 50:50, PEO 10k, 120% of swelling)[18]. It is remarkable to observe that in the studied covalent hybrid networks, especially in the 51:49 (lowest PEO content), the PEO phase made of PEO segments of 2.5k (4-arm stars of 10k), is well accessible to water which quickly penetrates the network and swells it efficiently which traduces the intimate homogeneity of PEO and PCL stars in the hybrid CAN resulting from the use of cross-reactive stars.

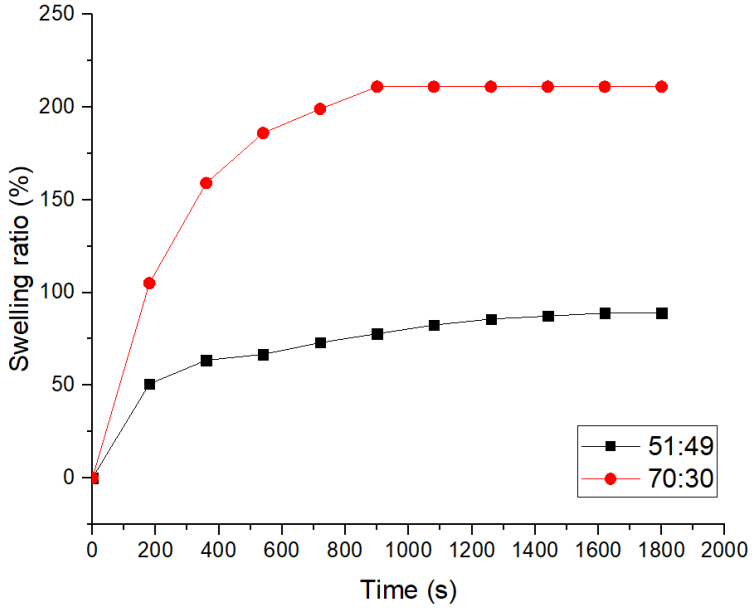

Figure 1: Swelling kinetics in water of the hybrid networks of both compositions.

V.3.1.3 Thermal properties of the networks

The thermal properties of the PEO-PCL hybrid networks were analyzed by DSC. Note that all the starting stars are semi-crystalline materials exhibiting a T_m around 60°C and a crystallinity degree of 76% for PEO4-FUR-10k and 60% for PCL4-MAL-8k, respectively. The DSC traces of the hybrid networks were recorded for both compositions (Figure 2 and S5).

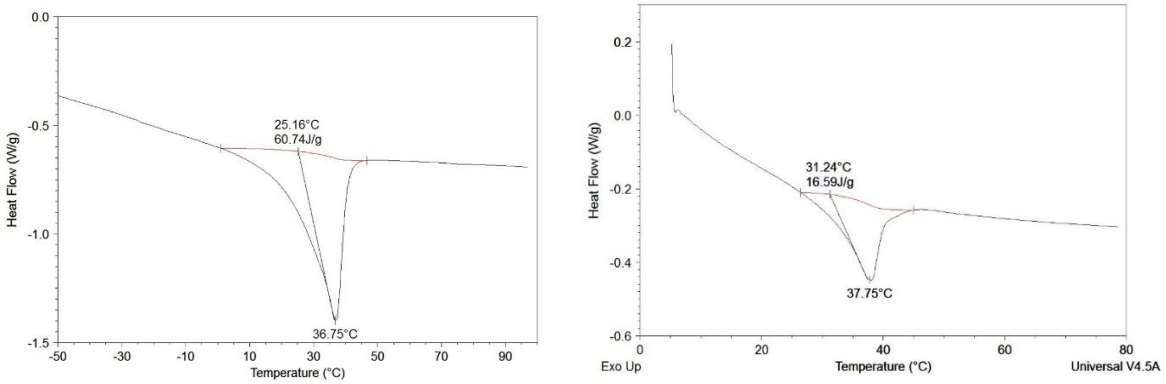

Figure 2: DSC traces for the 51:49 network in the dry state (left) and hydrated state (right).

They show one well-defined melting peak around 40°C evidencing the remaining ability of the material to crystallize even after crosslinking. These results are in contrast to

reported PCL:PEO IPN obtained by polymerization of acrylic end-capped PCL and PEO chains for which the PEO crystallization is prevented for networks with short PEO segments (2000 g/mol)[19,20]. The 4-arm star-shaped architecture of both PCL and PEO phases is most probably at the origin of the preservation of crystallinity of both phases in the present case. Indeed, if the PEO segment length is also short (2500 g/mol), four segments are connected at the same junction due to the star architecture which enriches locally the PEO phase allowing its crystallization.

To estimate the degree of crystallinity of the hybrid networks, we considered the proportion of both polymers in the network and take the average value. The melting enthalpy of a 100% crystalline PEO and PCL being 214J/g and 140J/g respectively, the crystallinity degree was estimated around 30-35% for both networks. As expected, the crystallinity decreases after crosslinking but remains quite significant. For the sake of comparison, a network formed by Diels-Alder addition between PCL-4FUR8k and PCL-4MAL8k exhibit a T_m at 44.4°C and a crystallinity degree of 37%[6], thus a quite similar reduction of the crystallinity degree and the melting temperature as compared to the stars before cross-linking. These PCL networks show temperature triggered shape-memory with excellent fixity and recovery. Therefore, such SM performances can be foreseen for the PEO:PCL hybrid networks. Interestingly, a DSC curve was recorded on the hydrated 51:49 network (Figure 2b). Only the PEO phase is expected to be swollen while the hydrophobic PCL should remain crystallized. Indeed, a crystallization peak is clearly observed around 40°C with a crystallinity degree of 12%, i.e. slightly less than the half of the dry sample. This confirms the complete swelling of the PEO phase and clearly evidences the ability of the PCL phase to keep its crystallinity after complete swelling of the hybrid network in water.

V.3.1.4 Mechanical properties of the networks

The mechanical robustness of the hybrid CANs was determined by tensile testing. The Young modulus, stress and elongation at break are reported for both networks' compositions in Table 2. As already observed in case of polyacrylate PEO/PCL IPN[20], the Young modulus and stress at break increase when the PEO content increases. The elongation at break (above 300% for the hybrid CANs) is higher than the reported one for IPN which levels at 200-250%[20]. Young modulus is also better compared of water SMP based on PEO and PTHF[28]. Nevertheless, the stress-strain curves (Figure S6) profile show a plateau after 50% elongation which can be attributed to stress-induced network debonding due to the mechanically triggered retro-Diels-Alder reaction[29]. As compared to non-covalent TPU systems for which yield point is reach around 25% elongation[18], the elastic deformation is thus two times higher for these CANs that appear thus well adapted for shape-memory experiments.

Table 2: Mechanical properties of networks of different compositions measured at room temperature in the dry and the hydrated state.

Composition PEO:PCL	**Hydration State**	**E (MPa)**	**σ (MPa)**	**ε (%)**
51:49	Dry	31	6.2	600
51:49	Hydrated	3.1	1.9	150
70:30	Dry	75	11.2	428
70:30	Hydrated	1.3	0.3	50

E: Young modulus, σ: stress at break, ε : elongation at break

Mechanical properties are obviously impacted by the water swelling. The stress-strain curves show a fully elastic profile, the plateau observed in the dry state disappearing (Figure S6). The hydration of the PEO segments increases their mobility and soften the samples so that the Young modulus is divided by 10 for the 51:49 network (Table 2, Figure S6) which is in line with reported TPU systems[18]. The stress and elongation at break are

also lower for hydrated samples as compared to dry ones. Nevertheless, even when the material is fully hydrated, it owns sufficient mechanical properties to be handled with an elongation at break still around 150% and stress at break of 1.9MPa for the 51:49 network. Water-sensitive shape-memory can thus be foreseen for networks of both compositions.

V.3.2 Shape-memory properties of the networks

V.3.2.1 Temperature-triggered SM of dry networks

As evidenced by DSC analysis, the hybrid CANs are semi-crystalline and should therefore exhibit temperature triggered shape-memory properties. The quantitative measurement of the fixity and recovery was performed by dynamic mechanical analysis (DMA) for 4 successive shape-memory cycles in the dry state (Figure 3a). The data collected from Figure 3a are gathered in Table S1 for the PEO/PCL 51:49 network. Very high fixity (98%) and recovery (97%) are obtained for each cycle except for the first training cycle[30] for which a recovery of 85% is reached. These results are as good as CANs entirely made of PCL (i.e. resulting of coupling PCL-4FUR and PCL-4MAL)[6] and as PEO/PCL IPN[19,20].

a)

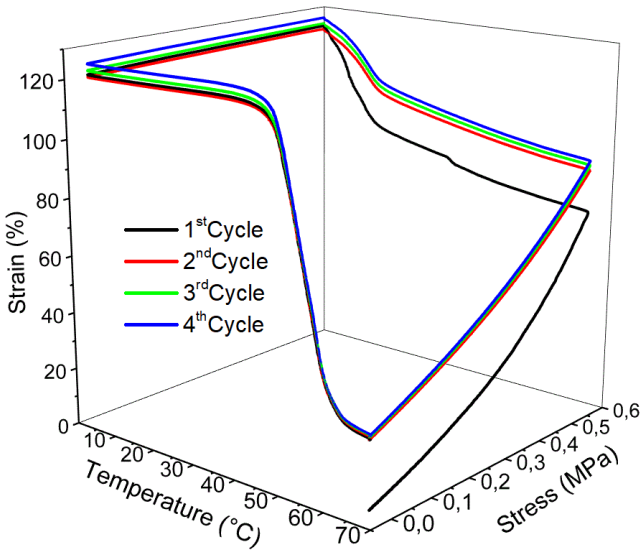

b)

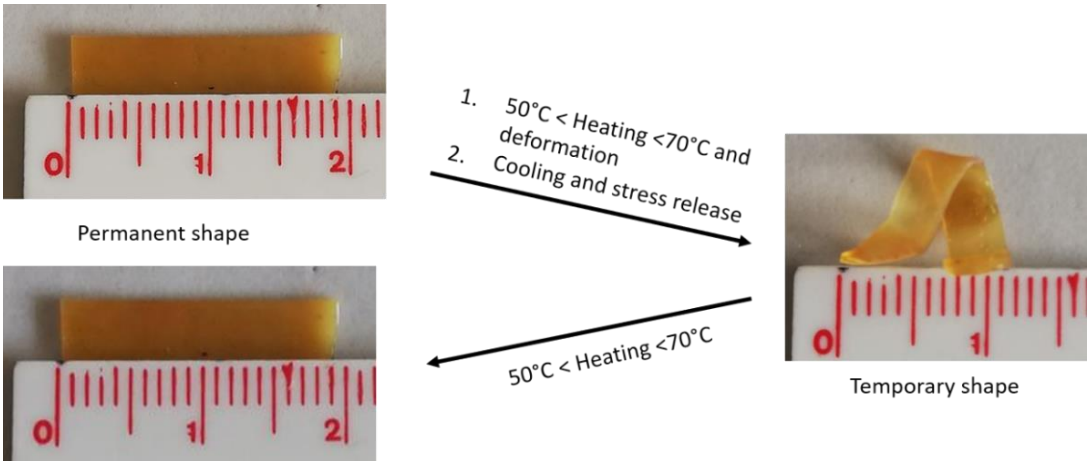

Figure 3: Temperature triggered shape-memory: a) 4 cycles recorded by DMA for the 51:49 network in the dry state (stress ramp: 0.06MPa/min; temperature ramp: 3°C/min on heating and cooling), b) 1 cycle for the 51:49 network in the dry state.

Interestingly, only a limited creep effect is observed from cycle to cycle for this PEO-PCL hybrid network as compared to similar furan/maleimide CANs composed of 100% PCL[6]. This creep phenomenon is caused by the occurrence of some stress-induced retro-Diels-Alder reactions at 65°C leading to the entropic relaxation of the disconnected polymer chains. This phenomenon is less pronounced for the PEO-PCL hybrid network most probably because of the lower elongation reached here, i.e. ~90%, as compared to ~150% for the pure PCL network.

Figure 3b illustrates the temperature-triggered SM of the 70:30 PEO/PCL hybrid network. This more rigid sample because of the high PEO content can be elastically deformed between 50°C and 70°C and keeps well the temporary shape after cooling to room temperature and stress release. By heating again to 65°C, the material recovers its initial shape (permanent shape) in a few seconds with excellent fidelity.

V.3.2.2 Water-triggered SM at room temperature

The water-triggered shape-memory was tested by immersing 0.5mm thick samples in water in order to swell the PEO segments of the network and provide them mobility. After equilibration during 60min at room temperature in water, the swollen material has doubled its volume and can be easily deformed, e.g. as a ring. It keeps the given temporary shape after sequential drying at room temperature and stress release (Figure 4). As evidenced from the measurement of the distance between ring edges on the dried ring (temporary shape) before and after stress release, a fixity close to 100% is obtained for CANs of both compositions. Then, immersing again the dry samples in water triggers the hydrated-shape recovery. As illustrated in Figure 4, the shape recovery is not complete even after reaching the swelling equilibrium, i.e. 45min immersion for the 51:49 and 20min for the 70:30. Nevertheless, a recovery above 80% is measured for the most hydrophilic 70:30 sample and about 75% for the 51:49 network that is comparable or even higher than reported data for other water triggered PEO/PCL systems[31,32,]. The crystallization of amorphous PCL segments that are oriented by the applied stress during room temperature drying of the sample to fix the temporary shape is responsible of the observed incomplete shape recovery, these PCL crystallites being stable towards rehydration.

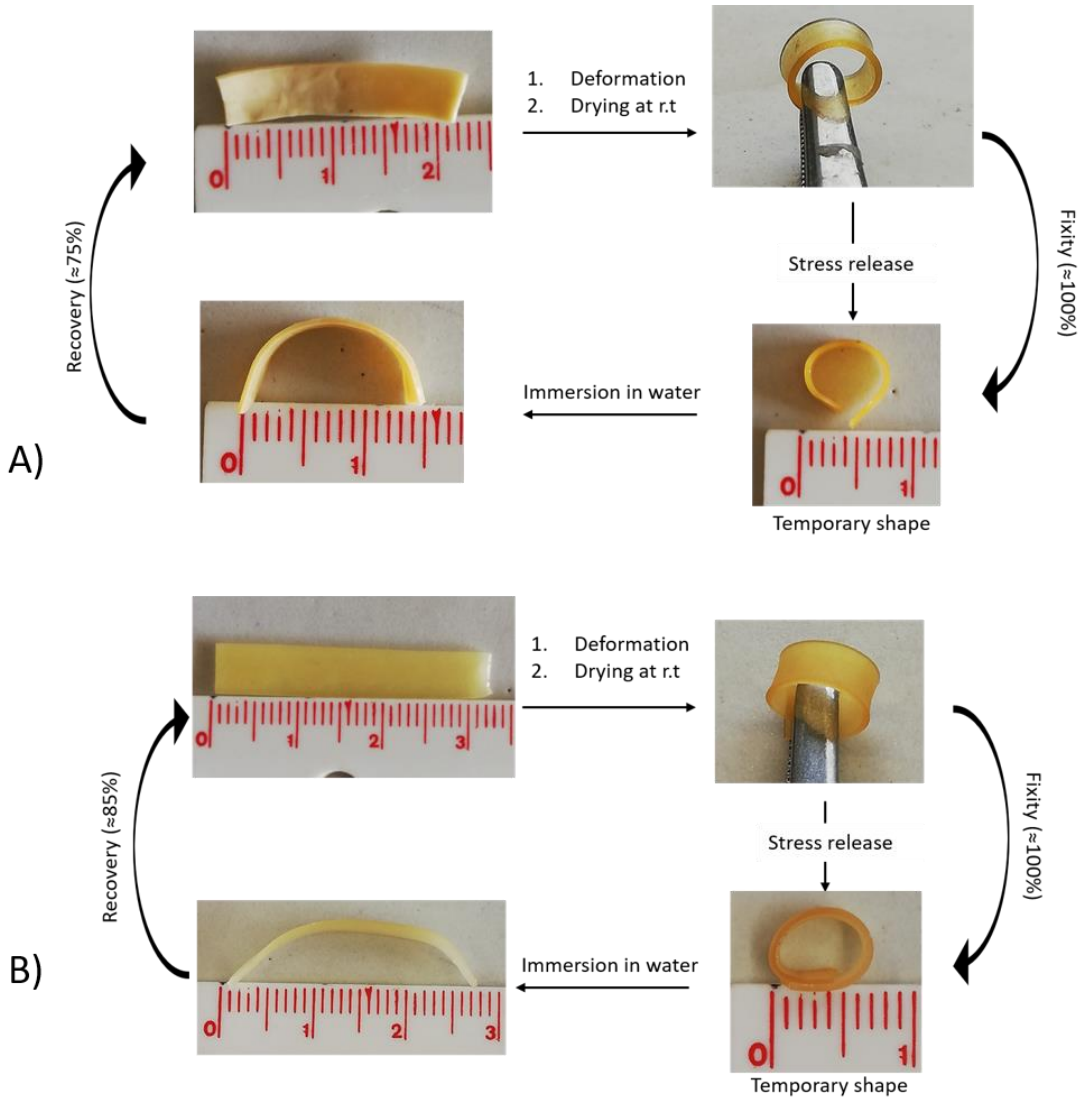

Figure 4: Water-triggered shape memory at room temperature of the PEO/PCL hybrid networks with a composition a) 51:49 b) 70:30.

V.3.2.3 Water-triggered shape transition of a thermally-fixed temporary shape

Having demonstrated the efficient temperature- and water-triggered shape-memory properties of the hybrid networks, the investigation of a first combination of these properties, i.e. the water-triggered relaxation of a thermally fixed temporary shape was considered. Storing a complex temporary shape by the thermal process is quite easy and quick because it does not require to evaporate the water at room temperature. In that process, both components, PCL and PEO are taking part to the temporary shape fixity

thanks to their crystallization. Besides, it is an advantage for some applications, notably in vivo applications, to trigger a shape modification without heating above the body temperature but simply by hydration. At a temperature remaining below 50°C (e.g. at the body temperature), the hydration of the PEO segments allows the partial release of the stored stress and the softening of the material, leading to a final shape (shape used in the final application) intermediate between the temporary and the permanent shape.

This process is illustrated for both materials compositions in Figure 5. The sample in the permanent shape is first heated at 65°C to melt all the crystallites before being deformed in the temporary shape by applying a stress, cooling at room temperature and releasing the stress. Finally, the sample is placed into a water bath at room temperature, so that the only PEO phase will swell and release the stress while the hydrophobic PCL is preserving the stored deformation. After complete hydration (30min or 20min) and a drying step of 24h, the final shape, intermediate between the temporary and the permanent shape is obtained and remains stable during time as far as the temperature is kept below 50°C. Noticeably, if the sample is heated again at 65°C and dried, the initial permanent shape is fully recovered in a few seconds (not shown).

As expected, the relaxation of the temporary shape increases with the PEO content of the networks. As a consequence, a final shape close to the temporary shape will be obtained for samples with low PEO content (Figure 5a) while a shape closer to the permanent shape will be reached for samples of high PEO content (Figure 5b).

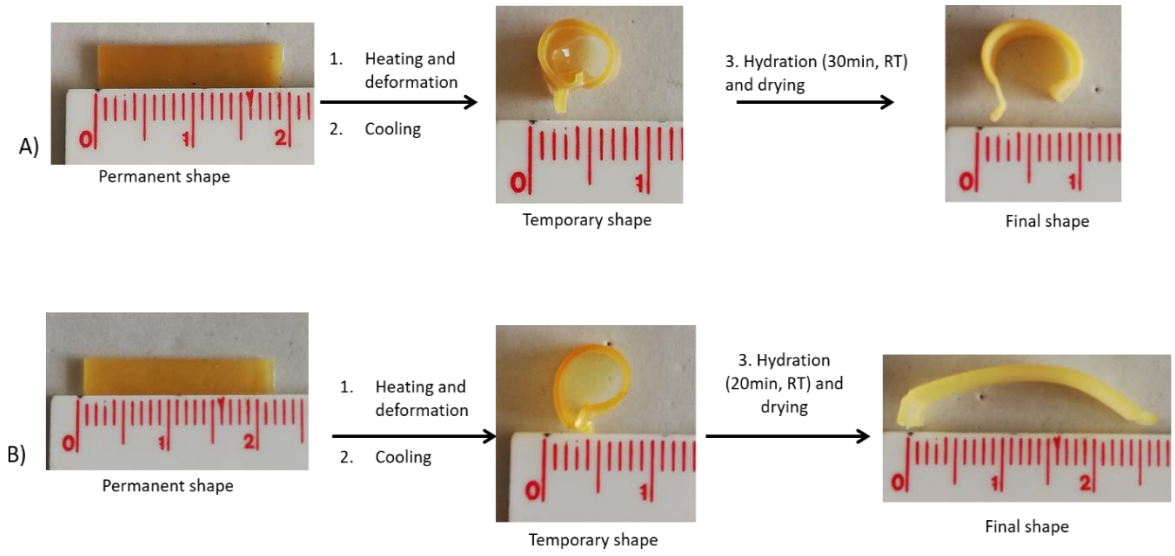

Figure 5: Illustration of the water-triggered shape transition of thermally stored temporary shape for the PEO/PCL hybrid networks with a composition a) 51:49 b) 70:30

V.3.2.4 Memory of multiple shapes

Another remarkable feature of this type of materials is their capacity to memorize in a temporary shape, two different final shapes that can be recovered depending on the applied trigger, i.e. temperature or water. For that purpose, a two-step programming of the material is necessary as described on Figure S7. The starting CAN shape defined by the crosslinking reaction happening during the covalent network formation (called "permanent shape" until now) will constitute the first memorized shape (shape 1-dry state). In the first programming step, the shape of this sample is modified into the second memorized shape (shape 2-dry state) by classical temperature shape programming, i.e. heating at 65°C to melt the material, deforming and cooling under stress followed by stress release. This shape 2 also exists in its hydrated version (shape2-hydrated state) after immersion in water. As seen above, only a partial release of the deformation occurs during the hydration step, especially for networks with moderate PEO content. Finally, the temporary shape, different from both shapes 1 and 2, is obtained by a second programming step, i.e. deforming at room temperature the water swollen shape 2, followed by drying then release of the stress. This dry sample is going to keep stable its

temporary shape as far as it is stored below 40°C and in a dry atmosphere. When shape 1 has to be recovered, it can be simply heated a few seconds at 65°C (Figure 6). On the other hand, the recovery of shape 2 is triggered by immersion in water during 20min. keeping the temperature below 40°C. Interestingly, heating the sample in its shape 2 converts it in the hydrated shape 1. This sequential recovery of shape 2 by sample hydration then shape 1 by further heating is especially interesting for surgery assisted by self-deploying medical devices.

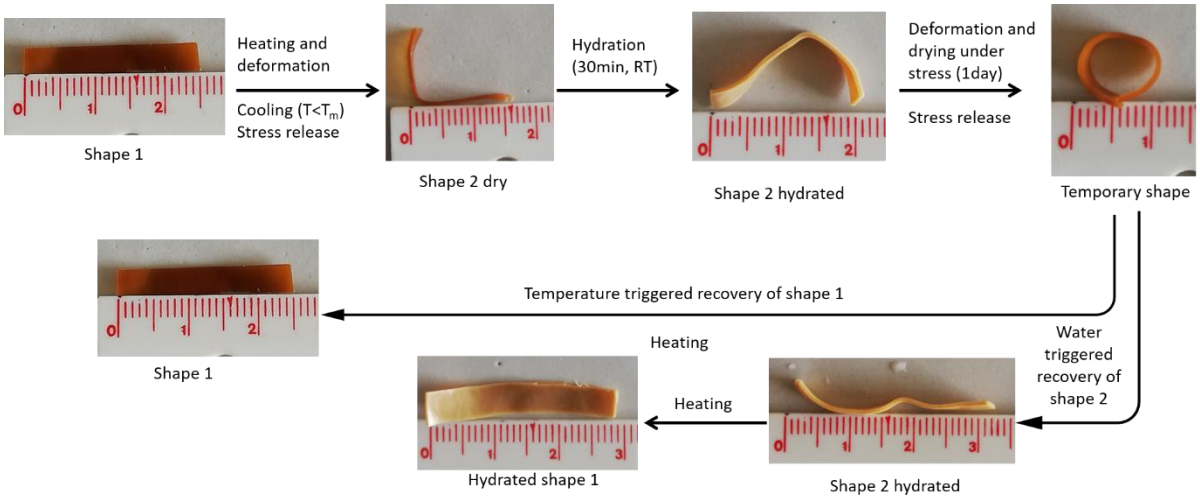

Figure 6: Multi stimulus shape-memory properties of the recycled 70:30 material.

V.3.3 Reconfiguration of the permanent shape

So far, the so-called permanent shape, i.e. the shape determined by the covalent crosslinking, was kept stable since heating processes were limited to 65°C. Nevertheless, thermo-cleavable furan-maleimide Diels-Alder adducts were purposely introduced to provide adaptable hybrid networks. Above 100°C, the cycloreversion, i.e. the retro Diels-Alder reaction significantly occurs[24,25]. Such CANs can advantageously be used for the reconfiguration of the permanent shape. As shown Figure 7, the pristine flat film is pressed into a complex 3D mold heated at 100°C. This temperature is kept constant for 24h to allow the retro Diels-Alder reaction to occur. After 24h, the temperature is reduced to 60°C and kept constant for 72h to form again the DA adducts and consequently restore the

network in a novel permanent shape (Figure 7). This 3D-reconfigured sample is now able to enter e.g. a temperature triggered SM cycle in which the memorized shape corresponds to the molded 3D object as exemplified Figure 7 (right part). A regional control of network reconfiguration can also be performed on the starting material (Figure S8).

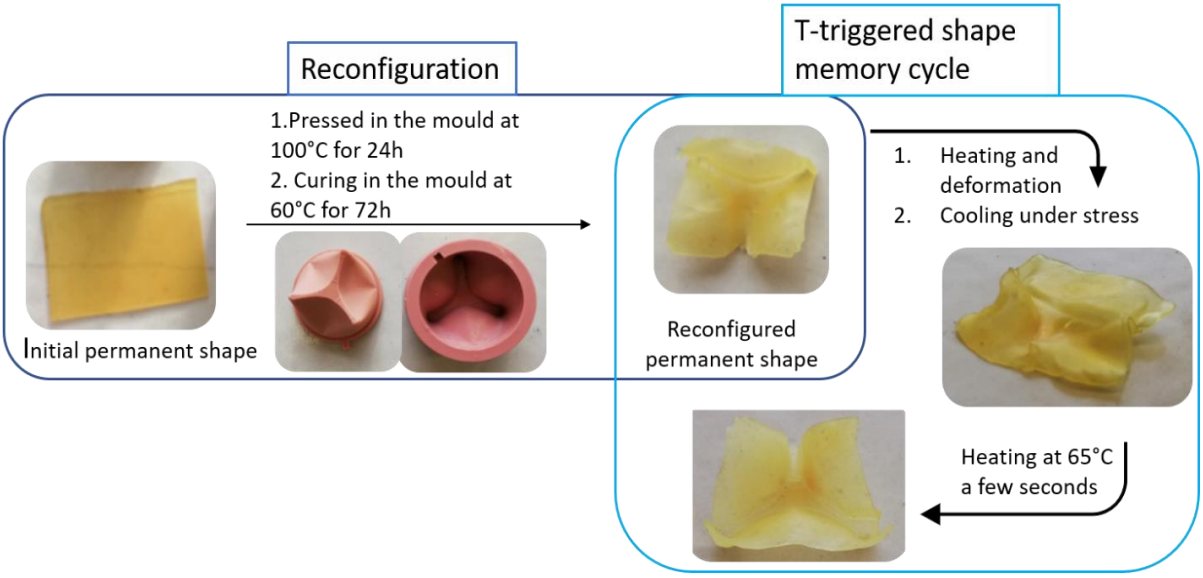

Figure 7: Reconfiguration of the flat sheet CAN in a 3D object and temperature triggered shape-memory of this reconfigured sample made of the 70:30 CAN.

V.3.4 Recycling of the networks

Owing to the significant cyclo-reversibility of the furan-maleimide Diels-Alder adduct above 100°C[24,25], it is possible not only to reconfigure the permanent shape but also to recycle the material as shown Figure S9. The recycled hybrid network is homogeneous and exhibits a slightly lower crosslinking density compared to the pristine material, as confirmed by swelling experiments in chloroform (Table 1-recycled). Indeed, network properties are a bit lower to those for the starting material, resulting in a lower elongation at break (Figure S6), which confirms that the reversibility of the reaction efficiently occurs during the recycling of the material and that reprocessing is not limited by the immiscibility of the two-star polymers. The swelling in water is also very similar to the one of the material before recycling (Table 1) which is in line with the fully preserved

water, thermo- and multi-triggered SM properties (Figure S9 and Figure 7). Indeed, the fixity and the recovery of the water and thermo- triggered shape-memory material are still the same than the pristine one (Table S2 and Table S3). The recycled material still crystalizes and the crystallinity degree is even slightly higher than before recycling (Figure S10), so that temperature shape-memory properties kept unchanged (Figure S9b). The 51:49 recycling is different of the one of the 70:30 because it is not blended then the material is not homogeneous resulting in lower mechanical properties compared than the one of the 70:30. Nevertheless, thermo- and water shape-memory properties were successfully tested.

V.3.5 Hydrolytic stability of the networks

PCL being hydrolytically degradable and since PEO facilitates water penetration in the network, the stability of the 51:49 sample in water at pH 7.4 was studied after 2 weeks and one month.

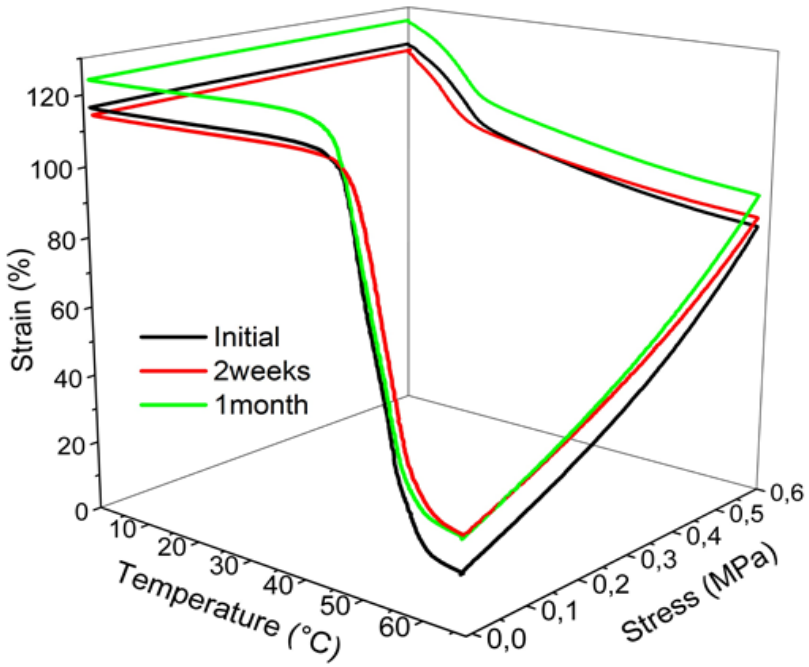

Figure 8: DMA analysis in the dry state of the 51:49 before ageing in water (black curve), after two weeks (red curve) and one month (green curve) of immersion in PBS phosphate buffer.

The integrity of the network is confirmed by swelling experiments in chloroform (Table 1). A moderate increase of the swelling ratio in chloroform indicates a limited number of bonds ruptures of the network and the insoluble fraction remains very high after one month of immersion in PBS. This very limited network degradation does not impact the temperature shape-memory properties that are well-preserved after one month as confirmed by DMA measurements (Figure 8 and Table S4). Mechanical properties after 2 months in PBS are still excellent (Figure S6 and Table S5) with a similar Young modulus compared to the non-degraded on, a lower elongation at break but a much higher stress at break.

V.4 Conclusion

Four-arm star-shaped PCL and PEO were successfully functionalized by maleimide and furan moieties, respectively. By optimizing the processing conditions, (i.e. temperature and time of extrusion, post annealing process, stoichiometry) hybrid networks have been obtained by chain-ends coupling via the formation of Diels-Alder adducts which are remarkably homogeneous knowing that these two polymers are immiscible. Playing on the molar mass of the PCL stars, networks of two different compositions (PEO/PCL 51:49 and 70:30) have been obtained. Even if the PEO and PCL stars are molecularly blended in the network owing to their cross-reactive coupling, both phases are still able to crystallize after crosslinking as demonstrated by DSC analysis of dry and water swollen materials. Therefore, both temperature and water triggered shape-memory properties are very efficient. Thanks to the covalent crosslinking, the elastic behavior holds until a deformation of 50% which is twice the value reported for TPU systems [18].

These results evidenced that thanks to the peculiar and well-defined structure of these CANs uniquely achieved by the blending of cross-reactive PEO and PCL homopolymers both having a 4-arm architecture, these hybrid networks exhibit crystallinity, mechanical robustness and water sensitivity. Consequently, advanced SM

properties can be achieved so as memorizing two different shapes that are recovered by different triggers, namely temperature and water. The insertion of Diels-Alder adducts in the network allowed for the first time to achieve recyclable and reconfigurable covalent PEO-PCL hybrid networks. In addition, no significant degradation of these hydrophilic polyester networks properties was observed after immersion during one month in PBS even for the most hydrophilic material containing 70% of PEO. These materials offer thus high opportunities for the development of biomedical applications especially in self-deployable devices for assisted complex surgeries. For example, the creation of efficient self-deploying esophageal stent can be performed[28].

V.5 References

1 A. Lendlein and O. E. C. Gould, *Nat Rev Mater*, 2019, **4**, 116–133.

2 C. J. Kloxin, T. F. Scott, B. J. Adzima and C. N. Bowman, *Macromolecules*, 2010, **43**, 2643–2653.

3 C. L. Lewis and E. M. Dell, *J Polym Sci B Polym Phys*, 2016, **54**, 1340–1364.

4 Y. Wu, Y. Wei and Y. Ji, *Polym Chem*, 2020, **11**, 5297–5320.

5 T. Defize, R. Riva, C. Jérôme and M. Alexandre, *Macromol Chem Phys*, 2012, **213**, 187–197.

6 T. Defize, R. Riva, J. M. Raquez, P. Dubois, C. Jérôme and M. Alexandre, *Macromol Rapid Commun*, 2011, **32**, 1264–1269.

7 T. Defize, R. Riva, J. M. Thomassin, C. Jérôme and M. Alexandre, *Macromol Symp*, 2011, **309–310**, 154–161.

8 Q. Zhang, M. Wang, H. Ao, H. Luo, X. Deng and Y. Wan, *Polym Test*, 2021, **96**, 107086.

9 G. J. M. Antony, S. T. Aruna, C. S. Jarali and S. Raja, *Polymer Bulletin*, , DOI:10.1007/s00289-020-03427-6.

10 T. Hu, S. Xuan, Q. Shu, Z. Xu, L. Shen, J. Li and X. Gong, *J Mater Chem C Mater*, 2021, **9**, 6568–6578.

11 Y. Chen, X. Zhao, C. Luo, Y. Shao, M. B. Yang and B. Yin, *Compos Part A Appl Sci Manuf*, 2020, **135**, 105931.

12 N. Lorwanishpaisarn, P. Kasemsiri, K. Jetsrisuparb, J. T. N. Knijnenburg, S. Hiziroglu, U. Pongsa, P. Chindaprasirt and H. Uyama, *Polym Test*, 2020, **81**, 106159.

13 Y. Guo, Z. Lv, Y. Huo, L. Sun, S. Chen, Z. Liu, C. He, X. Bi, X. Fan and Z. You, *J Mater Chem B*, 2019, 123–132.

14 J. M. Korde and B. Kandasubramanian, *Chemical Engineering Journal*, 2020, **379**, 122430.

15 M. Wu, P. Sukyai, D. Lv, F. Zhang, P. Wang, C. Liu and B. Li, *Chemical Engineering Journal*, 2020, **392**, 123673.

16 W. Zhang, X. Leng, M. Gao, Z. Wei, Y. Wang and Y. Li, *Polym Test*, 2021, **96**, 107099.

17 X. Gu and P. T. Mather, *Polymer (Guildf)*, 2012, **53**, 5924–5934.

18 X. Gu and P. T. Mather, *RSC Adv*, 2013, **3**, 15783–15791.

19 Y. Feng, S. Zhang, L. Zhang, J. Guo and Y. Xu, *Polym Adv Technol*, 2011, **22**, 2430–2438.

20 Y. Feng, H. Zhao, S. Zhang, L. Jiao, J. Lu, H. Wang and J. Guo, *Macromol Symp*, 2011, **306–307**, 18–26.

21 S. Buddhiranon, N. Kim and T. Kyu, *Macromol Chem Phys*, 2011, **212**, 1379–1391.

22 Z. Qiu, T. Ikehara and T. Nishi, *Polymer (Guildf)*, 2003, **44**, 3101–3106.

23 J. Li, Y. Zhang, Y. Jiacuo, Y. Shang, H. Huo and S. Jiang, *Polymer Bulletin*, 2012, **68**, 1405–1423.

24 J. A. Syrett, G. Mantovani, W. R. S. Barton, D. Price and D. M. Haddleton, *Polym Chem*, 2010, **1**, 102–106.

25 A. Gandini, D. Coelho and A. J. D. Silvestre, *Eur Polym J*, 2008, **44**, 4029–4036.

26 T. Defize, J. M. Thomassin, M. Alexandre, B. Gilbert, R. Riva and C. Jérôme, *Polymer (Guildf)*, 2016, **84**, 234–242.

27 L. Koenig and A. C. Angood, 1970, **1796**, 1787–1796.

28 R. Liang, H. Yu, L. Wang, B. U. Amin, N. Wang, J. Fu, Y. Xing, D. Shen and Z. Ni, *Chemistry of Materials*, 2021, **33**, 1190–1200.

29 Z. Wang and S. L. Craig, *Chemical Communications*, 2019, **55**, 12263–12266.

30 I. A. Rousseau, *Polym Eng Sci*, 2008, **48**, 2075–2089.

31 L. Sun and W. M. Huang, *Mater Des*, 2010, **31**, 2684–2689.

32 W. M. Huang, B. Yang, L. An, C. Li and Y. S. Chan, *Appl Phys Lett*, 2005, **86**, 1–3.

Supporting information

Synthesis of PCL-4OH (4000g/mol)

0,63g of pentaerythritol were transferred into a washed and dried round bottom flask and three azeotropic distillation, with dry toluene, were realized. 20mL of e-caprolactone (CL), previously distillated, were added into the pentaerythritol flask under N_2. The blend is then heated to 155°C in order to dissolve the pentaerythritol into the CL. The reactive medium is cooled down to 110°C and 20mL of tin(II) 2-ethylhexanoate 0,26M were added. The monomer conversion is followed by NMR ^{1}H and after 3h, the polymer is recovered by precipitation into heptane.

^{1}H NMR ($CDCl_3$, δ): 3,97 (t, 92H, -C$\underline{H}_2$-O-C(O)-); 3,53 (t, 8H, -C$\underline{H}_2$-OH); 2,22 (t, 92H, -O-C(O)-C$\underline{H}_2$-); 1,56 (m, 190H, -C(O)-CH_2-C$\underline{H}_2$-CH_2-C$\underline{H}_2$-CH_2-O-); 1,30 (m, 96H, -C(O)-CH_2-CH_2-C$\underline{H}_2$-CH_2-CH_2-O-). Quantitative conversion.

Synthesis of PCL-4COOH (8000g/mol)

50 g (25 mmol of hydroxyl function) of PCL-4OH were transferred into a previously dried round bottom flask and three azeotropic distillations with anhydrous toluene were carried out. Then, 200 mL of anhydrous DMF were added to the flask through a rubber septum with a flamed stain-less steel capillary. After complete solubilization, 2.75 g (27.5 mmol) of succinic anhydride and 3.9 mL (27.5 mmol) of triethylamine were successively added to the polymer solution. The solution was then stirred at 45°C overnight and the PCL-4COOH was successively precipitated in diethyl ether and methanol. A white powder is collected after filtration and drying under vacuum.

^{1}H NMR ($CDCl_3$,δ): 4,05 (t, 168H, H A + A'), 2,64 (s, 16H, H a + a'), 2,3 (t, 158H, H E), 1,64 (m, 316H, H B + D), 1,37 (m, 158H, H C). Functionalization: > 95%.

Synthesis of PCL-4MAL (8000g/mol)

20 g (9.5 mmol of carboxylic acid functions) of PCL-4COOH were transferred into a glass reactor previously dried. 80 ml of anhydrous CH_2Cl_2 were transferred to the reactor through a rubber septum using a flamed stainless-steel capillary. After the complete solubilization of the PCL, 2.3 g (11 mmol) of 4-(2-hydroxyethyl)-10-oxa-4-aza-tricyclo[5.2.1.0]dec-8-ene-3,5-dione, 2.27 g (11 mmol) of DCC and 0.134 g (1.1 mmol) of DMAP were transferred inside the reactor. After one night of reaction at room temperature the blend was filtrated in order to remove the DCU. The protected PCL-4MAL was recovered by precipitation in diethyl ether and in methanol, filtered and dried under vacuum. The polymer was then transferred into a glass reactor and heated at 105 ° C under vacuum for 6 h to eliminate furan and regenerate the maleimide functions. PCL-4MAL was

kept at room temperature. The functionalization was determined by ^{1}H NMR. The functional PCL was also characterized by SEC.

^{1}H NMR ($CDCl_3$, δ): 6,53 (s, 7,9H, H_{MAL}); 4,26 (t, 7,5H, H_{MAL}); 4,07 (t, 172H,-C<u>H</u>$_2$-O-C(O)-); 3,76 (t, 7,5H, H_{MAL}); 2,59 (s, 16H, O-C(O)-C<u>H</u>$_2$-C<u>H</u>$_2$-C(O)-O-MAL); 2,3 (t, 168H, -O-C(O)-C<u>H</u>$_2$-); 1,66 (m, 332H, -C(O)-CH$_2$-C<u>H</u>$_2$-CH$_2$-C<u>H</u>$_2$-CH$_2$-O-); 1,39 (m, 169H, -C(O)-CH$_2$-CH$_2$-C<u>H</u>$_2$-CH$_2$-CH$_2$-O).

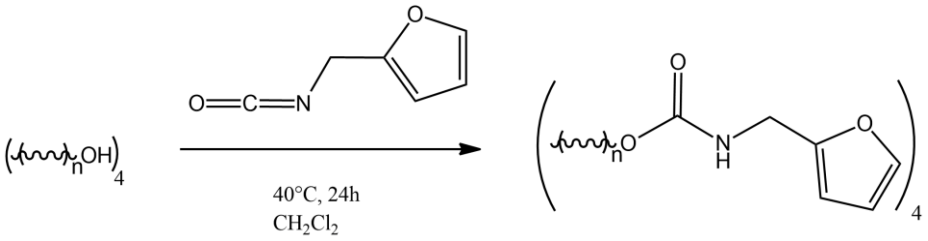

Scheme S1: Synthesis of PEO-4FUR from PEO-4OH (10.000g/mol)

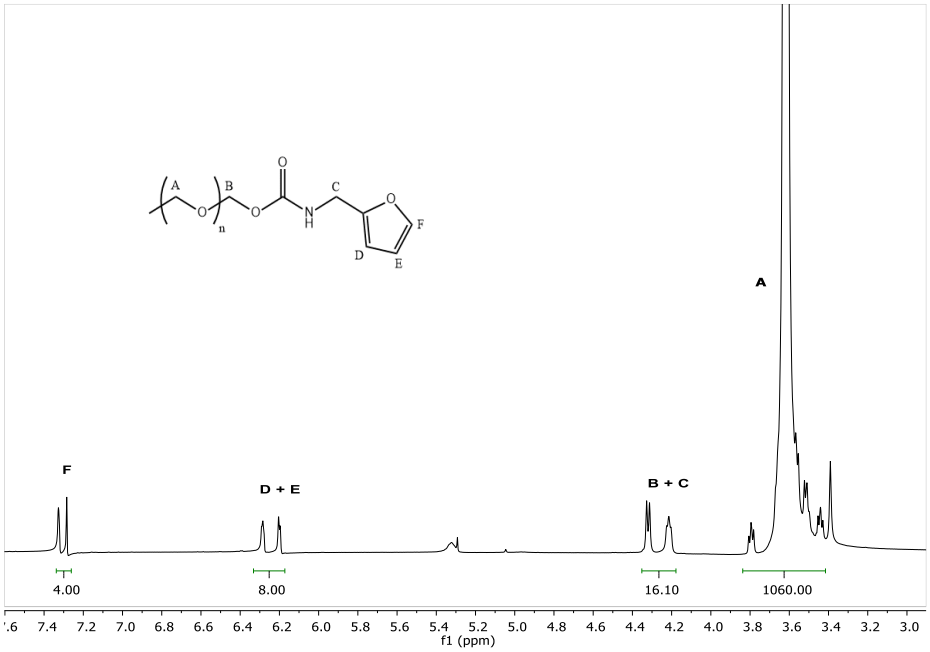

Figure S1: ^{1}H NMR spectrum of the PEO-4FUR

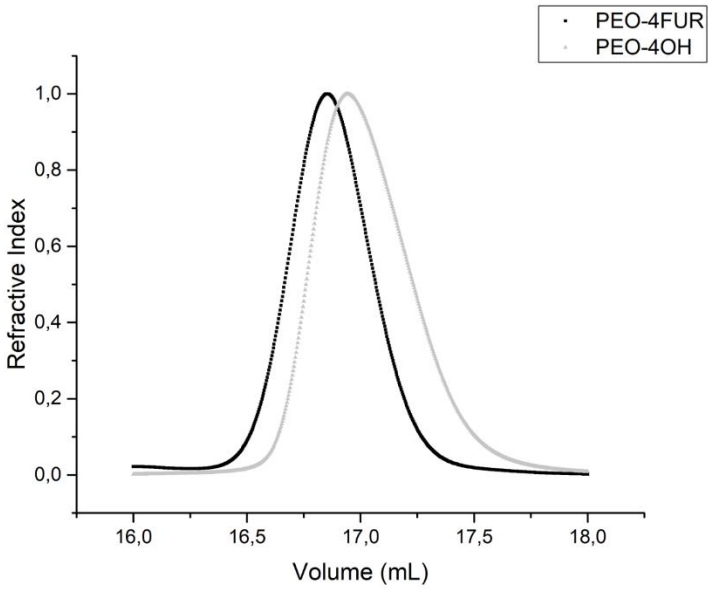

Figure S2: SEC chromatogram of the PEO-4FUR (black) and PEO-4OH (grey)

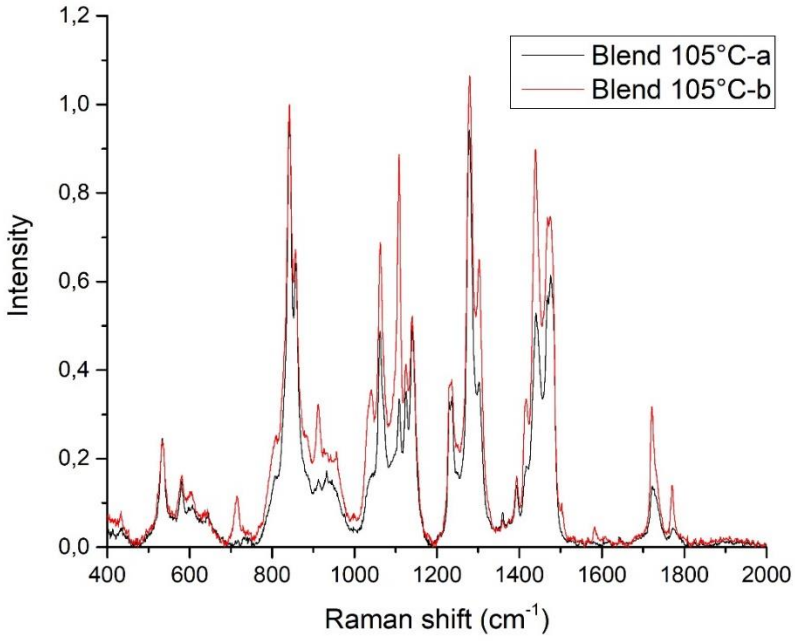

a)

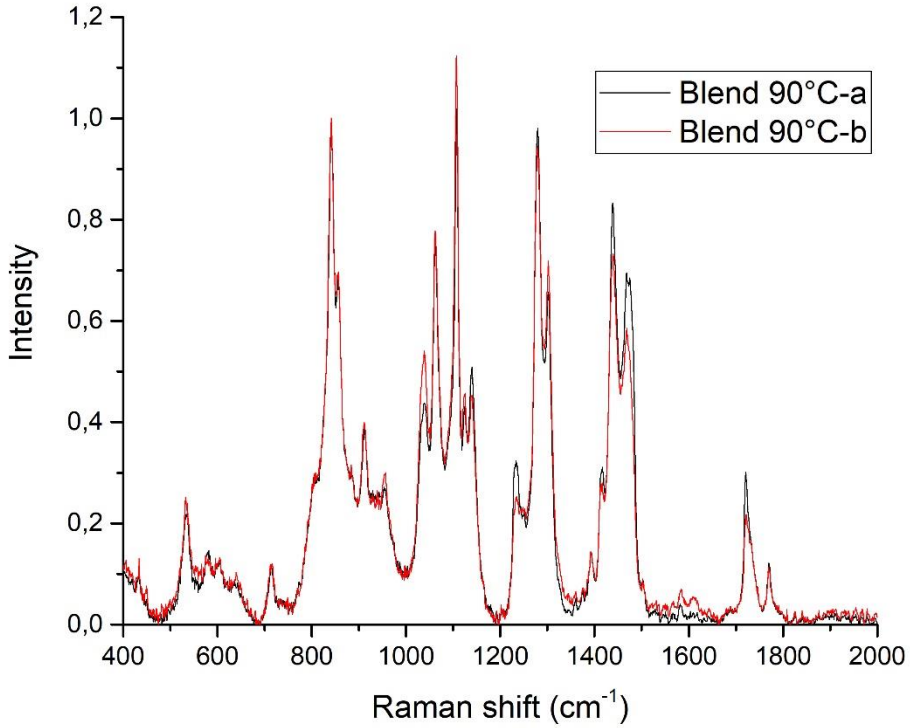

b)

Figure S3: Raman spectra on two different spots of the PEO-PCL mixture after melt blending at a) 105°C and b) 90°C (the two spots a and b giving the highest divergences over the 15 measured spectra were selected in both cases).

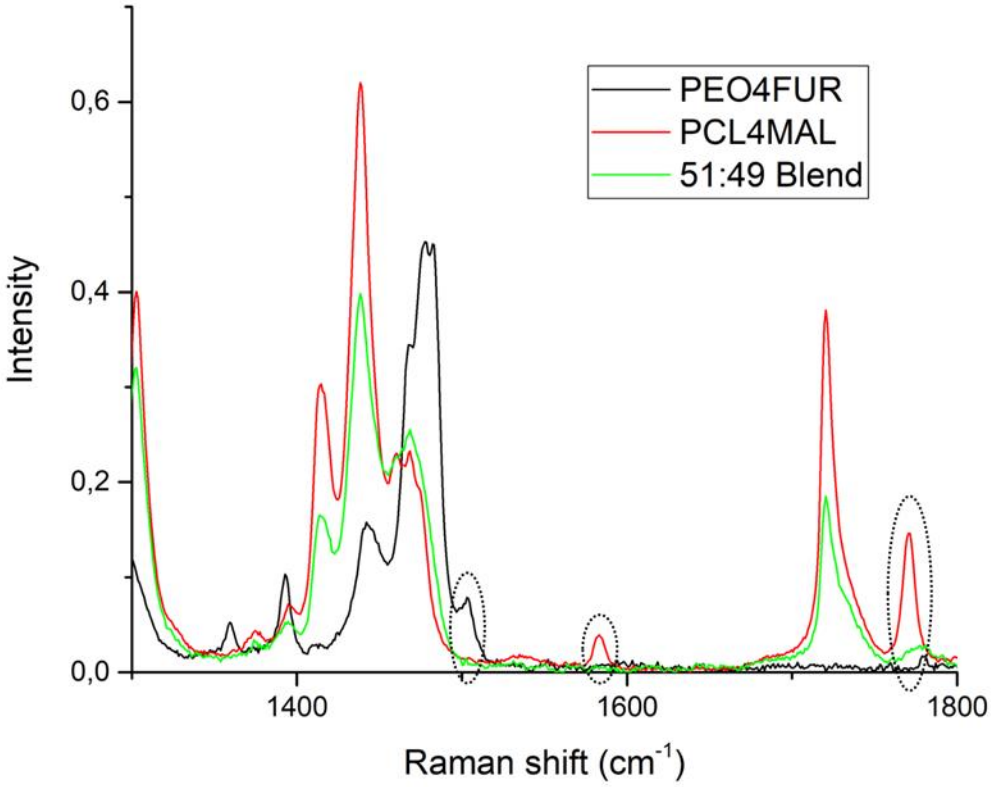

Figure S4: Raman spectra of the PEO-4FUR (black curve), PCL-4MAL (red curve) and the 51:49 blend after melt blending at 90°C and curing at 65°C for 72h (green curve). The dotted ovals highlight some bands characteristic of the furan (1503cm^{-1}) and maleimide (1587 and 1770cm^{-1}) end groups.

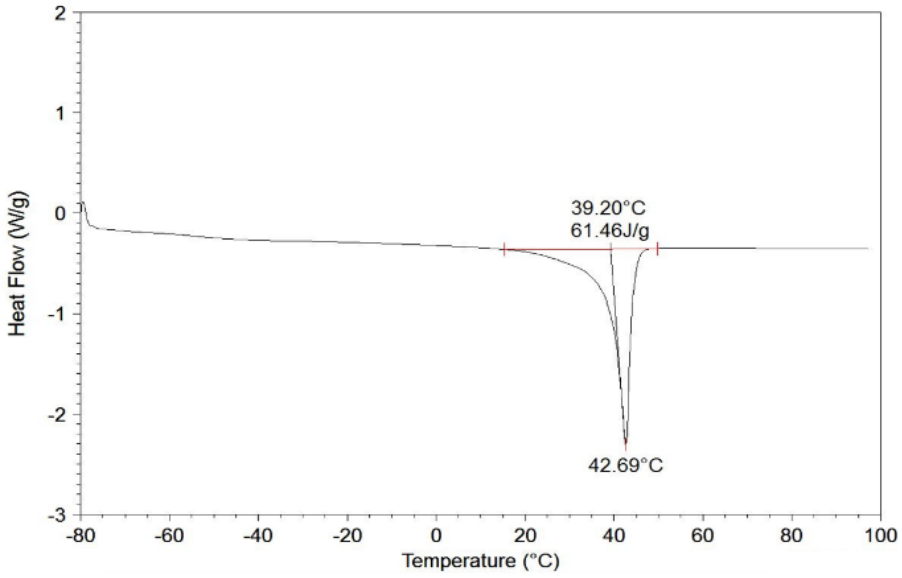

Figure S5: DSC trace for the 70:30 network.

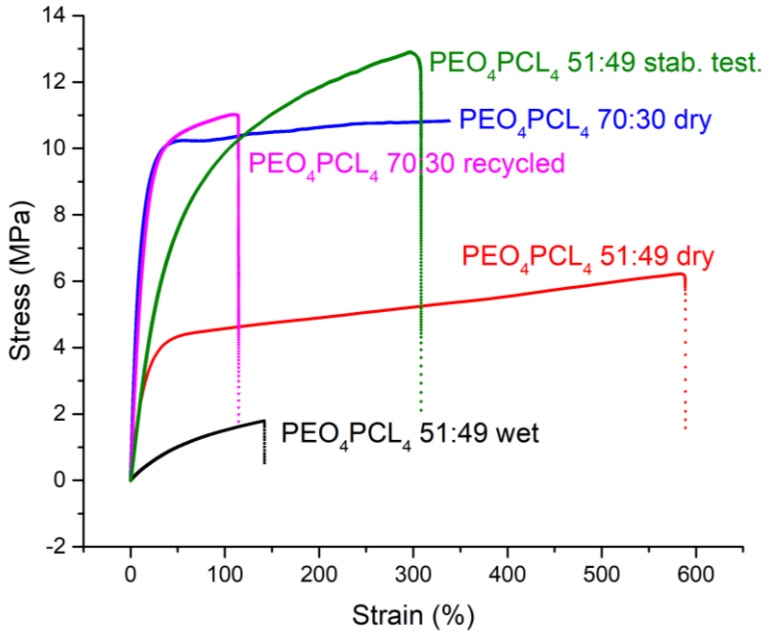

Figure S6: Stress-strain curves of the PEO-4FUR/PCL-4MAL8k (51:49) material at dry state (red), hydrated state (black) and after 2 months in PBS solution (green), the one of PEO-4FUR/PCL-4MAL4k (70:30) material at dry state (blue) and the one of PEO-4FUR/PCL-4MAL recycled (pink).

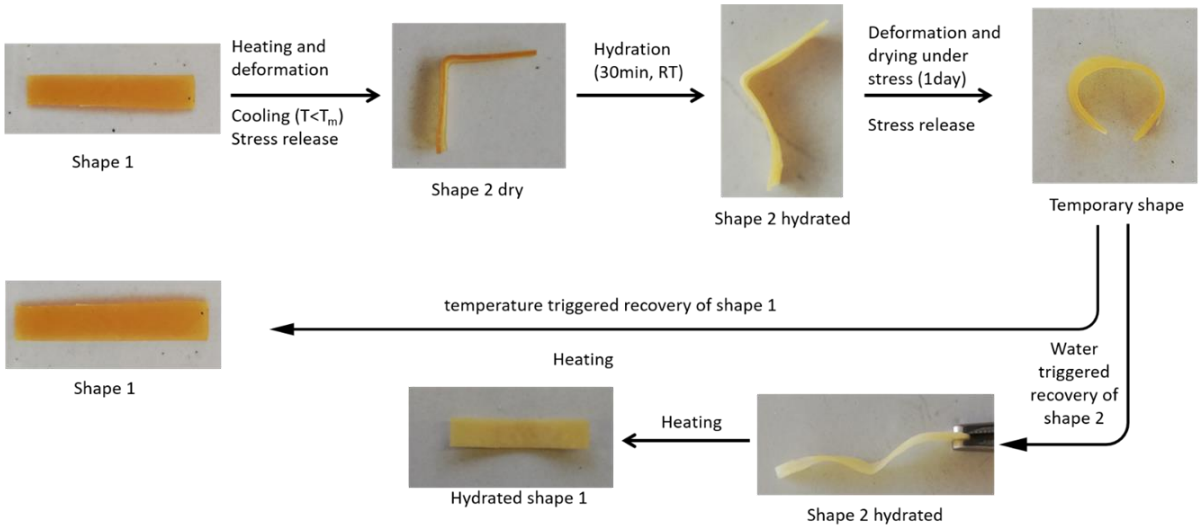

Figure S7: Multiple shape-memory of PEO/PCL network with the 51:49 composition.

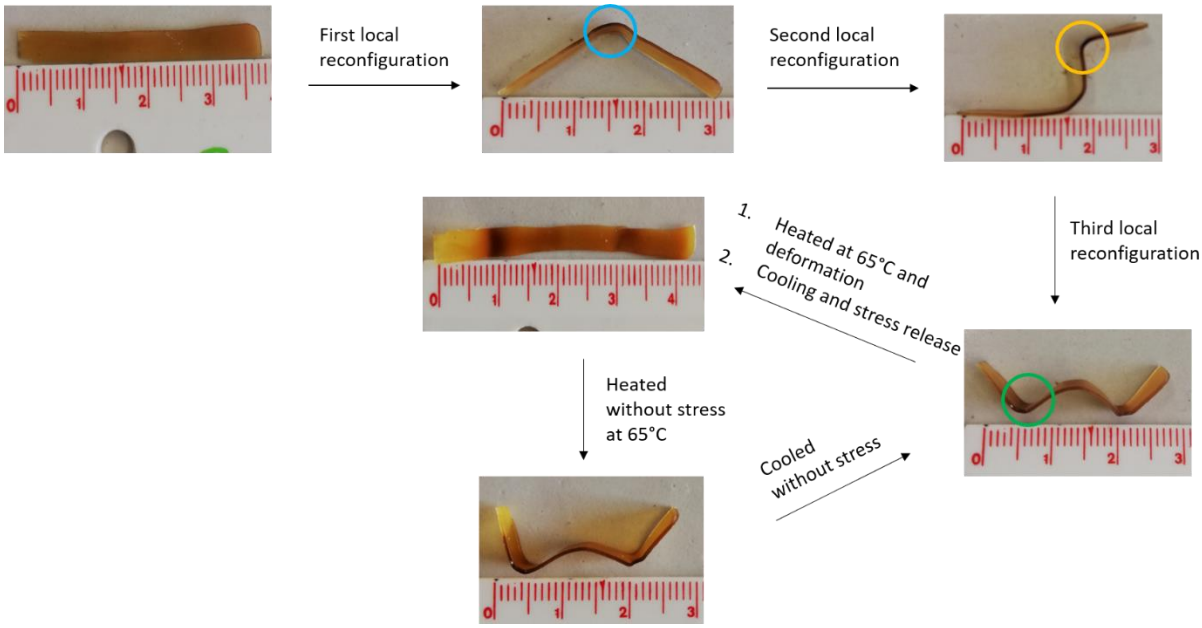

Figure S8: Local reconfiguration of the 51:49 shape-memory sample.

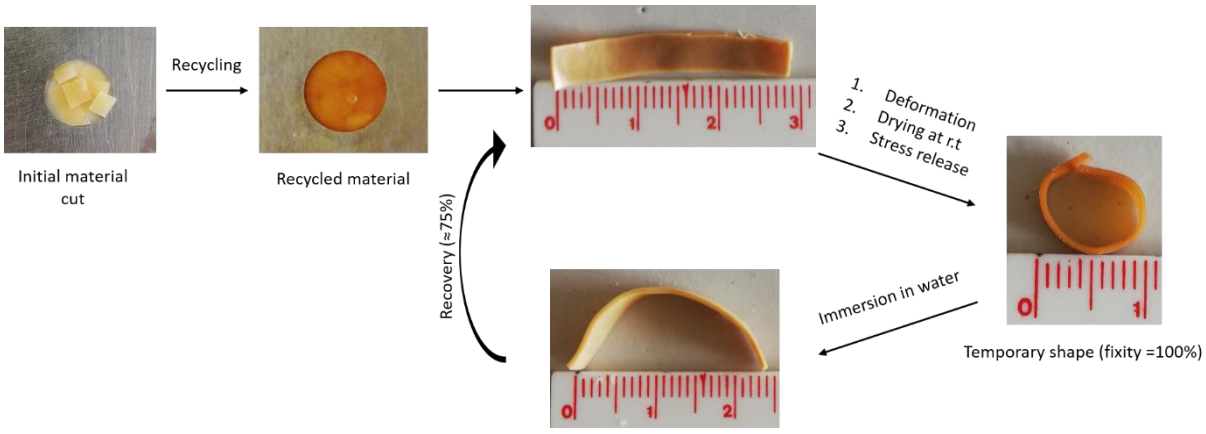

a)

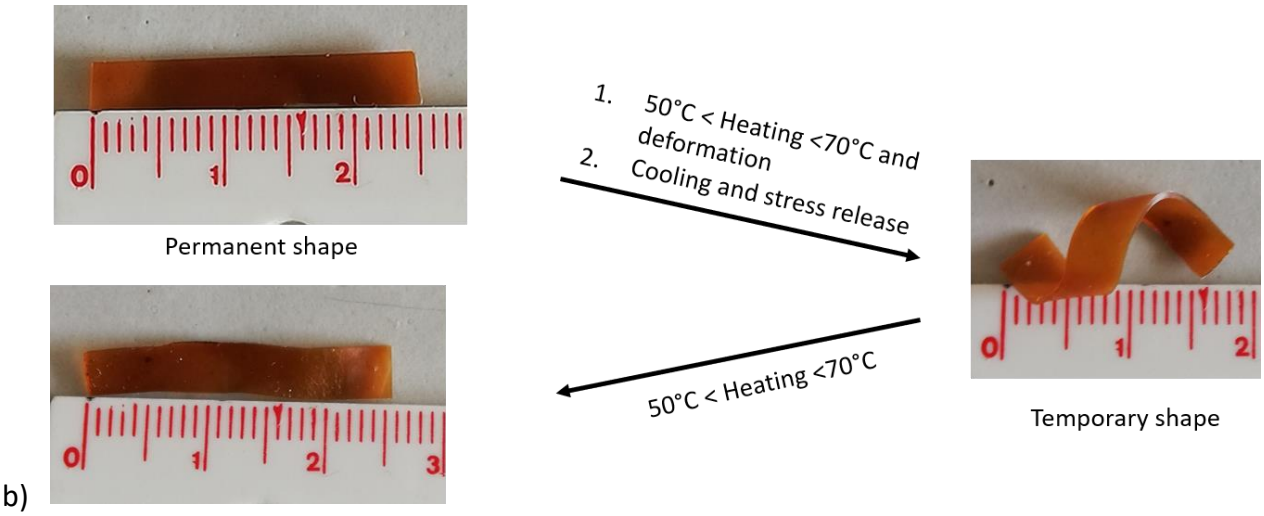

Figure S9: a) Sample before and after recycling process (left) and water shape-memory properties of the recycled 70:30 material (right). b) Thermo shape-memory properties of the recycled 70:30 material.

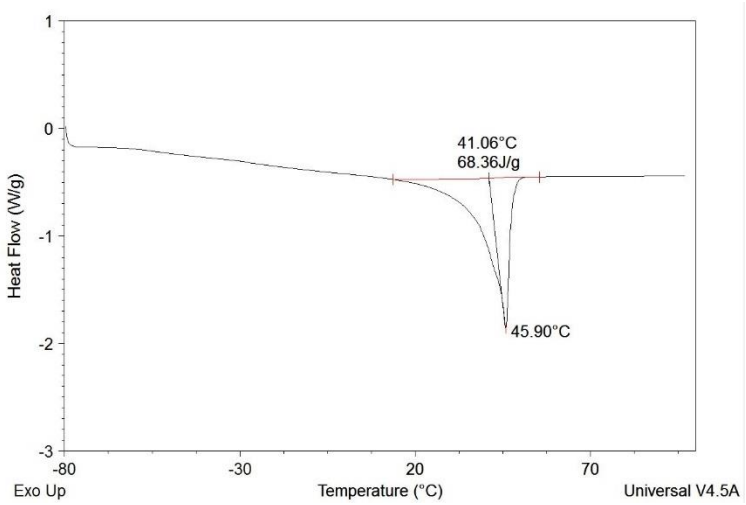

Figure S10: DSC traces for the recycled 70:30 network

Table S1: Temperature shape-memory properties of the 51:49 hybrid network as determined by DMA in the dry state.

Cycle number	**1**	**2**	**3**	**4**
Fixity ratio (%)	98	98	98	98

Recovery ratio (%)	85	97	97	97

Table S2: Fixity and recovery ratio of water triggered shape-memory for each kind of material.

Material	**51:49**	**51:49 Recycled**	**70:30**	**70:30 Recycled**
Fixity ratio (%)	≈100	≈100	≈100	≈100
Recovery ratio (%)	≈75	≈75	≈80	≈75

Table S3: Fixity and recovery ratio of temperature triggered shape-memory for each kind of recycled material.

Material	**51:49**	**51:49 recycled**	**70:30**	**70:30 Recycled**
Fixity ratio (%)	≈100	≈100	≈100	≈100
Recovery ratio (%)	≈100	≈100	≈100	≈100

Table S4: Temperature shape-memory properties of the 51:49 network after immersion in PBS

	Fixity ratio (%)				Recovery ratio (%)			
Immersion time **** ***Cycle number***	***1***	***2***	***3***	***4***	***1***	***2***	***3***	***4***
2 weeks	97	98	98	98	75	96	99	99
1 month	98	98	98	98	79	97	97	97

Table S5: Mechanical properties of the 51:49 material before and after hydrolytic test

Material	**E (MPa)**	**σ (MPa)**	**ε (%)**
51 : 49 before hydrolytic test	31	6.2	600
51 : 49 after hydrolytic test	43	12.9	310

Chapter VI: General conclusion and outlooks.

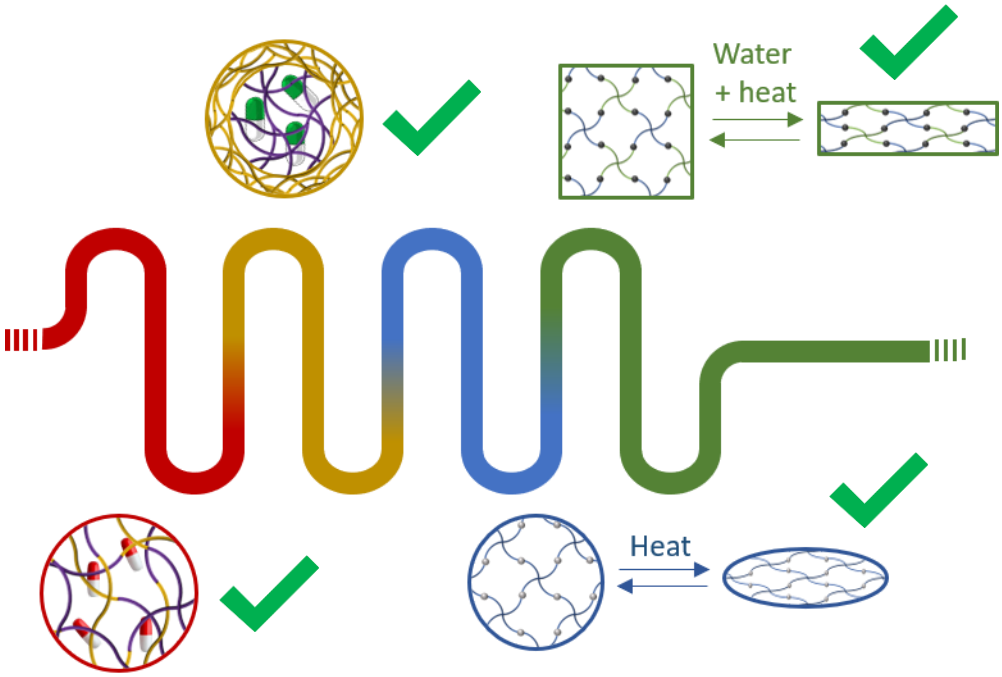

Chapter VI: General conclusion, discussions and outlooks

The different objectives targeted at the beginning of this thesis were mainly achieved. Well-defined microspheres made-of commercially available aliphatic polyesters largely used at present for biomedical applications and promising polyphosphoester polymers were successfully formulated according to a microfluidic process allowing the synthesis of a wide variety of drug-loaded microparticles with different drug-release profiles and functionalities discussed in detail in the VI.1 and VI.2 parts.

The formulation of microspheres containing PPE was optimized and microparticles with a size varying between 46.6µm and 59.8µm were obtained in the same conditions depending on the microsphere composition. The addition of a polyphosphoester component in a classic microspheres polyester matrix does not influence the encapsulation efficiency, compared to classic polyester microspheres, but allows to increase tremendously the drug-release kinetic, even when less than 10% of PPE is incorporated in microspheres. The complete release of the budesonide is tuned between 6h and 48h depending on the PPE proportion in the polymer matrix. The addition of a crosslinked PPE shell around a polyester core increases the microsphere size and allows to increase the drug-loading without modify the kinetic release/profile. Moreover, the microspheres containing PPE does not show any toxicity to HUVEC and Bfb cells but further cytotoxic tests must be required to ensure that these microspheres are not toxic and can be injected in human body.

One of the microfluidics' advantage is that the scaling-up is generally easier than in batch. Moreover, the microsphere's size, polydispersity, shape, structure and composition and consequently, the drug-loading and drug-release can be easily tuned by the modification of the microfluidic parameters which is very convenient for a supplier. The limiting step is the availability of large amount of PPE. Nevertheless, the Interreg In Flow project, which I had the pleasure to participate in, focused, among other things, on the development of a microfluidics-based innovative semi-industrial production process of cyclic phosphate monomers and their corresponding polyphosphoesters (co)polymers with an excellent control

of the macromolecular parameters. Typically, Dr Romain Morodo (CiTOS-ULiege) synthesized in flow 115g BEP monomer a day, by microfluidic technique, with an overall yield of 49% instead of 21% in batch[1] with a high purity allowing its (co)polymerization also according to a microfluidic process.

In the last two chapter, some shape-memory microspheres composed of PCL-4COU were formulated and UV crosslinked directly in flow and the temperature triggered shape-memory was tested. Considering the unique structure of the crosslinked PCL//PBEP microspheres, shape-memory were also successfully tested on these microparticles. Heating the microparticles to triggered the shape-memory can be problematic with biomedical applications in mind. That is why the incorporation of magnetite in microspheres was optimized with an EE around 99%, in order to have a shape-memory caused by a magnetic field. Another approach is to have a water-triggered shape-memory material by incorporating a hydrophilic component, the PEO, in a PCL matrix. This hybrid networks exhibit crystallinity, mechanical robustness and water sensitivity and consequently, two different shapes are memorized which are recovered by different triggers, namely temperature and water.

VI.1 Drug release kinetics tuning

The primary objective of this thesis was to modify the drug release kinetics by employing a biodegradable polymer alternative to polyester. The characteristics of the polymer, such as hydrophilicity, crystallinity, and free volume, play a crucial role in determining the drug release profiles. Polyphosphoesters have emerged as promising candidates for fine-tuning drug release from aliphatic polyester-based microspheres. They have already demonstrated successful applications in the development of drug-loaded nanocarriers and hydrogels for drug delivery purposes[2].

The initial approach involves modifying the composition of reference microspheres by incorporating polyphosphoesters (PBEP) into the polyester matrix. To achieve this, a diblock copolymer consisting of PLLA and PBEP was synthesized and the formulation was optimized. The model molecule chosen for drug-loading experiments was budesonide, so that the

formulation of budesonide loaded microspheres of various polymer blends was also optimized.

Encapsulation efficiency and drug release studies were conducted and compared to conventional loaded polyester microspheres. The results revealed that the encapsulation efficiency of budesonide remained similar when the same organic solvent was used for formulation. However, the drug release rate was significantly faster for the microspheres containing polyphosphoester. In fact, almost 100% of the budesonide was released within only 48 hours when 6.2wt% of PBEP was present in the particle matrix, whereas in the absence of PBEP, the drug release was only at 10% after 6 weeks.

The second approach involves the modification of the microspheres structure by formulating core-shell microspheres composed of a polyester core and a polyphosphoester shell. The measurement of encapsulation efficiency reveals that the addition of a shell is crucial for enhancing the drug-loading. Specifically, the drug-loading is nearly 20 times higher when a shell is added around a PDLLA core.

Furthermore, the addition of a polyphosphoester shell does not significantly impact the drug release profile compared to microspheres with a 100% PDLLA core-shell composition. In this case, the release is more sustained compared to previous formulations, with complete drug release occurring after 6 weeks.

Moreover, all kinds of microspheres containing polyphosphoester do not show any signs of cytotoxicity which is a highly positive aspect for potential biomedical applications. Nevertheless, further testing on immune cells and assessment of cellular functionality must be conducted to take the application in biomedical field of such microspheres one step further.

The variation in drug release profiles observed between different types of microspheres can hold significant implications, particularly in cases of chronic pain or Crohn's disease crisis. For instance, a combination of both types of microspheres could be formulated to achieve a novel drug release profile. Initially, the microspheres composed of a diblock copolymer would facilitate a faster release, providing immediate pain relief. Subsequently, the

core-shell microspheres would sustain the release of the drug, preventing pain over an extended period of time. This sequential release pattern could offer effective management and relief for conditions requiring both immediate and long-term pain control.

VI.2 Advanced microparticles functionality

The second objective of this work was to introduce functionality into the microspheres, which was achieved by formulating shape-memory microspheres. Core-shell microspheres composed of PCL and PBEP exhibited such properties. However, a notable issue was the leakage of the PCL core due to the limited crosslinking of the PBEP shell. To address this problem, chemically crosslinked PCL microspheres were formulated by using photoreactive star-shaped PCL stars.

Various deformation techniques were applied to obtain discs or rod-like microparticles. These microparticles exhibit excellent temperature triggered shape-memory properties even if the recovery of the rods is not complete considering that lemon-shape microparticles are obtained instead of spheres at the end of the shape-memory process. Furthermore, successful encapsulation of magnetite nanoparticles was achieved in these microspheres, with a loading of 5.4wt% with an EE of 98.7%. This loading that could be increased further if required, is comparable to magnetite-loaded microparticles reported by Uto et al. which demonstrated shape-memory microparticles induced by a magnetic field[3].

Such shape-memory microparticles could be advantageously used as embolic agent. The use of magnetite-loaded microparticles could allow their direct observation in the body by MRI facilitating the surgery. The deformation of such microparticles directly in flow presents an interesting challenge with significant biomedical implications. As mentioned earlier, this would allow for the formulation and deformation of microparticles on-site in a hospital or medical facility, enabling their immediate use. This capability opens up new possibilities for tailored and dynamic medical interventions, enhancing patient care and surgical outcomes.

However, it is important to note that the shape recovery of these microparticles is currently triggered by heat. The unloaded PCL microspheres undergo shape recovery upon direct heating, while the magnetite loaded ones can be triggered by a magnetic field, generating a Joule effect within the particles. It is crucial to consider that this local heating may pose a risk of tissue damages when used inside the body. To address this concern, the combination of cross-reactive poly(ethylene oxide) (PEO) and PCL stars in a hybrid network was investigated. We demonstrated that the resulting new shape-memory material allows both water and heat triggered shape recovery, enabling the programming of two different temporary shapes.

Following this thesis, the next step would be to formulate this innovative hybrid network as microspheres by the flow process. However, this is not straightforward, some challenges must be overcome. Firstly, if EtOAc is a common solvent for both PLC and PEO stars which could be used for the discontinuous phase, an aqueous continuous phase is to banish because the PEO will be dissolved in it. A hydrophobic continuous medium, such as an alkane, should rather be used as solvent for the continuous phase requiring a dedicated emulsifier to stabilize the microspheres.

Secondly, attention should be paid to avoid premature crosslinking of the furan-maleimide stars mixture if they are placed together in a single solution of the injecting syringe, preparing two solutions with each type of stars should be preferred to prevent this problem. Therefore, the microfluidic system should be accordingly adjusted in order to integrate a first mixing step of both stars solutions just before the droplet generation. Indeed, the mixing must be efficient enough to allow the Diels-Alder reaction between the cross-reactive stars.

Advantageously, the chain-ends of the PEO and the PCL stars could be functionalized by coumarin to fasten the coupling reaction by UV irradiation. In this way, both PEO and PCL stars could be mixed together in a single syringe and formulated by the cross-junction system. Considering that the PEO and the PCL are completely immiscible, two kinds of microparticles could be achieved depending on the relative rates of crosslinking and the phase-separation. If the crosslinking is faster than the phase-separation, homogeneous microspheres of an hybrid

network are expected . On the contrary, if the phase-separation occurs faster than the crosslinking reactions, Janus microparticles could be obtained [4]. Janus microspheres are very interesting for some applications because depending on the applied stimulus it would be possible to provoke the shape recovery only on one half of the microparticle. To favor the generation of Janus microparticles, we preconize feeding the core-shell device by two different syringes filled with each coumarin end-capped stars solution.

VI.3 Environmental concerns

As it was demonstrated all along this work, microfluidic processes are very powerful to produce well-defined microspheres. One aspect that was not yet considered is the sustainability aspect of the technique. This necessitates the use of simple, accessible and useful green metrics such as the environmental factor (EF) to measure the greenness of production processes. The EF measures the amount of waste generated by a process expressed in kg of waste per kg of product (eq (1))[5].

$$(1)\ EF = \frac{\sum m_{raw\ materials} + \sum m_{reagents} + \sum m_{solvents} - m_{desired\ product}}{m_{desired\ product}}$$

Of course, the EF factor alone is not enough to have a global idea of the sustainability of the technique but it is already a first indicator of some strengths and weaknesses of the process.

The EF value was calculated for each kind of formulated microspheres in the optimized conditions and gathered in the following table where $m_{raw\ materials}$ is the mass of polyester, polyphosphoester and API and PVOH, $m_{reagents}$ is the mass of photosensitizer and $m_{solvent}$ is the organic solvent. The water, used for the formulation and the purification is not considered in the expression of this factor.

Table 1 : EF calculation for each kind of microfluidic formulated API-loaded microspheres and for one sample of PCL obtained by nanoprecipitation (batch process).

Entry	Microspheres	Formulation conditions (entry + page)	$m_{raw\ materials}$ (g)	$m_{reagents}$ (g)	$m_{solvents}$ (g)	$m_{desired\ product}$ (g)	EF
1	PDLLA:bud	Entry 5 P70	1.285	0	1.35	$8.1\ 10^{-2}$	31.5
2	PLGA:bud	Entry 8 P70	1.285	0	1.35	$8.0\ 10^{-2}$	32
3	PLLA:bud	Entry 10 P70	1.285	0	1.995	$7.9\ 10^{-2}$	40.5
4	PLLA-*b*-PBEP bud	Entry 7 P74	6.085	0	1.995	$7.9\ 10^{-2}$	101
5	Blend 45:55 bud	Entry 1 P76	2.485	0	1.995	$7.9\ 10^{-2}$	55.7
6	Blend 80:20 bud	Entry 2 P76	2.485	0	1.995	$7.8\ 10^{-2}$	56.4
7	PDLLA//PBEP asp	Entry 1 P105	3.08	$2.4\ 10^{-3}$	1.35	$8.0\ 10^{-2}$	54.4
8	PCL//PBEP asp	Entry 2 P105	3.08	$2.4\ 10^{-3}$	1.35	$7.9\ 10^{-2}$	55.1
9	PDLLA//PDLLA asp	Entry 3 P105	3.08	0	1.35	$7.9\ 10^{-2}$	55.1
10	PDLLA asp	Entry 4 P105	3.04	0	0.675	$3.8\ 10^{-2}$	96.8
11	PCL network	Entry 8 P129	1.275	$2.7\ 10^{-3}$	1.35	$7.8\ 10^{-2}$	32.7
12	PCL:magnetite	P137	1.28	$2.7\ 10^{-3}$	1.545	$8.2\ 10^{-2}$	33.5
13	PCL: contrast agent	R.Riva conditions[A]	10.414	0	1.75	0.14	85.9
14	PCL: contrast agent (nano-precipitation)	R.Riva conditions[B]	58.29	0	35.13	0.7	132

[A]Organic phase composed of PCL 7.6w% and 3.3w% of contrast agent with a flow of 0.025mL/min; aqueous phase composed of PVOH = 2.5w% + KH_2PO_4 60g/L with a flow of 2mL/min, recovered product 90% with an EE of 29.3%. Mean diameter 200.3µm and PDI = $9.4\ 10^{-3}$.

[B]30mL of organic phase composed of PCL 0.1g/mL and contrast agent 0.043g/mL are processed in 600mL of PVOH solution 3w% containing KH_2PO_4 60g/L. Recovered product : 16.3% with an EE of 30%. Mean diameter 175.4µm and PDI = $1.3\ 10^{-2}$.

The EF values for each kind of microspheres varies from 31.5 to 96.8. The EF is influenced by the kind of used solvent (Entries 1 and 3) and slightly influenced by the encapsulation efficiency (Entries 7 and 9) because the amount of API is low compared to the

amount of solvent used. On the contrary, the EF is much higher when 5w% PVOH solution is used (entries 4, 7-9) and when the continuous phase flow increases (entries 4-6). This evidences that the continuous phase is predominantly impacting the EF. Core/shell microspheres formulation shows similar EF as bulk particles. Nevertheless, if the EF microfluidic values (Entry 13) is compared to nanoprecipitation technique (Entry 14) for the formulation of PCL microspheres, microfluidic formulation appears more sustainable than the nanoprecipitation, regarding the EF factor.

An ideal EF value is 0, whereas a higher EF means greater waste generation and subsequently leads to more pronounced negative environmental consequences. To decrease this EF value, the recycling of the continuous phase can be considered[5].A back-loop can be incorporated in the system to recycle the continuous phase if the organic and the aqueous phase are immiscible but in the case of partially miscible solvent, another separation process, as the distillation, must be implemented which is time and energy consuming. If it can be implemented to our system, the EF value would fall between 16.7 and 25.3, making continuous flow formulation relevant for a greener future.

VI.4 References

1. Morodo, R. *et al.* Accelerating the end-to-end production of cyclic phosphate monomers with modular flow chemistry. *Chem Sci* **13**, 10699–10706 (2022).
2. Ergul Yilmaz Z., C. J. Polyphosphoesters: New Trends in Synthesis and Drug Delivery Applications. *Macromol Biosci* 1745–1761 (2016) doi:10.1002/mabi.201600269.
3. Uto, K. & Ebara, M. Magnetic-responsive microparticles that switch shape at 37 °C. *Applied Sciences (Switzerland)* **7**, (2017).
4. Nisisako, T. Recent advances in microfluidic production of Janus droplets and particles. *Curr Opin Colloid Interface Sci* **25**, 1–12 (2016).
5. El Itawi, H., Fadlallah, S., Allais, F. & Perré, P. Green assessment of polymer microparticles production processes: a critical review. *Green Chemistry* **24**, 4237–4269 (2022).

Annexes

Soft Matter

PAPER

View Article Online
View Journal | View Issue

Cite this: *Soft Matter*, 2020, **16**, 10320

Switchable self-assembled capillary structures

Nicolas Vandewalle, *[a] Martin Poty,[a] Nathan Vanesse,[a] Jérémie Caprasse,[b] Thomas Defize[b] and Christine Jérôme[b]

Received 8th July 2020,
Accepted 24th September 2020

DOI: 10.1039/d0sm01251c

rsc.li/soft-matter-journal

Capillarity driven self-assembly is a way to create spontaneous structures along liquid interfaces in between bottom-up and top-down fabrication methods. Based on multipolar capillary interactions between elementary floating object, simple to complex structures can been achieved by designing objects with specific 3D shapes. We show herein that a switchable self-assembled structure can be obtained with a shape memory polymer. At a defined temperature of the liquid, the 3D shape of each elementary floating object changes, modifying the capillary interactions thus forcing the stable structure to disassemble and to form a new arrangement. Based on simulations and experiments, we study how this cooperative behavior induces metastable complex configurations.

1 Introduction

The spontaneous generation of order in systems made of numerous components, called self-assembly, is ubiquitous in biology and chemistry at the molecular level. Examples range from the formation of crystals to the formation of complex molecules. Self-assembly is now being intensely studied in chemistry, biology and materials engineering.[1] Moreover, self-assembly is also encountered from the micrometer up to the centimeter scales, offering opportunities to generate 2D and 3D elaborated structures with low cost and simple manipulations.[2] Extensive research demonstrated that the self-assembly of small-scale structures can be achieved along liquid interfaces, opening ways to inexpensive manufacture processes in between bottom-up and top-down forms of fabrication.[3–9]

Capillary driven self-assembly consists in suspending small objects at the water–air interface. Depending on the object weight, hydrophobicity and surface tension, the interface is slightly deformed, inducing a net force between the particles.[10–14] Vella and Mahadevan[14] rationalized this interaction for spheres, while Kralchevsky[11,12] considered non-spherical particles. In both approaches, any liquid deformation around an object (or a particle) defines a so-called capillary charge, and the interaction between two objects is given by the product of the capillary charges as well as a decreasing (Bessel) function of the object interdistance. While a spherical particle is characterized by a single capillary charge, a non-spherical particle could be characterized by a sum of capillary charges leading to multipolar effects.[13] Those multipolar interactions involve torque and orientational effects in addition to attractive/repulsive interactions.[13,15] Such multipolar effects were considered for example to explain the particular natural patterns forming along water–air interfaces with mosquito eggs and whirligig beetles.[16]

Based on multipolar capillary interactions, sophisticated self-assembled structures can therefore be envisioned, as already tested by our group.[7,8] In these earlier works, we 3D printed branched objects for producing either positive or negative charges located at the tips of the branches. We proved that large and ordered self-assemblies can be programmed by designing the shape of the objects: square and triangular lattices have been achieved.[7]

A step forward is to achieve a remotely configurable self-assembly. Changing the shape of the composing particles modifies the interactions between them and enables us to provoke or prevent the assembly. A programmable, reconfigurable and switchable self-assembly can thus be reached.[17] Earlier studies proposed to change the density of the liquid by adding salts.[18] The resulting modification of particle buoyancy triggers the reconfiguration of the assembly. More recently, we proposed to use an external magnetic field to actuate capillary charges placed on floating elastic objects,[19] allowing for reversing the self-assembling process.

The aim of this paper is to study the self-assembly of objects whose multipolar capillary interactions can be modified/activated by shape shifting using shape-memory polymer as material for manufacturing the objects. We study the different stable and metastable patterns that can be achieved, as the one illustrated in Fig. 1. Our work aims to provide original patterns by remotely switching the shape of objects.

[a] *GRASP, CESAM Research Unit, Institute of Physics B5a, University of Liège, B4000 Liège, Belgium. E-mail: nvandewalle@uliege.be*
[b] *CERM, CESAM Research Unit, Institute of Chemistry B6a, University of Liège, B4000 Liège, Belgium*

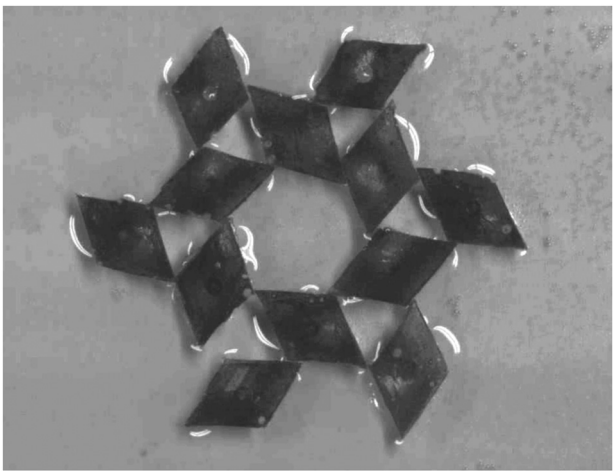

Fig. 1 Top view of a self-assembly made of 12 floating objects. Each one has a rhombus shape with edge length 1 cm, giving a scale to the picture. The picture captures the ephemera structure when a compact configuration disassembles. The symmetry of this metastable configuration emphasizes the cooperative motion of the particles.

2 Multipoles

According to ref. 14, the cylindrical liquid profile, being the liquid elevation z_i, at a position $\vec{r}$ from a spherical particle i centered on $\vec{r}_i$, is given by

$$z_i = Q_i K_0\left(\frac{|\vec{r}-\vec{r}_i|}{\lambda}\right) \quad (1)$$

where Q_i is called a capillary charge and corresponds roughly to a characteristic height for the meniscus deformation at some distance from the particle center, K_0 is the modified Bessel function of the second kind. The typical distance $\lambda = \sqrt{\gamma/\rho g}$, over which the liquid surface is deformed, is called the capillary length, which depends on surface tension γ, liquid density ρ and Earth gravitational acceleration g. This characteristic length is close to λ = 2.7 mm for water/air interfaces. When two distant particles, labelled i and j, are floating at the liquid surface, the interaction potential is given by

$$U_{ij} = -2\pi\gamma Q_i Q_j K_0\left(\frac{|\vec{r}_j-\vec{r}_i|}{\lambda}\right) \quad (2)$$

where the product of the capillary charges is found. This potential results from the superposition of the deformations z_i and z_j, which is assumed even if observations show that superposition principle is a crude approximation when particles come close together.[10] Nevertheless, it has been shown that this approximation is valid in most cases when the meniscus slope is not so important.[20] From eqn (2), both attraction and repulsion can be obtained, depending on the signs of the capillary charges Q_i and Q_j. For distant objects ($|\vec{r}_i - \vec{r}_j| \gg \lambda$), the decay of K_0 looks like an exponential decay.

When the object shape differs from a sphere,[15] or when the object is larger than the capillary length,[19] a superposition of capillary charges, has been proposed for describing the deformation of the liquid. The liquid elevation at position $\vec{r}$ around the object i is given by

$$z_i = \sum_{\alpha\in i} Q_\alpha K_0\left(\frac{|\vec{r}-\vec{r}_\alpha|}{\lambda}\right). \quad (3)$$

These capillary charges Q_α belonging to object i are the key ingredients of our work. The interaction between two multipolar objects i and j is simply given by the sum of all possible interactions between charges placed on both particles. One has

$$U_{ij} = -2\pi\gamma \sum_{\alpha\in i}\sum_{\beta\in j} Q_\alpha Q_\beta K_0\left(\frac{|\vec{r}_\beta-\vec{r}_\alpha|}{\lambda}\right), \quad (4)$$

that we will consider for the numerical modelling along this article.

In order to create a pattern, we 3D printed many multipolar objects having a rhombus shape. The internal angles of the rhombus are 60° and 120°. The side length is 1 cm, being much larger than the capillary length λ. The rhombus thickness is 0.5 mm. Those elementary units are floating thanks to partial wetting. In addition, we imposed positive and negative curvatures. In fact, we created two different types of rhombus, as illustrated in Fig. 2. The first type, as illustrated in Fig. 2(a),

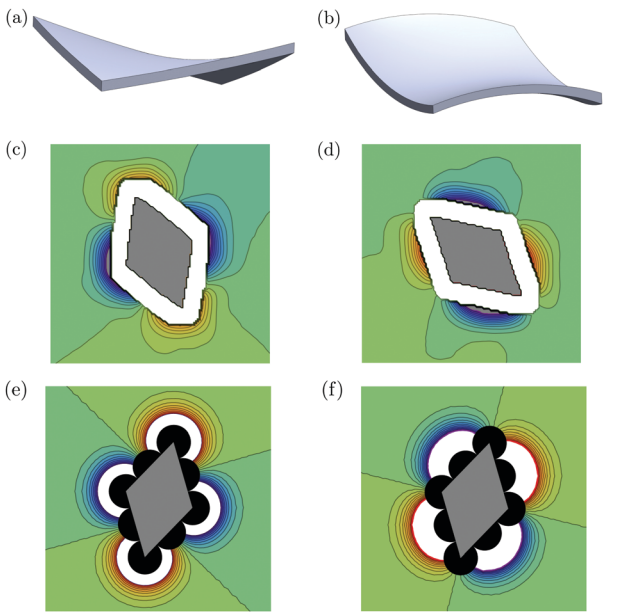

Fig. 2 (a) 3D view of a rhombus tile curved along the diagonals, with opposite curvatures. (b) 3D view of the same rhombus tile curved along the medians, with opposite curvatures. (c and d) Experimental profilometry of the liquid interface deformation around objects (a and b), respectively. The blue-green-red color scale indicates the elevation of the liquid interface in arbitrary units. Blue (red) corresponds to a negative (positive) capillary charge, while the green color corresponds to a flat unperturbed interface. The white region around each rhombus corresponds to high slopes characterized by large uncertainties within this profilometry method. (e and f) Using the same color code, simulation of the liquid elevation with eqn (3) in our simulations with objects corresponding to (a and b) respectively. Each rhombus is simulated using non-overlapping disks shown in black and associated to a capillary charge.

considers a positive and a negative curvature along the diagonals of the rhombus for creating respectively positive or negative capillary charges at the vertices. The second type of rhombus, as seen on Fig. 2(b), has curvatures along the medians of the rhombus for creating large liquid deformations along the sides of the rhombus.

Before building elaborated structures, we characterized the liquid interface deformation around each basic elements using a profilometry technique.[21] The experimental method is based on refraction of light through the deformed interface. A pattern is placed below the system and is recorded with zero deformation of the interface. When one or more objects are placed on the liquid interface, light refraction will modify the image of the pattern. By image correlation analysis, it is possible to obtain the gradients of the interface. By integration, the liquid profile is obtained. Liquid elevations of at least 10 μm are detected. Experimental liquid profiles around the particles are shown in a color scale in Fig. 2(c and d): red for positive deformation and blue for negative deformation.

The liquid elevation z around single floating tiles is shown in Fig. 2. The white region around each rhombus corresponds to strong gradients involving some indetermination of the liquid elevation after integration. Close to the objects, strong deviation from a flat interface are seen either at the vertices (c) or along the sides of the rhombus (d), as expected. Positive and negative capillary charges forming a quadrupolar system could be considered. Moreover, a slight negative capillary charge should be considered coming from the weight of the tile itself. Indeed, a non-curved tile deforms slightly the interface and a weak capillary interaction is observed between uncurved objects.

We have also considered a numerical model which considers rhombus shape made of 9 non-overlapping disks. One disk is placed at the center of the rhombus. Four disks corresponds to vertices. Four disks corresponds to the middle of the edges. Each disk could be the center of a capillary charge, as described by eqn (3). Two typical objects are shown in Fig. 2(e and f). A small grey rhombus is superimposed in order to give the orientation of the object. However, the object should be considered as the union of all disks. By placing capillary charges either at the vertices of the rhombus or along the sides of the rhombus, we obtain a good approximation of the liquid profile obtained in our experiments, as shown in Fig. 2. Please remark that the ninth capillary charge in the particle center is considered in order to provide a slight negative charge and attraction between objects. In the following work, we will consider this model in order to simulate capillary driven self-assemblies.

More capillary charges can be considered for describing the rhombus objects but this will inevitably increase the computation times when calculating the interaction potential eqn (4). We present herein the results with the minimum possible of charges in order to reproduce experimental observations. Moreover, adding more disks for modeling rhombi implies shorter interdistances that could result in another choice for the potential (4).

3 Self-assembled patterns

Considering both types of 3D printed objects, two different self-assembled patterns are obtained in experiments. Objects are placed at random on the water–air interface. Interactions drive the system into ordered clusters within seconds and without mechanical agitation. The more compact obtained experimental structures are illustrated in Fig. 3(a and b) when 12 floating objects comes together. A similar kind of self-assembled lattice has already been obtained in our earlier work on branched floating objects.[7] In fact, lacunes, *i.e.* missing tiles, may be present in the lattice and they are mainly due to initial conditions, *i.e.* initial positions and orientations of the particles. A small agitation of the water–air interface provides some annealing for the structure leading to a more compact and more symmetrical raft.[19] The key ingredient for reaching lattices is the use of both positive and negative charges on the objects allowing for both attractive and repulsive motions during self-assembly. It should be remarked that neighboring rhombi are still separated by a very thin layer of liquid at equilibrium, *i.e.* they are not completely in contact. This is probably due to the wavy contact line along the edge, leading to a repulsive interaction at short range.[22]

Rhombille tiling, as shown in Fig. 3(a), is obtained for vertex–vertex interactions. The rhombille tiling can be viewed as a regular hexagonal structure, each hexagon being made of three rhombi.[23] The hexagonal lattice has a symmetry $p6m$, while the hexagon centers have a symmetry $p3m1$, meaning that 3-fold and 6-fold local symmetries coexist in the structure.

When edge–edge interactions are dominating the system, the particles self-assemble into a 4-fold isohedral structure,[23] as shown in Fig. 3(b). The lattice is formed by the simple translation of the rhombus along the air–water interface. It is remarkable that completely different symmetries can be reached using similar rhombi objects but having different curvatures.

Based on the objects of Fig. 2(e and f) possessing 9 capillary charges, numerical simulations of self-assembly were performed. The objects are initially placed with random positions and orientations in the horizontal plane. The so-called steepest descent algorithm searches for small translations and rotations of the particles among numerous random moves, allowing only minimization of capillary energy, as given by eqn (4). Whatever the values of the charges Q_α in eqn (4), the minimum

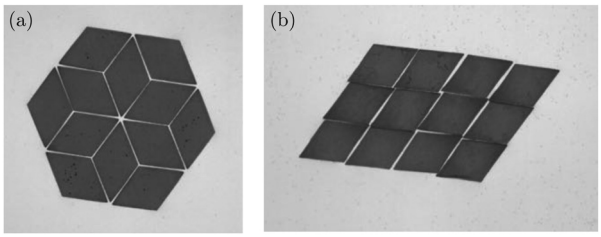

Fig. 3 Self-assemblies formed by 12 identical rhombi. Each rhombus has an edge length of 1 cm, giving a scale to the pictures. (a) Rhombille tiling obtained with tiles of Fig. 2(a), involving vertex–vertex interactions. (b) Isohedral tiling obtained with rhombi of Fig. 2(b), involving edge–edge interactions.

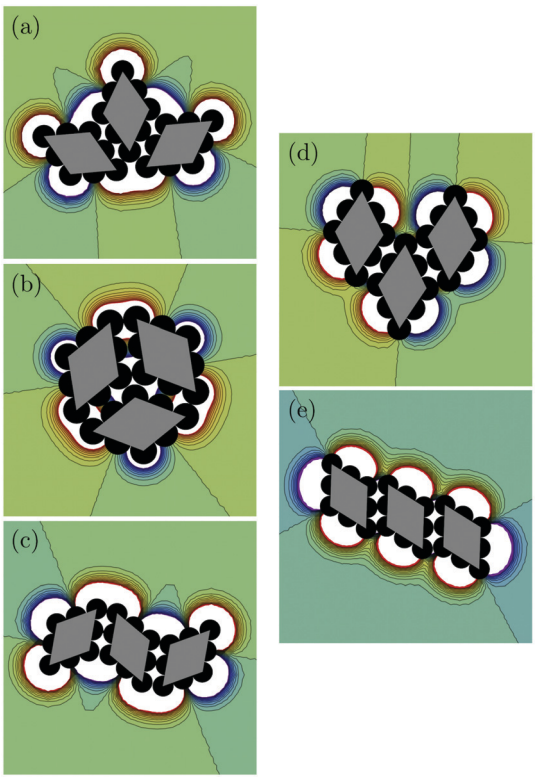

Fig. 4 All resulting patterns made of three objects, resulting from the simulations of capillary attractions and repulsions. The first column (a–c) shows the cases dominated by vertex–vertex interactions starting from different initial conditions. The right column (d and e) shows the cases dominated by edge–edge interactions. The blue-green-red color scale indicates the elevation of the liquid interface in arbitrary units. Blue (red) corresponds to a negative (positive) capillary charge, while the green color corresponds to a flat unperturbed interface.

is obtained when objects comes into contact. The resulting pattern is therefore independent on the scale of charge, *i.e.* the scale of interface deformation along the vertical z-axis.

Typical results for three interacting objects are shown in Fig. 4 for both types of rhombus. As expected, rhombille and isohedral patterns are obtained, therefore validating such a model. Although a low number of objects is considered, many different patterns result from self-assembly, emphasizing the importance of the initial conditions. All resulting patterns are illustrated in Fig. 4. Increasing the number of particles in simulations involve more defects in the lattices such that annealing is needed. Nevertheless, low number of objects are enough to show the symmetry of expected patterns. One should nevertheless remark that the isohedral pattern is not perfect, since there is a slight shift between neighboring rhombi. This effect, also observed in the picture of Fig. 3(b), can be reduced by considering smaller disks for the capillary charges describing the shape of the objects.

4 Switching behavior

Instead of 3D printing rigid tiles with specific curvatures, we 3D printed the negative of these tiles in order to create molds. A polymer can therefore be pressed in the molds. A shape-memory polymer has been developed for our purpose. Four-arm star-shaped poly-ε-caprolactone end-capped by reactive functions, *i.e.* furan or maleimide moieties, have been used for the preparation of the shape-memory particles (see Fig. 5). The functionalization of commercially available PCL-4OH chain-ends by maleimide or furan moieties to get the PCL-4MAL and PCL-4FUR, respectively, is a well optimized and already published process.[24,25] It was applied to PCL-4OH of a molar mass of 8000 g mol^{-1}.

In order to get the temperature triggered shape-memory objects, they were made of cross-linked semi-crystalline PCL. The chemically cross-linked PCL network is formed by mechanical mixing of an equimolar blend of PCL-4MAL and PCL-4FUR at 105 °C, followed by a thermal post-curing at 65 °C in a mold to allow Diels–Alder adduct formation leading to the network (Fig. 5). More precisely, 1 g of PCL-4FUR and 1 g of PCL-4MAL (M_n 8000 g mol^{-1}) stars were introduced in a 10 mL vial and molten at 105 °C in an oven. Few milligrams of carbon black were added in order to have a better contrast for future pictures and videos. Then the mixture was mechanically blended and collected in a home-made 3D-printed mold (see Fig. 6b), then cured at 65 °C during 24 h to obtain a crosslinked material. After this step, the formed PCL network has memorized the edge–edge shape (permanent shape) of the particles.

Then, these objects are heated again at 60 °C, *i.e.* above the melting temperature of the PCL network and placed in a second mold (Fig. 6a) to give them their vertex–vertex temporary shape after cooling in the mold at ambient temperature.

We decided to switch from vertex–vertex to edge–edge rhombus types. The melting temperature is around T_m = 60 °C. The water is therefore progressively heated from the bottom using electrical resistors. The increase of temperature may have two effects: (i) a modification of surface tension and (ii) the appearance of convective cells. We assume that they are weak effects. Indeed, the capillary length changes only by 4% in the temperature range such that the objects are still much larger than λ. By heating from below, convective rolls may appear below the interface, providing some agitation. If present, this source of fluid motion is however unable to separate the tiles from each other just before the transition. Once the transition temperature is reached, the change of symmetry is observed within a few seconds. A typical sequence

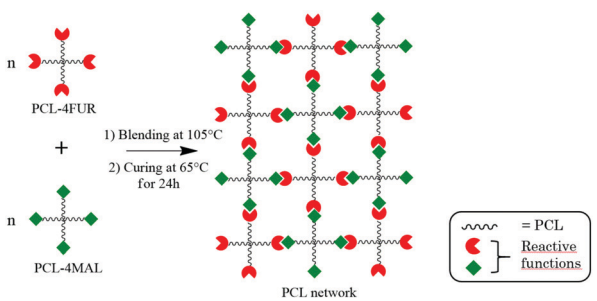

Fig. 5 Network formation using the Diels–Alder cycloaddition between furan and maleimide as reactive functions at the chain-ends of 4-arm star-shape PCL.

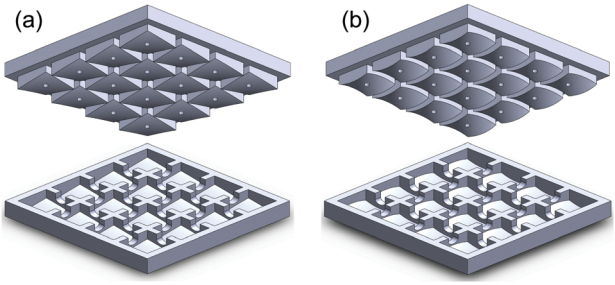

Fig. 6 Design of the molds used to give to the shape-memory particles: (a) the vertex–vertex temporary shape and (b) the edge–edge permanent shape.

of self-disassembly and reassembly into a new structure is given in Fig. 7. Starting from 6 rhombi in a flower configuration, *i.e.* with a 6-fold vertex in the center, the rhombi start to slide along each other and then rotate to switch to an isohedral lattice.

Changing the symmetry involves both fundamental moves for each rhombus: translation and rotation. When capillary charges migrate from vertices to edges, the translation of a rhombus along the edge of another one is cost effective with respect to the capillary energy. Indeed, the slight negative charge of each object favors translation for objects nearly in contact before rotations, as seen in the first stages shown in Fig. 7. Rotational events appears at the end of the shape switching process when capillary charges involve larger torques. At this step of the process, the centres of rotation correspond roughly to the tips of each rhombus.

We performed many experiments, varying the number of tiles as well as the initial configurations. We start from compact configurations only (without lacunes) but with a variable number of tiles. Two major behaviors should be distinguished. The first one, often encountered for a large number of tiles, is illustrated by the remarkable structure of Fig. 1 being the last step of a rearrangement starting from Fig. 3(a). In fact, the system is stuck in a metastable situation far from the expected isohedral structure. The transition is therefore incomplete. In fact, the migration of the capillary charges from vertices to edge centers allows for translation of tiles along the edges. However, the rotation of tiles is forbidden since particles are always in close interaction with two other neighbors, even in the last step of capillary charge migration. This behavior has been simulated

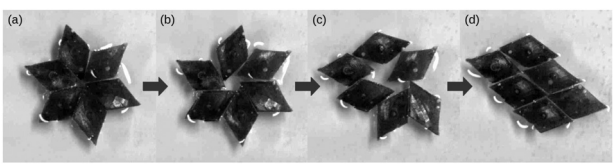

Fig. 7 Experiment of the reconfiguration of a self-assembly. Each rhombus has an edge length of 1 cm, giving a scale to the pictures. (a) Six rhombi are forming a flower-like rhombic configuration at $T < T_m$. (b and c) When the temperature of the liquid reaches T_m, the curvature of each rhombus changes to move the capillary charges from the vertex to the sides, causing the disassembly of the structure. (d) The final stable isohedral structure is found at the end of the irreversible process ($T > T_m$).

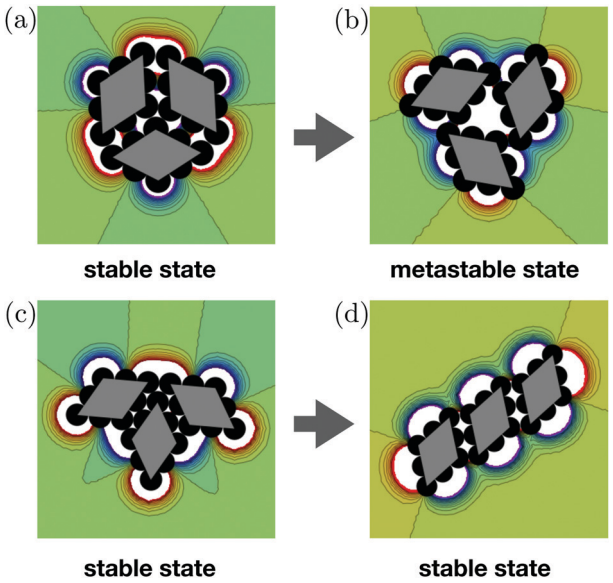

Fig. 8 Two initial different stable rhombic states are driven to a single stable isohedral state when capillary charges are transferred from vertices to sides. For the first compact configuration (a), a metastable state (b) is obtained for which three rhombi form a triangular configurations, as observed in Fig. 1. Another configuration (c) leads to a perfect isohedral stable state (d). The blue-green-red color scale indicates the elevation of the liquid interface in arbitrary units. Blue (red) corresponds to a negative (positive) capillary charge, while the green color corresponds to a flat unperturbed interface.

starting from 3 tiles forming a compact rhombille structure, as shown in the top row of Fig. 8. During the capillary charge migration along the edges, they move cooperatively forming a triangular shape in the center. The liquid deformation there is important since the superposition of three charges is observed there. Each rhombus has still 2 neighbors, but the rotation of each rhombus is unlikely since they are attracted towards the center of the triangle. The self-assembly of Fig. 1 is therefore a metastable configuration. In order to obtain the isohedral structure, this configuration should be annealed by interface fluctuations/agitation for separating objects from each other, allowing for rotations.

The second behavior is the one of Fig. 7: isohedral lattice is obtained at the end of the process. For that case, each rhombus has the opportunity to rotate. This has been simulated starting with three tiles, as shown in the bottom row of Fig. 8. From that experimental and numerical results, we can conclude that the initial configuration determines the occurrence or not of the metastable configuration.

5 Conclusions

In summary, we performed experiments and simulations for the capillary driven self-assembly of rhombic tiles, forming lattices. The curvature of the particles induce specific positions for the capillary charges involving different interactions and self-assembled lattices.

By using a shape memory polymer for creating particles, the self-assembly becomes responsive to the temperature of the liquid. The capillary charges can be transferred from vertices to edges. The resulting patterns disassemble and self-assemble again into new configurations, including metastable states.

The numerical simulations based on multipolar capillary charges are able to capture all observed phenomena, and could be applied to any other self-assembling objects forming complex structures.

Conflicts of interest

There are no conflicts to declare.

Acknowledgements

This work was financially supported by the CESAM Research Unit of the University of Liège.

Notes and references

1 G. M. Whitesides and B. Grzybowski, *Science*, 2002, **295**, 2418–2421.
2 M. Boncheva, D. A. Bruzewicz and G. M. Whitesides, *Pure Appl. Chem.*, 2003, **75**, 621–630.
3 N. Bowden, S. R. Oliver and G. M. Whitesides, *J. Phys. Chem.*, 2000, **104**, 2714–2724.
4 N. Bowden, F. Arias, T. Deng and G. M. Whitesides, *Langmuir*, 2001, **17**, 1757–1765.
5 P. W. Rothemund, *Proc. Natl. Acad. Sci. U. S. A.*, 2000, **97**, 984–989.
6 M. Mastrangeli, W. Ruythooren, J. P. Celis and C. V. Hoof, *IEEE Trans. Compon., Packag., Manuf. Technol.*, 2010, **1**, 133–149.
7 M. Poty, G. Lumay and N. Vandewalle, *New J. Phys.*, 2014, **16**, 023013.
8 N. Vandewalle, N. Obara and G. Lumay, *Eur. Phys. J. E: Soft Matter Biol. Phys.*, 2013, **36**, 127.
9 G. Lumay, N. Obara, F. Weyer and N. Vandewalle, *Soft Matter*, 2013, **9**, 2420–2425.
10 M. M. Nicolson, *Proc. Cambridge Philos. Soc.*, 1949, **45**, 288–295.
11 P. A. Kralchevsky and K. Nagayama, *Adv. Colloid Interface Sci.*, 2000, **85**, 145–192.
12 P. A. Kralchevsky and N. D. Denkov, *Curr. Opin. Colloid Interface Sci.*, 2001, **6**, 383–401.
13 K. D. Danov and P. A. Kralchevsky, *Adv. Colloid Interface Sci.*, 2010, **154**, 91–103.
14 D. Vella and L. Mahadevan, *Am. J. Phys.*, 2005, **73**, 817–825.
15 L. Botto, E. P. Lewandowski, M. Cavallaro and K. J. Stebe, *Soft Matter*, 2012, **8**, 9957–9971.
16 J. Voise, M. Schindler, J. Casas and E. Raphael, *J. R. Soc., Interface*, 2011, **8**, 1357–1366.
17 J. Bae, N. P. Bende, A. A. Evans, J. H. Na, C. D. Santangelo and R. C. Hayward, *Mater. Horiz.*, 2017, **4**, 228–235.
18 C. Mao, V. R. Thalladi, D. B. Wolfe, S. Whitesides and G. M. Whitesides, *J. Am. Chem. Soc.*, 2002, **124**, 14508–14509.
19 J. Metzmacher, M. Poty, G. Lumay and N. Vandewalle, *Eur. Phys. J. E: Soft Matter Biol. Phys.*, 2017, **40**, 108.
20 H. Cooray, P. Cicuta and D. Vella, *J. Phys.: Condens. Matter*, 2012, **24**, 284104.
21 F. Moisy, M. Rabaud and K. Salsac, *Exp. Fluids*, 2009, **46**, 1021.
22 L. Yao, L. Botto, M. Cavallaro, B. J. Bleier, V. Garbin and K. J. Stebe, *Soft Matter*, 2013, **9**, 779.
23 *Tilings and patterns*, ed. B. Grunbaum and G. C. Shepard, *Freeman*, 1987.
24 T. Defize, R. Riva, J. M. Raquez, P. Dubois, C. Jérôme and M. Alexandre, *Macromol. Rapid Commun.*, 2011, **32**, 1264–1269.
25 T. Defize, R. Riva, J. M. Thomassin, C. Jérôme and M. Alexandre, *Macromol. Symp.*, 2011, **309**, 154–161.

TAD chemistry : a very efficient reactive moiety for fast poly(ε-caprolactone) network crosslinking

Jérémie Caprasse, Raphaël Riva, Jean-Michel Thomassin, Christine Jérôme[1]

[1]CERM, University of Liège, CESAM-RU, Allée du Six Août, 13, 4000 Liège, Belgium

Abstract:

A chemically cross-linked and recyclable material with excellent shape-memory properties was formed by using the very efficient triazolinedione click chemistry between the 1,2,4-triazoline-3,5-dione (TAD) and the poly(ε-caprolactone) (PCL) functionalized by anthracene moieties. Concretely, a four arm PCL was functionalized by anthracene groups as chain-ends and this functional polymer was blended, in a mini extruder, with a bi-functional TAD (MDI-TAD) and then pressed in order to have a homogeneous film whose shape-memory properties can be determined. Compared to other thermo-reversible systems developed by our group[1–4], this one displays a better recovery, up to 97% for the first cycle, and no creep effect from cycle to cycle. Moreover, thanks to the high reactivity of the TAD moieties, no post-curing was required to obtain material with good mechanical properties. Finally, this material can be recycled by processing the degraded film with some MDI-TAD in the extruder.

Introduction:

Shape-memory polymers (SMPs) are physically or chemically cross-linked materials able to switch, under the action of a stimulus, from a previously fixed and stable temporary shape to its original shape, the permanent shape, programmed during the formation of the material. The stimulus used is generally the temperature and in this case they are so-called thermo-sensitive SMPs. SMPs are widely studied since few years for their interest in different fields many in packaging but also in other fields such as in the aerospace industry, smart textiles and as smart medical devices allowing minimal invasive surgery[2,5,6,7].

The semi-crystalline cross-linked poly(ε-caprolactone) is widely studied for this type of application. Indeed, when this cross-linked material is heated above the melting temperature

of the crystallites (around 50°C), the material becomes softer and can be deformed under stress. Then, the temperature decreases and when the crystallites are formed, the temporary shape is fixed even if the stress is released. Finally, if the polymer network is heated again without stress, due to the elasticity of the cross-linked chains, the material recovers its original shape.

The reversibility of the cross-links is an important factor for the recyclability and the reprocessability of the material. Different reversible reaction were considered, the photo-reversible[8–10], mechanically reversible[2,11,12,13] and more frequently the thermo-reversible reactions[2–4,11–14]. Many shape-memory polymers with thermo-reversible cross-links were investigated by our group. Firstly, the furan-maleimide[3] system, reversible above 100°C, demonstrates good mechanical and shape-memory properties (recovery >88% for the first cycle; fixity >99%). Moreover this Diels-Alder adduct presents good reprocessability and recyclability. Nevertheless, due to the high reversibility of this reaction, a creep effect occurs from cycle to cycle and considering that the reaction is relatively slow, a post curing of 48h is required to have a material with good mechanical properties. In order to avoid the creep effect of the material, the anthracene-maleimide couple was tested and studied[4]. This system was selected because of the higher stability of the formed adduct. DMA analysis confirmed this theory because a very small creep effect was observed from cycle to cycle and shape-memory properties were excellent (recovery >93% for the first cycle; fixity >99%). Nevertheless, a post-curing of 24h is still required to obtain a material with good mechanical properties and moreover, this material is no more recyclable because the temperature at which the reaction is reversible is above 250°C, temperature at which the polymer is degraded. The second drawback, the post-curing, can be avoided with the use of TAD derivative moieties. The TAD chemistry provides good yields in few minutes[15] thanks to the high reactivity of the azidocarbonyl derivatives. With this in mind, the TAD-indole system was developed[2] because the reaction with the indole is reversible at a temperature comprised between 90°C and 150°C, depending of the substituants on the indole molecule[13]. Shape-memory properties of this synthetized material were excellent (recovery >90% for the first cycle; fixity >99%) and this without any post-curing, as expected. This material can be reprocessed by solid state plasticity but the complete recyclability of the material is impossible because of the too dynamic reaction. A small creep effect is also observed from cycle to cycle.

Considering all these results the anthracene-TAD system has to be tested because it would combine the high stability of the adduct, avoiding the creep effect, and the high reactivity of the TAD, avoiding the creep effect. Moreover this couple is reversible above 50°C under mechanical stress, allowing the reprocessability and the recyclability of the material.

Experimental section:

Materials:

Toluene, dichloromethane (CH_2Cl_2) and diethyl ether (from Chem-Lab) as well as N,N-dimethylformamide (DMF), succinic anhydride, triethylamine (NEt_3), 9-anthracenemethanol, dicyclohexylcarbodimide (DCC) and 4-dimethylaminopyridine (DMAP) from Aldrich were used as received. 4-arm star-shaped PCL bearing hydroxyl groups at the end of each arm (Mn=8000 g/mol, PCL-4OH) were kindly provided by Perstorp-caprolactones. The synthesis of the 4,4'-(methylenebis(4,1-phenylene))bis(3H-pyrazole-3,5(4H)-dione) (MDI-TAD) and the 4-(2-hydroxyethyl)-10-oxa-4-aza-tricyclo[5.2.1.0]-dec-8-ene-3,5-dione were reported elsewhere.[14,16]

Synthesis of PCL-4COOH

50 g (25 mmol of hydroxyl function) of PCL-4OH were transferred into a previously dried round bottom flask and three azeotropic distillations with anhydrous toluene were carried out. Then, 200 mL of anhydrous DMF were added to the flask through a rubber septum with a flamed stain-less steel capillary. After complete solubilization, 2.75 g (27.5 mmol) of succinic anhydride and 3.9 mL (27.5 mmol) of triethylamine were successively added to the polymer solution. The solution was then stirred at 45°C overnight and the pink-purple solution containing the PCL-4COOH was successively precipitated in diethyl ether and methanol. A white powder is collected after filtration and dried under vacuum.

1 H NMR (CDCl3 ,δ): 4.05 (t, 168H, H A + A'), 2.64 (s, 16H, H a + a'), 2.3 (t, 158H, H E), 1.64 (m, 316H, H B + D), 1.37 (m, 158H, H C). Functionalization: > 95%.

Synthesis of Four-Arm Star-Shaped Anthracene- Bearing PCL (PCL-4ANTHR)

20 g (9.5 mmol of carboxylic acid functions) of PCL-4COOH were transferred into a previously round-bottom flask and three azeotropic distillations with anhydrous toluene were carried

out. Then, 60 ml of anhydrous CH_2Cl_2 were transferred to the flask through a rubber septum using a flamed stainless steel capillary. After the complete solubilization of the polymer, 2.37g (11.4 mmol) of 9-anthracenemethanol, 0.14g (1.14 mmol) of DMAP and 2.35g (11.4 mmol) of DCC were sequentially transferred inside the flask. After one night of reaction at room temperature and the filtration of the dicyclohexylurea (DCU) formed during the reaction, PCL-4ANT was recovered by successive precipitation in diethyl ether and methanol, filtered and dried under vacuum to obtain a slight yellow powder. The extent of functionalization was evaluated by 1 H NMR.

1 H NMR (CDCl3 ,δ): 8.51 (s, 3H, H g), 8.34-8.3 (d, 6H, H c), 8.05-8.01 (d, 6H, H f), 7.58-7.46 (m, 12H, H d + e), 6.17 (s, 6H, H b), 4.05 (t, 176H, H A + A'), 2.62 (t, 16H, H a + a' + x), 2.3 (t, 168H, H E), 1.64 (m, 336H, H B + D), 1.37 (m, 168H, H C). Functionalization: 75%.

Preparation of the PCL networks

Networks are formed during the extrusion in the melted state followed by a thermal curing. Typically, 4g of PCL-4ANTH and 0.32g of MDI-TAD were grinded together and injected in a 6 cm^3 co-rotating twin screw mini-extruder (Xplore, DSM). They were melt-blended at 120°C during 15min at 150rpm. The blend is collected in a 0.5mm thick mold and processed by compression molding at 120 °C and 75 bars during 1h in order to obtain a flat sheet shape of material.

Swelling experiment

The cross-linked material was immersed in chloroform for 24h at room temperature in order to reach its swelling equilibrium. The resulting gel was collected carefully and weighted in order to determine the quantity of solvent absorb by the cross-linked polymer. Then, the material was dried under vacuum until constant weight in order to determine the insoluble fraction. The swelling ratio and the insoluble fraction were calculated thanks to these equations (1) and (2).

$$\text{Swelling ratio} = \frac{\text{weight of the swollen material} - \text{weight of the dried material}}{\text{weight of the dried material}} * 100 \quad (1)$$

$$\text{Insoluble fraction} = \frac{\text{weight of the dried material}}{\text{weight of the initial material}} * 100 \qquad (2)$$

Characterization techniques

Proton nuclear magnetic resonance (^{1}H NMR) spectra were carried out by a Bruker Avance 400 apparatus at 25 °C at 400MHz in the Fourier-transform (FT) mode and using $CDCl_3$ as solvent. Size exclusion chromatography (SEC) analysis were recorded in THF at 45°C with a throughput of 1ml.min^{-1} on a Viscotek 305 TDA liquid chromatograph equipped with 2 PSS SDV linear M columns calibrated with polystyrene standards. Differential scanning calorimetry (DSC) was performed on a DSC Q500 (TA Instruments) calibrated with indium. The sample is inserted at 20°C and a temperature ramp of 10°C.min^{-1} is applied to reach -80°C. After 5min of temperature stabilization, the same temperature ramp is applied until 100°C. This cooling down-heating cycle is repeated and the melting temperature (T_m) and the melting enthalpy (ΔH_m) are recorded during the second heating ramp. Shape-memory properties were determined with a DMA Q800 (TA Instruments) using the tensile film clamp in controlled force mode. The sample (5mm x 5mm x 0.5mm) is introduced and then heated at 65°C. After 5min of temperature stabilization, a stress ramp of 0.06MPa.min^{-1} is applied to reach 0.3MPa. The sample is cooled-down under stress to 0°C and the temperature is maintained for 5min after that, the stress is released and the fixity can be determined at this stage. Still in absence of stress, the sample was heated to 65°C and the recovery can be determined. This cycle is repeated four times.

Results and Discussion:

The chains-ends functionalization of the PCL-4OH was realized by a two reactions of esterification previously described.[1] The first one converts the alcohol chains-ends into carboxylic acids thanks to the anhydride succinic in presence of triethylamine and the second one is a Steglich esterification in order to convert the –COOH chains-ends into anthracene by using 9-anthracenemethanol (Figure 1)

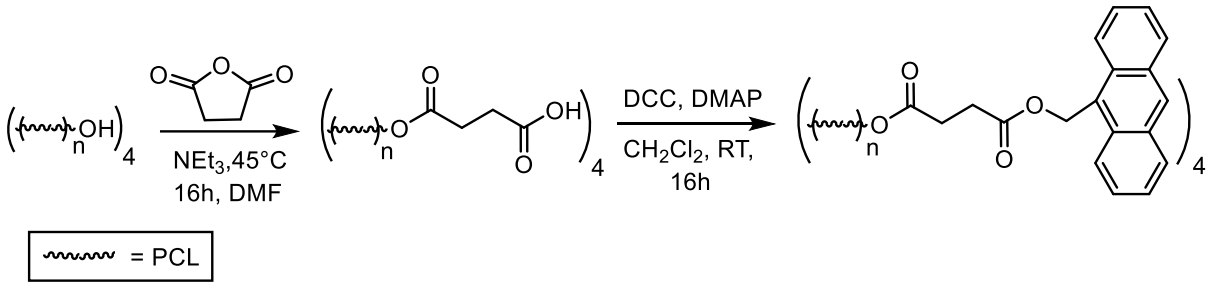

Figure 1: two step chains-ends functionalization by anthracene

For the first reaction, the complete conversion of the hydroxyl groups is reached because the peak corresponding to the -C<u>H</u>$_2$-OH (δ=3.63ppm) disappeared completely and a new peak at 2.65ppm, corresponding to the -C(O)-CH$_2$-CH$_2$-C(O)- protons (g+g'), appeared. As regards to the Steglich esterification, five different signals appeared at δ= 6.16; 7.5; 8.00; 8.30 and 8.50ppm (peaks h, j, l, i and k) corresponding to the nine protons of the anthracene group. Moreover, the signal corresponding to the -C<u>H</u>$_2$OH from the 9-anthracenemethanol shift from 5.64 to 6.16. This means that there is no more 9-anthracenemethanol in the final product. Nevertheless, the conversion of the –COOH chains-ends, which is calculated by comparison of the integral of the anthracene-C<u>H</u>$_2$O- (peak h) and the integral of the g+g' protons is equal to 80%. This non-quantitative reaction is directly visible on the NMR spectra because there is a small peak (x) inside the g+g' peak characteristic to the unreacted chain ends. This percentage of functionalization means that there is at least, in average, three functionalized arms on the four, which is enough to have the formation of a network.

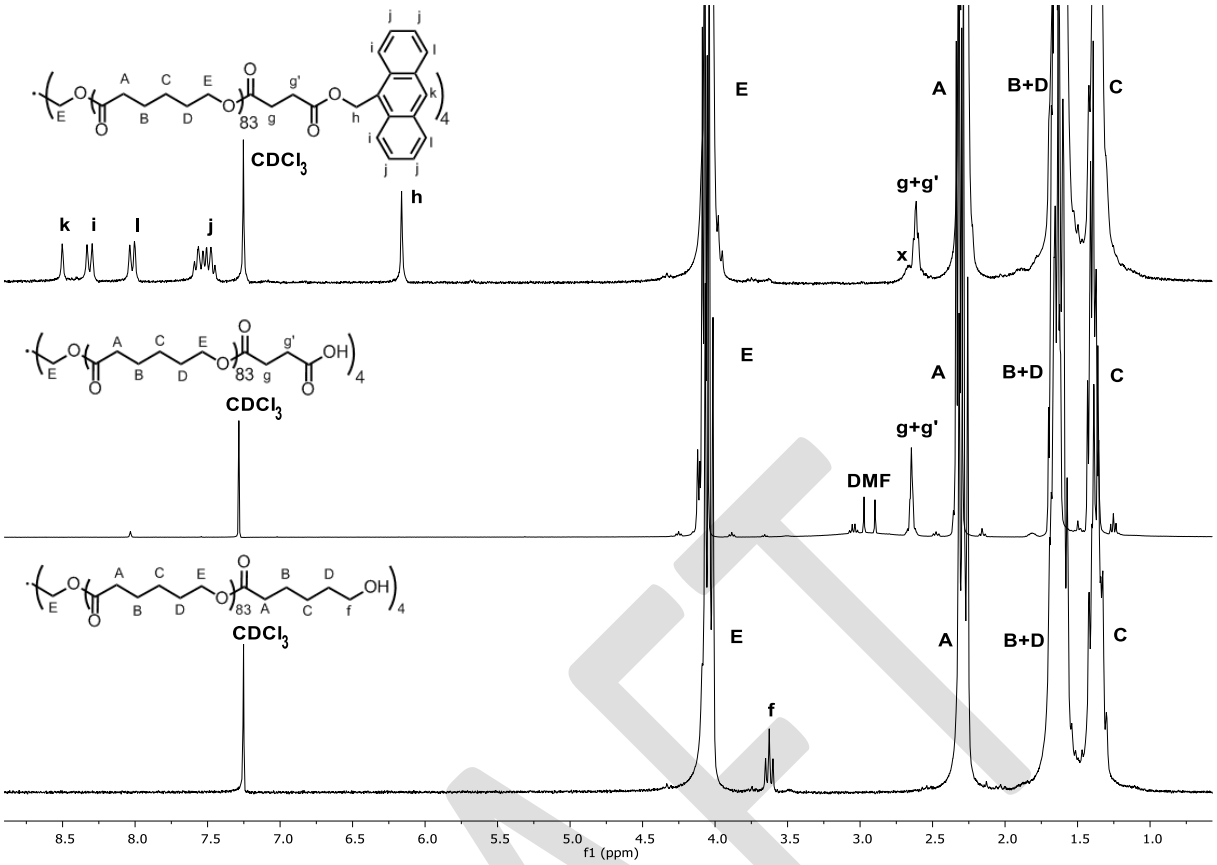

Figure 2: ^{1}H NMR spectra of the anthracene functionalization

The average degree of polymerization ($\overline{DP}$) is calculated, thanks to the integrals of one proton of the repetitive unit (peak A, Figure 2) and the integral of one proton of the chain end (peak f, Figure 2), following this equation:

$$\overline{DP} = \frac{I_A/2}{I_f/8}$$

The average degree of polymerization and the percentage of functionalization for each type of PCL are reported in this Table:

PCL type	$\overline{DP}$ (^{1}H NMR)	M_w (^{1}H NMR)	%conversion (^{1}H NMR)	M_w/M_n (SEC)
PCL-4OH	83	9400	-	1.26
PCL-4COOH	84	9800	>99%	1.22
PCL-4ANTH	89	11300	80%	1.34

Table 1: Functionalized poly(ε-caprolactone) parameters

The size exclusion chromatography provides the poly-dispersity index of the macromolecular chains. The SEC values, even if they are corrected by Mark-Houwink coefficient, are not accurate because star-shape polymers are used and the hydrodynamic volume of these types of molecules is different compared to a linear polymer with the same molar masse. Moreover, there is also an impact of the end-groups on the elution volume because they can change the hydrodynamic volume of the star-shape polymer. Finally, no degradation of the PCL chains is observed during the different functionalization steps.

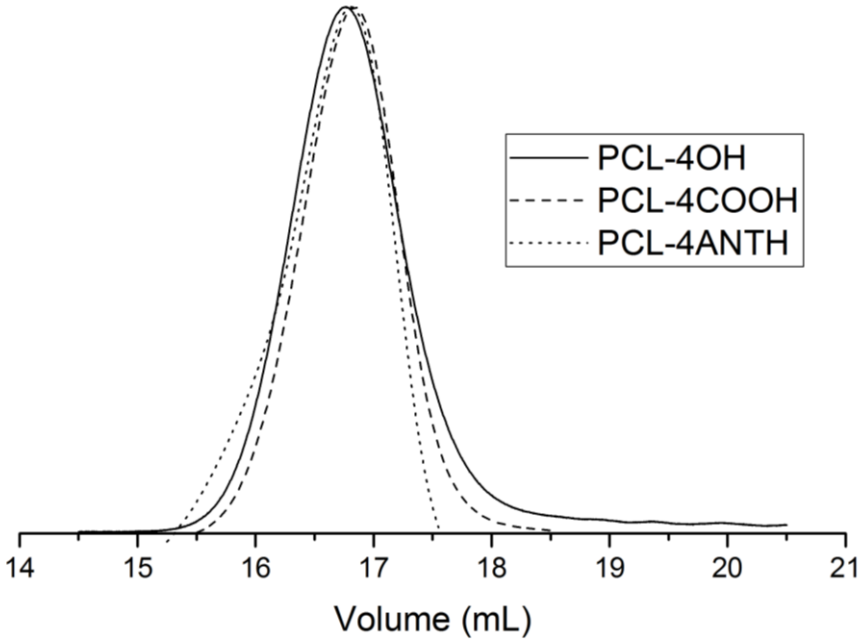

Figure 3: SEC chromatograms of the PCL functionalization steps.

A melting temperature of 45°C is obtained by DSC for the PCL-4ANTH with a crystallinity degree of 45%, which suits for shape-memory applications.

The second component of the mixture, the MDI-TAD reagent, was synthetized in three steps with high yield described by Billiet and al.[14]

PCL networks were obtained by mixing PCL-4ANTH and MDI-TAD in stoichiometric amount. These two reagents were grinding together to provide a nice homogeneous powder. The precursor blend is injected in the mini-extruder at 120°C. This temperature was chosen, on one hand, in order to confer some mobility to the PCL-chains and consequently allow a

better mixing. And on the other hand, at this temperature, the equilibrium of the reaction between these species is shifted to the left and normally avoiding the cross-linking inside the extruder since the reaction between anthracene and TAD is supposed to be reversible above 50°C. Nevertheless, the working temperature cannot be above 150°C because above this temperature, the degradation of the MDI-TAD occurs.

In spite of this temperature, during the melting process, the torque inside the mini-extruder increase directly and sharply which indicates that the cross-linking reaction occurs anyway. One reason of this is that the reaction with the MDI-TAD is very fast and dynamic. After 15min of mixing, two types of material were collected by the extruder outlet, the first one was an inhomogeneous brown and yellow material and the second one is a homogeneous brown and translucent material from which a piece cut and analyzed by swelling experiment in chloroform. A cross-linked material is obtained with a swelling ratio of 1200% and an insoluble fraction of 98.5%. These results confirm that the reaction of the MDI-TAD and the PCL-4ANTH is significant, even at 120°C, and highly cross-linked compared to other previously developed systems.[1]

The inhomogeneous material is then reprocessed by compression molding into a flat sheet shape mold at 100°C and 75 bars during 1h. After this treatment, a homogeneous brown film is recovered and a piece of this film is drawn in order to be analyzed by swelling experiment in chloroform. After 48h in the solvent, the sample is collected and a swelling ration of 1500% and an insoluble fraction of 93.5% are calculated. In order to reach the same cross-linking density than those of the other material, a kinetic study, based on swelling experiment is realized. This was realized at 65°C in an open air oven. This temperature allows chains mobility, because it is above the T_m of the PCL, and the reaction between anthracene chain-ends and MDI-TAD is more favorable. After 24h of thermal curing, the swelling ration and the insoluble fraction were respectively equal to 1400% and 94% and these value were still the same after 72h of post-curing. For the following experiments, all the samples were prepared from this flat sheet shape.

The crystallinity degree of the final film is analyzed by DSC, since the shape-memory properties are directly linked to the ability of the material to fix the temporary shape. In this

case, it is equal to 36% with a melting temperature of 40°C which is comparable to other systems studied by our group.[1,2]

The shape-memory properties of the formed material were determined by dynamical and mechanical analysis (DMA) by conducting stress-relaxation tests at 65°C. The experiment is composed of four consecutive cycles during which the fixity, i.e. the ability of the material to keep its temporary shape during the stress release at 0°C, and the recovery, i.e. the ability of the material to recover its original shape, were calculated with these equations.

The fixity ratio:

$$R_f = \frac{\text{Strain after stress release}}{\text{Strain after stretching and cooling}} * 100$$

The recovery ratio:

$$R_r = \frac{\text{Strain after stress release before reheating} - \text{strain after reheating at cycle}N}{\text{Strain after cooling under stress} - \text{strain after reheating at cycle } (N-1)} * 100$$

From curves on the Figure 4, the fixity ratios are above 99% for each cycle. The recovery is not fully complete for the first cycle (97%) because of the training phenomenon but this value is excellent compared to the other systems already tested by our group[1-3] . For the other cycles, the recovery ratio is above 99%. Moreover, a very limited creep effect is observed from cycle to cycle for this system, which means that there is no adduct dissociation at this temperature and consequently, it is very stable. Considering all these results, this type of reversible system is very promising.

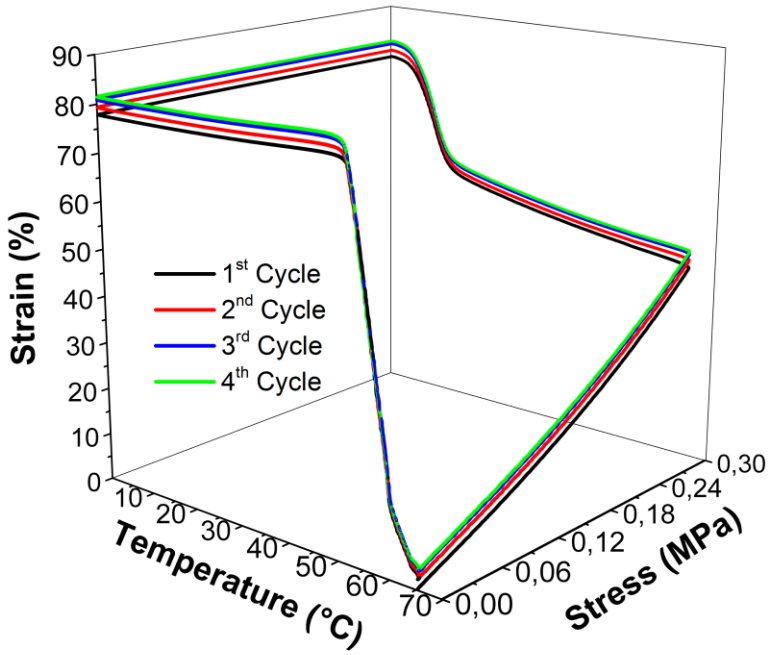

Figure 4 : Shape-memory experiment at 65°C

The anthracene-TAD adduct was also selected for its thermal and mechanical reversibility above 50°C[11,12]. The reversibility of the reaction was firstly tested by rheology but the results were not concluding even at higher temperature. The sample was then pressed at 120°C in order to increase the formation of the starting materials. After three hours at 120°C, the film is recovered and a small piece is analyzed by swelling experiment in chloroform. The degraded film is a bit more brittle than the initial film which indicates that the cross-linking density is lower than before and this is confirmed by the swelling experiment with a swelling ratio of 3100% and an insoluble fraction of 73%. In order to prove the reversibility of the reaction, the film was then placed in the oven at 65°C during 72h and after this post-curing treatment, swelling experiment was done and the results were exactly the same. These results suggest that there is no reversibility of this system but rather a degradation of the triazolinedione derivative. To prove this hypothesis, a new film was prepared, following the same conditions except for the degradation step. Instead of applying a temperature of 120°C, the film was placed in the press at 150°C for three hours in order to degrade it totally. Indeed, after this heating treatment, the film was much more brittle than before, indicating that the cross-linking density is much lower compared to the initial film. A swelling experiment was

realized on a piece of this material and after few hours, the material is completely disintegrated in the chloroform confirming that the cross-linking ratio is very weak.

The recyclability of the material was tested by cutting the degraded material in very small pieces and mixing it with 50% of the initial MDI-TAD quantity (0.15g) in the extruder with the same conditions than before. Once again, the torque increases sharply and after 15 minutes of blending, an inhomogeneous material is collected by the extruder output. Then, it was pressed in the flat sheet shape mold at 100°C and 75 bars for 30 minutes. The recovered film was browner than before but the hand-tested mechanical properties were better. Then, a piece of this film was cut and a swelling experiment was realized. The swelling ratio was equal to 2200% and the insoluble fraction was equal to 63%. Shape-memory properties were then tested by DMA but, sadly, the film breaks in the first cycle because the material is not very homogenous probably due to the excessive amount of added MDI-TAD. Indeed, some MDI-TAD spots were visible into the film. Another film was realized by adding 25% of the initial quantity of MDI-TAD (75mg). After the same processing way, a homogenous film with good mechanical properties was obtained. Swelling experiment was realized and the swelling ratio and the insoluble fraction were respectively equal to 3700% and 41%. DMA measurements were realized but once again, the film breaks in the first cycle due to the too low cross-linking.

Nevertheless, a qualitative study of shape-memory behavior was realized for each film, before and after recycling. These tests consist to heat a rectangular piece of the film at 65°C, allowing the fusion of the crystallites and the deformation of the material upon mechanical stress. This deformed shape was fixed by cooling slowly the material to room temperature in order to fix the temporary shape. The permanent shape is recovered, in less than one second, by heating again the material at 65°C without stress. Figure!!

Conclusion:

Poly(ε-caprolactone) was successfully functionalized by anthracene moieties with a conversion ratio around 80% and without any degradation of the polymer chains. A new type of shape-memory material was obtained after the blending of this PCL with MDI-TAD into the extruder at 120°C and after a compression molding at 100°C and 75 bars, a thin film of the material was recovered. The recovery and the fixity ratios were excellent and compared to the other systems developed by our group, the recovery of this material is really outstanding.

Moreover, there was a very small creep effect that appears from cycle to cycle but it is very limited compared to other systems.

After the degradation of the film at 150°C for three hours, a very brittle material was obtained, suggesting that the cross-linking ratio decrease and the MDI-TAD is degraded by this thermal treatment instead of a reversible reaction between the anthracene and the TAD moieties because there is no new cross-linking of the material after a post-curing of three days at 65°C. By adding some MDI-TAD and mixing it with the degraded film into the extruder, a homogeneous and cross-linked material was obtained. Unfortunately, DMA tests cannot be performed because of the film break. Nevertheless, from an almost completely uncross-linked material, a new film with good mechanical properties was obtained.

Bibliography:

1. Defize, T., Riva, R., Jérôme, C. & Alexandre, M. Multifunctional Poly (ε -caprolactone) -Forming Networks by Diels – Alder Cycloaddition : Effect of the Adduct on the Shape-Memory Properties. *Macromol. Chem. Phys.* **213,** 187–197 (2012).

2. Defize, T. *et al.* Reversible TAD Chemistry as a Convenient Tool for the Design of (Re)processable PCL-Based Shape-Memory Materials. *Macromol. Rapid Commun.* **38,** 1–7 (2017).

3. Defize, T. *et al.* Thermoreversibly crosslinked poly(ε-caprolactone) as recyclable shape-memory polymer network. *Macromol. Rapid Commun.* **32,** 1264–1269 (2011).

4. Defize, T., Riva, R., Thomassin, J. M., Jérôme, C. & Alexandre, M. Thermo-reversible reactions for the preparation of smart materials: Recyclable covalently-crosslinked shape memory polymers. *Macromol. Symp.* **309–310,** 154–161 (2011).

5. Lendlein, a. Biodegradable, Elastic Shape-Memory Polymers for Potential Biomedical Applications. *Science (80-.).* **296,** 1673–1676 (2002).

6. Lendlein, A. & Kelch, S. Shape-Memory Effect From permanent shape. *Angew. Chemie* **41,** 2034–2057 (2002).

7. Julich-gruner, K. K., Löwenberg, C., Neffe, A. T., Behl, M. & Lendlein, A. Recent Trends

in the Chemistry of Shape-Memory Polymers. 527–536 (2013).

8. Schenck, G. O., von Wilucki, I. & Krauch, C. H. Photosensibilisierte Cyclodimerisation von Cumarin. *Chem. Ber.* **95,** 1409–1412 (1962).

9. Kaur, G., Johnston, P. & Saito, K. Photo-reversible dimerisation reactions and their applications in polymeric systems. *Polym. Chem.* **5,** 2171–2186 (2014).

10. Chung, C., Roh, Y., Cho, S. & Kim, J. Crack Healing in Polymeric Materials via Photochemical [2 + 2] Cycloaddition. *Chem. Mater.* **16,** 3982–3984 (2004).

11. Gossweiler, G. R. *et al.* Mechanochemical activation of covalent bonds in polymers with full and repeatable macroscopic shape recovery. *ACS Macro Lett.* **3,** 216–219 (2014).

12. Roy, N. & Lehn, J. M. Dynamic Covalent chemistry: A facile room-temperature, reversible, diels-alder reaction between anthracene derivatives and n-phenyltriazolinedione. *Chem. - An Asian J.* **6,** 2419–2425 (2011).

13. Houck, H. a. *et al.* Design of a thermally controlled sequence of triazolinedione-based click and transclick reactions. *Chem. Sci.* **8,** 3098–3108 (2017).

14. Billiet, S. *et al.* Triazolinediones enable ultrafast and reversible click chemistry for the design of dynamic polymer systems. *Nat. Chem.* **6,** 815–821 (2014).

15. De Bruycker, K. *et al.* Triazolinediones as Highly Enabling Synthetic Tools. *Chem. Rev.* **116,** 3919–3974 (2016).

16. Heath, W. H. *et al.* Degradable cross-linkers and strippable imaging materials for step-and-flash imprint lithography. *Macromolecules* **41,** 719–726 (2008).